Adipogenesis in Rodent Skin, The Dermal Adipose Layer: What Signals Adipocyte Development in the Lower Dermis?

DAVIES, OLIVIA,STEPHANIE,EVELYN

DAVIES, OLIVIA,STEPHANIE,EVELYN (2015) *Adipogenesis in Rodent Skin, The Dermal Adipose Layer: What Signals Adipocyte Development in the Lower Dermis?*, Durham theses, Durham University. Available at Durham E-Theses Online: http://etheses.dur.ac.uk/11156/

Adipogenesis in Rodent Skin, The Dermal Adipose Layer: What Signals Adipocyte Development in the Lower Dermis?

Olivia Stephanie Evelyn Davies

MSCR Biological Sciences

School of Biological and Biomedical Sciences
Durham University

2014

Research into adipogenesis has become increasingly more fundamental as our understanding of diabetes and obesity develops. Adipose tissue (fat) exists in many depots throughout the body. While widely known that there is a subcutaneous adipose depot beneath the skin, more recently a separate dermal adipose layer, within the lower dermis of rodent skin, has been found. However, the developmental origins and timings of adipogenesis in this dermal layer are not well characterised. This thesis aims to study adipogenesis within this layer, by creating an in vivo-like model and investigating signalling pathway effects.

Firstly, the hypothesis of an inhibition signal from the upper dermis and the role of the G0/G1 switch gene 2 (G0S2) in the dermal adipose tissue was explored. Experiments showed G0S2 expression in the lower dermis during development. PPARγ has been shown as the main regulator of adipogenesis, together with C/EBPα. The potential role of PPARγ in early adipogenesis was investigated, using immunofluorescence analysis.

Microarray analysis studies previously showed molecular differences between in vitro and in vivo, therefore model systems, more closely related to in vivo conditions, are necessary. An organ culture and a cell culture model were developed. The cell culture model, using 3D cell spheres, proved most useful to investigate signalling in adipocyte development. The EGF/EGFR, TGFβ/BMP and KGF/KGFR pathways were studied, by supplementing cultures with an activator or inhibitor of the receptor of each pathway. Differential levels of oil red O staining and therefore adipocyte formation, were observed.

In conclusion, this work was found to suggest commitment of the cells to the adipocyte lineage begins earlier, than from when microarray data was collected. While not conclusive, it provides an insight and direction for further studies, in terms of PPARγ and potential adipogenic inhibition signals in the upper dermis, as well as a model system.

Table of Contents

List of Tables

Chapter 2

Chapter 3

Chapter 4

Chapter 5

List of Illustrations

Chapter 1

Chapter 2

Chapter 3

Chapter 4

Chapter 5

List of Appendices

Abbreviations

2D	2-dimensional
3D	3-dimensional
ANOVA	Analysis of Variance
BAT	Brown adipose tissue
BMP	Bone morphogenetic protein
BMPR	Bone morphogenetic protein receptor
BMZ	Basement membrane zone
cDNA	Complementary deoxyribonucleic acid
C/EBP	CCAAT enhancer binding protein
DAPI	4',6-diamidine-2'-phenylindole dihydrochloride
DEJ	Dermal epidermal junction
DMEM	Dulbecco's modified eagle's medium
DMSO	Dimethyl sulfoxide
dN	Postnatal day (newborn)
'E' or 'e'	Embryonic day
EDTA	Entylenediaminetetraacetic acid
EDU	5-ethynyl-2'-deoxyurindine
EGF	Epidermal growth factor
EGFR	Epidermal growth factor receptor
EGF+	EGF pathway activator
EGF-	EGF pathway inhibitor
ESCs	Embryonic stem cells
FACs	Fluorescence activated cell sorting
FBS	Foetal bovine serum
FGF	Fibroblast growth factor
FGFR	Fibroblast growth factor receptor
FITC	Fluorescein isothiocyanate
GEDI	Gene expression dynamics expector
G0S2	G0/G1 switch gene 2
H&E	Haematoxylin and Eosin
IF	Immunofluorescence analysis
KGF	Keratinocyte growth factor
KGFR	Keratinocyte growth factor receptor
LSSU	Life sciences support unit
MEM	Minimal Essential Medium
MOM	Mouse on mouse
mRNA	Messenger ribonucleic acid
MSCs	Mesenchymal stem cells
ORO	Oil red O
PBS	Phosphate buffered saline
PFA	Paraformaldehyde
PPAR	Peroxisome proliferator activated receptor
RCM	Relative centrifugal force
RNA	Ribonucleic acid
RNAi	Ribonucleic acid interference
RPM	Revolutions per minute
RT-PCR	Reverse transcriptase - polymerase chain reaction
TGF	Transforming growth factor
TZD	Thiazolidinedione
WAT	White adipose tissue

Declaration

The Organ Culture Model was established as part of joint research with Sarah Morris. The intention was to create a model to study adipogenesis. E14.5 to E18.5 spheres were also created jointly as a basis for further investigation of earlier adipogenesis.
Therefore, Chapters 1, 2, 3, 5, and 6 are my individual contribution. Chapter 4, establishing the models, the organ culture model was conducted as part of joint research and the 3D spheres, however the cell culture model system comparing 2D, 3D and 3D to 2D and supplementing with factors was my own contribution.

Statement of Copyright

Acknowledgements

I would like firstly to thank Professor Colin Jahoda for providing the opportunity to conduct this research and directing my path of research in terms of experiments, and also providing continual support and suggestions throughout the course of the masters. I would also like to thank the members of Professor Colin Jahoda's research group: Hilary Prescott, Karl Gledhill, Aaron Gardner, Arianna Bianchi and Shu Wei Li for technical support throughout my laboratory research.

I would like to acknowledge Kamila Wojciechowicz for forming the basis of this project in terms of a direction of study and enabling the use of microarray data for further analysis.

I would like to mention also Craig Manning for equipment and protocol advice and those people in the LSSU who efficiently conducted all the timed matings required, including Heather Crawford and Claire Robinson.

I gratefully thank Adina Mihai for providing 3T3 F442A cells and Weiju Wu for providing a sample of EDU for testing.

Importantly, I acknowledge Sarah Morris for helping to establish a culture model and providing endless entertainment during antibody incubations.

CHAPTER 1:

Introduction

1.1. The Skin

Skin is a vital organ that constitutes the outer layer of the body and plays several crucial roles including those involved in insulation and protection from the external environment (Igarashi et al. 2005; Millar 2005). Mammalian skin has many essential similarities between species. In simple terms, from the outside in, the skin is composed of, an epidermis and a dermis (Figure 1.1). Underneath the dermis is a layer which is termed the subcutis or hypodermis and which is primarily adipose tissue and therefore often known as the subcutaneous layer. These defined layers are in fact divided into many sub-layers in which the cell morphology differs (Figure 1.1). A dermal-epidermal junction also exists between the epidermis and dermis.

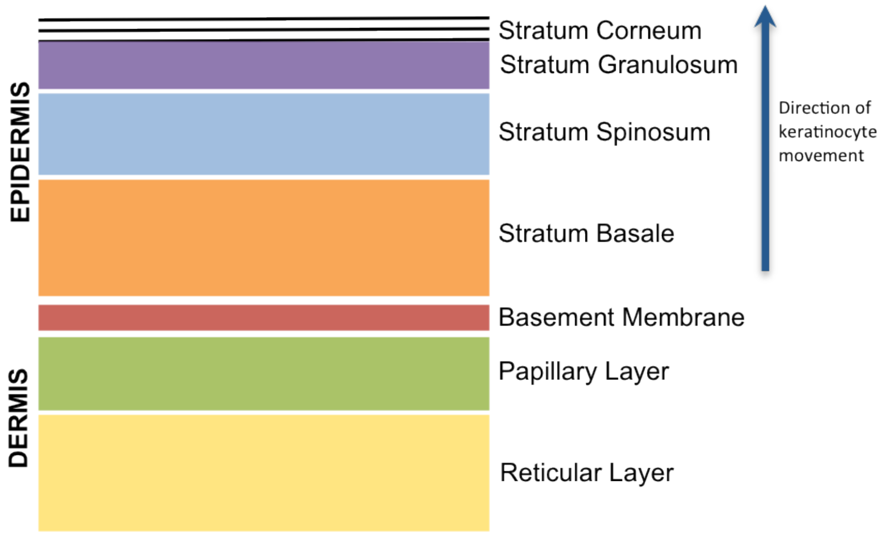

Figure 1.1: Schematic of the layers within the skin. The skin is divided into the epidermis, dermis and basement membrane, but within them are further sub-layers. The direction of keratinocyte movement is labelled. (Adapted from McGrath *et al.* 2004; McGrath *et al.* 2008; Wojciechowicz 2012)

The skin is associated with many different tissues including those of vascular and nervous origin (Kanitakis 2002) (Figure 1.2). The skin also has a number of appendages including hair follicles and sebaceous glands (pilosebaceous units) and apocrine and eccrine sweat glands, which differ in their distributions across the body. For example, in some regions, including the palms of human skin, skin is glabrous and does not have any hair follicles (Montagna 1974; McGrath *et al.* 2004).

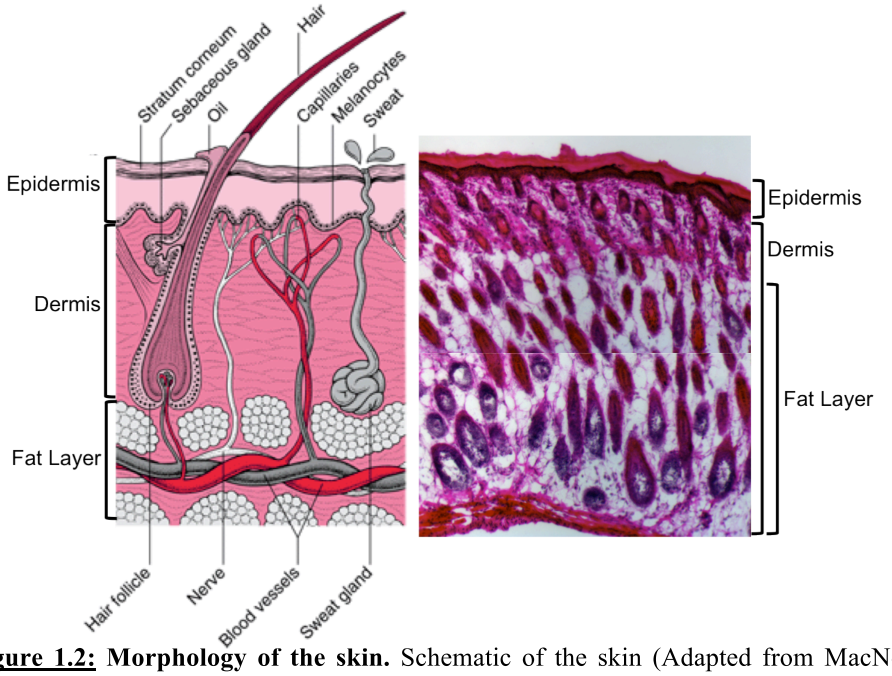

Figure 1.2: Morphology of the skin. Schematic of the skin (Adapted from MacNeal 2014) compared with Haematoxylin and Eosin staining of 7 day old mouse back skin conducted during this project. Follicles protrude into the adipose (fat) layer.

1.1.1. Epidermis

The epidermis and its associated appendages are of ectodermal origin in embryogenesis (Kanitakis 2002). The main cellular component of the epidermis is composed of keratinocytes, which differentiate as they move through the skin from the inner to the outer layer of the epidermis where they become flattened cornified corneocytes, thus the epidermis is continuously self-renewing. The basal layer contains the stem cell population. Cells are shed at the skin surface by desquamation and new cells are generated from a stem cell population at the basal layer (Bouwstra *et al*. 2003; Moore and Lemischka 2006). The epidermis is subdivided into a number of layers (Figure 1.1). The stratum corneum is the outermost layer and therefore the main protective barrier (Bouwstra *et al*. 2003). Cells in the layers beneath move up through the epidermis, as annotated in Figure 1.1. Keratinocytes contain many structural proteins, including keratin filaments, and lipids. These fibrous proteins increase in number as the keratinocytes move through the epidermis in the differentiation process and make up the majority of the cytoskeleton (Downing 1992). Each layer can be distinguished by the morphology and differentiation state of the keratinocytes, molecularly shown by changes in cytokeratin expression (Franssen *et al.* 2004).

As well as keratinocytes, there are other cell types present including Langerhans cells, melanocytes and Merkel cells (Kanitakis 2002). Intercellular junctions, including gap and adherens junctions as well as desmosomes, allow cell-to-cell contact throughout the epidermis (Kanitakis 2002). This is fundamental to maintaining the structure until the stratum corneum where the desmosomes have been permitted to degrade prior to exfoliation from the surface (Downing 1992). During the differentiation of the keratinocytes, they develop many membrane-bound lamellar bodies, composed mainly of lipids, which are later secreted to form intercellular lamellae (Downing 1992; Bouwstra *et al.* 2003). As well as a number of lamellar proteins, the epidermis has a high lipid content, from phospholipids to ceramides and cholesterol; The majority of which are part of the stratum corneum (Downing 1992; Bouwstra *et al.* 2003). These play a significant role in making the epidermal barrier impermeable to water.

1.1.2. Dermal-Epidermal Junction

At the dermal-epidermal junction (DEJ) is the basement membrane zone (BMZ), a specialized structure containing multiple extracellular matrix components including collagen fibres, secreted by basal keratinocytes and dermal fibroblasts (Kanitakis 2002). This junction is important for adhering the epidermis to the dermis and is also involved in the exchange of metabolites between the two. Crucially it is also involved in the interactive signalling between the dermis and epidermis. Anchoring fibrils are present to join the two layers (Burkhard and Ruppert 1981; Kanitakis 2002).

1.1.3. Dermis

The dermis is an elastic connective tissue layer of mesodermal origin, which provides mechanical support for the skin (Kanitakis 2002; Bouwstra *et al.* 2003). Its cellular content consists mainly of fibroblasts and in addition dendrocytes and mast cells are also present. The spindle-shaped fibroblasts synthesise all the extracellular fibres present in the dermis (Kanitakis 2002). Structurally dermis can be defined as a fibrous collagen network populated with relatively few cells. Meshworks of collagen and elastic fibres create the dermis, making the skin both durable and mobile. The dermis also contains a number of nerves, blood vessels and lymphatics (Montagna 1974) and houses the epithelial skin appendages.

1.2. The Adipose Organ

The adipose organ not only acts as energy storage, insulation and protection but also the body’s largest endocrine organ, influencing cells and tissues across the body (Gesta *et al.* 2007; Poulos *et al.* 2009). Adipose tissue, commonly known as fat, is made up of several different cell types: mainly adipocytes, but also endothelial cells, blood cells, fibroblasts and macrophages (Rosen *et al.* 1999). The organ is made up of anatomically distinct depots including subcutaneous and visceral (Cinti 2007) and crucially its structure and functions differ between locations. For example, visceral adipose tissue is involved in increased risk of insulin resistance, while the subcutaneous adipose tissue is not (Rosen and MacDougald 2006). In accordance with this, gene expression also varies between depots (Gesta *et al*. 2007).

Adipocytes and adipose tissue play important roles in obesity and diabetes, through adipocyte hypertrophy and adipocyte recruitment (Wang *et al*. 2006). Research into adipogenesis has grown in response to the current obesity epidemic (Gesta *et al.* 2007; Billon *et al*. 2008). Obesity being an increase in adipocyte number and size whereby a balance between energy intake and expenditure does not exist (Gesta *et al.* 2007; Billon *et al*. 2008). Obesity can cause insulin resistance and has been found to be a major causal factor of many diseases, including type 2 diabetes, cardiovascular disease and some cancers (Gesta *et al*. 2007). A better understanding of adipogenesis may therefore be beneficial to the treatment and prevention of obesity and associated diseases.

1.2.1. Adipocytes

The main cellular component of adipose tissue is adipocytes. The proteins e.g. adipokines that these cells secrete are important for many functions, including blood pressure, energy balance and angiogenesis (Lau *et al.* 2005; Rosen and MacDougald 2006; Lefterova and Lazar 2009). Mature adipocytes are able to store and synthesise a high quantity of lipids and rapidly release them (Rosen and MacDougald 2006). These cells differ from other cells that can carry lipids, in that they contain large lipid droplets contained within perilipin (Greenberg *et al.* 1991; Gesta *et al.* 2007). Leptin is a hormone secreted by mature white adipocytes thought to be involved in regulating fat mass and energy balance (Gregoire *et al.* 1998; Martin *et al.* 1998).

Two main types of adipocyte can characterize mature adipose tissues. White adipocytes contribute to white adipose tissue (WAT) and brown adipocytes to brown adipose tissue (BAT), though tissues are not necessarily solely one or the other (Avram *et al.* 2005). WAT and BAT have opposite functions (Billon *et al.* 2008). White adipose cells contain a single lipid droplet (Spiegelman 2013). Brown adipocytes have a lower lipid content but more mitochondria for their involvement in heat dissipation during thermogenesis (energy usage) and their importance in preventing hypothermia (Spiegelman 2013) while WAT is involved in excess energy storage (Rosen and MacDougald 2006; Billon *et al.* 2008; Farmer 2008; Lefterova and Lazar 2009). BAT decreases in volume after birth (Gesta *et al*. 2007). There are more brown adipocytes in rodents than in humans for the burning of energy (Gray *et al.* 2006).

It was originally thought that depots of adipose tissue were exclusively white or brown, but it was discovered that many of them comprise of a mix of both white and brown adipocytes in both rodents and humans (Gray *et al*. 2006). One suggested reason for the introduction of brown adipocytes into white depots is to prevent obesity (Gray *et al.* 2006). The brown adipocytes that develop in white adipose tissue are not of the same origin as original brown fat (Seale *et al.* 2008; Spiegelman 2013). Thus brown adipocytes can be defined as; classical brown adipocytes, whereas beige adipose cells which develop in white depots are often referred to as brite cells (Petrovic *et al.* 2010).

The gene expression profiles of these adipocytes are, for the best part, the same. However, certain genes e.g. uncoupling protein-1 (UCP-1) are only expressed by one type, in this case brown adipocytes and it is involved in heat dissipation (Gray *et al.* 2006; Spiegelman 2013). Brown adipocytes are distributed in the interscapular region and develop earlier in foetal development than white adipocytes, which develop neonatally in rodents and during midgestation in humans (Gesta *et al*. 2007).

1.2.2. Origins of Adipose Tissue

Despite the interest in adipose tissue and its potential for therapeutic applications, relatively little is actually known about their origins. They are thought to develop from mesenchymal stem cells (MSCs) and before that from mesoderm (Billon *et al.* 2008). MSCs can differentiate into adipocytes, osteoblasts, chondrocytes and connective tissue (Figure 1.3). However, due to the precursor cells (preadipocytes) not presenting any morphological changes and the lack of definitive cell-specific markers, the lineage of MSCs towards adipocytes is yet to be clearly defined (Billon *et al.* 2008). The fact that adipocytes exist in separate adipose tissue depots, which exhibit different developmental gene expression profiles (Gesta *et al.* 2006), suggests they may be of differing developmental origin (Billon *et al.* 2008). Likewise, the variation in gene expression may be related to the differing metabolic functions of the individual fat depots. For example, adipose tissue in the breasts and thighs is more sensitive to sex hormones than other adipose tissue depots (Billon *et al.* 2008). Are there separate types of preadipocytes for distinct adipose depots?

It has been suggested that adipocytes may arise from neuroectoderm and neural crest as the neural crest stem cells generated had adipogenic potential in culture (Billon *et al.* 2007; Takashima *et al.* 2007; Billon *et al.* 2008). *In vivo* it has been found that only cephalic adipose depots arise from neural crest, which further suggests that adipose tissues come from different origins, but when do these cells become committed to adipocyte lineages and do their functions differ? It may be that only specific depots are linked to obesity and associated diseases (Gesta *et al.* 2007; Billon *et al.* 2008). One hindrance to our understanding of the lineage of different adipose depots is therefore the relative lack of specific markers (Billon *et al.* 2008) There are now some markers associated with adipogenesis e.g. CD24, however early adipogenic markers are less well characterised (Rodeheffer *et al*. 2008).

It has been suggested that developmental genes and those involved in pattern formation including Hox genes may be important in the isolated development of different adipose depots, e.g. HoxA5, HoxA4 and HoxC8 are more highly expressed in intraabdominal adipocytes while HoxA10 and HoxC9 are more highly expressed in subcutaneous adipocytes (Gesta *et al.* 2006; Gesta *et al*. 2007).

Atit *et al.* (2006) investigated the developmental origin of mouse skin dermis and traced the lineage suggesting that interscapular fat and dermis arise from the same origin in the dermomyotome. Muscle also can develop from this dermomyotome, i.e. if muscle formation is inhibited, adipocytes will be produced. It was thought that these brown and white adipocytes developed from the same mesenchymal progenitor, but now some research shows otherwise. Seale *et al.* (2008) used lineage-tracing studies to find that white and brown adipocytes develop from different origins. For example, brown fat and skeletal muscle arise from the same lineage white fat does not.

Driskell *et al.* (2013) found that by embryonic day 18.5 (e18.5), the upper dermis and lower dermis had become separate. The fibroblasts present were originating from two different lineages. The upper dermis and the dermal papilla from one and the lower dermis, reticular fibroblasts and preadipocytes from the other (Driskell *et al.* 2013). This suggests that at some point before e18.5, the upper dermis was responsible for hair follicle formation and the lower dermis for adipogenesis.

1.2.3. Adipogenesis

Adipogenesis is the development of lipid-containing adipocytes from their precursor cells (Gregoire *et al.* 1998). Mesenchymal stem cells develop into preadipocytes that have become committed. These then differentiate into adipocytes (Rosen and MacDougald 2006; Billon *et al.* 2008). Four stages are involved in this second process; growth arrest, mitotic clonal expansion, early differentiation and terminal differentiation as shown in Figure 1.3 (Gesta *et al.* 2007). The need for the mitotic clonal expansion step is controversial as some say differentiation occurs without it. Some describe adipogenesis more simply as a two-step process; determination followed by terminal differentiation (Rosen and MacDougald 2006). Determination, similar to early differentiation is the stage at which the stem cell becomes committed to a preadipocyte. Terminal differentiation is the process by which preadipocytes become mature adipocytes.

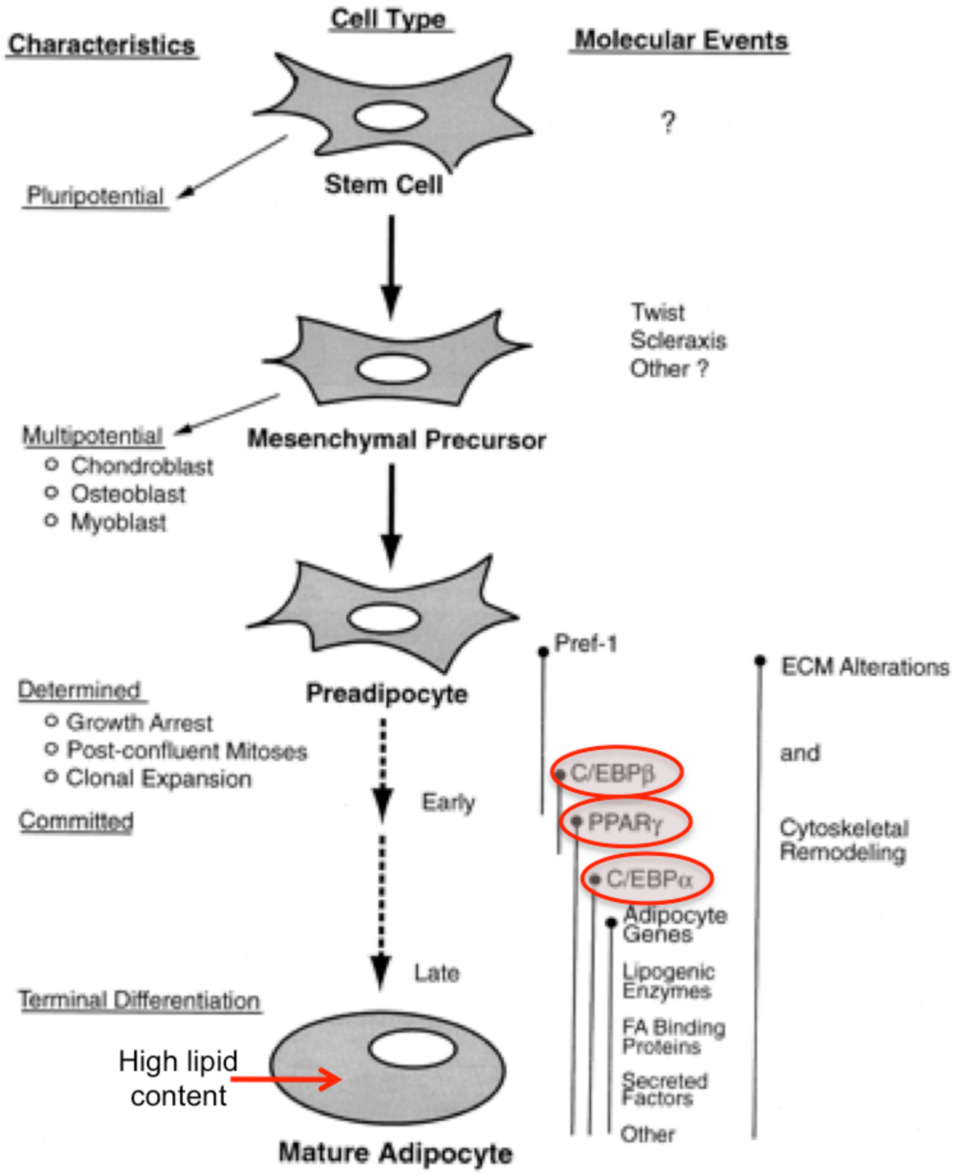

Figure 1.3: **The Stages in Adipocyte Differentiation**. Several key molecular events that occur are shown on the right. Time periods are represented by vertical lines. Two key transcription factor families, PPAR and C/EBP are highlighted (red circles). A mature adipocyte contains a high lipid content. Adapted from Gregoire *et al.* 1998.

Adipocyte development occurs during embryogenesis and continues postnatally (Mandrup and Lane 1997). While fat in terms of adipocytes is not visible in the early stages of embryonic development morphologically, changes in gene expression have started to occur, though the exact timing of these changes is largely unknown. There are a number of transcription factors and genes involved in adipogenesis, crucially PPARγ (Peroxisome Proliferator Activated Receptor gamma) and the CEBP (CCAAT enhancer binding protein) family (Figure 1.3). What is understood of their roles will be discussed later (see sections 2.1 and 3.1). The study of these expression patterns is significant to understanding the mechanism by which adipogenesis occurs.

It has been found that there are many *in vivo* versus *in vitro* differences, particularly in early adipogenesis when cells become committed preadipocytes (Rosen and MacDougald 2006). There is thought to be a bout of cell division before differentiation occurs as shown in the 3T3 cell lines (Rosen and MacDougald 2006).

1.3. Hair Follicle Involvement

Mouse skin develops alongside hair follicle formation. Hair follicles are structures that contain both epithelial and dermal elements. The epithelial root sheaths exist around the hair shaft and the dermal cells form the dermal papilla important for continuous hair growth (Sperling 1991; Millar 2002). Hair follicle formation begins in embryogenesis and involves signalling between epithelium and mesenchyme to orchestrate the development and differentiation into the component parts of a hair follicle (Hardy 1992; Millar 2002). The signalling was discovered relatively early in developmental studies by experiments recombining epidermis and dermis from mouse and chick skin at different embryonic stages (Millar 2002).

Hair follicle initiation is triggered by a signal from the mesenchyme (“first dermal signal”) and starts with thickening in the basal layer of the epidermis forming the hair placode (Hardy 1992; Botchkarev and Sharov 2004). The cells orientate and their adhesion changes (Nanba *et al*. 2000; Tumbar e*t al.* 2003; Botchkarev and Sharov 2004). With a signal from the epithelial placode, underneath this thickening in the epidermis, dermal cells become locally denser and cluster in preparation to form the follicular papilla or dermal papilla (Paus *et al.* 1999; Botchkarev and Sharov 2004). This is called the dermal condensate which produces a “second dermal signal” allowing the epithelial placode cells to proliferate into the dermis and encase the developing dermal papilla (Millar 2002). The epithelial cells then signal to each other to proliferate and differentiate to form the inner root sheath and hair shaft (Millar 1999; Millar 2002).

There are different types of hair follicles. In mice, the guard/primary hair follicles are induced between e14.5 and e16.5. Secondary hair follicles (awl, auchene and zig-zag) are induced from e16.5 to postnatal day 0.5 (0.5dN) (Sundberg and Hogan 1994).

There is developing interest in the relationship hair follicles play with developing fat cells (Hausman and Martin 1982; Wojciechowicz *et al.* 2008). Fat in the lower dermis develops close to the lower region of the hair follicles and adipogenesis initiation occurs after downgrowth of the follicles (Hausman *et al.* 1981). When the hair follicles are actively growing during anagen the fat layer is at its thickest stage, which suggests that there is an interaction involved (Wojciechowicz *et al*. 2013). Hausman *et al.* (1981) suggested that the cells required for adipogenesis were transported down from the upper dermis with the development of the hair follicles, thus inferring a developmental relationship between the two processes. A recent study by Wojciechowicz *et al.* (2013) suggests differently that the cells in the lower dermis prior to birth become the dermal fat layer as opposed to preadipocytes being transported with the follicles. Both studies still find an association between lipid and hair follicle development, thus their signalling and molecular regulation may be linked. It may be that many of the factors associated with hair follicle growth could play a role in adipogenesis and vice versa (Wojciechowicz *et al.* 2008; Festa *et al.* 2011)

A developed hair follicle continues to cycle through stages of hair growth throughout postnatal life. There are three main phases. The first being anagen, during which signals between the epithelial cells and the dermal cells lead to the development of the hair matrix which differentiates into the inner root sheath and the hair shaft (Oliver and Jahoda 1988; Taylor *et al.* 2000; Oshima *et al.* 2001; Millar 2002). This is followed by catagen where the lower parts of the follicle undergo apoptosis and then telogen where the follicle is in a resting phase prior to a new growth cycle (Millar 2002). There is also another phase called exogen which is known as the "shedding phase" The hair follicles are also capable of responding to androgens at different stages, e.g. causing beard hair follicles in adolescent males to become larger (Millar 2002).

There are two stem cell populations within in the skin; one at the basal layer and the other within the outer root sheath of the hair follicles. The latter regenerates the hair and sebaceous glands (Moore and Lemischka 2006).

1.4. The Dermal Adipose Layer

Most work into adipogenesis has been conducted using *in vitro* cell lines e.g. 3T3 cells and the differentiation differences specific to certain depots are not clearly classified (Rosen and MacDougald 2006). During the embryonic stages of development the dermis splits into distinctly separate regions, referred to as the upper and lower dermis. These can be distinguished by the development of adipose tissue, which only occurs in the lower dermis, visible as the white layer in Figure 1.4. The adipocytes develop around the base of the follicles (Hausman *et al.*1981). It was previously found that embryonic adipocyte precursor cells in the lower dermis could be labelled with C/EBPα, which suggested that fat might be developing there (Wojciechowicz *et al.* 2008).

It is known that within the subcutaneous adipose tissue beneath mouse skin there exist many layers. The dermal layer is not always considered separate from the underlying subcutaneous layers; however, in mice they are divided by a muscle layer – the panniculus carnosus (Cinti 2007; Schmidt and Horsley 2012; Wojciechowicz *et al.* 2013). Jahoda's lab has recently found this dermal fat layer to be of a separate developmental origin from that of the underlying subcutaneous adipose layer early on during embryonic development thus suggesting that these are in fact two separate depots. Skin from embryonic day 14/14.5 was then transplanted under the kidney capsule showing that fat can develop without subcutaneous tissue influences (Wojciechowicz *et al.* 2013).

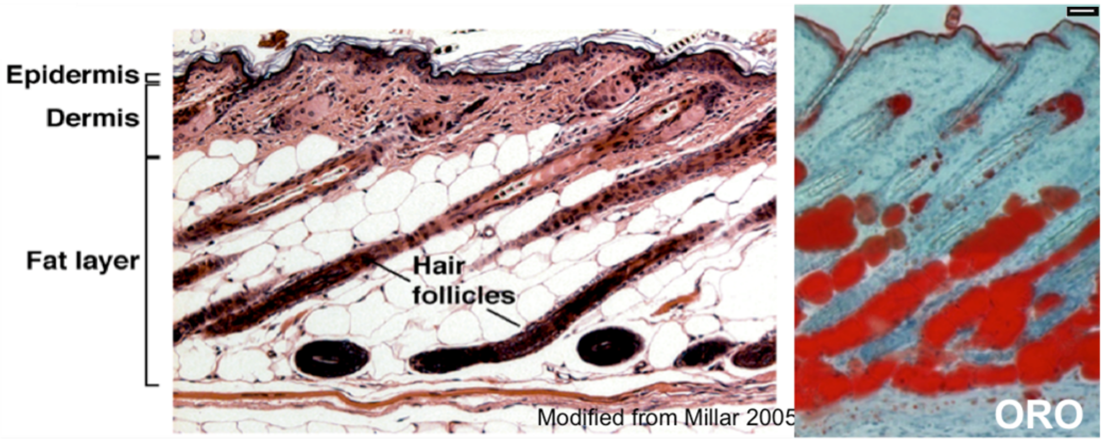

<u>Figure 1.4:</u> Skin structure in a postnatal mouse. Sections were stained with Haematoxylin and counterstained with Eosin. Image of a 28 day mouse (left) shows the fat layer of the lower dermis clearly as the white area (Adapted from Millar 2005) The right side is a comparison from a 17 day mouse where the adipocytes are stained red with oil red O (Adapted from Wojciechowicz *et al.* 2013) Scale bar 30μm.

1.5. Blood Vessels

Blood vessels are present in the dermis and subcutaneous layer of the skin and are available to provide the skin with nutrients and to remove waste. They also are important in preventing dramatic changes to body temperature by vasodilation and vasoconstriction (MacNeal 2014). Vasodilation occurs when the vessels dilate and move near the surface of the skin to allow heat to be lost and vasoconstriction involves the narrowing of the vessels, which also move deeper into the skin to limit heat loss from the skin's surface. They can be seen represented in the skin in figure 1.2.

Blood vessel formation, also known as vasculogenesis or angiogenesis, starts before and also occurs alongside adipogenesis, during which it has been suggested that the developing preadipocytes and capillaries interact (Fukumura *et al.* 2003; Hausman and Richardson 2004; Hausman and Hausman 2006; Wang *et al*. 2006). A study using PPARγ negative construct showed that when angiogenesis was inhibited, adipogenesis was also inhibited (Gurnell *et al.* 2000; Hausman and Hausman 2006). Hausman *et al.* (1981) suggested a link between hair follicles, adipocytes and capillaries.

1.6. Molecular Involvement

A complex array of factors regulates the development of adipocytes from mesenchymal stem cells (MSCs). These include transcription factors and intermediates from a number of signalling pathways (Rosen and MacDougald 2006; Chapter 5). There are two main families of factors involvement in adipogenesis. The CCAAT enhancer binding protein (C/EBP) family and the peroxisome proliferator activated receptor (PPAR) family (Figure 1.3). These are discussed in further detail in Chapters 2 and 3.

Microarrays also suggest there are other factors which contribute and may be important markers of adipogenesis. Markers are important for tracking the development and location of cells and therefore further understanding developmental processes, e.g. adipogenesis. Several markers of mature adipocytes have been discovered in mouse skin. These include C/EBPα, FABP4, PPARγ, adiponectin and adipsin (Birsoy *et al.* 2011; Wojciechowicz *et al.* 2013). However, little is understood about the formation of adipocytes in rodents and therefore the origin of adipose tissue in the skin. With the discovery of a dermal adipose layer separated from the subcutaneous adipose layer, there is increased interest in the origins of different adipose depots and the timings of development. In order to determine the origin of these dermal adipocytes and the timing of events, early markers are important. A marker of pre-adipocyte tissue could allow us to follow the development more closely.

Wojciechowicz *et al.* (2008) found that cells in the lower dermis were labelled with C/EBPα before birth around e17 to e18 in preadipocyte cells (Wojciechowicz *et al.* 2008). Fatty acid binding protein 4 (FABP4) expression was studied in mouse skin with the earliest labelling in the lower dermis being found at e16 and increasing between e17 and e19 (Wojciechowicz *et al.* 2013). mRNA expression of FABP4 using RT-PCR on laser captured tissue was significantly higher in the lower dermis. FABP4 shows the usefulness of markers in the study of development. It was expressed in the lower dermis before the accumulation of lipids and therefore shows there is already a developmental difference between the upper and lower dermis.

1.7. Studying development using Rodents

There are numerous reasons why in many instances the laboratory mouse is a suitable animal model for research into adipogenesis. In comparison with other animal models used in research, e.g. pigs (Hausman and Richardson 2004), mice breed quickly with a high success rate and their small size enables mice to be more easily maintained. They share many similarities with human development and have been widely used in many research fields thus suitable techniques and protocols have already been established. Knockout and transgenic mouse models have been fundamental in establishing the significance of a number of genes in development. Conditional knockouts using a system specific promoter can enable studies on one developmental system, however, development is complex and *in vitro* methods are also still used. Although not perfect, in many respects mouse skin is very similar to human skin and therefore represents a suitable and accessible experimental model for much scientific research. In this project an *in-vivo* like method using mouse back skin and *in vitro* culture methods was used.

The gestational period is around 21 days in a laboratory mouse (CD1 or FVB). Work on mouse back hair by Wojciechowicz *et al.* (2013) has shown that the first wave of follicles (guard hairs) start to form at e14.5 which is followed by the second wave (awl and auchene hairs) at e16.5. The zigzag hairs then develop at e18.5 (Wojciechowicz *et al.* 2013). Terminal adipocytes were found around the base of the guard hairs at e18.5 although unevenly distributed along the anterior-posterior axis (Wojciechowicz *et al.* 2013). Only one or two days after birth were adipocytes distinctly visible throughout a lower dermal layer and this layer continued to thicken alongside the developing hair follicles.

1.8. Why study Adipogenesis? Obesity and related disorders

There are a number of different metabolic disorders, which are due to metabolic imbalance. These include lipodystrophy or obesity, which can in turn result in hyperglycaemia, hyperlipidemia, insulin resistance and diabetes and that can be caused by both genetic and environmental defects (Camp *et al.* 2002; Trayhurn 2005; Gesta *et al*. 2006; Lefterova and Lazar 2009). Adipogenesis is not as well defined as other developmental processes, but as research develops, its role is understood to be of increasing importance. Further understanding of adipogenesis and the roles of adipocytes will certainly further our knowledge of the causes of diabetes and obesity in order to optimally treat these diseases (Camp *et al.* 2002).

Obesity is a growing worldwide concern and is on the rise, resulting in growing interest in adipogenesis (Gesta *et al.* 2006; Siersbæk *et al.* 2012; Spiegelman 2013). Obesity is both increased adipocyte number (hyperplasia) and increased adipocyte size (hypertrophy) (Couillard *et al.* 2000; Camp *et al.* 2002) also known as, 'an imbalance between energy intake and energy expenditure' (Billon *et al.* 2008). Healthy levels of excess fat are stored mainly in adipocytes, whereas when an individual is obese, large amounts of fat are stored in other tissues because the levels are too high to be stored in adipose tissue (Camp *et al.* 2002). This build up of fat in other tissues, including muscle, liver and pancreatic tissue may be a possible cause of obesity-related type 2 diabetes mellitus (Unger 2002; Camp *et al.* 2002). The location of the excess fat deposits determines the level of risk in getting these metabolic disorders (Gesta *et al.* 2006).

Now named as playing a fundamental role in metabolism, adipose tissue is considered a target for novel therapies for the treatment of obesity and related metabolic disorders including diabetes and atherosclerosis (Camp *et al*. 2002). In adult mice, BAT secretes less cytokines and adipokines compared with WAT. Lefterova and Lazar (2009) suggest that changing adipocytes from white to brown might be a method of treating obesity as brown adipocytes are also involved in lipid oxidation (Farmer 2008).

The quantification of adipogenesis is much less detailed in relation to other developmental systems. In general there is still a great deal to be understood in terms of development of fat, in particular the recently detected dermal fat layer and early adipogenesis (initiation). Microarray data has suggested a number of factors to be upregulated during the process and some variation from that known from *in vitro* studies (Soukas *et al.* 2001). However, whether these are specific to fat development or indirectly involved via hair follicle or blood vessel development is yet to be determined?

It is clear that a significant number of signalling pathways and molecules influence adipogenesis and cause transcriptional events to occur, many of which are still being discovered. PPARγ and C/EBPα are just two of many factors involved. Not only are transcription factors involved but there is also the potential for the involvement of microRNAs, hair follicles and the development of blood vessels (angiogenesis).

1.9. Thesis Aims

From the recent knowledge of the existence of a distinct adipose depot in the lower dermis of the skin separate from the subcutaneous compartment, the focus of this study was on this dermal adipose layer and to further our knowledge on adipogenesis in rodent back skin. More specifically, the work aimed to investigate the developmental question of when the cells become committed to becoming adipocytes in rodents and what causes these cells to become committed. Why is it only the lower dermal cells that undergo adipogenesis?

Chapter 2 followed on from the work carried out by Wojciechowicz (2013) in the host laboratory. She produced microarray data of the upper and lower dermis of mouse back skin. This chapter aimed to analyse further what can be found out about the molecular basis of adipogenesis in the dermal adipose layer. The expression of one gene previously implicated in adipogenesis (G0/G1 switch gene 2), flagged up in these microarrays was also investigated.

Late adipogenesis involving the differentiation of adipocytes is well defined compared with early adipogenesis (Gesta *et al*. 2006). The genetics of how many and in which way the stem cells become committed to the adipocyte lineage is not as well classified, thus need to look earlier to see at which stage influence development. One major factor widely recognised as crucial to adipogenesis *in vitro* and *in vivo* is PPARγ.

The PPAR receptors are now considered important therapeutic targets. They are key in the regulation of adipogenesis and the lipid balance. Therefore, by looking in detail at the roles of these receptors, efficient treatments for metabolic disease is a viable option (Evans *et al.* 2004). There is still much speculation into the role PPARγ plays in early adipogenesis, because there are differences between *in vitro* and *in vivo* studies. Chapter 3 aimed to further elicit the importance of PPARγ in early adipogenesis in expression studies.

As the dermal adipose layer is recent in discovery, this project focused on developing our understanding of this layer in rodents. It can be difficult to study the effects of many molecules via overexpression and knockout studies because these often have lethal effects. Studies involving conditional ablation may be difficult if specific promoters are not known. There is therefore a need for *in vivo*-like models to be created. A major part of this project involved the development of a suitable model system to study adipogenesis (Chapter 4). The overall aim was to investigate the role of key signalling pathways in dermal adipogenesis (Chapter 5). To do this an experimental model was required; this model system was then used to investigate the signalling pathway question.

It is also important to investigate how signalling from developing skin or hair follicles stimulates the production of dermal fat. It is not yet known why it is only the lower dermis and not the upper dermis that develops into fat and at what point the lower dermal cells become committed to the adipocyte lineage? The microarray data used in chapter 2 was in fact from e17 to e19. However, it is thought that adipocytes start to develop even earlier (Wojciechowicz *et al.* 2013; Driskell *et al.* 2013). The work in chapters 4 and 5 looked at developing a suitable model system at e16.5 and conducting signalling pathway analysis at this age. The main hypothesis was therefore that commitment to the adipocyte lineage starts earlier than e17 and so more influence on the development of adipocytes should be observed earlier than e17. FABP4 labelling of the lower dermis has suggested that it has already separated from the upper dermis by e16, though it may be that differences develop even earlier in association with hair follicle initiation. E14.5 3-dimensional culture was also investigated to determine whether there were differences between e14.5 and e16.5 and adipogenesis starts earlier.

CHAPTER 2:

Rodent Skin Dermis Microarray Analysis and Development of the G0S2 Gene Expression Profile

2.1. Introduction

Many stages of development, in particular those that occur earlier, are not visible morphological changes, but instead occur at the molecular level, i.e. gene expression. There are a number of different genes, which correspond to a complex network of responses, involved in adipogenesis. The basic process involves fibroblast-like preadipocytes differentiating into adipocytes containing lipid-droplets and this involves a transcriptional cascade (Lefterova and Lazar 2009; Siersbæk *et al.* 2012) A complex array of factors regulate the development of adipocytes. The genetic reprogramming in adipogenesis includes a number of transcription factors, and is also affected by hormones, cytokines and nutrients (Fève 2005). Several signalling pathways have been implicated in adipogenesis including the BMP pathway and the EGF/EGFR pathway (Chapter 5).

Throughout research into adipogenesis, some genes have been recognised as the main regulatory genes. Those crucial to adipogenesis and referred to as the master regulators include CCAAT/enhancer-binding proteins (C/EBPs) and the nuclear receptor, peroxisome proliferator-activated receptor gamma (PPARγ) (Gregoire *et al.* 1998; Farmer 2006). There are also other factors that have been found important more recently, including Krüppel –like factors (KLFs) (Banerjee *et al.* 2003; Birsoy *et al.* 2008; Siersbæk *et al.* 2012), Krox20 (Chen *et al.* 2005), Wingless, INT-1 proteins (Wnts) and cell-cycle proteins (Lefterova and Lazar 2009). Siersbæk *et al.* (2012) show the existence of hotspots in the chromatin where several transcription factors bind, which suggests that the factors talk to each other and influence each other's behaviour. For example, KLF4 and Krox20 interact with each other (Lefterova and Lazar 2009).

There are two main waves of transcriptional activity in adipogenesis (Siersbæk *et al.* 2012). The first wave is thought to involve early factors including C/EBPβ/δ, KLFs, cAMP response element binding protein (CREB), early growth response 2 (Krox20) and sterol regulatory element binding protein 1c (SREBP-1c) (Siersbæk *et al.* 2012). The second wave fundamentally involves PPARγ and C/EBPα (Siersbæk *et al.* 2012).

2.1.1. Late Adipogenesis

Late adipogenesis is better characterised than early adipogenesis. PPARγ2 is expressed late in adipogenesis. First C/EBPβ binds to PPARγ binding sites and this could mean that it aids the binding of PPARγ (Siersbæk *et al.* 2011; Siersbæk *et al.* 2012). Many hotspots of transcription factors exist close to the PPARγ, which suggests the involvement of many pathways in inducing PPARγ (Siersbæk *et al.* 2011; Siersbæk *et al.* 2012). PPARγ is discussed further in Chapter 3. C/EBPβ as well as being expressed during early adipogenesis, is also present in mature adipocytes (Lefterova *et al.* 2008; Siersbæk *et al.* 2012). C/EBPα/β or PPARγ in mature adipocytes are required for the maintenance of adipogenic genes (Lefterova *et al.* 2008) and they interact with each other. PPARγ and C/EBPα activate adipogenic genes, which enables the terminal differentiation of adipocytes (Fève 2005).

2.1.2. Microarrays

There are many techniques used to look at the role of certain genes throughout development. These include the use of *in vitro* preadipocyte cell lines and mesenchyme-derived precursor cells as well as knockout mouse models (Farmer 2006).

Most of the research into the molecular basis of adipogenesis has been investigated using *in vitro* cell lines or primary cell cultures (Siersbæk *et al.* 2012). However, more recently *in vivo*-type studies, ‘global approaches’ have been deemed necessary to confirm the molecular mechanisms, because there are microarray differences between *in vivo* and *in vitro* (Wojciechowicz 2012). Much interaction between transcription factors has shown the integration of signalling pathways (Siersbæk *et al.* 2012).

Microarrays have been conducted for a number of different tissue types. They are a way of finding out with factors are expressed during a developmental process. Wojciechowicz (2012) in the Jahoda lab produced microarrays from the dermis to study fat development in the skin. These were from embryonic day 17 (e17), e18 and e19. While analysis was conducted on the lower dermis to observe those genes that were significantly upregulated and hence might be important in adipogenesis, little was looked at in terms of the upper dermis. Do preadipocytes become committed via a positive or negative signal, i.e. are certain fat-related genes switched off in the upper dermis or are certain fat-related genes switched on in the lower dermis? As well as this, the microarrays could now be taken back earlier, because it is considered adipogenesis starts earlier.

Expression profiling through microarray analysis has aided the discovery of many factors involved in adipogenesis (Soukas *et al.* 2001; Farmer 2006). Krox20 (Egr2), being one such early factor is involved in C/EBPβ activation (Farmer 2006).

2.1.3. The C/EBP Family

The CCAAT enhancer binding protein family includes C/EBPα, -β and -δ. Mouse models showed the importance of these genes in adipogenesis (Wang *et al.* 1995). Abnormal fat development occurs when C/EBP genes have been deleted. For example, homozygous deletion of C/EBPα in mice resulted in lipid accumulation failure in adipocytes and decreased expression of the adipose tissue marker, UCP-1 (Wang *et al.* 1995). Members of the C/EBP family not only play a role in embryonic development but also in the maintenance of mature adipocytes.

Knocking out C/EBPα in the whole body leads to early fatality of the newborn mice (Wang *et al.* 1995; Lefterova and Lazar 2009). However, when rescued, there was still no WAT, but BAT is present. Removing C/EBPα in adult mice caused a reduction in WAT (Mandrup and Lane 1997; Wu *et al.* 1999; Yang *et al.* 2005; Lefterova and Lazar 2009). It is more important for WAT formation, compared with BAT (Linhart *et al.* 2001; Farmer 2006). Many promoters of adipocyte-specific genes have binding sites for C/EBPα (Mandrup and Lane 1997). C/EBPα is needed for adipocyte differentiation as shown when its anti-sense RNA was expressed in 3T3-L1 preadipocyte cells (Lin and Lane 1992; Mandrup and Lane 1997). This resulted in the prevention of differentiation and also the blocking of its own expression, which suggests C/EBPα may also be required for maintenance of the differentiated state (Mandrup and Lane 1997). C/EBPα is also thought to induce the arrest of mitotic activity of the preadipocytes, while C/EBPβ and C/EBPδ are expressed in the dividing cells (Mandrup and Lane 1997). C/EBPβ has a higher adipogenic potential than C/EBPδ (Mandrup and Lane 1997). C/EBPβ and C/EBPδ are thought to be transcriptional activators, which act earlier in the developmental process than C/EBPα (Lefterova and Lazar 2009). CEBPα involved in terminal differentiation of adipocytes (Gerhold *et al.* 2002). C/EBPβ is needed to induce PPARγ and C/EBPα (Farmer 2006; Lefterova and Lazar 2009). CEBPs also have a later role maintaining mature adipocytes (Darlington *et al.* 1998).

C/EBPβ is involved in adipogenesis both *in vivo* and *in vitro* (Siersbæk *et al.* 2012). Profiling of C/EBPβ binding shows that before differentiation is induced it binds with many chromatin regions, thus it may actually be involved early in preadipocytes (Siersbæk *et al.* 2011; Siersbæk *et al.* 2012).

Using a mouse model which does not have C/EBPβ, Tanaka *et al.* (1997) have shown that the embryonic fibroblast cells have decreased adipogenic capabilities and those cells derived from C/EBPβ and -δ double knockouts are unable to differentiate into mature adipocytes (Fève 2005).

2.1.4. The PPAR Family

Three main subtypes exist within the peroxisome proliferator-activated receptor family. PPARγ, PPARα and PPARδ, also known as PPARβ exhibit high similarity in their amino acid sequences (Kliewer *et al.* 1995; Mandrup and Lane 1997). These receptors bind with retinoid X receptors (RXRs) to PPAR responsive elements (PPREs) (Mandrup and Lane 1997; Michalik *et al.* 2002).

The nuclear receptor, PPARγ has been found to be necessary for adipogenesis both in early differentiation and later maintenance of mature adipocytes (Rosen *et al.* 1999; Gesta *et al.* 2007) and this in particular is looked further in chapter 3. Thiazolinedone (TZD) drugs used to treat diabetes target PPARγ (Lehman *et al.* 1995; Mandrup and Lane 1997; Lefterova *et al.* 2008). Out of the three subtypes, PPARγ is the most adipogenic-specific, highly expressed in adipose tissue and rarely found to be expressed in other tissues, as shown by ectopic expression in NIH 3T3 cells (Brun *et al.* 1996; Mandrup and Lane 1997). The fundamental value of PPARγ is true of *both in vitro* and *in vivo* studies (Farmer 2006).

PPARα and PPARβ/δ are also thought to some extent to play a role in adipogenesis (Evans *et al.* 2004), though *in vivo* they are distributed differently and expressed to different degrees by activation of different ligands (Mandrup and Lane 1997). PPARδ is expressed in adipose tissue, though precisely when is unclear (Mandrup and Lane 1997). PPARα is more highly expressed in brown adipose tissue than white adipose tissue (Kliewer *et al.* 1995, Mandrup and Lane 1997).

PPARγ is thought to control and trigger the expression of many adipose-related genes. Development of brown fat requires a number of extra molecular factors. These include peroxisome proliferator-activated receptor γ coactivator 1 (PGC1) and PRDM16 (Spiegelman 2013). Also uncoupling protein 1 (UCP1) is crucial to brown fat development. Its expression causes increased energy expenditure of brown adipocytes (Gray *et al.* 2006). UCP1 expression is regulated by PPARs as well as other important regulators, including CEBP family members. The PPARs associate with a PPAR response element in the promoter of UCP1 (Sears *et al.* 1996; Gray et al. 2006).

It is also important to note that PPARγ interacts with the C/EBP family during adipogenesis. PPARγ and C/EBPα are considered the master regulators of adipogenesis (Rosen *et al*. 2002; Farmer 2006). While C/EBPα cannot work alone without PPARγ, PPARγ can allow adipocyte development in the absence of C/EBPα (Rosen *et al.* 1999; Farmer 2006). Together PPARγ is expressed upstream of C/EBPα but downstream of CEBPβ. There is a degree of colocalization between C/EBPα and PPARγ and 60% of genes upregulated in adipogenesis are bound by both factor (Lefterova *et al*. 2008; Lefterova and Lazar 2009). PPARγ expression can recover adipogenesis in C/EBPα-deficient MEFs (Rosen *et al.* 2002; Lefterova and Lazar 2009). The exact role and interaction between these major regulators is largely unknown. It could be a question of compensation, because of the importance of adipose tissue to survival.

C/EBPα and PPARγ interact with each other during development. While the knockout animals are embryonic lethal, heterozygous PPARγ knockouts show reduced C/EBPα expression and C/EBPα null mice show reduced PPARγ expression (Barak *et al.* 1999; Wu *et al.* 1999; Fève 2005). However, while overexpressing PPARγ2 in C/EBPα null embryonic fibroblast cells can re-establish adipogenesis, opposingly overexpressing C/EBPα in PPARγ null embryonic fibroblasts cannot (Wu *et al.* 1999; Rosen *et al.* 2002; Fève 2005). Fève (2005) suggests that PPARγ2 may therefore be key while C/EBPα may just be required to maintain PPARγ2 expression, but they are both essential.

C/EBPβ and C/EBPδ are first expressed after hormonal induction (Cao *et al.* 1991; Farmer 2006; Mandrup and Lane 1997). It is then thought that C/EBPα and PPARγ are activated. C/EBPα then maintains its own expression allowing the continued expression of many adipogenic genes needed in terminally differentiated adipocytes (Mandrup and Lane 1997). As well as this, PPARγ also interacts with C/EBPα to activate each other's expression (Wu *et al.* 1999; Farmer 2006).

Many experiments have shown conflicting results. For example mice that don't express C/EBPβ and C/EBPδ still express C/EBPα and PPARγ but adipose tissue formation is incapable of developing correctly (Tanaka *et al.* 1997). This may be because of the importance of C/EBPα and PPARγ in adipogenesis that alternative means of activating them can occur when C/EBPβ and C/EBPδ activity has been inhibited (Farmer 2006).

2.1.5. Cell Cycle Proteins

It is thought that proliferation occurs prior to differentiation, since cells are induced to conduct adipogenesis when they are in a state of confluency (Farmer 2006). This is known as the mitotic clonal expansion step. When the proliferation step is inhibited, adipogenesis cannot occur which suggests it is necessary for the activation of adipogenic genes (Tang *et al.* 2003; Farmer 2006). After this the cell-cycle arrests. G0 to G1 cell cycle switch due to contact inhibition (Otto and Lane 2005; Lefterova and Lazar 2009).

Cell cycle proteins implicated in adipogenesis include D-type cyclins, cyclin-dependent kinases 4 and 6 (Cdk4/6), retinoblastoma family (Rb), p107 and p130 (Farmer 2006). The E2F family is highly recognised for its role in adipogenesis as cell cycle proteins (Farmer 2006). Krox20 has also been implicated in the reintroduction of preadipocytes into the cell cycle (Farmer 2006).

2.1.6. KLFs

KLFs are zinc-finger transcription factors whose functions include both stimulatory and inhibitory functions (Lefterova and Lazar 2009). For example, KLF6 and KLF15 are also involved in inducing adipogenesis (Li *et al.* 2005; Mori *et al.* 2005; Farmer 2006; Lefterova and Lazar 2009). Contrastingly, KLF2 suppresses adipogenesis (Wu *et al.* 2005; Famer 2006). This was found when KLF2 was overexpressed in 3T3-L1 cells (Wu *et al.* 2005; Lefterova and Lazar 2009).

These KLFs also interact with PPARγ and C/EBP family members. KLF4 important early on in differentiation transactivates C/EBPβ (Birsoy *et al.* 2008; Lefterova and Lazar 2009). C/EBPβ and C/EBPδ act together with KLF5 on the PPARγ2 promoter and mice with KLF5 knocked out exhibit adipose tissue deficiency (Oishi *et al.* 2005; Farmer 2006; Lefterova and Lazar 2009). KLF15 also acts alongside the CEBP family with C/EBPα (Mori *et al.* 2005; Lefterova and Lazar 2009).

2.1.7. G0-G1 Switch Gene 2

The G0/G1 switch gene 2 (G0S2) has been implicated in adipogenesis. It directly inhibits the lipolytic enzyme, adipose triglyceride lipase (ATGL) (Yang *et al.*

2010; Heckmann *et al.* 2013) and is thought to be inhibiting proliferation and holding the stem cells quiescent (Heckmann *et al.* 2013), acting as a tumour suppressor gene. In mouse 3T3-L1 and human SGBS (Simpson-Golabi-Behmel syndrome) preadipocytes, G0S2 mRNA and protein expression increased as cell growth ceases prior to terminal differentiation of preadipocytes (Zandbergen *et al.* 2005; Heckmann *et al.* 2013). The SGBS cell line, originating from an SGBS patient's adipose tissue, alongside mouse 3T3 cells are useful tools in the study of adipogenesis (Fischer-Posovszky *et al.* 2008). G0S2 was found influenced by bone morphogenetic protein 2 (Bmp2) in mouse embryos (Bachner *et al.* 1998; Heckman *et al.* 2013).

Jahoda's laboratory previously flagged up G0S2 expression in the adipose microarrays as a potential marker of adipocyte development. G0S2 mRNA expression was found in both the upper and lower dermis (Wojciechowiz *et al.* 2013). At e18.5, G0S2 expression is limited to brown and white adipose tissue and also later in adult adipose tissue (Cristillo *et al.* 1997; Zandbergen *et al.* 2005; Heckmann *et al.* 2013). This chapter aimed to investigate in more detail the role of G0S2. It is unclear whether G0S2 actively prevents cell cycle continuation.

Transactivation, gel shift and chromatin immunoprecipitation assays show that G0S2 is a direct target of PPARγ (Zandbergen *et al.* 2005). Thus if it is found to be crucial to adipogenesis, it could be a useful marker of PPARγ activity and late adipocyte development.

2.1.8. Other Factors

There are significant number of transcription factors involved in adipogenesis; not just those discussed above but also many others. These include aP2, Hsl, glucocorticoids, STAT proteins and also clock proteins, e.g. brain and muscle amt-like protein 1 (Bmal1), sterol regulatory element-binding transcription factor 1 (SREBP1) and Rev-erba (Lefterova and Lazar 2009; Siersbæk *et al.* 2011). Ectopically expressing a dominant negative of SREBP-1c inhibits preadipocyte differentiation and conversely overexpressing SREBP-1c leads to increased adipogenesis (Kim and Spiegelman 1996; Farmer 2006).

Glucocorticoids are clearly important in inducing adipogenesis *in vitro*, but their roles *in vivo* still remain vague (Siersbæk *et al.* 2011). STAT5A and glucocorticoid receptor (GR) are present in many of the same chromatin regions (Siersbæk *et al.* 2011)

Expressing STAT5A leads to adipocyte differentiation and activation of PPARγ in fibroblasts not originally adipogenic (Floyd and Stephens 2003; Farmer 2006).

There are a number of known inhibitory factors of adipogenesis, which are increasingly suppressed during differentiation (Farmer 2006). For example, the forkhead transcription factor, FoxO1. This is suppressed by insulin, which also induces SREBP-1c activity (Farmer 2006). Some of the KLFs as mentioned in section 2.1.6, e.g. KLF2 also have an inhibitory effect on adipogenesis. Interferon-regulatory factors (IRFs) e.g. IRF3 and IRF4 suppress differentiation (Eguchi *et al.* 2008; Lefterova and Lazar 2009) as well as GATA-binding proteins 2 and 2, which also prevent terminal differentiation of preadipocytes (Rosen and MacDougald 2006; Lefterova and Lazar 2009).

Microarray data showed that the molecular mechanisms of adipogenesis are complex. As well as these, extracellular signals including growth factors can influence adipogenesis including bone morphogenetic proteins (BMPs) and fibroblast growth factors (FGFs), many of which are discussed in chapter 5 on signalling pathways.

A lot of research has been conducted recently into the control of adipogenesis in terms of preadipocyte differentiation into terminal adipocytes. Thus, much more is understood about the molecular mechanisms of late adipogenesis in comparison with early adipogenesis from the commitment of stem cells. It has also been considered that different fat depots develop in different ways, which is why it is important to study each depot. In this case, the focus is on the newly identified dermal fat layer, which is separate from the subcutaneous fat layer beneath the skin.

This chapter aimed to elucidate further the dermal adipose layer in terms of the molecular mechanisms involved. Genespring was used to produce microarrays of the upper dermis to investigate the potential of any inhibitors of adipogenesis. The microarrays were already analysed for the lower dermis to investigate the normal adipogenic pathway, but whether the upper dermis microarrays showed any potential influences on the adipogenic process was never investigated.

The G0/G1 switch gene 2 (G0S2) present in the arrays list was also investigated by immunofluorescence analysis. This was to look at the role and expression of (at the time) a relatively under-investigated gene involved in adipogenic differentiation in the novel adipogenic depot in mouse skin dermis.

2.2. Materials and Methods

2.2.1 Microarray Analysis

2.2.1.1 Use of GeneSpring® GX11.0 Software to generate Upper Dermis Microarray Data

The microarray samples were prepared by Kamila Wojciechowicz at Durham University (UK) and Mouse Genechips 430 2.0 (Affymetrix) were used to generate the data. Three different embryonic ages were used: e17, e18 and e19 and three samples of the upper dermis from each age (Table 2.1).

Table 2.1: Upper Dermis Samples used from the Array Data for the 3 Different Embryonic Ages

Embryonic age	**17**	**18**	**19**
Samples	KW1	K1	K1I
	KW3	K3	K1II
	KW5	K5	E1-19

GeneSpring was used to normalise the data and create a comparison of the samples from the three different ages by ANOVA.

The workload type was selected as 'Biological Significance' and then the data was loaded. 3 parameters were selected by time point e17, e18 and e19 and the statistical test chosen was the Analysis of Variance (ANOVA). To select significant genes, the p-value was set at 0.05. These significant genes were then filtered on a fold change of 2. 3 microarray lists were created comparing the upper dermis at e17 against e18 and e19 and also comparing e18 with e19.

2.2.1.2. GEDI Analysis

The Gene Expression Dynamics Expector (GEDI) (Version 2.1) was used to analyse expression profiles. The generated comparison lists were used to input into GEDI. Normalised not raw values were generated and imported into an Excel Document (Microsoft). It was then modified for use in GEDI (Figure 2.1). Cell A1 contained '}Static', B1 'DESC' and D1 showed the total number of data sets '45101'. What was compared was entered in E1, 'E17vsE18vsE19' and A2 contained '}$'. 'DESC' replaced gene symbol in B2. Probe set IDs and the corresponding fold changes were entered under these headings, as shown in Figure 2.1.

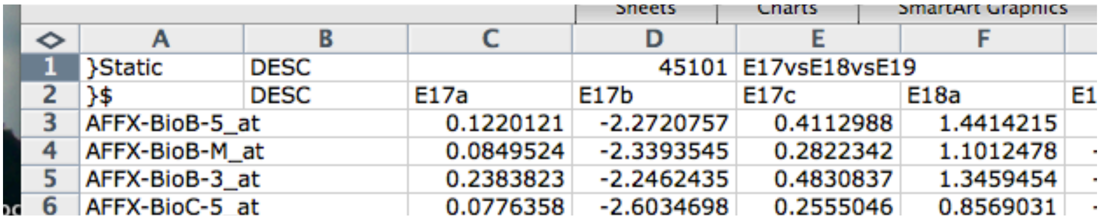

	A	B	C	D	E	F
1	}Static	DESC		45101	E17vsE18vsE19	
2	}$	DESC	E17a	E17b	E17c	E18a
3	AFFX-BioB-5_at		0.1220121	-2.2720757	0.4112988	1.4414215
4	AFFX-BioB-M_at		0.0849524	-2.3393545	0.2822342	1.1012478
5	AFFX-BioB-3_at		0.2383823	-2.2462435	0.4830837	1.3459454
6	AFFX-BioC-5_at		0.0776358	-2.6034698	0.2555046	0.8569031

Figure 2.1: **Screenshot to show the formatting for GEDi analysis**

The document was then saved as a text file and input into GEDI which produced 25 x 26 square grids based on trends.

2.2.2. Immunofluorescence Analysis of G0S2

G0S2 was investigated in mouse back skin, both embryonic (e14.5, e16.5 and e18.5) and postnatal (0-3 hours, 1-day and 3-days), obtained from mice from timed matings as described in section 3.2.2.1.

Skin cut from the back of each specimen was rolled or orientated flat and put into Tissue-Tek® O.C.T.™ compound (Sakura, Agar Scientific, Netherlands), then snap frozen in liquid nitrogen and kept at −80°C. Skin sections (7 µm), were cut on a cryostat (LEICA CM 3050S) and attached to ColorFrost®Plus slides (Thermo Shandon Ltd, Cheshire, UK). The slides were dried for 2 hours at room temperature, and then used for immunofluorescence staining.

Slides were fixed in 4% PFA (Appendix I) for 15 minutes, rinsed in PBS (Appendix I) and then permeabilised in 0.2% Triton-X for 15 minutes. The slides were then washed again in PBS for 3 minutes and blocked in 10% donkey serum for 1 hour. 3 x 5 minutes washes were conducted in PBS before the slides were incubated overnight at 4°C with the primary antibody against G0S2 (1:100, rabbit polyclonal from Proteintech). 3 x 5 minutes washes were conducted and then the slides were incubated with a fluorescent secondary donkey anti-rabbit antibody (1:500) for 1 hour at room temperature. 3 more PBS washes were conducted and then the slides were mounted in vectashield and coverslipped and stored in the dark at 4°C. All the incubation steps were conducted in the dark in a humidity chamber.

2.3. Results

2.3.1. Microarray Analysis

Data from three samples of 3 different ages from the upper dermis was inputted into GeneSpring to produce 3 different microarray lists. Under 2-fold there was a high number of results produced. E17 compared with E18 produced 2526 results, E17 compared with E19 produced 3203 results and E18 compared with E19 produced 173 results. This was significantly lower by E19. The data was input into GEDI to investigate clusters. There was variability found in samples from the same age, e.g. for e17, 2 GEDI maps looked similar but the third was different (Figure 2.2). This was unreliable because the data sets produced different results. Therefore, one data set from each age was removed and the data was re-entered into GEDi (Figure 2.3).

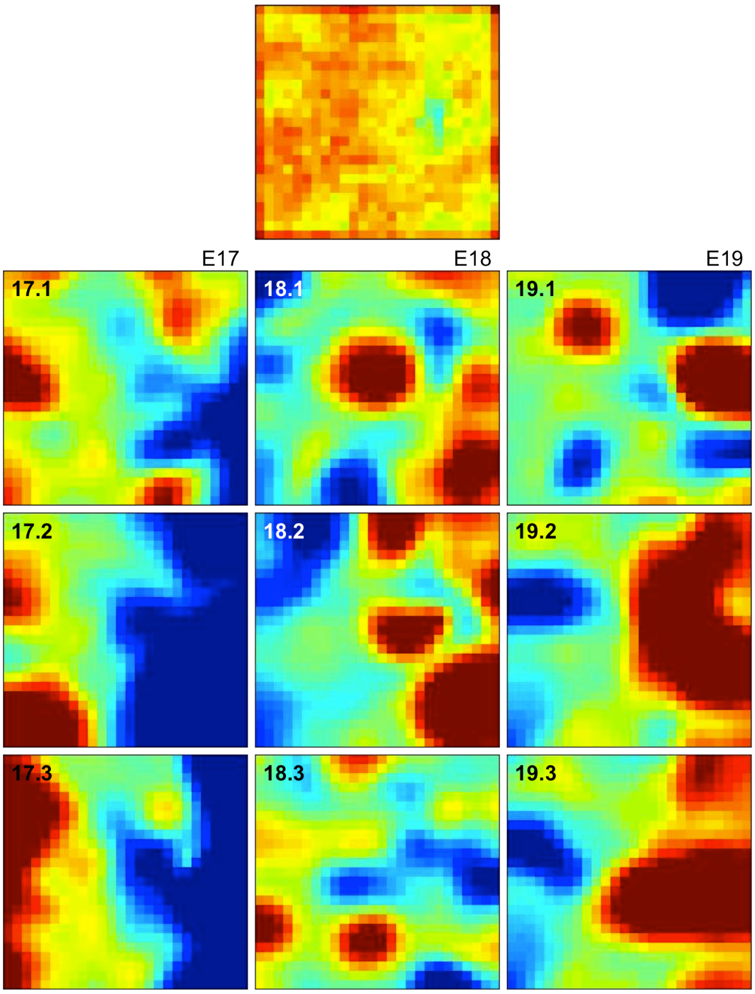

<u>Figure 2.2:</u> Analysis of Microarray Data of the Upper Dermis using GEDI. 3 different ages shown and 3 samples from each. GEDI maps, showing clusters of upregulation and downregulation in 25 by 26 grids.

Removing one from each, showed more similar clusters. These were then used to observe a cluster, early in e17. There were more genes expressed between e17 and e18 and more similarities between e18 and e19.

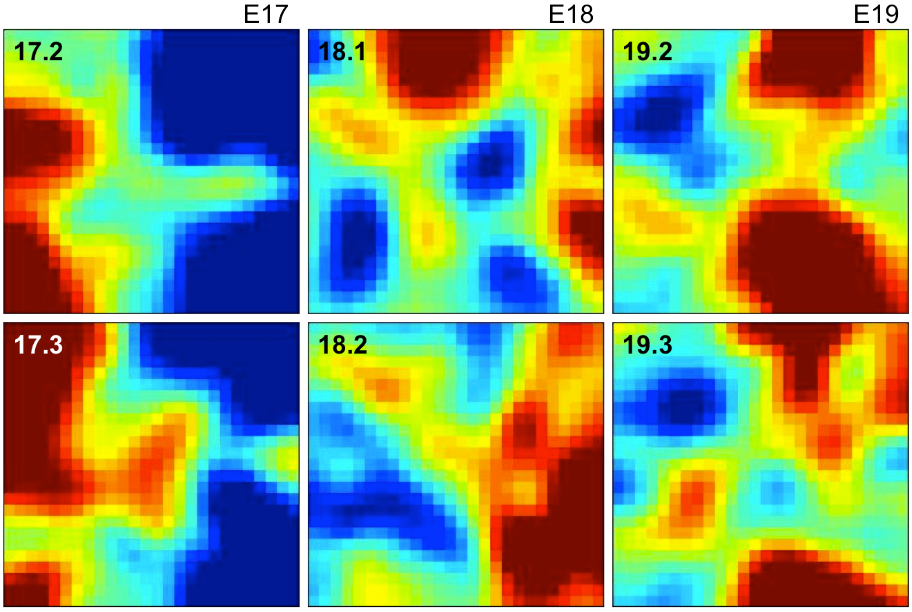

<u>Figure 2.3:</u> Analysis of Microarray Data of the Upper Dermis using GEDI. 3 different ages shown and 2 samples from each. GEDI maps, showing clusters of upregulation and downregulation in 25 by 26 grids.

Upon analysing the microarray lists, a few genes were flagged up. For example, SPARC-like 1. This gene was present in the lower right corner of the GEDI maps, where it is clear the expression changes from blue to red, high to low (Figure 2.3). This was downregulated significantly 5.31 fold change between e17 and e18 and more so 7.22 fold change by e19 from e17, suggesting early involvement. Osteoglycin and Calmodulin 1 were also down regulated from e17 and e19 (Table 2.2). Serine racemase conversely is unregulated more than 10 fold between e17 and e19.

Table 2.2: Four genes expressed more than 2 fold in upper dermis microarrays

<u>Gene Title</u>	<u>Gene Symbol</u>	<u>FC e17 vs e18</u>	<u>FC e18 vs e19</u>	<u>FC e17 vs e19</u>
SPARC like 1	**SPARCl1**	-5.308625	-	-7.2157235
Serine racemase	**Srr**	4.7332816	2.1253738	10.126023
Osteoglycin	**Ogn**	-3.4252784	-3.1587124	-10.819469
Calmodulin 1	**Cal1**	-5.282315	-	-4.6968126

‘-‘ represents downregulation

2.3.2. G0/G1 Switch Gene 2 (G0S2)

2.3.2.1. Postnatal Mouse Back Skin

The antibody was a sample, kindly donated by Proteintech, Europe which was tested first in postnatal mouse skin, to observe the working capability of the antibody and the presence of G0S2 in the skin. After 0 to 3 hours, the skin showed labelling of

G0S2 in the skin dermis, under the base of the follicles, where adipocytes form (Figure 2.4). The labelling of G0S2 was speckled through the cells.

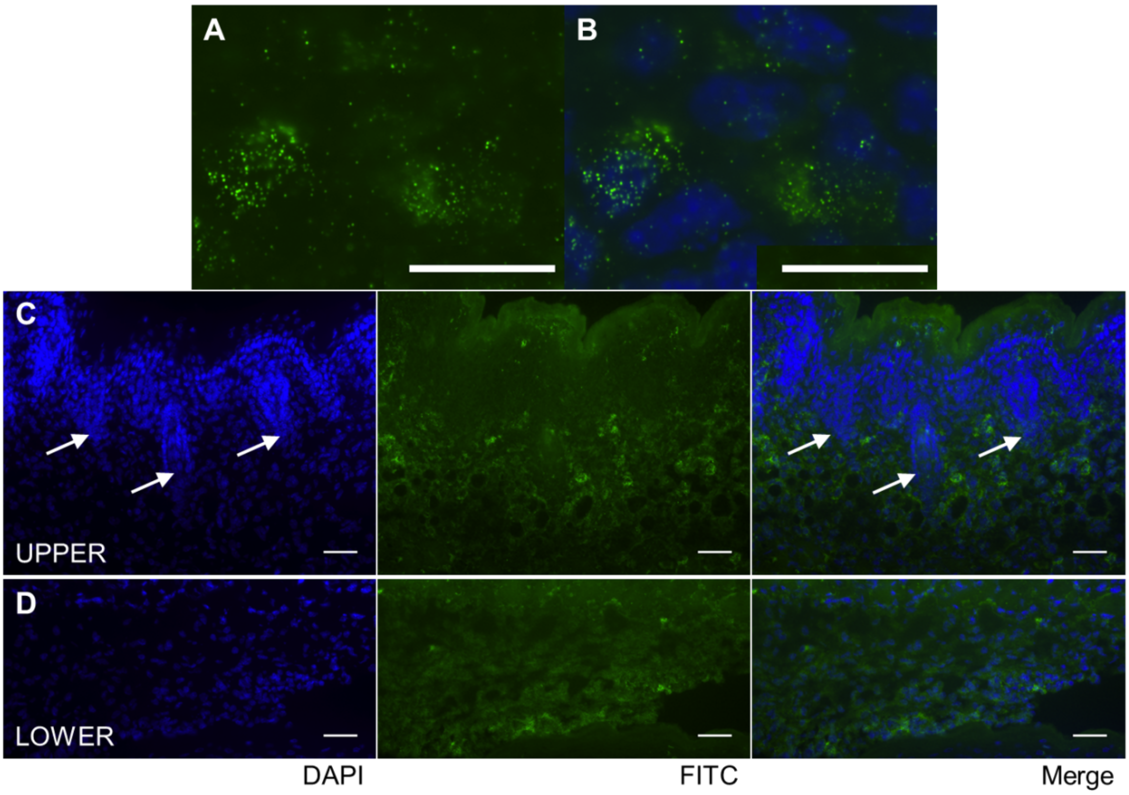

<u>Figure 2.4:</u> Analysis of G0S2 (Proteintech) expression in 0-3 hour newborn mouse back skin. Sections cut at 7μm, stained with an antibody against G0S2 and counterstained with DAPI. From left to right; DAPI, FITC, and merge (DAPI/FITC). FITC represents the fluorescent labelling of G0S2. (**A,B)** Magnified cells show speckled labelling Fluorescent images were taken using a Zeiss Axio Imager M1. Base of hair follicles labelled (arrows). (**A,B**) scale bar = 12μm. (**C,D**) scale bar = 40μm.

After 1 day (1dN), newborn mouse back skin showed positive labelling of G0S2, particularly around the base of the hair follicles (Figure 2.5E), but also there was a degree of positive labelling in the upper dermis (Figure 2.5C). A similar distribution was also seen in 3-day mouse back skin with a few cells labelled in the upper dermis, but also still present around the follicles (Figure 2.6). Negative controls were conducted by omitting the G0S2 antibody incubation step, but still incubating with the fluorescent secondary antibody to show, if present, the level background fluorescence.

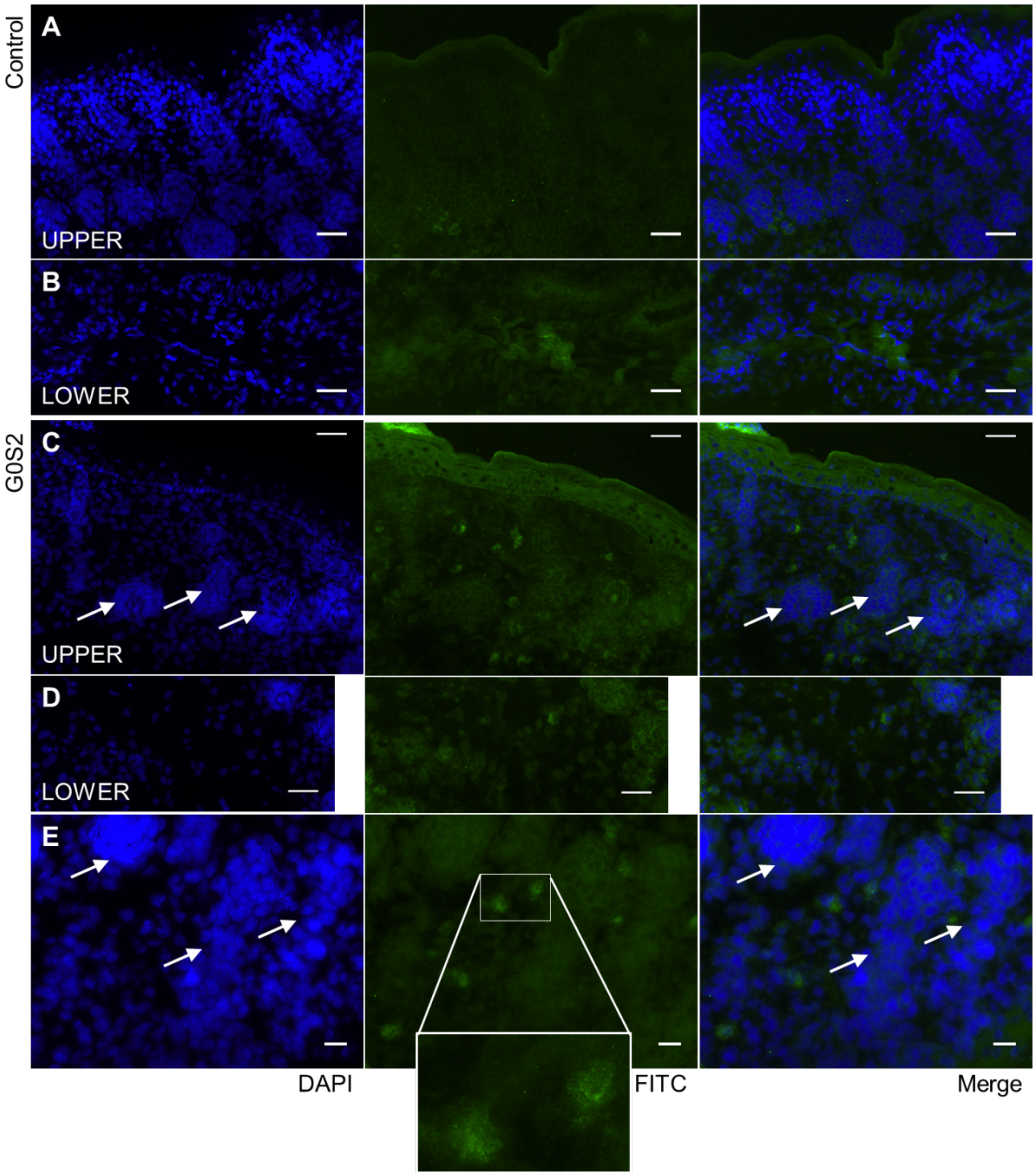

<u>Figure 2.5:</u> Analysis of G0S2 (Proteintech) expression in 1-day newborn mouse back skin. Sections cut at 7μm, stained with an antibody against G0S2 and counterstained with DAPI. From left to right; DAPI, FITC, and merge (DAPI/FITC). FITC represents the fluorescent labelling of G0S2. (**A,B**) Controls showing no fluorescently labelled G0S2 expression. (**C-E**) labelled using G0S2 primary antibody. Inset shows a magnified image of the positive G0S2 labelling in cells. Hair follicles in the skin labelled, demonstrating their position (arrows). Fluorescent images were taken using a Zeiss Axio Imager M1. (**A-D**) scale bar = 40μm. (**E**) scale bar = 15μm.

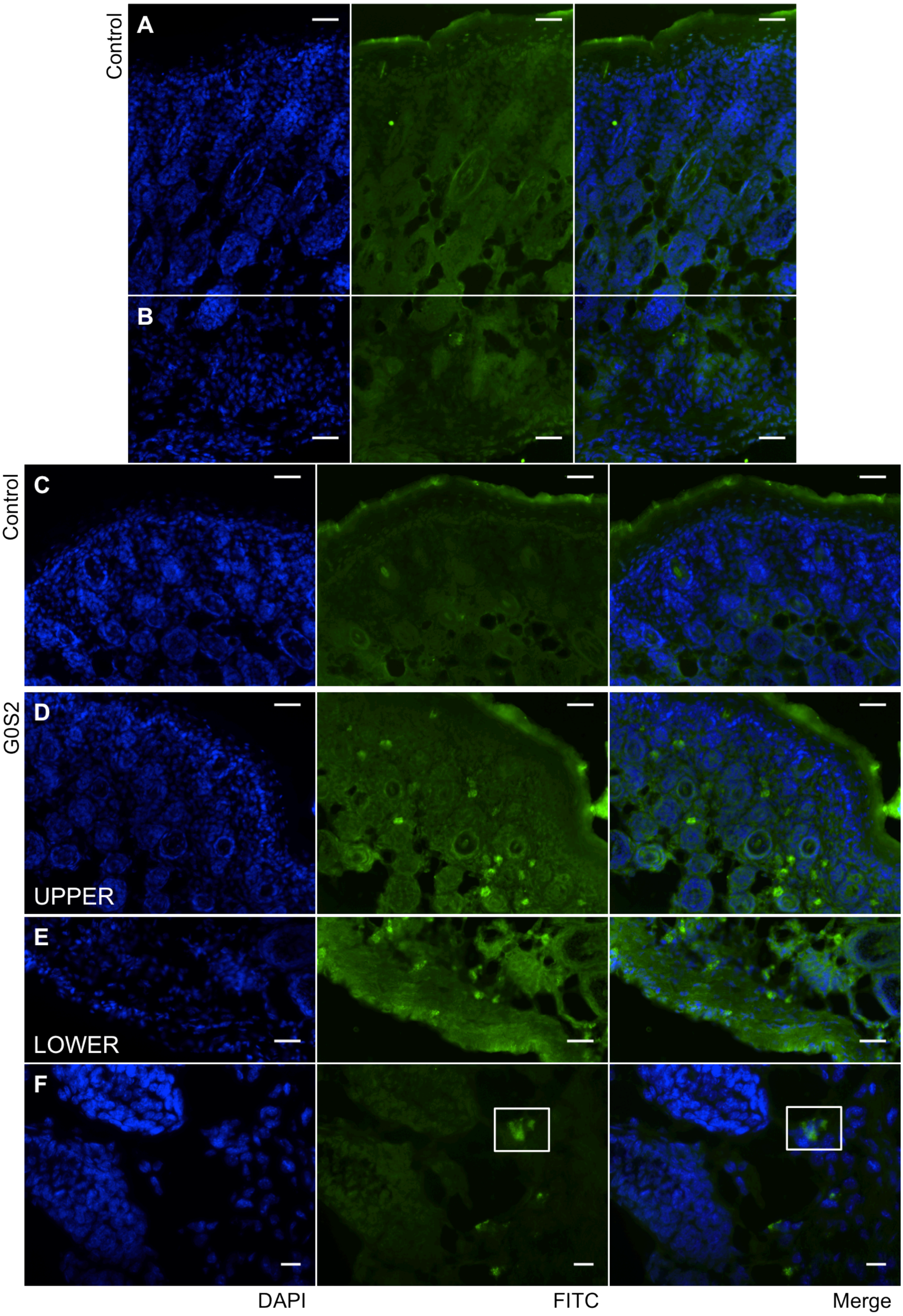

Figure 2.6: **Analysis of G0S2 (Proteintech) expression in 3-day newborn mouse back skin.** Sections cut at 7µm, stained with an antibody against G0S2 and counterstained with DAPI. From left to right; DAPI, FITC, and merge (DAPI/FITC). FITC represents the fluorescent labelling of G0S2. (**A-C**) Controls showing no fluorescently labelled G0S2 expression. (**D-F**) labelled using G0S2 primary antibody. Positive G0S2 expression highlighted (white squares). Fluorescent images were taken using a Zeiss Axio Imager M1. (**A-E**) scale bar = 40µm. (**F**) scale bar = 15µm.

2.3.2.2. Embryonic Mouse Back Skin

Going back to embryonic day 18.5, G0S2 was expressed in the developing embryonic skin (Figure 2.7).

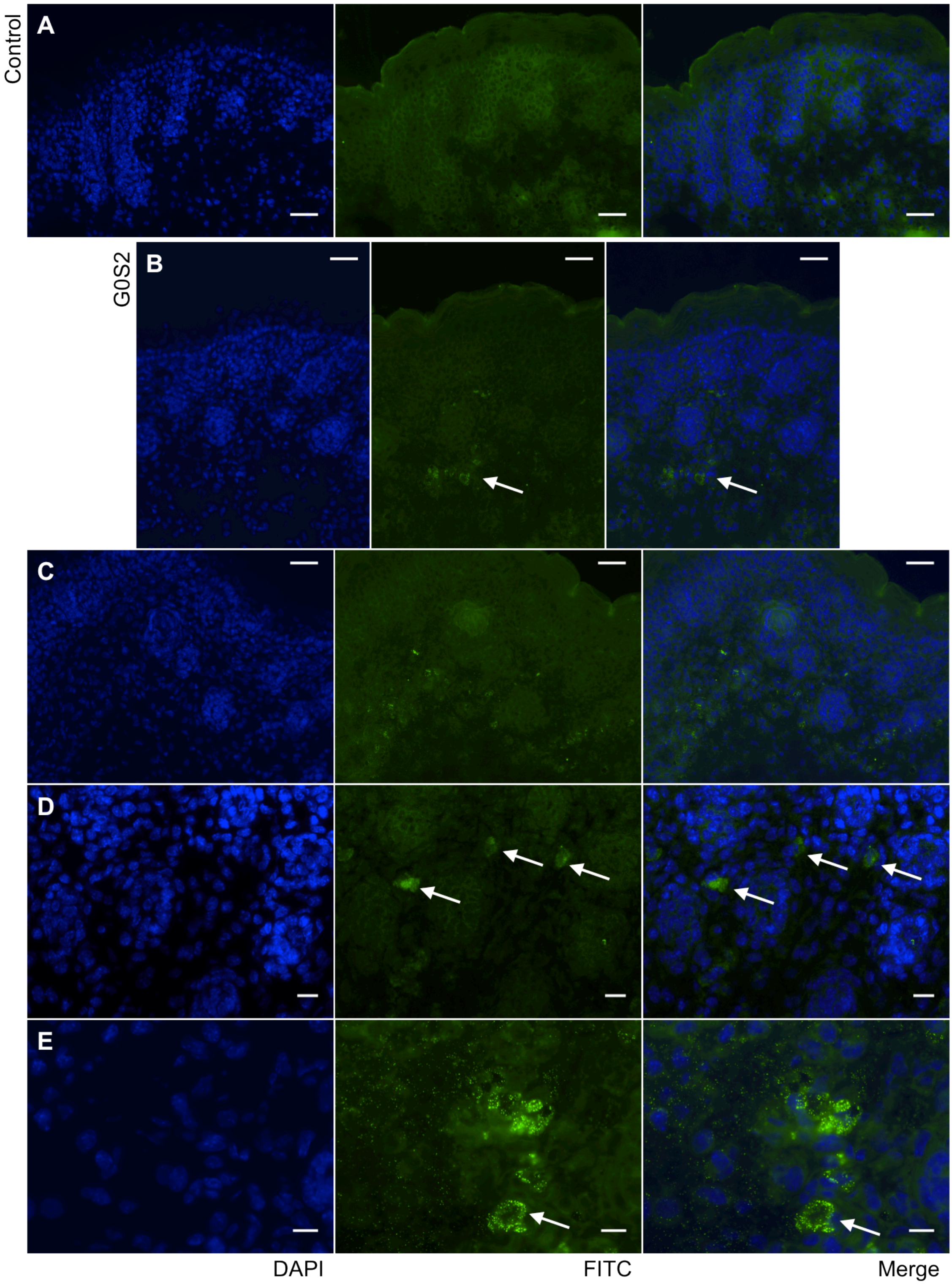

Figure 2.7: Analysis of G0S2 (Proteintech) expression in 18.5-day embryonic mouse back skin. Sections cut at 7μm, stained with an antibody against G0S2 and counterstained with DAPI. From left to right; DAPI, FITC, and merge (DAPI/FITC). FITC represents the fluorescent labelling of G0S2. (**A**) Control showing no fluorescently labelled G0S2 expression. (**B-E**) labelled using G0S2 primary antibody. G0S2 labelled cells shown (arrows). Fluorescent images were taken using a Zeiss Axio Imager M1. (**A-D**) scale bar = 40μm. (**E**) scale bar = 15μm.

In comparison with the background staining shown in the negative controls, there were some G0S2 labelled cells present in the lower dermis of the skin at e18.5 (Figures 2.7B and C). However, earlier in e16.5 (Figure 2.8) and also e14.5 (Figure 2.9), there were no positively labelled cells for G0S2 detected, which suggested, it acted from around e18.5.

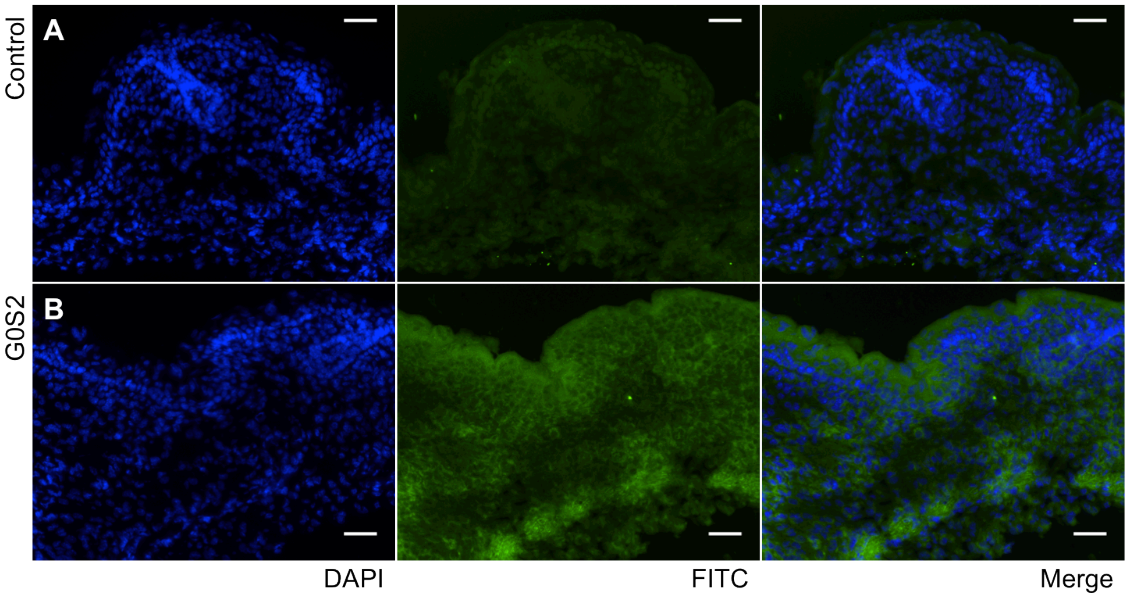

Figure 2.8: **Analysis of G0S2 (Proteintech) expression in 16.5-day embryonic mouse back skin.** Sections cut at 7μm, stained with an antibody against G0S2 and counterstained with DAPI. From left to right; DAPI, FITC, and merge (DAPI/FITC). FITC represents the fluorescent labelling of G0S2. (**A**) Control showing no fluorescently labelled G0S2 expression. (**B**) labelled using G0S2 primary antibody. Fluorescent images were taken using a Zeiss Axio Imager M1. Scale bar = 40μm.

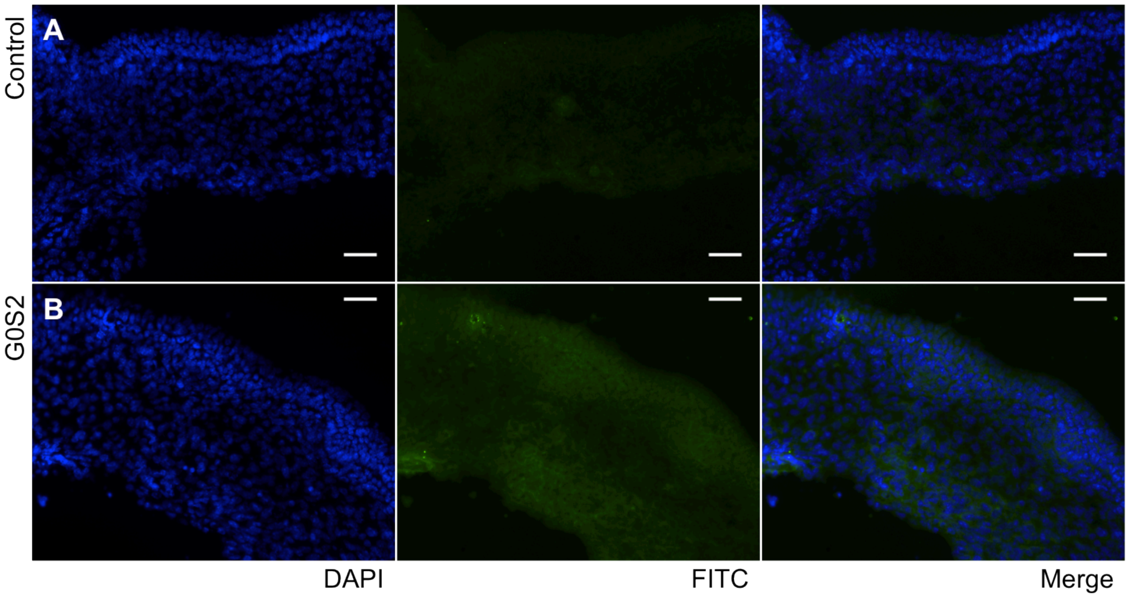

Figure 2.9: **Analysis of G0S2 (Proteintech) expression in 14.5-day embryonic mouse back skin.** Sections cut at 7μm, stained with an antibody against G0S2 and counterstained with DAPI. From left to right; DAPI, FITC, and merge (DAPI/FITC). FITC represents the fluorescent labelling of G0S2. (**A**) Control showing no fluorescently labelled G0S2 expression. (**B**) labelled using G0S2 primary antibody. Fluorescent images were taken using a Zeiss Axio Imager M1. Scale bar = 40μm.

2.4. Discussion

2.4.1. Microarray Analysis

Microarray analysis was previously conducted to investigate the lower dermis and compare the upper and lower dermis (Wojciechowicz 2012), but microarray lists were not created to look at a comparison across the ages in solely the upper dermis. There were significantly more highly expressed genes between e17 and e18 and e17 to e19 compared with between e18 and e19. This suggests that most of the signalling that occurs in development of the upper dermis takes place earlier, around e17, potentially e16 or even e14 though dermis microarrays had not been developed this early.

GEDI analysis showed that there were differences in the expression profiles within the upper dermis at one age. Either this makes the data sets unreliable or it could show that the expression varies in different areas of the upper dermis. For example, there may be different genes detected near the epidermis in comparison with near the lower dermis as different cells are developing. It could also be that the sample point is where a developing follicle is and so the expression profiles are more related to the developing follicle than interfollicular dermal cells.

The thought is that in actual fact, because the depots and more recently the dermal adipose layer have been found of different developmental origins that gene expression may in fact differ between depots. Macotela *et al.* (2012) found that when adipocyte precursor cells were taken from different depots, both subcutaneous and visceral, they had contrasting patterns of gene expression. It may be important to characterise gene expression for each depot. This chapter aimed to characterise potential inhibitory adipogenic signals of the upper dermis in relation to the dermal adipose depot.

Four genes of interest were selected that showed significant differences in expression across the three ages in the upper dermis. SPARC (Secreted protein, acidic, cysteine-rich) like 1 (SPARCl1) was found to be significantly downregulated between e17 and e18 and further by e19. It could be suggested that this gene is required to inhibit adipogenesis in the upper dermis before the cells differentiate. Like SPARC, its name suggests that it may also be associated with inhibiting adipogenesis. Liu and colleagues (2014) found that SPARCl1 was expressed in the Visceral Stromal-Vascular Fraction (SVF) and therefore expressed visceral, but not subcutaneous. Perhaps it is also expressed in the dermis, but not the subcutaneous adipose tissue, separating its functioning in the skin. This may be a signal of inhibition in the upper dermis. This is an interesting idea, but one that requires experimentation to observe what occurs in the upper dermis when SPARCl1 expression is removed, e.g. by a knockout mouse model. Potentially it is already expressed before e17.

Comparatively, serine racemase was upregulated between e17 and e19. Serine racemase is involved in the regulation of insulin and glucagon release and therefore Type 2 diabetes (Tsai *et al.* 2010). This regulation may be associated with its upregulation in the upper dermis later than adipocytes are suggested to develop, thus it may be maintaining upper dermal cells in a non-adipogenic state. As more adipogenic signals start to influence the dermis, e.g. C/EBPα around e18, this serine racemase becomes more highly expressed in the upper dermis to prevent adipocyte differentiation from occurring. Chapter 4 shows that dermal cells are capable of differentiating into adipocytes in cell spheres from as early as e14.5, so perhaps the upper dermis requires an inhibition of the adipogenesis signal. If serine racemase expression was removed from the upper dermis would it lead to adipogenesis throughout the dermis or would overexpression in the lower dermis inhibit adipocyte formation? These are foundations for interesting experiments in relation to serine racemase. For example, to test this hypothesis, serine racemase could be downregulated or inhibited in the upper dermis. Most of the research found links serine racemase with diabetes but not adipogenesis, so this could be an interesting avenue to explore.

Osteoglycin was downregulated in the microarrays between e17 and e19. Insenser *et al.* (2012) found that osteoglycin expression was increased in obese patients, which suggests osteoglycin stimulates or maintains adipocyte formation. The downregulation and therefore decrease of osteoglycin in the upper dermis, where no adipose tissue develops correlates with this results found by Insenser *et al.* (2012). There is a reduction in positively associated adipocyte factors in the upper dermis around the time adipogenesis is occurring. Further work could look at overexpressing osteoglycin in the upper dermis to observe if adipocytes can form.

Calmodulin 1 was also found to exhibit reduced expression between e17 and e19. Graves *et al.* (1985) found that the adipocyte insulin receptor has a calmodulin binding domain. Insulin receptor defects are thought to be associated with obesity, though the link in humans is not well characterised (Hotamisligil *et al.* 1995). However, a factor associated with insulin could be linked with adipogenesis in the skin, therefore changes in expression of calmodulin 1 in the skin dermis could be an interesting avenue to explore, in terms of the regulation of dermal adipogenesis.

An understanding of the expression profiles of adipocyte development may not only help further our understanding of what is involved in adipogenesis, but also might enable the identification of some pre-adipocyte markers to help with the study, with the aid of earlier microarray studies as well.

2.4.2. G0S2

G0S2 was found expressed in the dermis in the microarrays and also by immunofluorescence staining. G0S2 was not found significantly expressed in the upper dermis microarrays, suggesting its importance in the lower dermis development and therefore, adipogenesis. Expression in the skin dermis from e18.5 and further in postnatal mouse skin was found, which matches that found by Wojciechowicz (2012). It was detected in the lower dermis and around the base of the follicles where adipocytes develop. This proved positive for the association of G0S2 with adipogenesis, however, it was not found to be an early signal. The labelling of G0S2 was speckled in the cells. This was similar to that found by Yang *et al.* (2010).

At the time that this project was conducted, relatively little was known by way of the role of G0S2 in adipogenesis. However, more recently it has been strongly implicated in adipogenesis. It has been determined to have an *in vivo* role, as well as *in vitro* (Choi *et al.* 2014). Choi *et al.* (2014) showed that G0S2 knockout mice developed with reduced adipose mass. It was found important from mitotic clonal expansion right through to terminal differentiation (Choi *et al.* 2014) and this correlates with the findings that G0S2 was expressed in the later ages (section 2.3.2). In pigs, G0S2 was found to increase over the course of adipogenesis both *in vitro* and *in vivo* (Ahn *et al.* 2013). This corresponds with the result that there was more strong antibody labelling in the postnatal skin (section 2.3.2). G0S2 is therefore important for adipogenesis and is controlled by PPARγ (Choi *et al.* 2014), which is highly implicated in adipogenesis.

CHAPTER 3

PPARγ: What does it really do? *In Vitro* and *In Vivo* Immunofluorescence Analysis

3.1. Introduction

3.1.1. Structure and Function of PPARγ

Peroxisome proliferator-activated receptor gamma (PPARγ) is a member of the nuclear hormone receptor superfamily and is a ligand-activated transcription factor (Mandrup and Lane 1997; Michalik *et al.* 2002; Lehrke and Lazar 2005; Lefterova and Lazar 2009). There are other PPARs, including PPARβ/δ and PPARα. PPARβ/δ has been found to be upregulated in the early stages of adipogenesis and is required to initiate PPARγ and other genes in the process. PPARγ has four main domains: the DNA binding domain (C domain), the ligand-binding domain (E/F domain), the hinge region (D domain) and the N-terminal domain (A/B domain) (Michalik *et al.* 2002). The E/F domain is involved in the ligand-dependent receptor function, while the A/B domain is involved in the ligand-independent receptor function (Michalik *et al.* 2002).

Two PPARγ protein isoforms exist, named PPARγ1 and PPARγ2. The majority of PPARγ2 protein is specific purely to adipocytes (Zhu *et al.* 1995). While both isoforms are involved in adipogenesis, PPARγ2 is more dominant (Zhang *et al.* 2004). There are many endogenous ligands of PPARγ, including the prostaglandin PGJ_2 and members of the 5-HETE family, e.g. 5-oxo-HETE (O'Flaherty *et al.* 2005). Though there are many ligands that have been found *in vitro,* not all of them have yet to be found of importance *in vivo* (Bishop-Bailey and Wray 2003; Lefterova and Lazar 2009).

Upon ligand to receptor binding, a conformational change causes the co-repressor to be released and opens up a docking site for the co-activator (Tontonoz and Spiegelman 2008; Lefterova and Lazar 2009). This triggers the expression of target genes, which contain PPAR responsive elements (PPRE) (Michalik *et al.* 2002). PPARγ dimerizes with retinoid X receptors (RXRs) (Gerhold *et al.* 2002; Michalik *et al.* 2002). While it is widely known that PPARγ is important in adipogenesis, which genes it targets are partly unrecognised. Some include the *LEP* gene encoding Leptin, Lipoprotein lipase (Schoonjans *et al.* 1996), G0/G1 switch gene 2 (Zandbergen *et al.* 2005; see Chapter 2) and the *UCP2* and *CD36* genes (Matsusue *et al.* 2003). Expression profiling during differentiation suggests that many genes are regulated by PPARγ, though the mechanisms are largely unknown. (Perera *et al.* 2006; Lefterova *et al* 2008). Therefore regulation of gene expression by PPARγ is not fully understood. It is important to understand how the transcriptional activity of PPARγ works to clarify its role in adipogenesis.

PPARγ has been found to be involved in lipid accumulation and adipogenesis. As well as this, PPARγ plays a role in a number of different processes. These include macrophage maturation, inflammation control and many functions of mature adipocytes, including insulin sensitivity and lipid metabolism (Barak *et al.* 1999; Lefterova *et al*. 2008). The gene is becoming increasingly more important due to its association with syndrome X and diabetes. Thus it is implicated in obesity, which is becoming an increasingly large problem amongst the population. Humans with PPARγ dominant negative mutations show lipodystrophy, insulin resistance and hypertension, which implicate PPARγ in diabetes (Gray *et al.* 2006).

PPARγ interacts with several coregulators, which include the coactivator PGC-1a which helps activate a number of transcription factors during adipogenesis, including nuclear respiratory factor 1 (NRF-1) (Lin *et al.* 2005; Farmer 2006). The p160 coregulators also associate with PPARγ and lead to modifications of the chromatin (Farmer 2006). Some factors also act as corepressors. Yu *et al.* (2005) showed that by RNAi knockdown of two factors SMRT and NcoR, PPARγ target genes are expressed more, suggesting that these factors work with PPARγ activity to repress it (Picard *et al.* 2004; Farmer 2006).

The three PPARs are distributed differently throughout the adult body with the majority of PPARα and PPARγ in the liver and adipose tissue (Evans *et al.* 2004). PPARβ/δ is expressed throughout the body (Evans *et al.* 2004). In rodents, PPARγ expression is limited to BAT by day 18.5 of gestation and to the central nervous system from day 13.5 to 15.5 (Michalik *et al*. 2002).

3.1.2. The Master Regulator of Adipogenesis

PPARγ has long been recognised as one of the master regulators of adipogenesis along with CCAAT/enhancer-binding proteins (C/EBP) (Lefterova and Lazar 2009). It is thought to be involved in all stages of adipogenesis: the commitment of preadipocytes, the differentiation into adipocytes and the survival and maintenance of terminal adipocytes (Rotman *et al.* 2006). It has been shown to be both necessary and sufficient for differentiation of white and brown adipocytes (Tontonoz *et al.* 1994; Rosen *et al.* 2002; Gray *et al.* 2006; Tontonoz and Spiegelman 2008; Lefterova *et al.* 2008; Lefterova and Lazar 2009). As described in chapter 2, members of the C/EBP family (C/EBPα and C/EBPδ) interact with PPARγ in adipogenesis (Wu *et al.* 1996).

Research using adipocyte cell lines, e.g. the 3T3-L1 cell line, have been used to investigate the functions of PPARγ in adipogenesis (Tang *et al*. 2003; Lefterova and Lazar 2009). PPARγ activators induce 3T3-L1 preadipocytes to differentiate (Chawla and Lazar 1994). Not only have 3T3-L1 cells been used to show that PPARγ is a main regulator, but also what affects PPARγ expression. How PPARγ is controlled has been determined by supplying the cells in culture with various factors and monitoring PPARγ transcriptional activity. For example, PKA stimulators were found to inhibit PPARγ expression, while thiazolidinedione (TZD) induced it (Gerhold *et al.* 2002; Watanabe *et al.* 2003).

Inducing expression of PPARγ can lead to the formation of adipocytes from cells that are not normally adipogenic (Tontonoz *et al.* 1994; Mandrup and Lane 1997). For example, Hu *et al.* (1995) showed that myoblasts cultured with PPARγ accumulate lipids and express markers indicative of adipocytes, therefore undergoing transdifferentiation (Gerhold *et al.* 2002). The presence of PPARγ agonist rosiglitazone can cause the cells to all differentiate into adipocytes and decrease osteoblast formation (Ali *et al.* 2005: Rotman *et al.* 2006). While these gain-of-function experiments are useful to understanding the function of PPARγ they do not show whether it is indeed necessary for adipogenesis, thus loss-of-function experiments are also beneficial (Rosen *et al.* 1999).

Mouse models have been used to show the importance of PPARγ *in vivo* as well as *in vitro*. However, as with many of the loss-of-function/knockout mouse models involved in the study of adipogenesis, in the absence of PPARγ the mice are embryonic lethal (Barak *et al.* 1999; Gray *et al.* 2006). Barak *et al.* (1999) generated PPARγ-deficient mice whereby the mutation caused the knockout of both the DNA binding and ligand binding functions. No homozygous null embryos survived past the midembryonic stage (Miles *et al.* 1999; Rosen *et al*. 1999), whereas the heterozygotes could survive, thus chimeric methods were more insightful. It was found that embryonic stem cells (ESCs) that don't express PPARγ are incapable of developing into adipocytes.

Gray *et al.* (2006) used a dominant-negative PPARγ mouse model, called P465L PPARγ, generated by homologous recombination. The mice had normal levels of adipose tissue, though under closer inspection their brown adipocytes had one large lipid droplet. White adipose tissue, while appearing normal recruited less brown *adipocytes* and there was less UCP1 expression (Gray *et al.* 2006). PPARγ in this case is thought to have more of an effect on brown adipocytes than white adipocytes. It was also possible to ablate specifically PPARγ2, which decreased the lipid content of brown adipocytes (Zhang *et al.* 2004).

PPARγ2 was specifically knocked down with homologous recombination in white adipose tissue (Koutnikova *et al.* 2003). Those homozygous (PPAR$\gamma^{hyp/hyp}$) mice that survive after birth are severely lipodystrophic with virtually no WAT. In response PPARγ1 mRNA was found to increase. Homozygous mice appeared normal at birth, but post-natally the lack of PPARγ2 affected WAT development, though it did not appear to impede BAT development. Muscle compensates metabolically so the lipodystrophy is only temporarily detrimental to those homozygous mice that survive. Zhang *et al.* (2004) also found that PPAR$\gamma 2^{-/-}$ mice were able to survive but less WAT had developed and the adipocytes were smaller in size, fewer lipids had accumulated and they exhibited reduced expression of adipogenic genes. Compared with the wild-type mice there was no difference in the weight of BAT depots, liver, spleen or heart.

PPARγ also has a role in the maintenance of mature adipocytes (Imai *et al.* 2004; Zhang *et al.* 2004), since knocking out PPARγ after adipose tissue formation causes the loss of fat over time as well as hyperlipidemia (He *et al.* 2003; Evans *et al.* 2004). PPARγ has therefore been found to function in both adipocyte differentiation and maintenance. Koutnikova *et al.* (2003) also found this to be the case.

3.1.3. Recent Hypotheses

While the current hypothesis is that PPARγ is crucial to adipogenesis, its exact role and timing of involved in different adipose depots *in vivo* is unclear. In microarray analysis of embryonic dermis, the Jahoda group found mRNA expression of PPARγ *in vivo* between e17 and e18 in mouse skin, but not the differential expression that might have been expected between the upper and lower dermis. Wojciechowicz (2012) in Jahoda's lab used immunofluorescent analysis to look at the expression of PPARγ in embryonic mouse back skin. However, it was not detected in the lower dermis, where the dermal fat layer has been found to develop. Several explanations were suggested; one that the epitopes for the PPARγ protein in the skin dermis were obscured so the antibodies couldn't bind. Secondly, that the PPARγ protein is not present in the lower dermis at the time points analysed (e17, e18 and e19). Thirdly, while PPARγ may be crucial to the regulation of the early stages of adipogenesis in other fat depots, this may not be the case for the dermal fat layer: Its development may be regulated differently.

Fourthly, the antibodies used may not have been appropriate for back skin and therefore showed non-specific staining or background staining (Wojciechowiz 2012). Another possibility is that while the gene is being expressed the protein is not being produced, or not accumulating in the nucleus. Perhaps in skin the importance of PPARγ rests in adipocyte differentiation and maintenance and less so at initiation and lineage commitment. Vernochet *et al.* (2002) suggested that in cell culture the media may cause the commitment of cells to the adipogenic lineage and in fact PPARγ only then has a role in differentiation post commitment (Rotman *et al.* 2006). PPARγ was found not to be required for lineage commitment and the establishment of brown adipocytes, but necessary for their development (Barak *et al.* 1999). Since this gene is widely recognised for its involvement in inducing adipogenesis (see above), it is important to look closely at its expression in developing skin by accurate and reliable means.

To address these questions over the role of PPARγ in the formation of the dermal fat layer, a positive control is required to clarify that the antibodies used are effective and reliable. In this chapter, several different PPARγ antibodies were tested *in vitro* using the 3T3-F442A cell line. PPARγ expression is expressed in 3T3 cell nuclei 42-60 hours after they have been induced to differentiate down the adipogenic lineage (Morrison and Farmer 1999; Wojciechowicz 2012). Immunofluorescent analysis using an anti-PPARγ antibody is an appropriate method to determine whether staining is localised to the nucleus and thus PPARγ is being expressed. Both induced and non-induced cells were stained for PPARγ. While the timings *in vitro* are well understood, they are less clear *in vivo*. After the uncertainties and questions raised by the work of Wojciechowicz (2012) the aim of this chapter was to unequivocally describe the expression of PPARγ during development of the dermal fat layer. Here *in vivo* PPARγ expression was studied in skin from embryonic day 14.5 to 5 day newborn mice. Dermal cell spheres were also created to look at PPARγ expression solely in developing dermal cells taken from embryonic day 14.5 mouse back skin.

3.2. Materials and Methods

3.2.1. In Vitro Analysis – The 3T3 F442A Cell Line

3.2.1.1. Preadipocyte Cell Culture and Maintenance

Cryofrozen 3T3-F442A cells (kindly donated by Adina Mihai, Durham University) were rapidly defrosted in a water bath. The cells were brought up in 12ml of pre-warmed 3T3 cell media (Appendix II) in a T75 flask and incubated at 37°C in 10% CO_2.

After 24 hours, the media was poured off and the T75 rinsed with sterile PBS to remove excess media. 10ml of a solution of trypsin (0.25%) in EDTA (Gibco) was added before the flask was returned to the incubator for several minutes until the cells detached. Then trypsinization was stopped by adding another 10 ml 3T3 cell media before transferring the suspension to a 15ml centrifuge tube (Falcon) prior to centrifugation at 1000rpm for 5 minutes (Hermle Z400 Bench top centrifuge). The cell pellet was resuspended in 1ml fresh 3T3 cell media and the cells were counted. The cells were seeded at 60-70% confluence in 6 well plates. Some wells contained sterile coverslips for the cells to adhere to prior to immunofluorescence staining. The coverslips had been soaked in acid ethanol for 24 hours and washed twice in Phosphate buffered saline (PBS: Appendix I) before being transferred to 35ml dishes. The plates were returned to the incubator at 37°C in 10% CO_2.

3.2.1.2. Inducing Adipogenesis

Two days after the cells had reached confluence, the cells were stimulated with differentiation medium (Appendix II) to induce adipocyte formation. One plate was not supplied with differentiation media but was allowed to continue growing in normal 3T3 cell media as a non-induced control.

After 2 days one induced and one non-induced 6 well plate was taken out of culture for PPARγ immunofluorescence analysis. The other plate was left in culture to develop into adipocytes to ensure the differentiation process would be successful at producing fat.

After a further 24 hours the culture medium was changed to insulin media (Appendix II). These cells were incubated for another 2 days at 37°C in 5% CO_2. The media was then changed back to the 3T3 cell media for another 10 days.

3.2.1.3. Oil red O Analysis of 3T3 F442A Cells

After 10 days, oil red O analysis was conducted to determine whether the adipocyte differentiation had occurred. The cells were washed in PBS and then fixed in calcium formal (Appendix I) for 10 minutes. The wells were then immediately stained or stored in PBS at 4°C prior to staining.

An incubation with 60% isopropanol was followed by 10 minutes with a working solution of oil red O. A short wash in 60% isopropanol was then used to remove any excess oil red O followed by two careful washes in PBS. The cells were then stored in PBS at 4°C before pictures were taken.

3.2.1.4. PPARγ Immunofluorescence Analysis in Vitro

Immunofluorescent staining of PPARγ was carried out on cells after 2 days of incubation with differentiation media and also non-induced 3T3 cells after 2 days. Five different PPARγ antibodies were used (Table 3.1).

Table 3.1: Summary of primary antibodies and conditions used for immunofluorescent staining *in vitro*

Antibody/ Factor Name	Manufacturer	Raised in	Clonality (P/M*)	Dilution	Fixation	Blocking serum
PPARγ-2	Affinity Bioreagents	Rabbit	P	1:500	Acetone	Donkey
PPARγ (B-5) (sc-271392)	Santa Cruz	Mouse	M	1:100	Acetone	Goat
PPARγ (E-8) (sc-7273)	Santa Cruz	Mouse	M	1:100	Acetone	Goat
Anti- PPARγ (ab19481)	Abcam	Rabbit	P	1:100	PFA	Donkey
Anti- PPARγ (AHP1461)	Abd Serotec	Rabbit	P	1:50	Acetone PFA	Donkey

* P - polyclonal; M – monoclonal
Acetone/PFA – Slides were fixed in either ice-cold acetone or 4% paraformaldehyde

Table 3.2: Details of the corresponding secondary antibodies used for immunofluorescent staining

Secondary Antibody		Manufacturer	Dilution
Donkey anti rabbit (FITC)	AlexaFluor^{R} 488	Invitrogen	1:500
Goat anti mouse (FITC)	AlexaFluor^{R} 488	Invitrogen	1:500

Cells were grown on square coverslips, therefore, staining was conducted in the wells, making sure during each wash, coverslips were washed underneath. Coverslips were first washed twice in 1x phosphate buffered saline (PBS-appendix 1) for 2 minutes to remove all media prior to fixation. Cells were fixed in either ice-cold acetone for 10 minutes or 4% paraformaldehyde (PFA – Appendix I) for 15 minutes (see table 3.1). Cells that were to be incubated with the anti-PPARγ antibody from Abd Serotec were fixed with both acetone and PFA, because this antibody had not been tested on frozen sections. Coverslips fixed in acetone were then allowed to dry before being rinsed in PBS, while coverslips fixed in PFA were rinsed in PBS, then permeabilised with 0.5% Triton-X for 5 minutes, and then rinsed again in PBS. Cells were then blocked with 20% donkey serum (Sigma, MO, USA) or goat serum (Sigma, MO, USA) in PBS for 30 minutes (see table 3.1). The wells were then washed for two minutes in PBS and cells then incubated with the primary antibodies (Table 3.1) in 1% donkey or goat serum/PBS overnight at 4°C.

The wells were washed three times in PBS for 5 minutes and incubated with a corresponding secondary antibody (Table 3.2) for 1 hour at room temperature. 4′,6-diamidine-2′-phenylindole dihydrochloride (DAPI) (KPL, Maryland, USA) was added for 3 minutes at a dilution of 1:1000. Incubations were carried out in the dark to prevent the coverslips from drying out and the fluorescence fading. Three more 5-minute PBS washes were conducted before mounting the coverslips onto blank slides in anti-fade Mowiol. Slides were kept at 4°C in the dark. Immunofluorescence analysis was performed on a Zeiss Axio Imager M1 microscope with Volocity software.

For each type of fixation, blocking step and secondary antibody, negative controls were performed, where cells were not exposed to the primary antibodies, but incubated with 1% donkey (or goat) serum/PBS. They were exposed to the same corresponding secondary antibodies to determine if there was any non-specific staining. Other controls were conducted using the 3T3 cells that had not been induced to differentiate.

3.2.2. In Vitro Analysis – Dermal Cell Spheres

3.2.2.1. Origin, Maintenance and Breeding of Rodents

Back skin from 14.5-day embryonic mice was taken from mice of the FVB strain from the Durham University Life Sciences Support Unit (LSSU). They were kept at 21°C, 55% humidity on a 12 hour light/dark cycle. They were fed on the Harlan Teklad 2013 Rodent Maintenance diet and watered *ad libitum*.

Vaginal plug analysis was used to obtain skin from embryos at the specific age. The presence of a vaginal plug the morning after breeding pairs had been kept together was used as an indication of a successful mating and the embryos were noted at 0.5 days gestation at this point. Animals were killed using CO_2/cervical dislocation. Back skin was microdissected from embryonic mice (see section 3.2.3.2).

3.2.2.2. Production of Single Cell Suspensions from Mouse Dermis

Skin pieces obtained from foetal mouse back skin were put in a 6% Pancreatin/5% Trypsin cocktail in Earle's solution (1:1:2, Appendix III) at 4ºC for 90 minutes. Fine tweezers were then used to carefully prise apart the dermis from the epidermis. Dermal pieces were transferred to sterile Earle's solution before being incubated in a warm working solution of DNase I (Sigma)/Collagenase II (Sigma) (Appendix III) at 37C for 15-20 minutes. Mechanical dissociation was carried out with a 1ml pipette to form a single cell suspension of the dermis. The suspension was diluted with 2ml of 10% FBS-MEM and filtered through a cell filter (Fisher), before being centrifuged at 1000rpm for 5 minutes. The supernatant was carefully poured off leaving a cell pellet, which was resuspended in 1ml of 10% FBS / MEM.

3.2.2.3. Preparing 3-dimensional Spheres in Culture

Spheres were created by pipetting 10μl drops containing 6000 cells onto the petri dish lids, evenly spaced and not too close to the edge. 25ml of sterile distilled H_20 was put into each petri dish and the drops were suspended over this to prevent them from drying out. Petri dishes containing 25ml of sterile distilled H_20 but no spheres were placed above and below before being transferred to the incubator (37C, 5% CO_2). See Chapter 4, figure 4.5 for diagram of 3D culture set up.

3.2.2.4. Obtaining 3-dimensional Spheres for Analysis

After two days the dermal cells had aggregated and formed spheres. 10-15 spheres were collected and snap frozen in liquid nitrogen suspended in Tissue-Tek® O.C.T.™ compound (Sakura, Agar Scientific, Netherlands), before being stored at -80C. This was repeated each day for 5 days and two blocks were frozen down each day. Spheres collected were therefore from e14.5 plus 2, 3, 4, 5, and 6 days.

Sections were cut from each sample time point at 7um on a cryostat (LEICA CM 3050S) and then allowed to dry for 2 hours at room temperature.

3.2.2.5. PPARγ Immunofluorescence Analysis of e14.5 Spheres

Three of the PPARγ antibodies were used; Santa Cruz E-8, Abcam and Abd Serotec. The Affinity Bioreagents PPARγ-2 antibody was not used due to limiting quantities. The slides were stained as described in section 3.2.1.3 and negative controls incubated with only the secondary antibodies and not the primary PPARγ antibodies were conducted alongside for each replicate.

3.2.2.6. Oil red O Analysis of e14.5 Spheres

Oil red O staining was conducted on the spheres after 2, 3, 4, 5 and 6 days. Sections (10μm) were cut from the frozen spheres on a cryostat (LEICA CM 3050S) and attached to ColorFrost®Plus slides (Thermo Shandon Ltd, Cheshire, UK). Slides were left to dry at room temperature for 1hour 30 minutes and then washed in PBS (3x 5 minutes) followed by fixation in calcium formal (Appendix I) for 1 hour. They were then incubated with 60% isopropanol (Sigma) for 15 minutes and stained with a working solution of oil red O (Appendix I) for 15 minutes. Slides were briefly washed in 60% isopropanol to remove excess oil red O and then rinsed in water. They were counterstained by dipping each slide in Shandon instant haematoxylin (Thermo Scientific, Cheshire, UK) and then rinsed in water. Slides were mounted in pre-warmed glycergel (DakoCytomation Inc. California, USA) and coverslipped. Images were taken on a Zeiss Axio Imager (M1) microscope using Volocity software.

3.2.3. In Vivo Analysis – Rodent Back Skin

3.2.3.2 Preparation of Skin Sections

Rodents were maintained and timed matings obtained as described in section 3.2.2.1, and back skin was obtained from mouse embryos at e14.5, e16.5, e18.5 and from newborn mice after 1, 2, 3 and 5 days (Table 3.2). Additional skin samples were taken from an 18.5 day-old embryonic rat, of the Lister black hooded strain, also provided by the LSSU (Durham University).

Skin cut from the back of each specimen was rolled or orientated flat and put into Tissue-Tek® O.C.T.™ compound (Sakura, Agar Scientific, Netherlands), then snap frozen in liquid nitrogen and kept at −80°C. Skin sections (7 µm), were cut on a cryostat (LEICA CM 3050S) and attached to ColorFrost®Plus slides (Thermo Shandon Ltd, Cheshire, UK). The slides were dried for 2 hours at room temperature, and then used immediately for immunofluorescence staining or haematoxylin and eosin (H&E) staining.

Skin from 5dN mice was also cut from wax blocks. This involved the skin being fixed in 4% PFA and dehydrated in alcohol before being embedded in paraffin. Wax sections were cut using a microtome and then floated on distilled water to keep flat before being adhered to slides, with care taken to remove all bubbles. This process was conducted on a hot plate where the slides were left overnight to dry out.

3.2.3.3. PPARγ Immunofluorescence Analysis in Vivo

Once the effects of the different antibodies had been established *in vitro* on cells from the 3T3 F442A cell line, these antibodies were tested *in vivo* on rodent back skin apart from the PPARγ (B-5) Santa Cruz antibody which was not used *in vivo*, because it didn't look to have potential specificity *in vitro*.

Immunofluorescence analysis (IF) was conducted on a number of different ages with different combinations of fixation and specimen types as shown in Table 3.3.

Table 3.3: Summary of ages and specimen types the listed primary antibodies were tested on using immunofluorescence staining.

	Age (days)	Type	Section	PPARγ			
				ABR	Santa Cruz	Abcam	Abd Serotec
Embryonic	14.5	Mouse	Frozen			✓	✓
	16.5	Mouse	Frozen			✓	✓
	18.5	Mouse	Frozen			✓	✓
		Rat			✓		
Newborn	1	Mouse	Frozen			✓	✓
	3	Mouse	Frozen			✓	✓
	4	Mouse	Frozen	✓	✓		
	5	Mouse	Paraffin				✓

3.2.3.3.1. Frozen sections (IF)

All four antibodies were tested on frozen sections. The staining protocol was conducted in the same way as is described in section 3.2.1.3 except that sections were attached to slides as opposed to coverslips and so incubations were not conducted in wells of 6 well plates, but instead carried out in a humidity chamber to prevent the sections drying out. Each step was carried out for the same length of time and the conditions, as well as respective secondary antibodies used are listed in table 3.4. Samples incubated with the Abd Serotec PPARγ antibody were subjected to no fixation as well as both acetone and PFA fixation steps, because there was no pre-indication as to which would be more successful, if any.

Table 3.4: Table showing the primary antibody manufacturers, respective secondary antibodies and the conditions used in immunofluorescence staining of frozen sections *in vivo*

Manufacturer	Blocking serum	Dilution	Fixation	Secondary Antibody
Affinity Bioreagents	Donkey	1:500	Acetone	Donkey anti-rabbit (FITC)
Santa Cruz	Goat	1:100	Acetone	Goat anti-mouse (FITC)
Abcam	Donkey	1:100	PFA	Donkey anti-rabbit (FITC)
Abd Serotec	Donkey	1:50	No fixation	Donkey anti-rabbit (FITC)
			Acetone	
			PFA	

3.2.3.3.1.1. Mouse on Mouse Protocol

When staining in skin sections, using an antibody raised in mouse, some steps are needed to prevent the antibody staining everything. A mouse on mouse (MOM) kit (Vecta FMK-2207) was used for the Santa Cruz E-8 antibody in skin sections. The immunofluorescence staining was also conducted without using the MOM kit to act as a control. See Appendix II for all working solutions.

Sections were fixed in ice-cold acetone for 10 minutes and then air-dried, before being washed twice for 2 minutes in PBS. The slides were incubated in the ‘mouse blocking reagent working solution’ for 1 hour and then washed twice in PBS for 2 minutes. Next was an incubation in the ‘’diluent working solution’ for 5 minutes and the excess was tipped off. The primary antibody from Santa Cruz was diluted in the ‘diluent working solution’ and the slides were incubated in it for 30 minutes and then washed a further 2 times in PBS for two minutes. The ‘biotinylated anti-mouse reagent’ was then put on the slides and left for 10 minutes and washed off 2 times for 2 minutes in PBS. The slides were lastly incubated in the ‘fluorescin avidin DCS working solution’ for 5 minutes and washed twice in PBS for 5 minutes before being mounted in Vectashield.

3.2.3.3.2. Paraffin Sections (IF)

Slides with 5dN mouse skin paraffin sections attached were allowed to cool and then de-paraffinised thoroughly in histoclear twice for 5 minutes each. The sections were then hydrated through a graded series of washes in ethanol. This started with 2 x 3 minutes in 100% ethanol then 2 x 2 minutes in 95% ethanol and finally 2 x 2 minutes in 70% ethanol. The slides were then washed twice in water for 5 minutes.

An antigen retrieval step using a 10mM sodium citrate buffer, pH6 (appendix 1) was conducted by suspending the slides in a beaker containing this buffer and placing in a microwave for 20 minutes. This was then left to cool for 15 minutes before the slides were rinse in PBS.

Immunfluorescence staining was then continued in the same way as frozen sections blocking with 20% donkey serum and using the Abd Serotec PPARγ antibody at a concentration of 2.5μg/ml in 1% donkey serum/PBS (see section 3.2.1.3).

3.3. Results

3.3.1. 3T3 F442A Cells in Culture

In order to first investigate the different PPARγ antibodies *in vitro*, 3T3 F442A cells were brought up from frozen and put into culture in 6-well plates. Pictures were taken of these cells to show they were healthy and confluent before the media was changed to induce adipocyte differentiation (Figure 3.1). These images showed that some of the cells were already spontaneously differentiating because some clearly had lipid droplets in (Figure 3.1F).

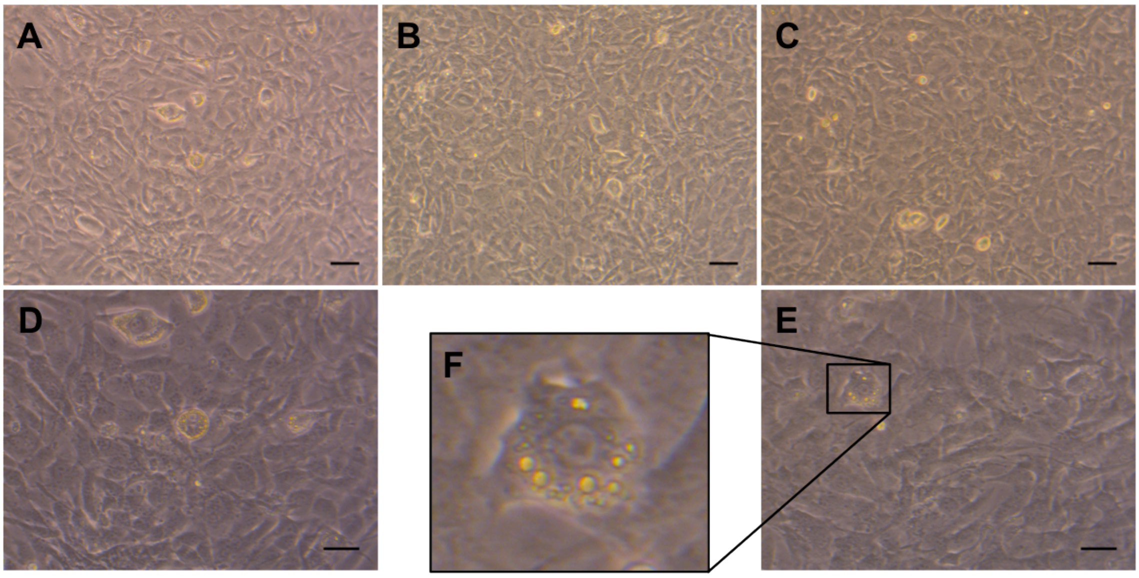

<u>Figure 3.1:</u> **Images of 3T3 F442A cells in culture before the addition of adipogenic media.** Cells have proliferated and adhered to the coverslips. (**A-C**) lower resolution. (**D,E**) higher resolution. (**F**) zoomed in image to show representation adipocyte containing lipid droplets. Images were taken using a Zeiss Axiovert 10. (**A-C**) scale bar = 65μm. (**D,E**) scale bar = 40μm.

One 6-well plate was then supplied with an adipogenic induction media to induce differentiation and another 6-well plate was supplied with the normal DMEM cell culture media. After 2 days of incubation and before the cells were immunofluorescently stained for PPARγ, observations of lipid droplet accumulation in the cells were made. They showed a certain degree of differentiation in the untreated cultures (Figures 3.2A-C), but a much higher proportion of cells differentiating in those with adipogenic medium (Figures 3.2D-F).

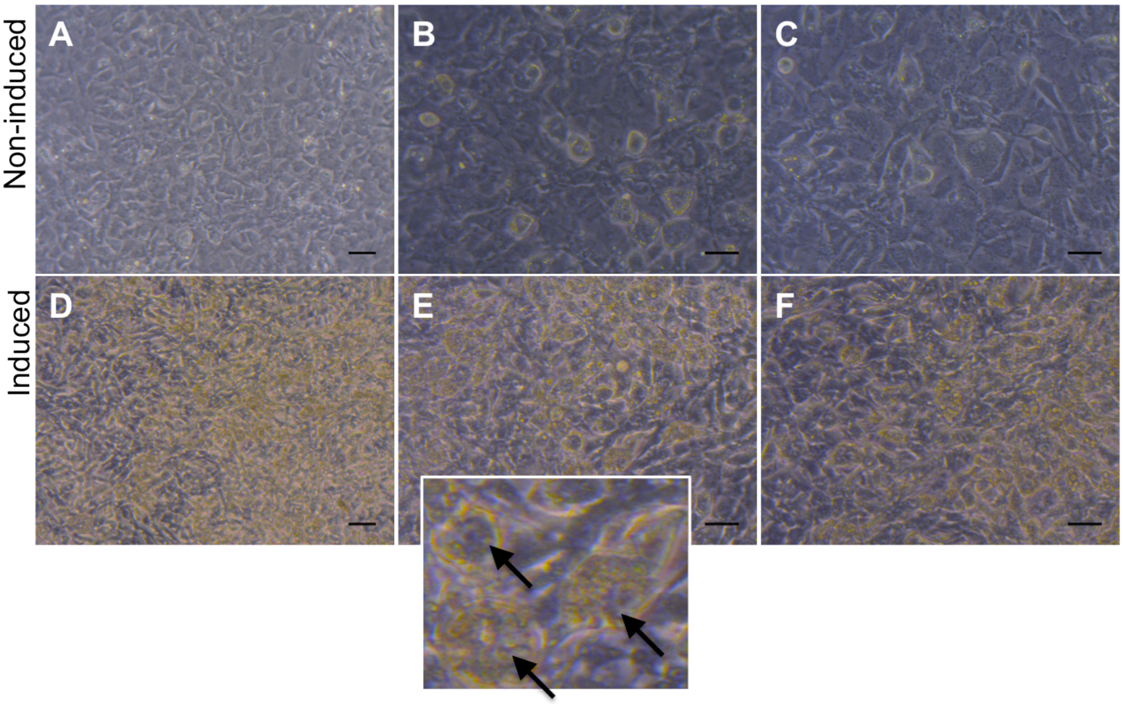

Figure 3.2: **Images of 3T3 F442A cells in culture after the change of culture media.** (**A-C**) not induced to differentiate. (**D-F**) induced to differentiate. Arrows label adipocytes. Images were taken using a Zeiss Axiovert 10. (**A,D**) scale bar = 65μm. (**B,C,E,F**) scale bar = 40μm.

The cells were fixed for staining from 2 days after addition of adipogenic medium. Some wells were left for 10 days to show that the cells fully differentiated into terminal adipocytes. Cells that were stained with oil red O to show the presence of lipids in the cells revealed a substantial amount of red coloration implicating successful differentiation of the cells (Figure 3.3). Visualisation of the individual cells was not easy because of the degree of confluence.

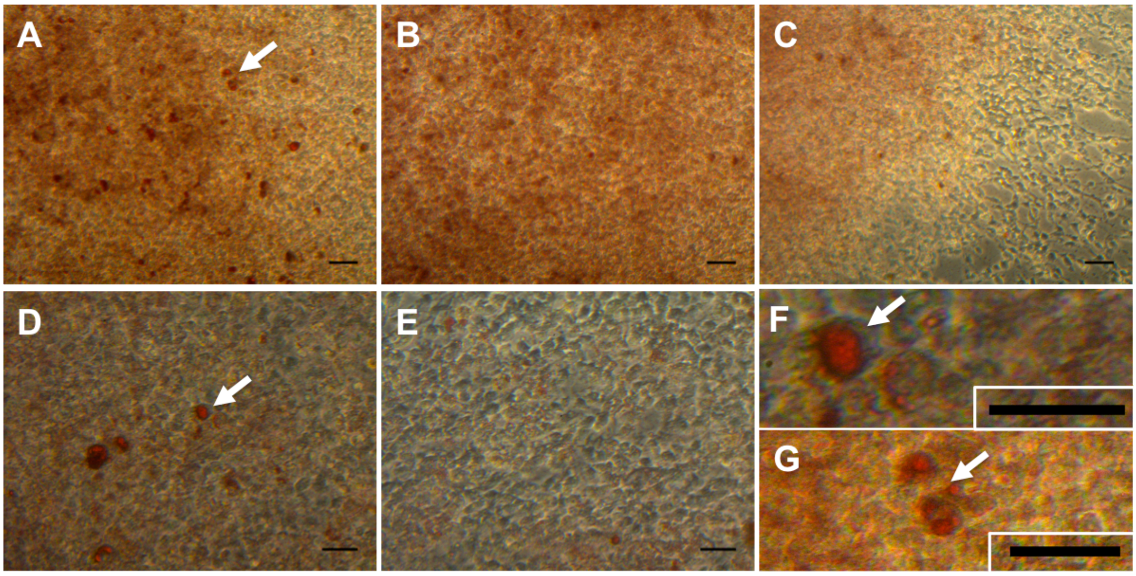

Figure 3.3: **Oil red O analysis of 3T3 F442A cells after 10 days in culture.** (**A-C**) lower resolution. (**D,E**) higher resolution. (**F,G**) magnified image to show lipid droplets that have been stained red. Images were taken using a Zeiss Axiovert 10. (**A-C,G**) scale bar = 65μm. (**D-F**) scale bar = 40μm.

3.3.2. In vitro versus in vivo Immunofluorescent Staining of PPARγ

The role and timing of PPARγ involvement in adipogenesis *in vitro* is well documented. Thus PPARγ immunofluorescent staining of the 3T3-F442A *in vitro* cell line was conducted with the aim of evaluating the working capabilities of five different primary antibodies of PPARγ, prior to investigating its activities *in vivo.* Cells were induced to differentiate into adipocytes using adipogenic medium and after 2 days were stained for PPARγ expression. Other cells were left in culture without being induced to differentiate to control the effects of the adipogenic medium. Negative controls using no antibody binding to PPARγ, but only the fluorescent secondary antibody were conducted to show the level of background staining present and thus help determine a positive result.

The antibody, PPARγ B-5 from Santa Cruz was observed to stain the cultured 3T3 cells which had been induced to differentiate, but labelling revealed general background staining and was not specific to cell nuclei (Figure 3.4). Similarly in the non-induced cultures, the staining was clearly not nuclear (Figure 3.5) in that the blue nuclear stain, DAPI, did not correspond with the green fluorescence of the PPARγ antibody. Therefore it was decided that this antibody would be of no use for studying adipogenesis in developing mouse back skin *in vivo*.

The next antibody investigated was a polyclonal antibody against PPARγ2 from Bioaffinity Reagents. As represented in Figure 3.6 this revealed a high degree of positive nuclear expression though interestingly more so in the cultured cells that had not been incubated with adipogenic medium (Figure 3.7). There was however a lot of background cytoplasmic staining with this antibody. This was not the case for the PPARγ E-8 antibody from Santa Cruz (Figure 3.8) which revealed clear nuclear staining of cells in differentiation medium, though not in every nucleus which is to be expected as not all the cells turn into adipocytes simultaneously. When the cells in normal medium were stained with this antibody (Figure 3.9), far fewer had positively stained nuclei. Lipid-droplets were observed in both the induced and non-induced 3T3 cells left in culture for longer than 2 days, which suggests that some of the cells spontaneously differentiate.

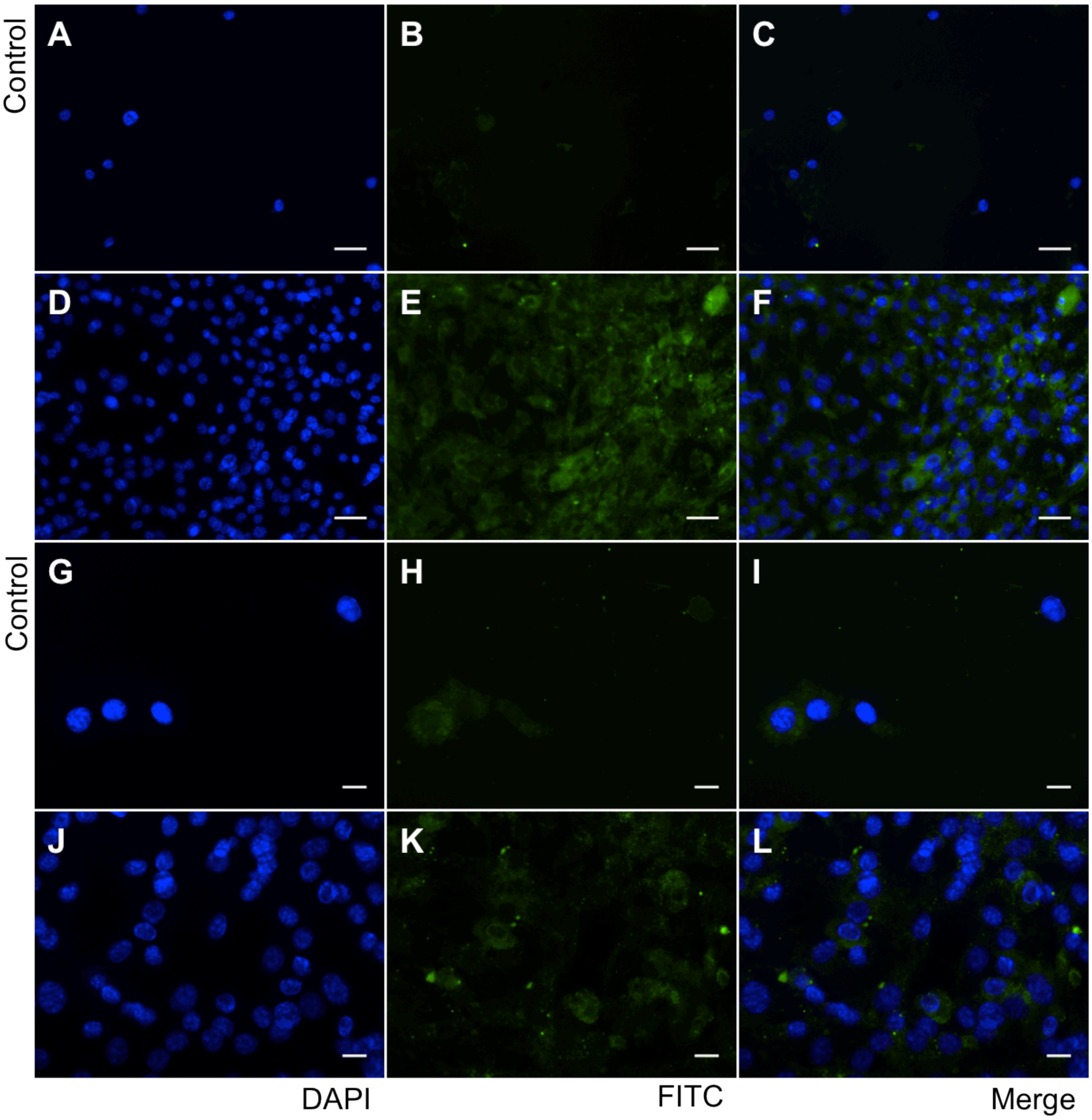

<u>Figure 3.4:</u> Analysis of PPARγ B-5 (Santa Cruz) expression in 3T3 F442A cells induced to differentiate. Adherent cells stained with an antibody against PPARγ and counterstained with DAPI. From left to right; DAPI, FITC, and merge (DAPI/FITC). FITC represents the fluorescent labelling of PPARγ. (**A-C,G-I**) Controls showing no fluorescently labelled PPARγ expression. (**D-F,J-L**) labelled using PPARγ primary antibody. Fluorescent images were taken using a Zeiss Axio Imager M1. (**A-F**) scale bar = 40μm. (**G-L**) scale bar = 15μm.

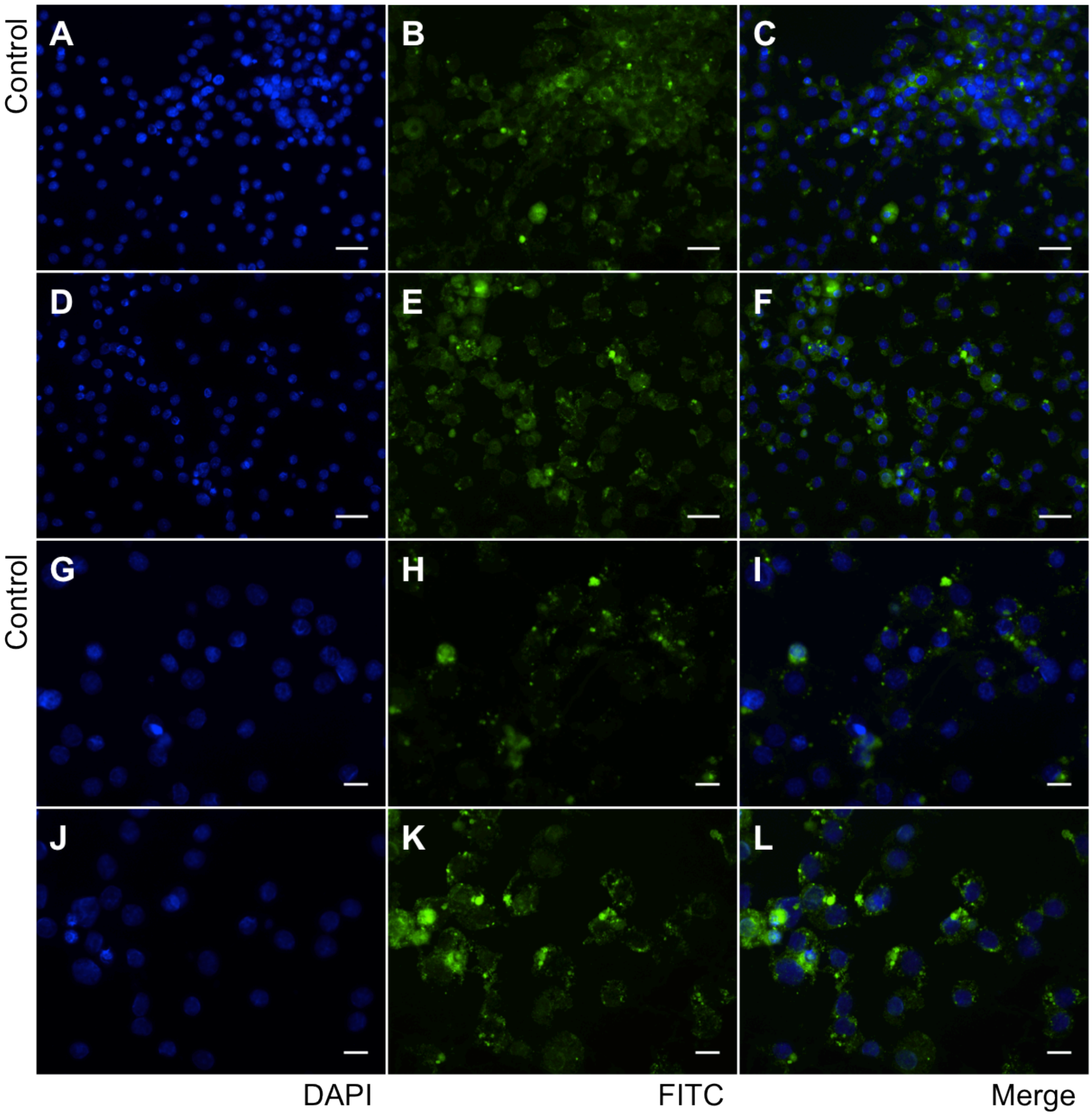

Figure 3.5: Analysis of PPARγ B-5 (Santa Cruz) expression in 3T3 F442A cells not induced to differentiate. Adherent cells stained with an antibody against PPARγ and counterstained with DAPI. From left to right; DAPI, FITC, and merge (DAPI/FITC). FITC represents the fluorescent labelling of PPARγ. (**A-C**,**G-I**) Controls showing no fluorescently labelled PPARγ expression. (**D-F**,**J-L**) labelled using PPARγ primary antibody. Fluorescent images were taken using a Zeiss Axio Imager M1. (**A-F**) scale bar = 40μm. (**G-L**) scale bar = 15μm.

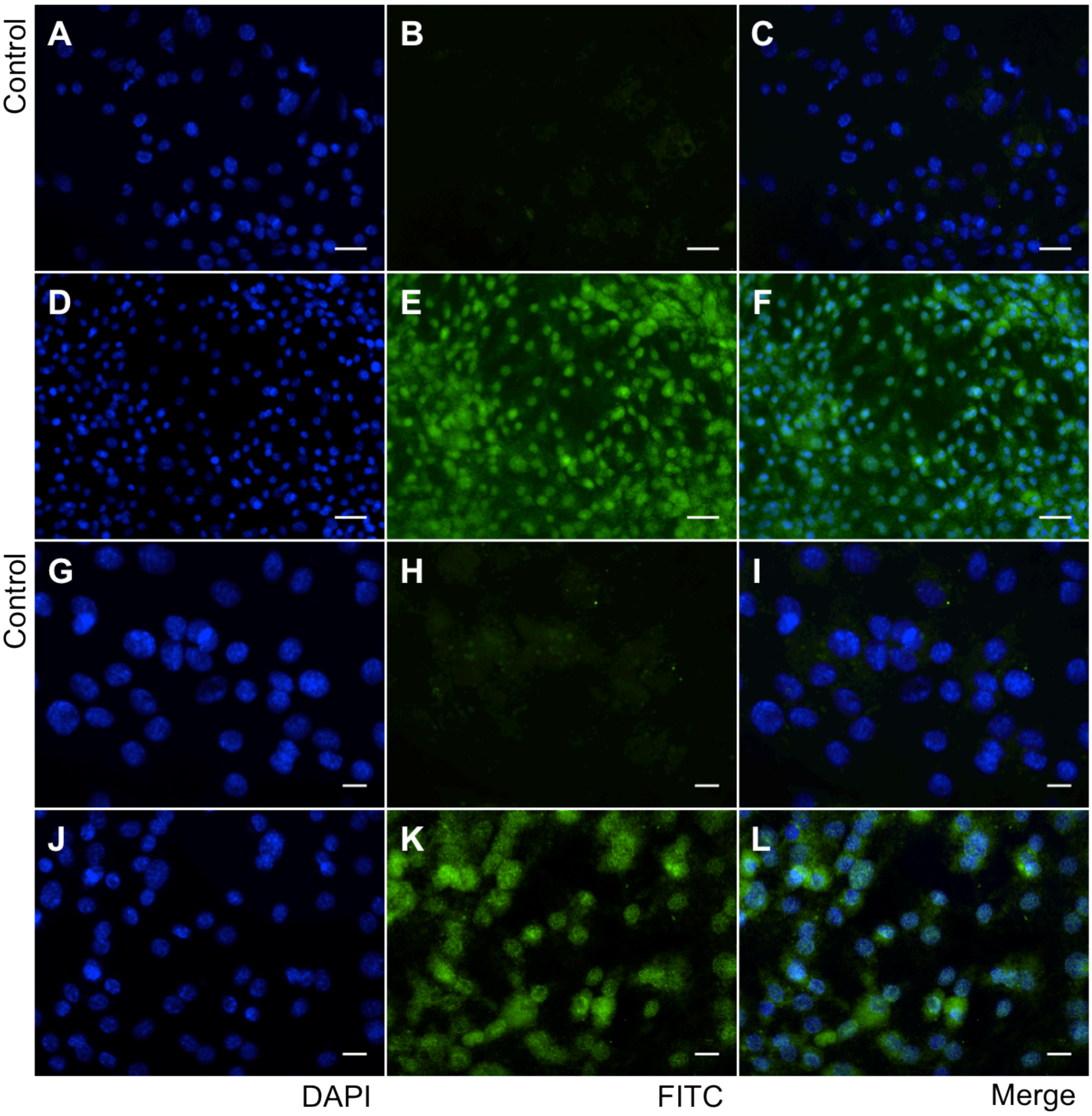

Figure 3.6: Analysis of PPARγ2 (Affinity Bioreagents) expression in 3T3 F442A cells induced to differentiate. Adherent cells stained with an antibody against PPARγ and counterstained with DAPI. From left to right; DAPI, FITC, and merge (DAPI/FITC). FITC represents the fluorescent labelling of PPARγ. (**A-C,G-I**) Controls showing no fluorescently labelled PPARγ expression. (**D-F,J-L**) labelled using PPARγ primary antibody. Fluorescent images were taken using a Zeiss Axio Imager M1. (**A-F**) scale bar = 40μm. (**G-L**) scale bar = 15μm.

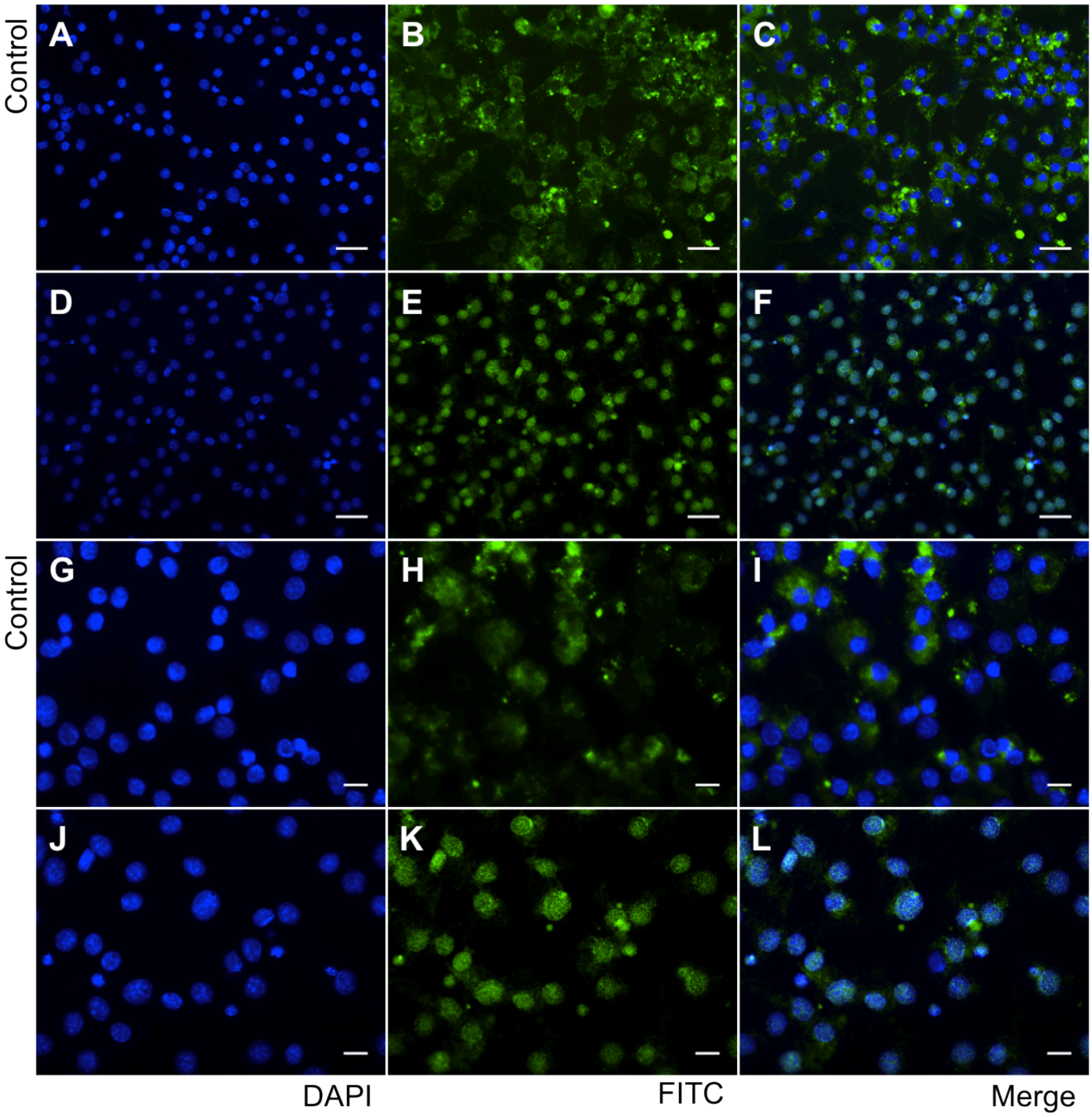

Figure 3.7: Analysis of PPARγ2 (Affinity Bioreagents) expression in 3T3 F442A cells not induced to differentiate. Adherent cells stained with an antibody against PPARγ and counterstained with DAPI. From left to right; DAPI, FITC, and merge (DAPI/FITC). FITC represents the fluorescent labelling of PPARγ. (**A-C,G-I**) Controls showing no fluorescently labelled PPARγ expression. (**D-F,J-L**) labelled using PPARγ primary antibody. Fluorescent images were taken using a Zeiss Axio Imager M1. (**A-F**) scale bar = 40μm. (**G-L**) scale bar = 15μm.

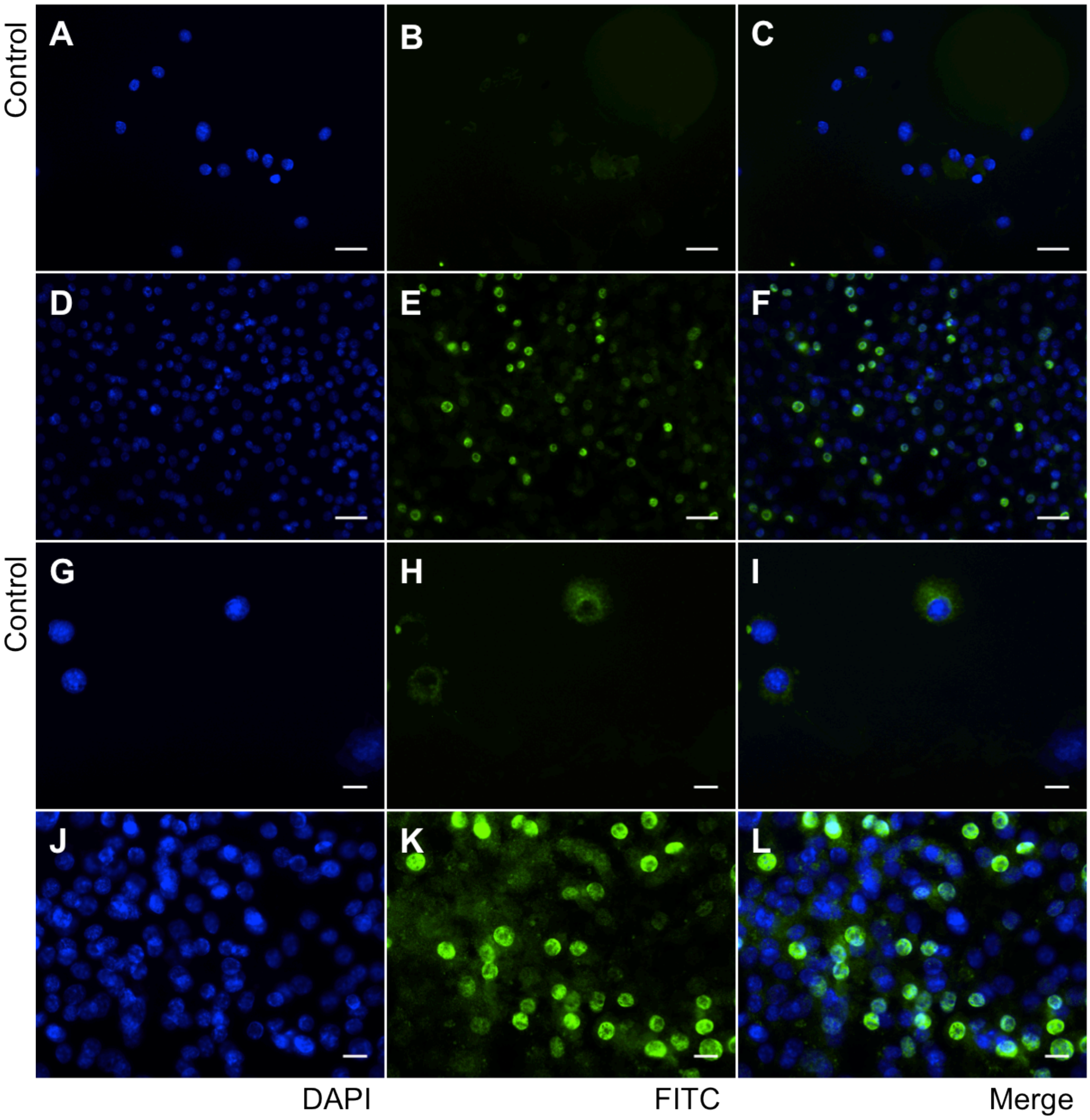

Figure 3.8: Analysis of PPARγ E-8 (Santa Cruz) expression in 3T3 F442A cells induced to differentiate. Adherent cells stained with an antibody against PPARγ and counterstained with DAPI. From left to right; DAPI, FITC, and merge (DAPI/FITC). FITC represents the fluorescent labelling of PPARγ. (**A-C,G-I**) Controls showing no fluorescently labelled PPARγ expression. (**D-F,J-L**) labelled using PPARγ primary antibody. Fluorescent images were taken using a Zeiss Axio Imager M1. (**A-F**) scale bar = 40µm. (**G-L**) scale bar = 15µm.

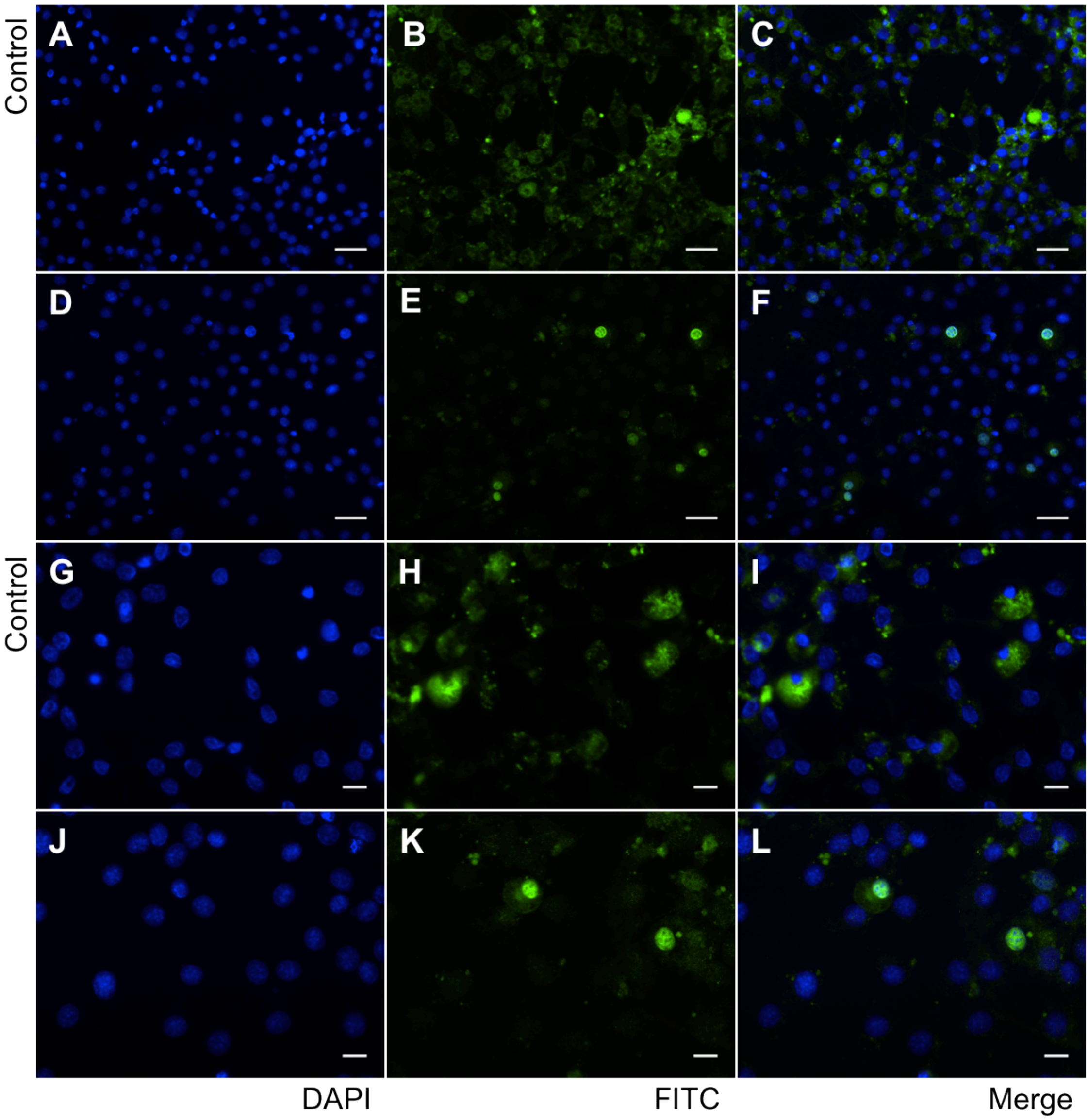

Figure 3.9: Analysis of PPARγ E-8 (Santa Cruz) expression in 3T3 F442A cells not induced to differentiate. Adherent cells stained with an antibody against PPARγ and counterstained with DAPI. From left to right; DAPI, FITC, and merge (DAPI/FITC). FITC represents the fluorescent labelling of PPARγ. (**A-C,G-I**) Controls showing no fluorescently labelled PPARγ expression. (**D-F,J-L**) labelled using PPARγ primary antibody. Fluorescent images were taken using a Zeiss Axio Imager M1. (**A-F**) scale bar = 40μm. (**G-L**) scale bar = 15μm.

The results found using the two PPARγ primary antibodies from Affinity Bioreagents and Santa Cruz (Number E-8) were deemed positive and these two antibodies were subsequently used to further investigate PPARγ expression *in vivo*.

With the knowledge that PPARγ has been found expressed postnatally (Rotman et al. 2006), back skin from 4 day-old newborn mice was first immunofluorescently stained with both antibodies. While *in vitro* there was positive nuclear staining for PPARγ, there was little to suggest positive expression *in vivo*. Some staining was observed in the upper dermis, though it was difficult to tell if this was nuclear (Figure 3.10). Hair follicles appeared to be stained throughout, although more strongly in the upper dermis. At a higher magnification (Figure 3.11) there was little evidence of labelling in the lower dermal cells surrounding the follicles where adipocytes are present or developing. This staining was repeated with the same results.

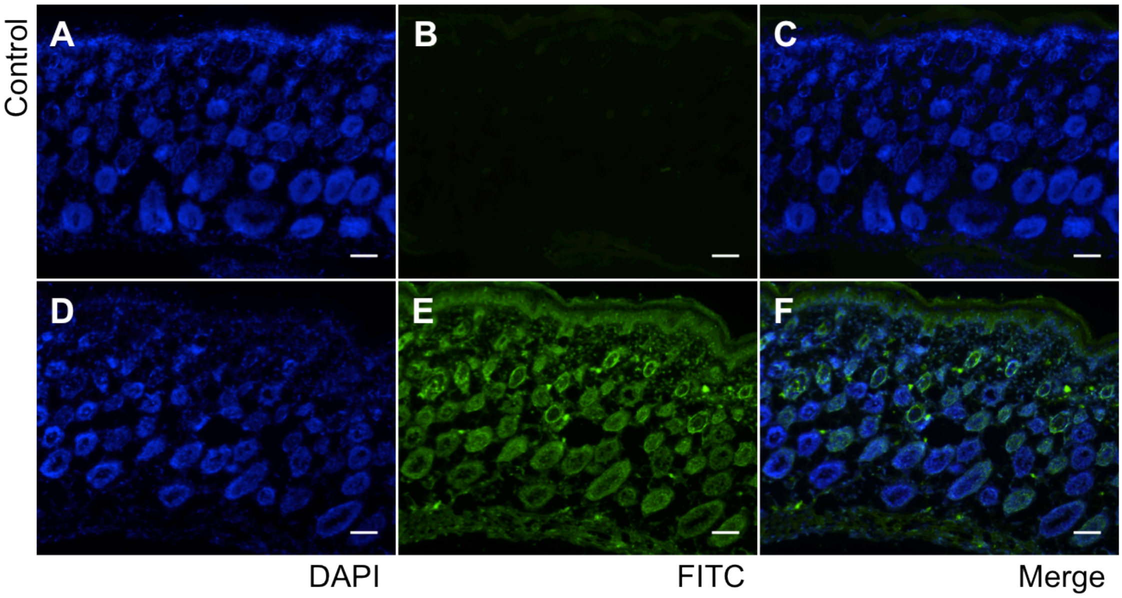

Figure 3.10: Analysis of PPARγ2 (Affinity Bioreagents) expression in 4-day newborn mouse back skin. Sections cut at 7μm, stained with an antibody against PPARγ and counterstained with DAPI. From left to right; DAPI, FITC, and merge (DAPI/FITC). FITC represents the fluorescent labelling of PPARγ. (**A-C**) Controls showing no fluorescently labelled PPARγ expression. (**D-F**) labelled using PPARγ primary antibody. Fluorescent images were taken using a Zeiss Axio Imager M1. Scale bar = 65μm.

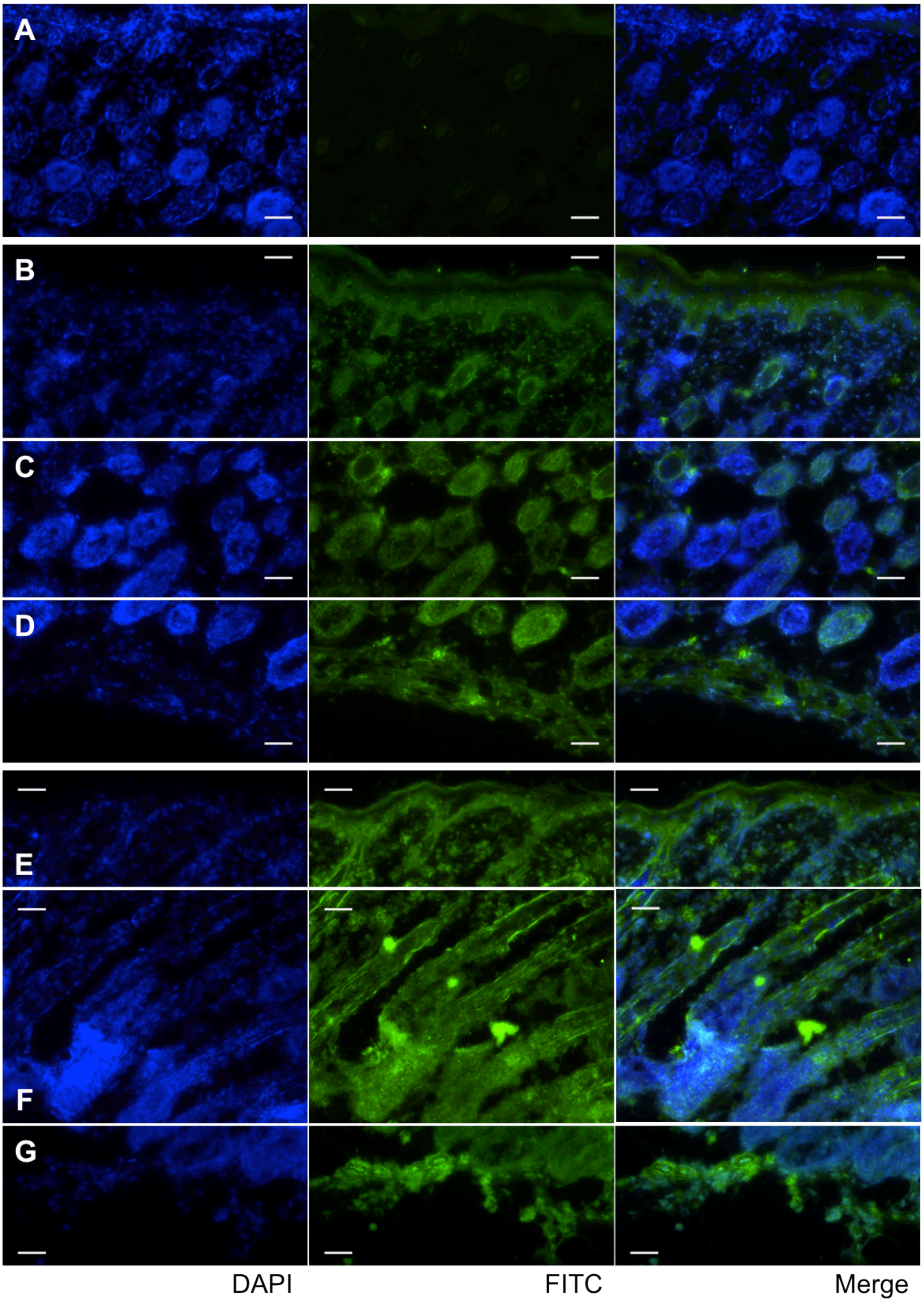

Figure 3.11: Analysis of PPARγ2 (Affinity Bioreagents) expression in 4-day newborn mouse back skin (different view). Sections cut at 7μm, stained with an antibody against PPARγ and counterstained with DAPI. From left to right; DAPI, FITC, and merge (DAPI/FITC). FITC represents the fluorescent labelling of PPARγ. (**A**) Control showing no fluorescently labelled PPARγ expression. (**B-G**) labelled using PPARγ primary antibody, showing two different views of the follicles through the skin sections. Fluorescent images were taken using a Zeiss Axio Imager M1. Scale bar = 40μm.

The Santa Cruz (PPARγ E-8) antibody was a mouse monoclonal, so a mouse on mouse kit (MOM) was used to stain 4-day newborn skin sections to prevent staining of endogenous mouse immunoglobulins. Some controls without using the MOM kit were also conducted to observe its effectiveness. Without the MOM kit fluorescent analysis of both PPARγ in the skin and the negative controls using only the fluorescent secondary antibody (Figure 3.12) showed non-specific staining throughout the skin and no obvious nuclear staining of adipocytes. Comparatively, with the MOM kit (Figure 3.13), the PPARγ staining showed what appeared to be some more specific staining, though the negative controls without primary antibody incubation also exhibited a similar pattern. Therefore, it was not deemed reliable positive staining for PPARγ.

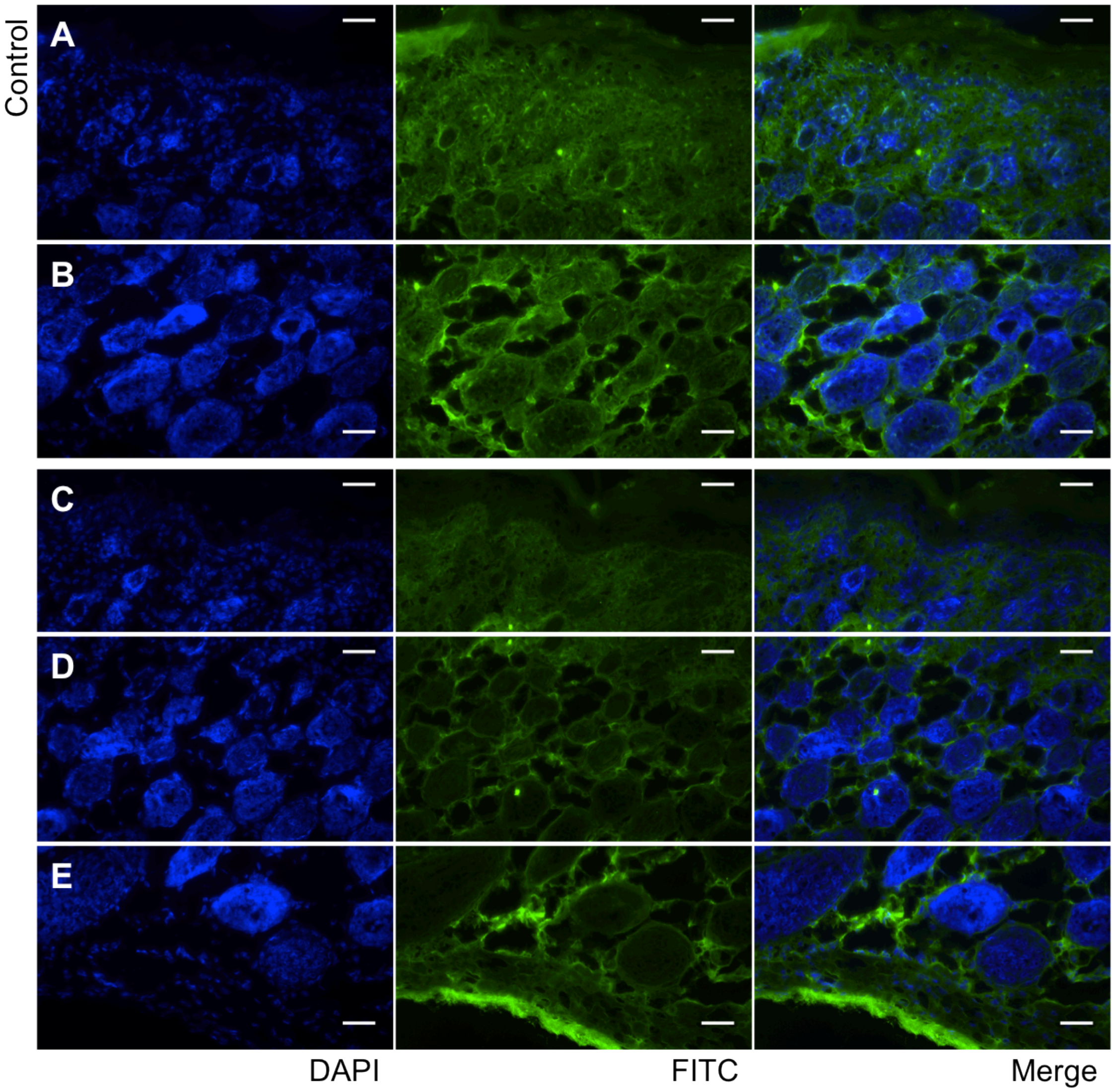

Figure 3.12: Analysis of PPARγ E-8 (Santa Cruz) expression in 4-day newborn mouse back skin without using the MOM kit. Sections cut at 7μm, stained with an antibody against PPARγ and counterstained with DAPI. From left to right; DAPI, FITC, and merge (DAPI/FITC). FITC represents the fluorescent labelling of PPARγ. (**A,B**) Control showing no fluorescently labelled PPARγ expression, 2 images to represent upper and lower levels of the skin. (**C-E**) labelled using PPARγ primary antibody, 3 images top to bottom show the different levels through the skin. Fluorescent images were taken using a Zeiss Axio Imager M1. Scale bar = 40μm.

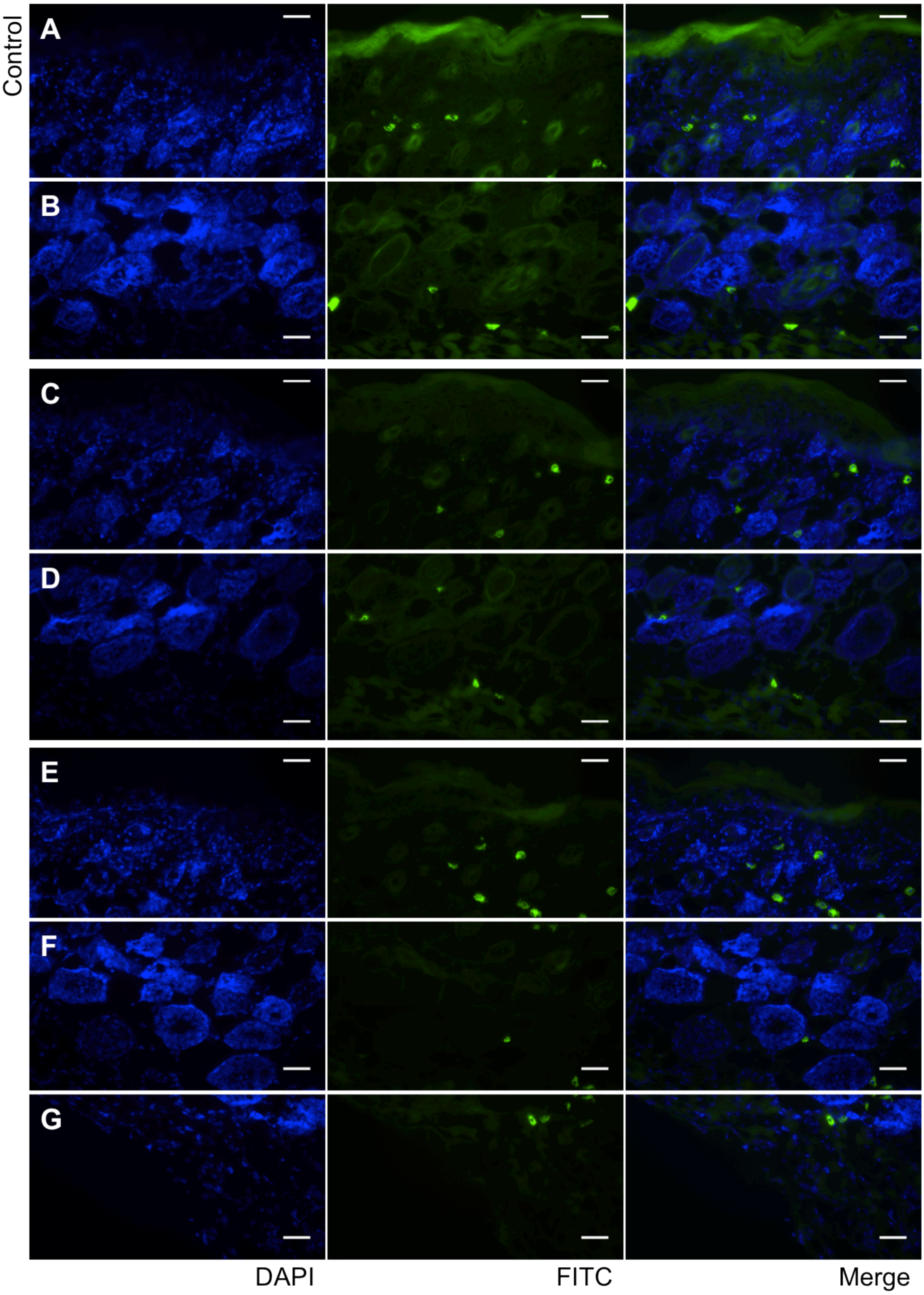

Figure 3.13: **Analysis of PPARγ E-8 (Santa Cruz) expression in 4-day newborn mouse back skin using a MOM kit.** Sections cut at 7μm, stained with an antibody against PPARγ and counterstained with DAPI. From left to right; DAPI, FITC, and merge (DAPI/FITC). FITC represents the fluorescent labelling of PPARγ. (**A,B**) Control showing no fluorescently labelled PPARγ expression, 2 images to represent upper and lower levels of the skin. (**C-G**) labelled using PPARγ primary antibody, showing two different views and the different skin levels. Fluorescent images were taken using a Zeiss Axio Imager M1. Scale bar = 40μm.

Due to the non-specific staining in mouse skin, the PPARγ E-8 (Santa Cruz) antibody was tested in rat skin as well. Late embryonic rat skin from 18.5 days was available and at this point early adipocytes are present and developing in the skin. The results illustrated in Figure 3.14, show a speckled distribution of staining (Figures 3.14D, E and F). However, cells that appeared to be positively labelled in the FITC fluorescent images, when combined with the DAPI staining did not appear to show nuclear marking, though the labelling did differ from the negative control (Figures 3.14A-C).

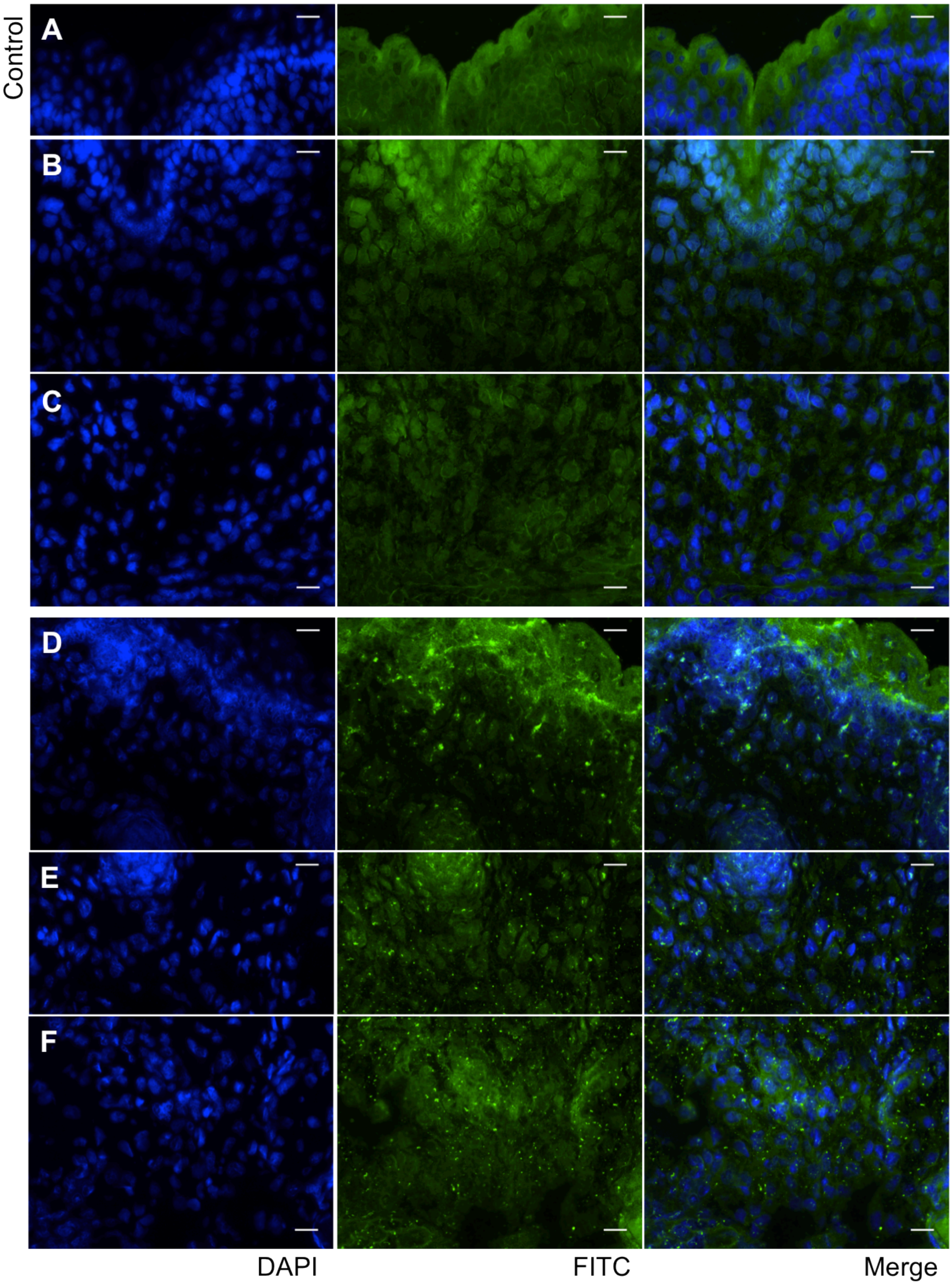

Figure 3.14: **Analysis of PPARγ E-8 (Santa Cruz) expression in 18.5-day embryonic rat back skin.** Sections cut at 7μm, stained with an antibody against PPARγ and counterstained with DAPI. From left to right; DAPI, FITC, and merge (DAPI/FITC). FITC represents the fluorescent labelling of PPARγ. (**A-C**) Control showing no fluorescently labelled PPARγ expression, 2 images to represent upper and lower levels of the skin. (**D-F**) labelled using PPARγ primary antibody, 3 images top to bottom show the different levels through the skin. Fluorescent images were taken using a Zeiss Axio Imager M1. Scale bar = 40μm.

Both *in vitro* and *in vivo* analysis of the three anti-PPARγ primary antibodies – Santa Cruz B-5, Santa Cruz E-8 and Affinity Bioreagents – were not found to be sufficiently reliable, because of the contrasts between them. Two further different antibodies for PPARγ were then investigated in order to find an antibody that could be deemed reliable *in vivo*.

Firstly, an antibody from Abcam was tested in 3T3 F442A cells induced to differentiate into adipocytes. This showed some staining in a proportion of the cells as would be expected as not all the cells will be undergoing differentiation, however it is not limited to the nuclei of the cells (Figure 3.15). Cells that were not in adipogenic medium showed background staining of the cell cytoplasm, but not the nuclei (Figure 3.16), more so than the cells induced to differentiate.

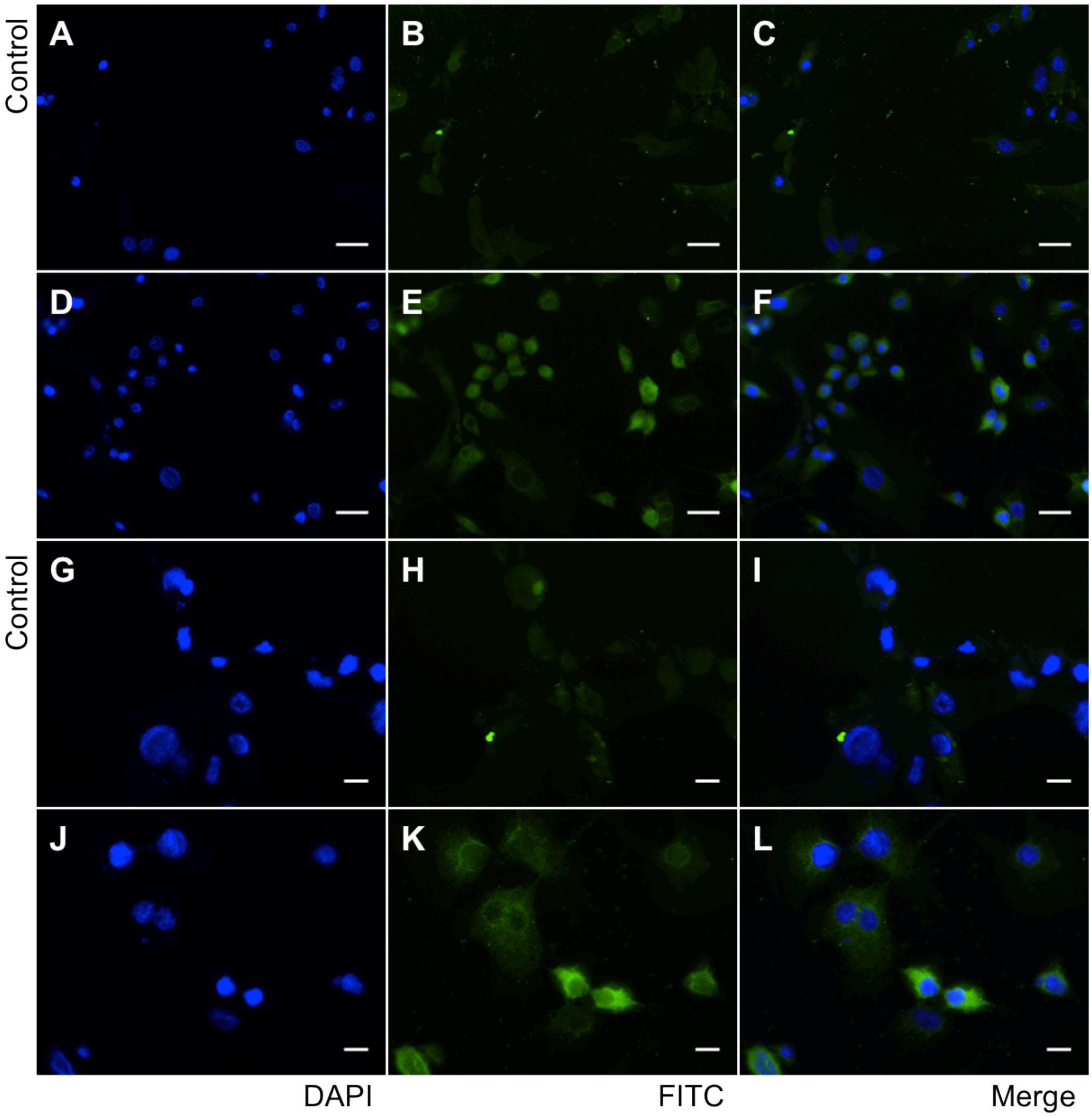

Figure 3.15: Analysis of PPARγ (Abcam) expression in 3T3 F442A cells induced to differentiate. Cells grown on coverslips were stained with an antibody against PPARγ and counterstained with DAPI. From left to right; DAPI, FITC, and merge (DAPI/FITC). FITC represents the fluorescent labelling of PPARγ. (**A-C,G-I**) Controls showing no fluorescently labelled PPARγ expression. (**D-F,J-L**) labelled using PPARγ primary antibody. Fluorescent images were taken using a Zeiss Axio Imager M1. (**A-F**) scale bar = 40μm. (**G-L**) scale bar = 15μm.

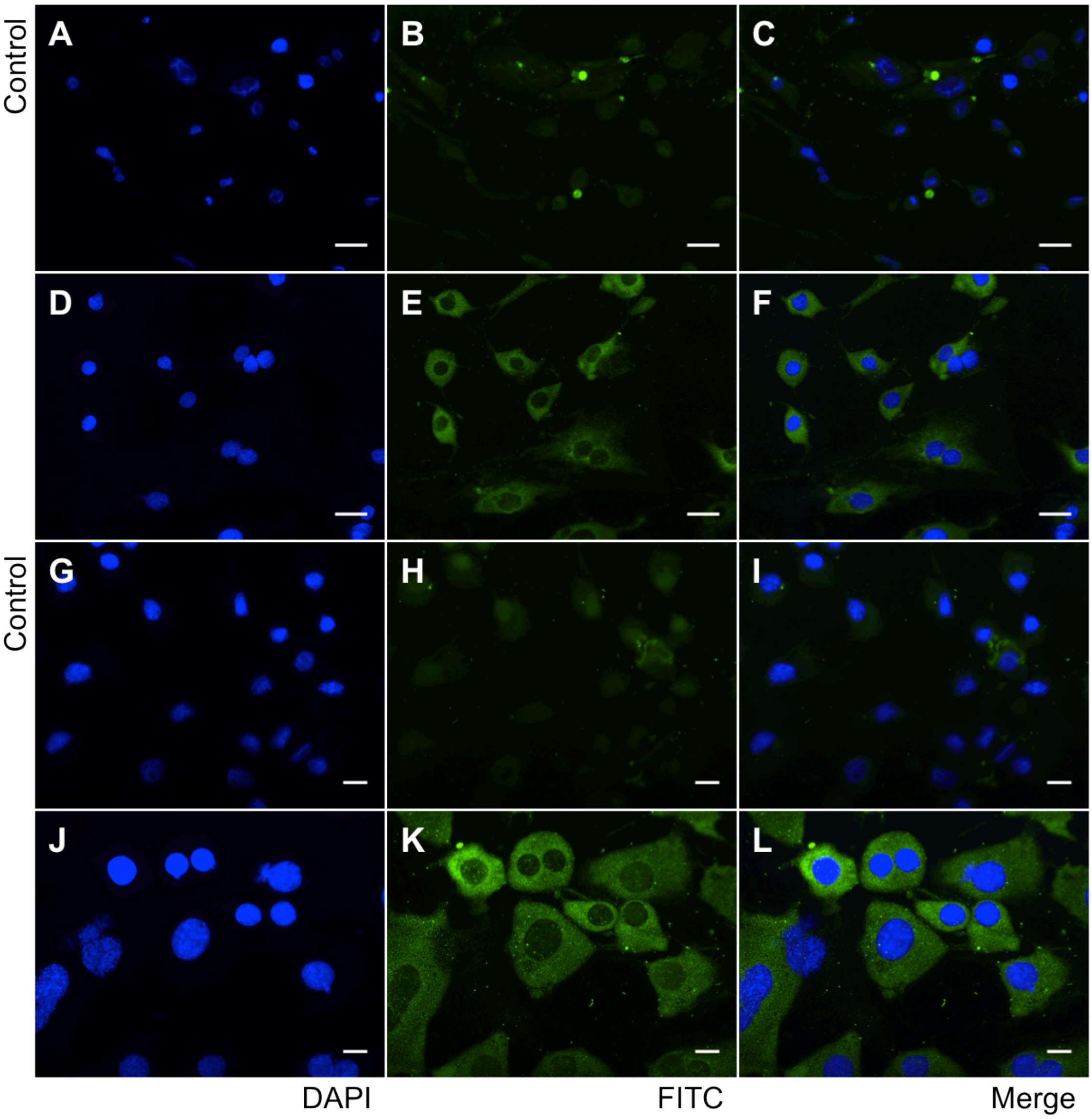

Figure 3.16: Analysis of PPARγ (Abcam) expression in 3T3 F442A cells not induced to differentiate. Cells grown on coverslips were stained with an antibody against PPARγ and counterstained with DAPI. From left to right; DAPI, FITC, and merge (DAPI/FITC). FITC represents the fluorescent labelling of PPARγ. (**A-C,G-I**) Controls showing no fluorescently labelled PPARγ expression. (**D-F,J-L**) labelled using PPARγ primary antibody. Fluorescent images were taken using a Zeiss Axio Imager M1. (**A-F**) scale bar = 40μm. (**G-L**) scale bar = 15μm.

This antibody (Abcam) was then used to investigate PPARγ expression *in vivo* using mouse back skin of a variety of ages, both embryonic and postnatal (e14.5, e16.5, e18.5, 1dN and 3dN). These results are illustrated in figures 3.14-3.18. At both postnatal day 1 (Figure 3.17 and day 3 (Figure 3.18), the basal layer of the epidermis and cells at the periphery of hair follicles were positive for PPARγ, more so after 1 day than 3 days. There was no evidence of any positive PPARγ labelling in cells of the lower dermis. In comparison the controls displayed little background staining, suggesting that the basal epidermal layer was genuinely positive for PPARγ, though this was not nuclear staining (Figures 3.17E and K and Figure 3.18H).

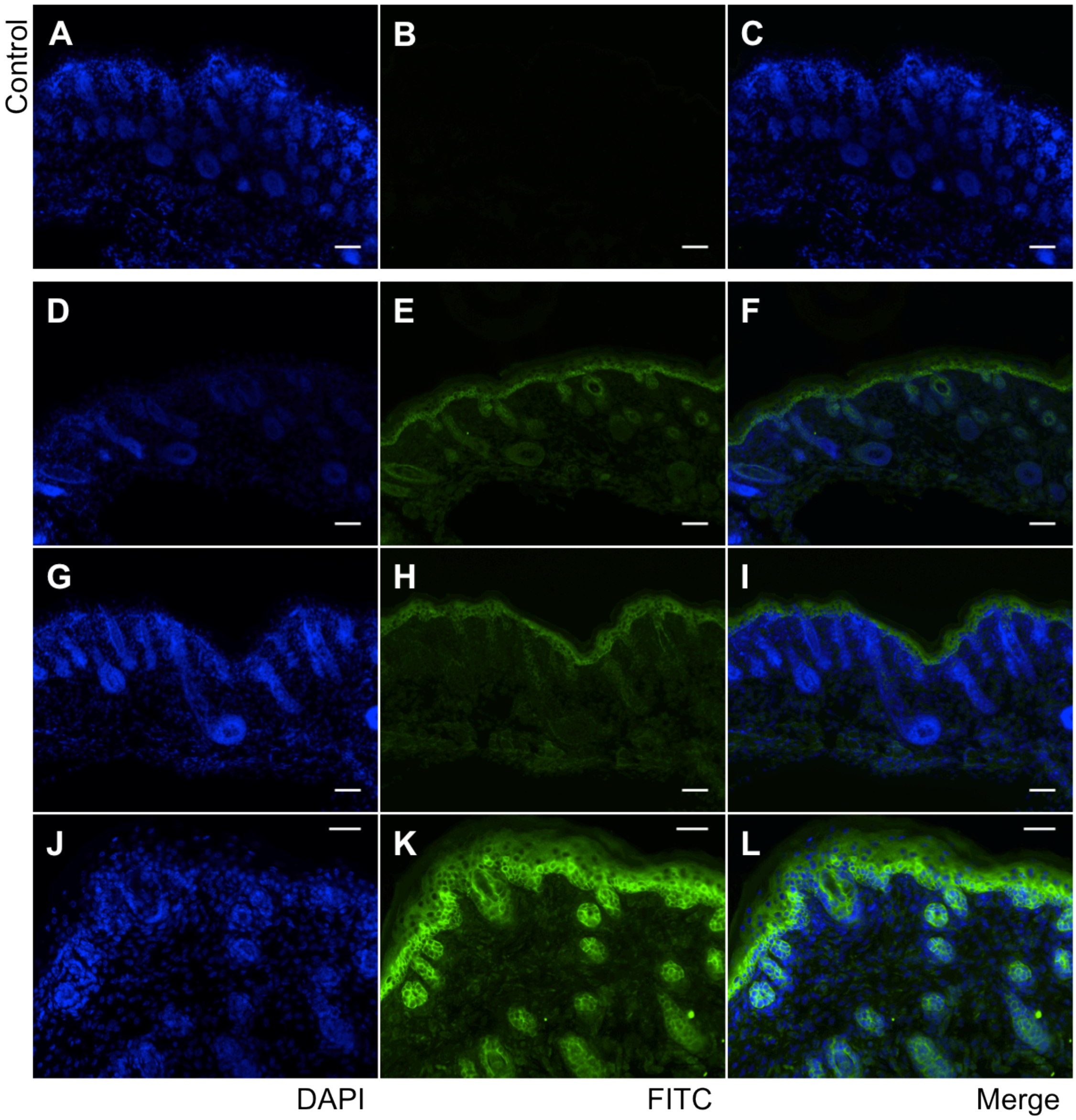

<u>Figure 3.17:</u> Analysis of PPARγ (Abcam) expression in 1-day postnatal mouse back skin. Sections were cut at 7μm and stained with an antibody against PPARγ (Abcam) and counterstained with DAPI. From left to right; DAPI, FITC, and merge (DAPI/FITC). FITC represents the fluorescent labelling of PPARγ. (**A-C**) Control showing no fluorescently labelled PPARγ expression. (**D-L**) labelled using PPARγ primary antibody, showing two different views of the hair follicles. Fluorescent images were taken using a Zeiss Axio Imager M1. (**A-I**) scale bar = 65m. (**J-L**) scale bar = 40μm.

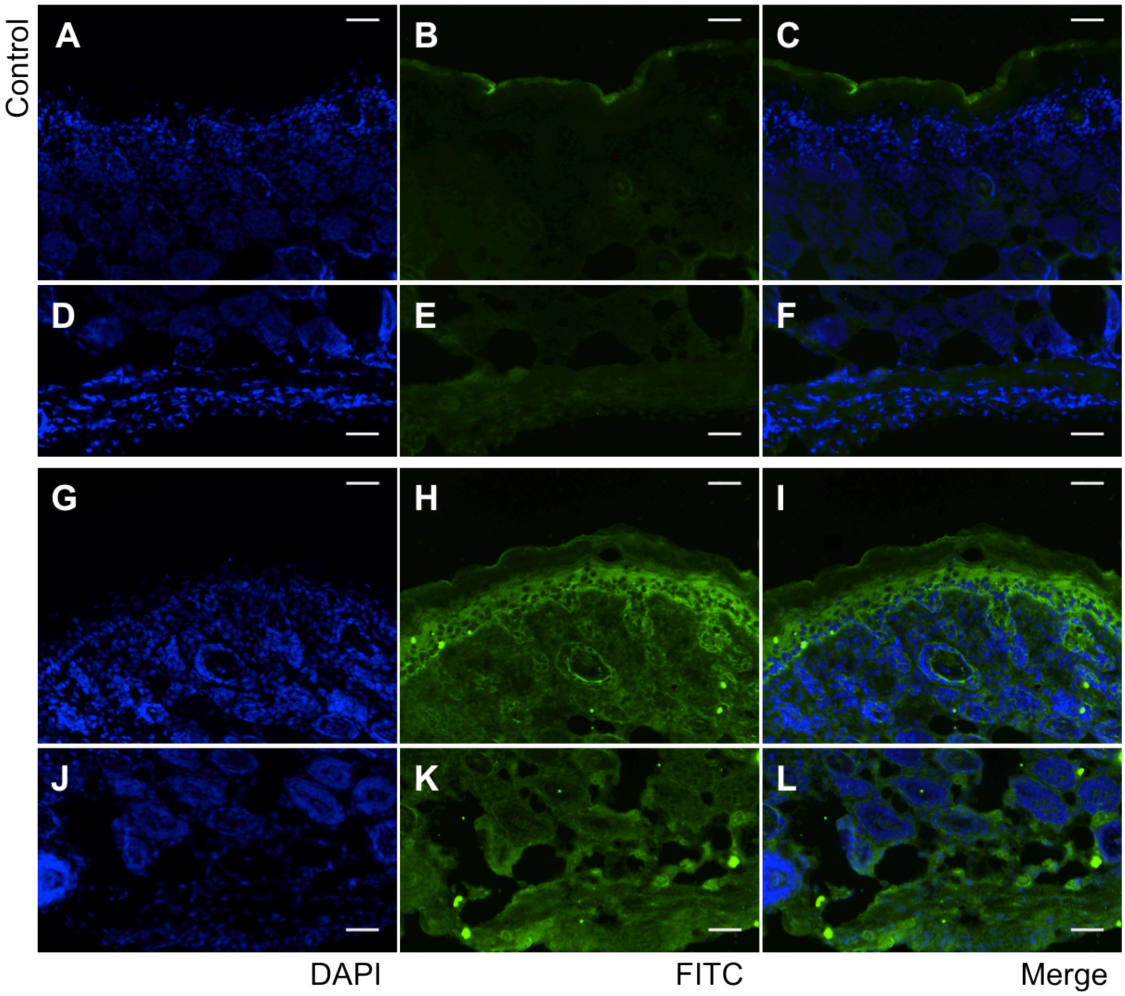

Figure 3.18: Analysis of PPARγ (Abcam) expression in 3--day postnatal mouse back skin. Sections were cut at 7μm and stained with an antibody against PPARγ (Abcam) and counterstained with DAPI. From left to right; DAPI, FITC, and merge (DAPI/FITC). FITC represents the fluorescent labelling of PPARγ. (**A-F**) Controls showing no fluorescently labelled PPARγ expression, 2 images to represent upper and lower levels of the skin. (**G-L**) labelled using PPARγ primary antibody, 2 images to represent upper and lower levels of the skin. Fluorescent images were taken using a Zeiss Axio Imager M1. Scale bar = 40μm.

In younger skin, little staining was seen at 14.5 days though at e16.5 and clearly at 18.5 days, the basal epidermal layer was clearly stained with bright fluorescence (Figures 3.20 and 3.21) in the same pattern seen postnatally (Figures 3.17 and 3.18). By e18.5 there was also some staining present in the developing follicles, reflecting the newborn picture. However there was no evidence of nuclear staining in cells of the lower dermis, where adipocytes develop.

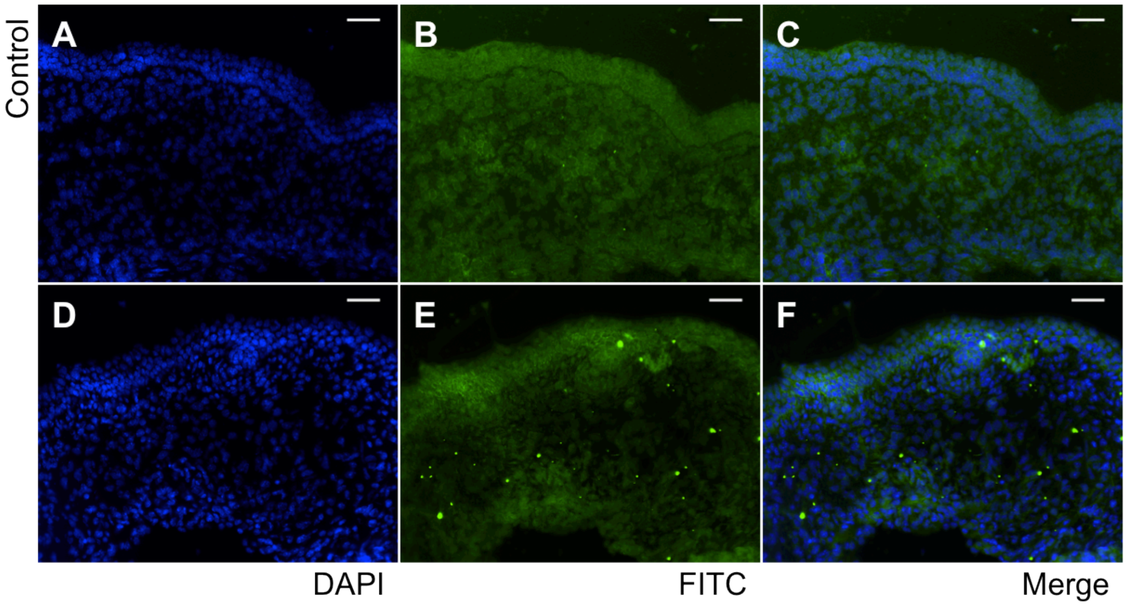

Figure 3.19: **Analysis of PPARγ (Abcam) expression in 14.5-day embryonic mouse back skin.** Sections were cut at 7μm and stained with an antibody against PPARγ (Abcam) and counterstained with DAPI. From left to right; DAPI, FITC, and merge (DAPI/FITC). FITC represents the fluorescent labelling of PPARγ. (**A-C**) Controls showing no fluorescently labelled PPARγ expression. (**D-F**) labelled using PPARγ primary antibody. Fluorescent images were taken using a Zeiss Axio Imager M1. Scale bar = 40μm.

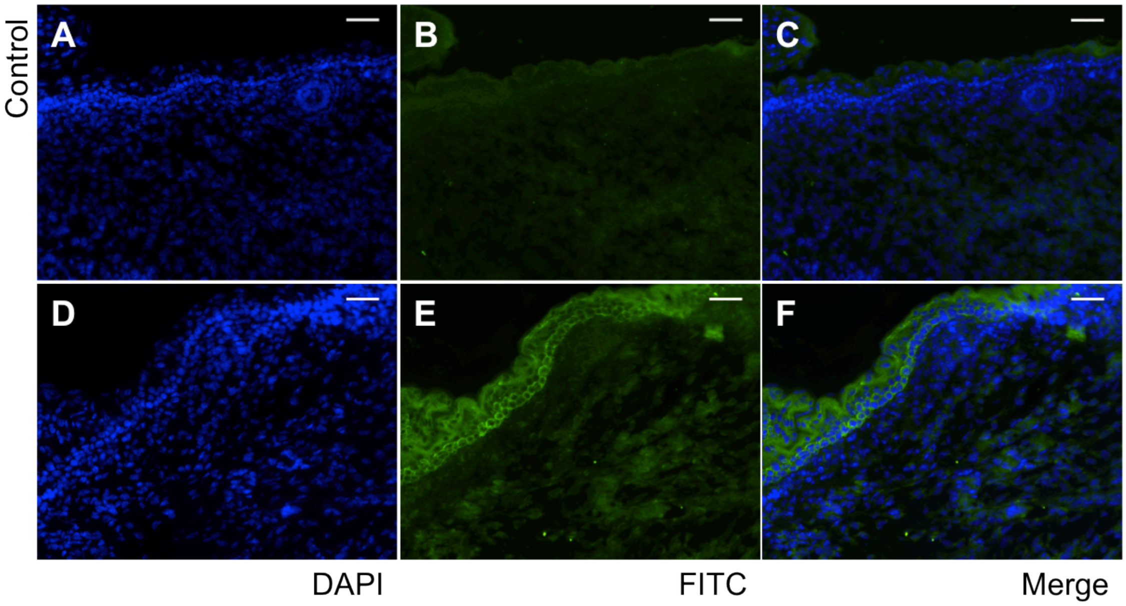

Figure 3.20: **Analysis of PPARγ (Abcam) expression in 16.5-day embryonic mouse back skin.** Sections were cut at 7μm and stained with an antibody against PPARγ (Abcam) and counterstained with DAPI. From left to right; DAPI, FITC, and merge (DAPI/FITC). FITC represents the fluorescent labelling of PPARγ. (**A-C**) Controls showing no fluorescently labelled PPARγ expression. (**D-F**) labelled using PPARγ primary antibody. Fluorescent images were taken using a Zeiss Axio Imager M1. Scale bar = 40μm.

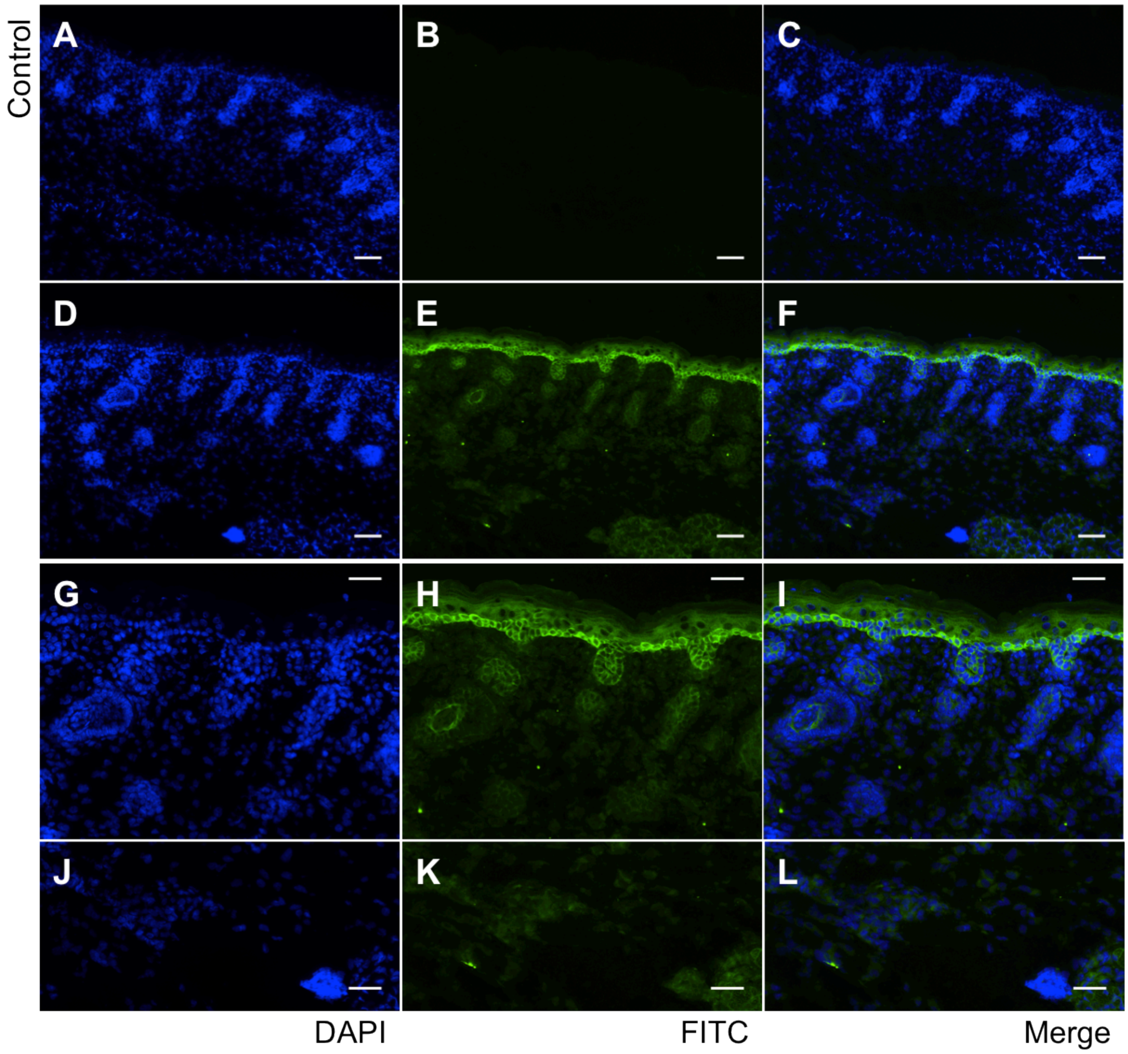

Figure 3.21: Analysis of PPARγ (Abcam) expression in 18.5-day embryonic mouse back skin. Sections were cut at 7μm and stained with an antibody against PPARγ (Abcam) and counterstained with DAPI. From left to right; DAPI, FITC, and merge (DAPI/FITC). FITC represents the fluorescent labelling of PPARγ. (**A-C**) Controls showing no fluorescently labelled PPARγ expression. (**D-L**) labelled using PPARγ primary antibody, showing a lower (**D-F**) and a higher (**G-L**) magnification. Fluorescent images were taken using a Zeiss Axio Imager M1. (**A-F**) scale bar = 65m. (**G-L**) scale bar = 40μm.

The fifth anti-PPARγ antibody was supplied by ABD Serotec. As this antibody had not previously been used for immunofluorescence on frozen sections before, it was first tried on the cultured 3T3 cells using two different fixation procedures, acetone and PFA. When the cells were fixed in acetone, both the induced and the non-induced 3T3 cells showed evidence of nuclear PPARγ staining (Figures 3.22 and 3.24). However, when fixed with PFA, the cells only demonstrated cytoplasmic staining for both induced (Figure 3.23) and not induced (Figure 3.25) cultures. Some of the cells also appeared to have shrunk and become distorted during the fixation process (Figure 3.23).

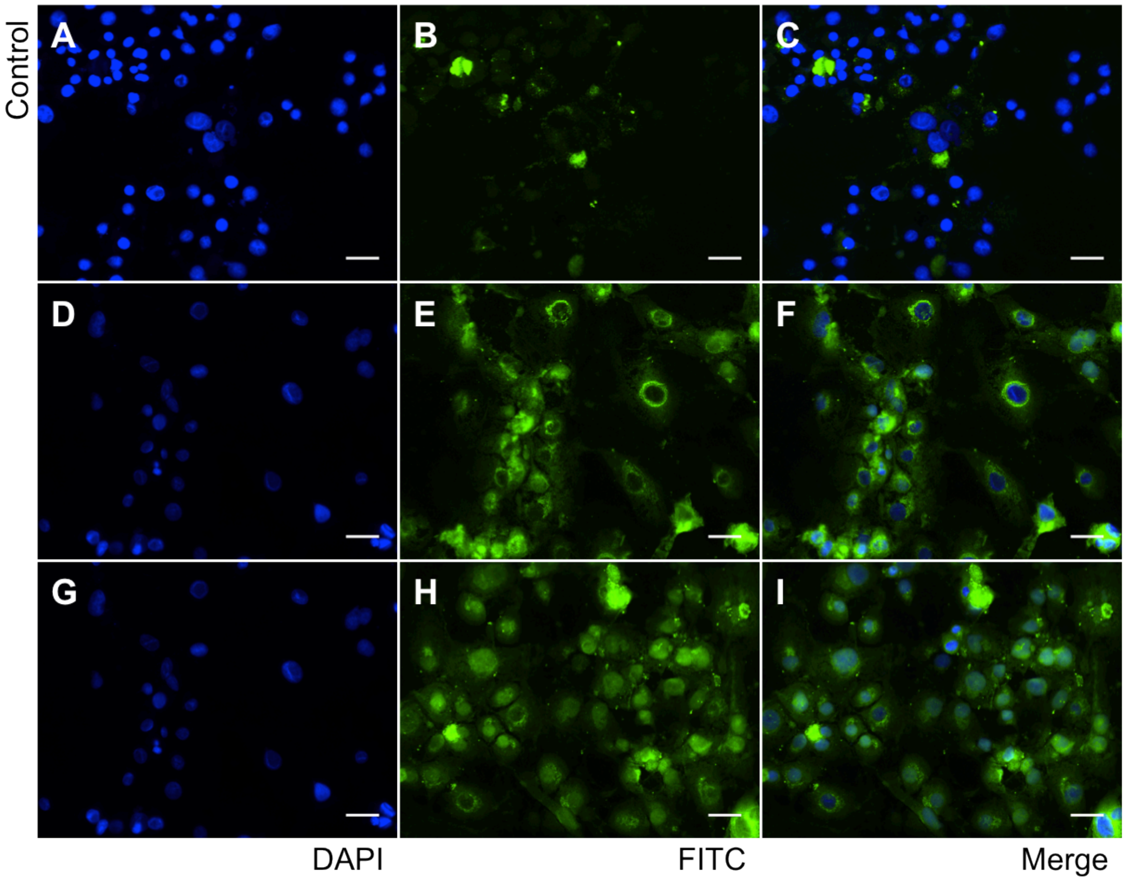

<u>Figure 3.22:</u> Analysis of PPARγ (Abd Serotec) expression in 3T3 F442A cells induced to differentiate and fixed in acetone. Adherent cells fixed with acetone and stained with an antibody against PPARγ (Abd Serotec) and counterstained with DAPI. From left to right; DAPI, FITC, and merge (DAPI/FITC). FITC represents the fluorescent labelling of PPARγ. (**A-C**) Controls showing no fluorescently labelled PPARγ expression. (**D-I**) labelled using PPARγ primary antibody. Fluorescent images were taken using a Zeiss Axio Imager M1. Scale bar = 40μm.

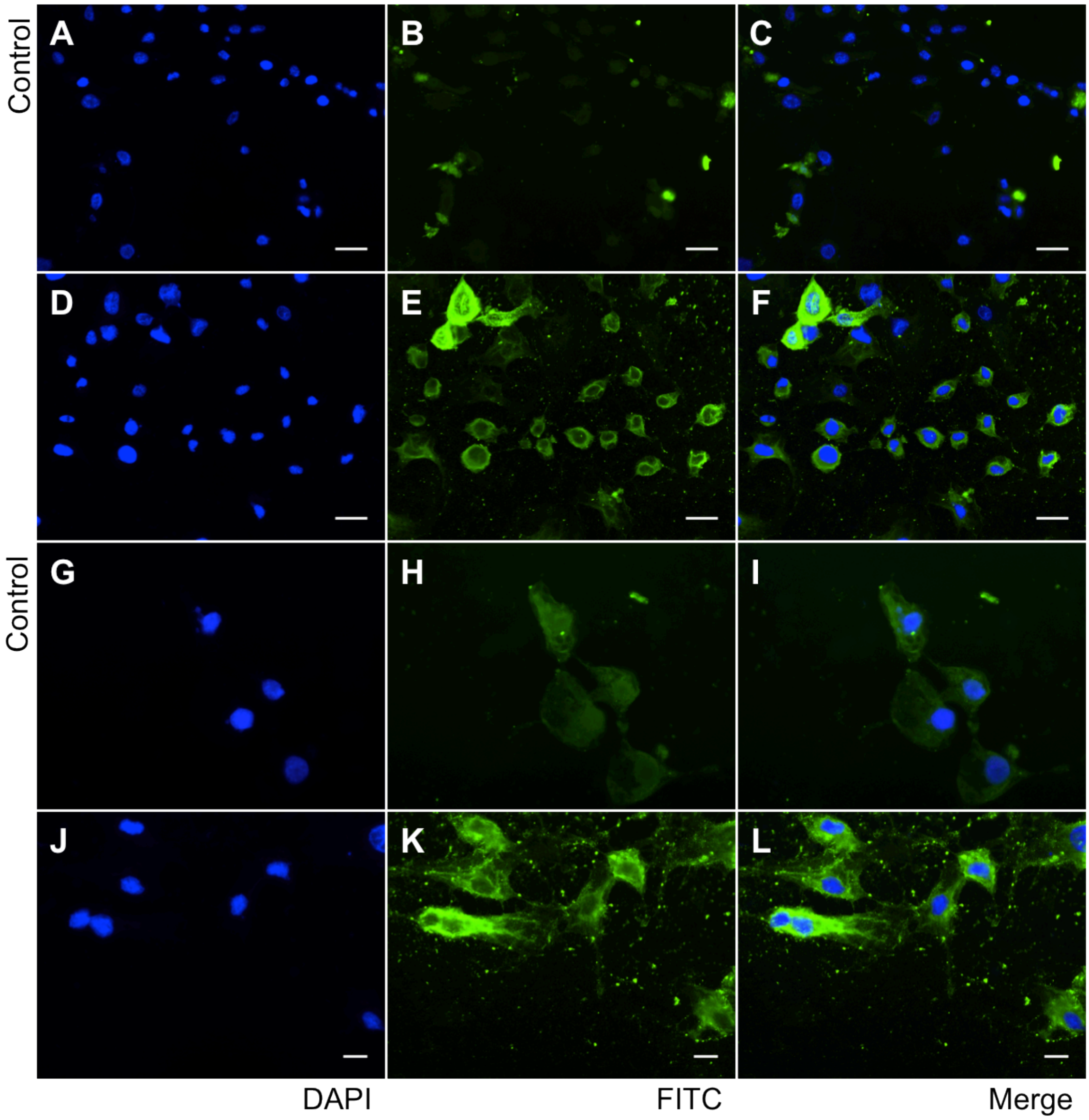

Figure 3.23: **Analysis of PPARγ (Abd Serotec) expression in 3T3 F442A cells induced to differentiate and fixed in PFA.** Adherent cells fixed with 4% PFA and stained with an antibody against PPARγ (Abd Serotec) and counterstained with DAPI. From left to right; DAPI, FITC, and merge (DAPI/FITC). FITC represents the fluorescent labelling of PPARγ. (**A-C**) Controls showing no fluorescently labelled PPARγ expression. (**D-I**) labelled using PPARγ primary antibody. Fluorescent images were taken using a Zeiss Axio Imager M1. (**A-F**) scale bar = 40μm. (**G-L**) scale bar = 15μm

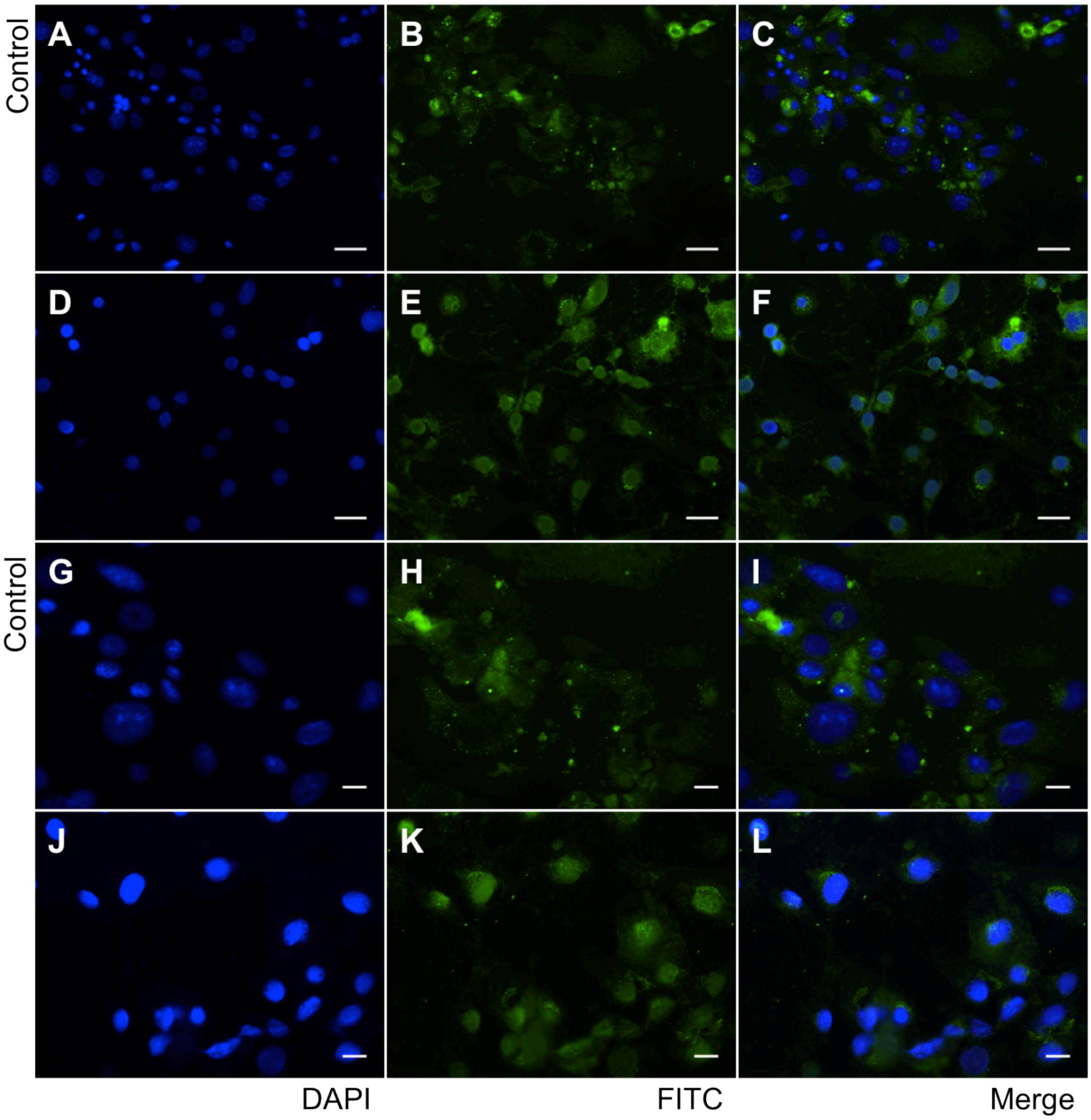

Figure 3.24: Analysis of PPARγ (Abd Serotec) expression in 3T3 F442A cells not induced to differentiate and fixed in acetone. Adhered cells fixed with acetone and stained with an antibody against PPARγ (Abd Serotec) and counterstained with DAPI. From left to right; DAPI, FITC, and merge (DAPI/FITC). FITC represents the fluorescent labelling of PPARγ. (**A-C**) Controls showing no fluorescently labelled PPARγ expression. (**D-I**) labelled using PPARγ primary antibody. Fluorescent images were taken using a Zeiss Axio Imager M1. (**A-F**) scale bar = 40μm. (**G-L**) scale bar = 15μm.

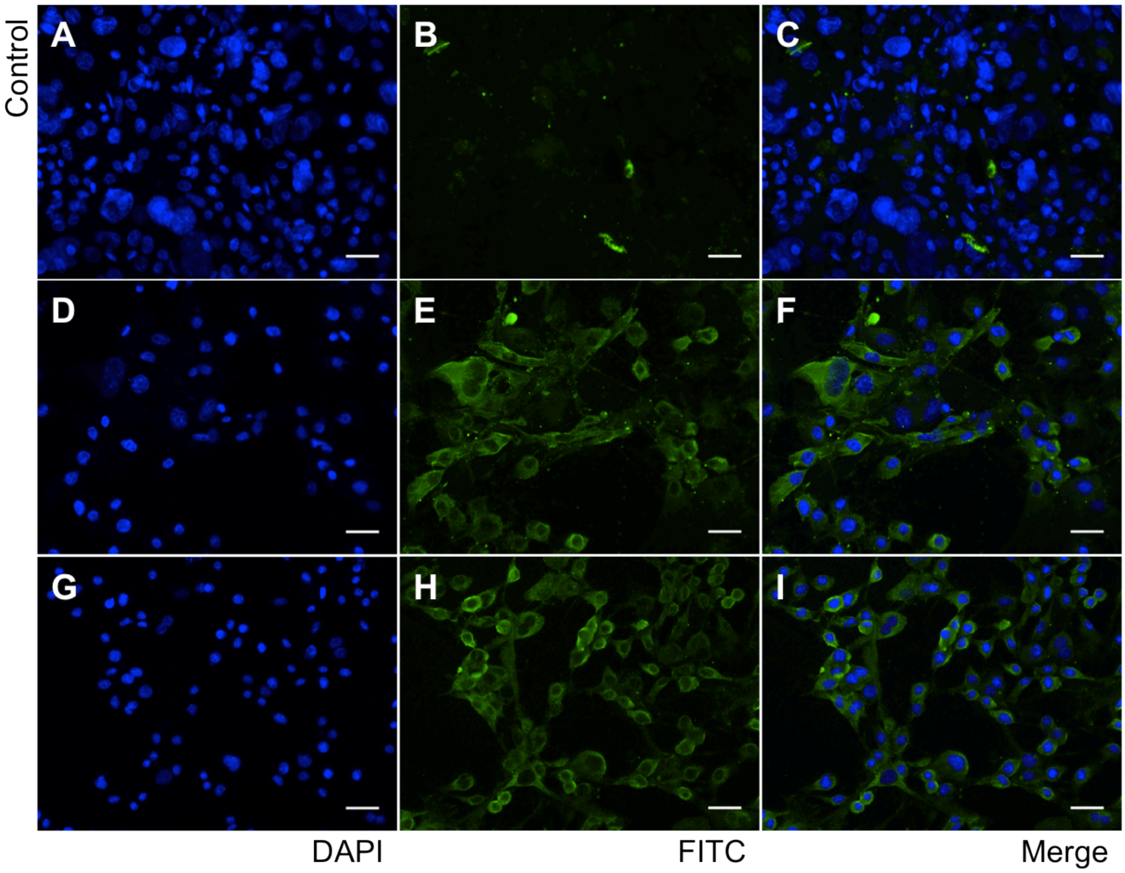

<u>Figure 3.25:</u> Analysis of PPARγ (Abd Serotec) expression in 3T3 F442A cells not induced to differentiate and fixed in PFA. Adherent cells fixed with 4% PFA and stained with an antibody against PPARγ (Abd Serotec) and counterstained with DAPI. From left to right; DAPI, FITC, and merge (DAPI/FITC). FITC represents the fluorescent labelling of PPARγ. (**A-C**) Controls showing no fluorescently labelled PPARγexpression. (**D-I**) labelled using PPARγ primary antibody. Fluorescent images were taken using a Zeiss Axio Imager M1. Scale bar = 40μm.

This anti- PPARγ antibody from Abd Serotec was then used to study PPARγ expression in embryonic and postnatal mouse back skin. Both acetone and PFA fixation techniques were used, as wells as a no fixation step. In the early embryonic ages, only even background staining of the skin was observed after protocols using either no fixation or acetone fixation (Figures 3.26 2 and 3 and Figure 3.27 1). When fixed in 4% PFA, some positive staining was found in the upper dermis (Figures 3.26 4 and 3.27 2). However, this did not coincide with the DAPI labelling and so did not represent nuclear expression. The same distribution in the upper dermis was seen with e18.5 (Figure 3.28) and 1 day newborn mouse back skin, after PFA fixation (Figure 3.29). By postnatal day 3, the positive staining was less obvious (Figure 3.30). Therefore, overall little specificity was identified in relation to the staining of PPARγ *in vivo.*

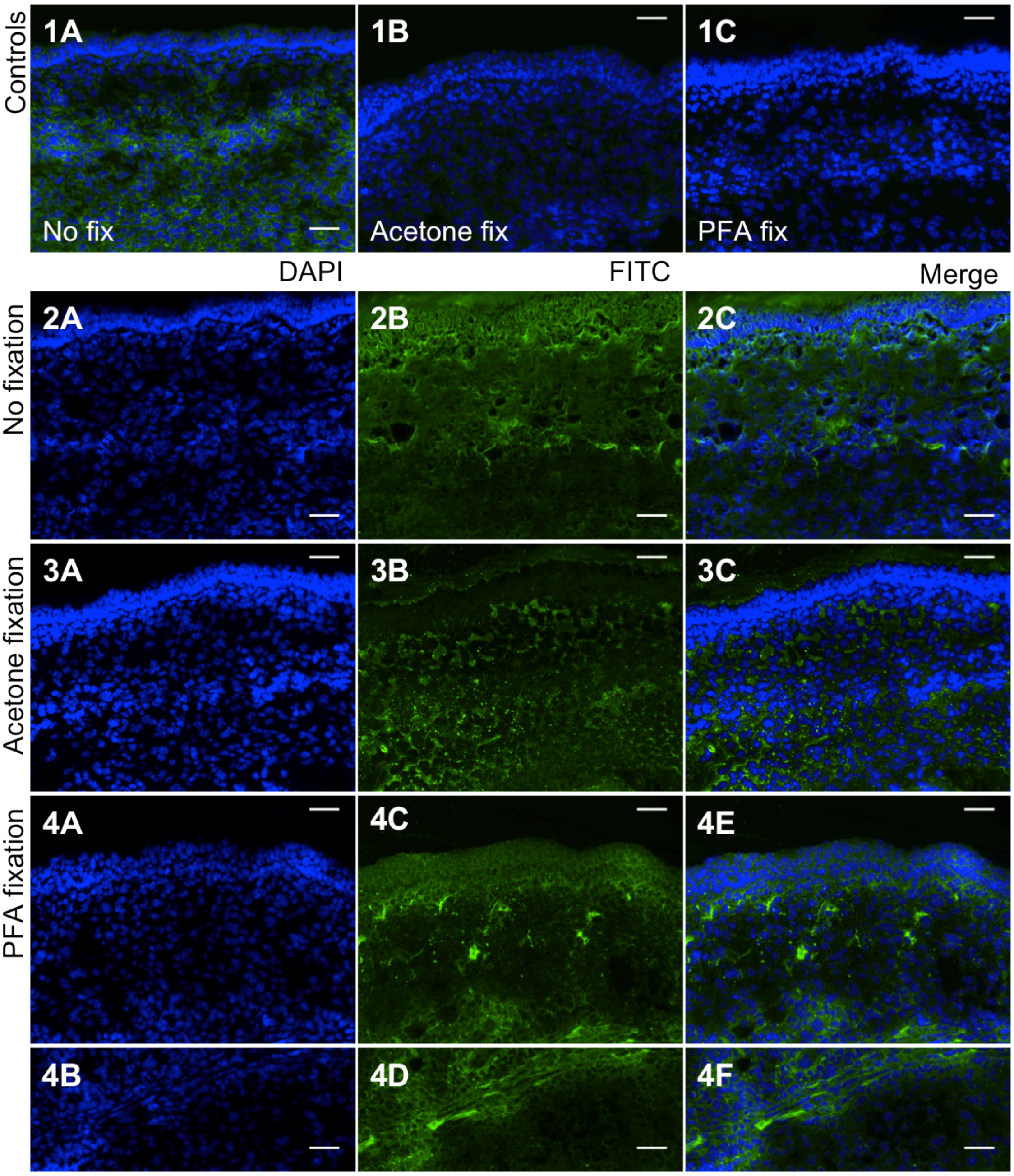

Figure 3.26: Analysis of PPARγ (Abd Serotec) expression in 14.5-day embryonic mouse back skin. Sections were cut at 7μm and stained with an antibody against PPARγ (Abd Serotec) and counterstained with DAPI. From left to right; DAPI, FITC, and merge (DAPI/FITC). FITC represents the fluorescent labelling of PPARγ. (**1A-C**) Controls showing 3 merged images with no fluorescently labelled PPARγ expression. (**1A**,**2**) No fixation step. (**1B**,**3**) Fixed in acetone. (**1C**,**4**) Fixed in 4% PFA. (**4A, B**) Upper and lower views of the skin. (**2-4**) labelled using PPARγ primary antibody. Fluorescent images were taken using a Zeiss Axio Imager M1. Scale bar = 40μm.

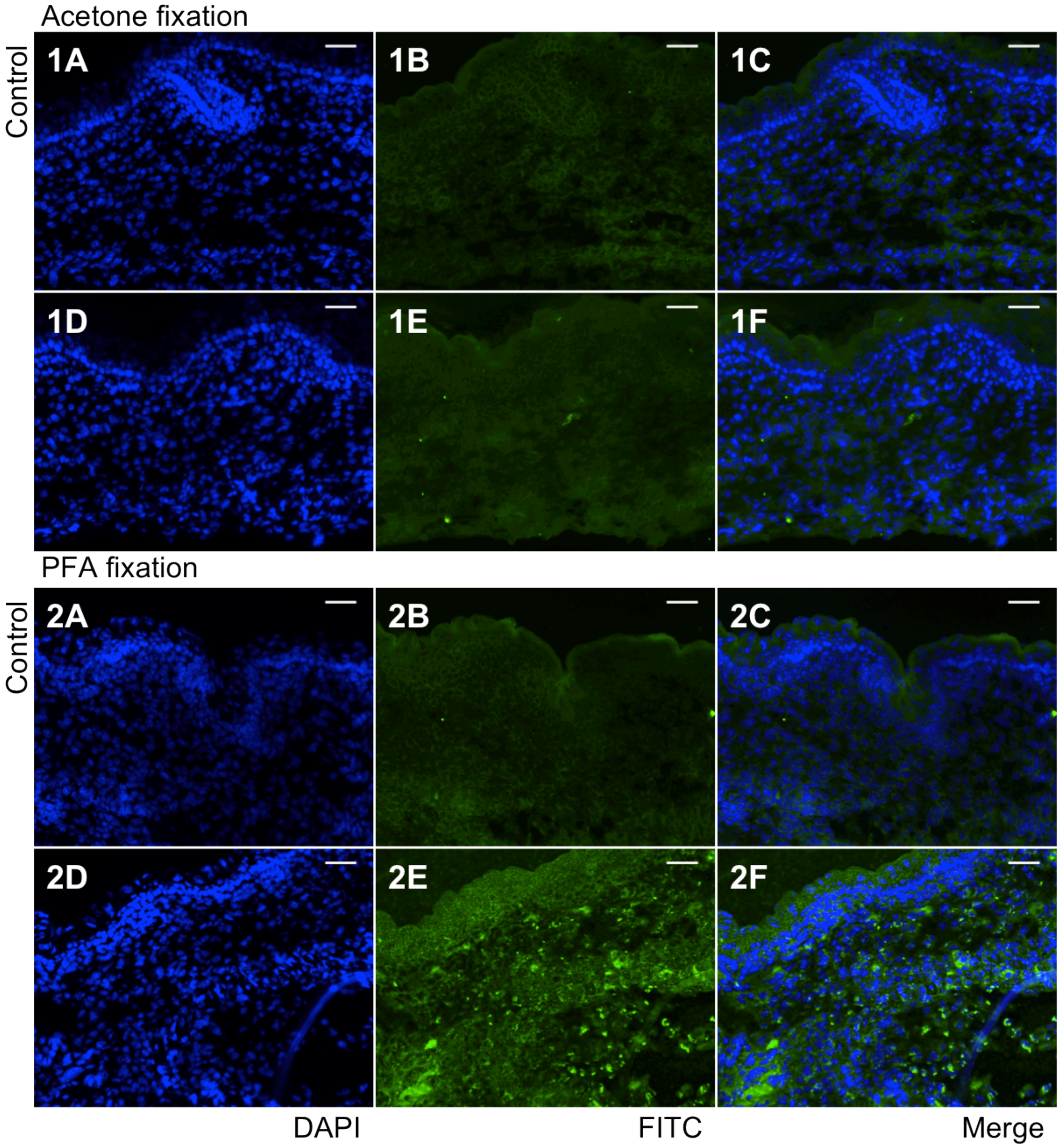

Figure 3.27: Analysis of PPARγ (Abd Serotec) expression in 16.5-day embryonic mouse back skin. Sections were cut at 7μm and stained with an antibody against PPARγ (Abd Serotec) and counterstained with DAPI. From left to right; DAPI, FITC, and merge (DAPI/FITC). FITC represents the fluorescent labelling of PPARγ. (**1A-C**,**2A-C**) Controls showing no fluorescently labelled PPARγ expression. (**1**) Fixed in acetone. (**2**) Fixed in 4% PFA. (**1D-F**,**2D-F**) labelled using PPARγ primary antibody. Fluorescent images were taken using a Zeiss Axio Imager M1. Scale bar = 40μm.

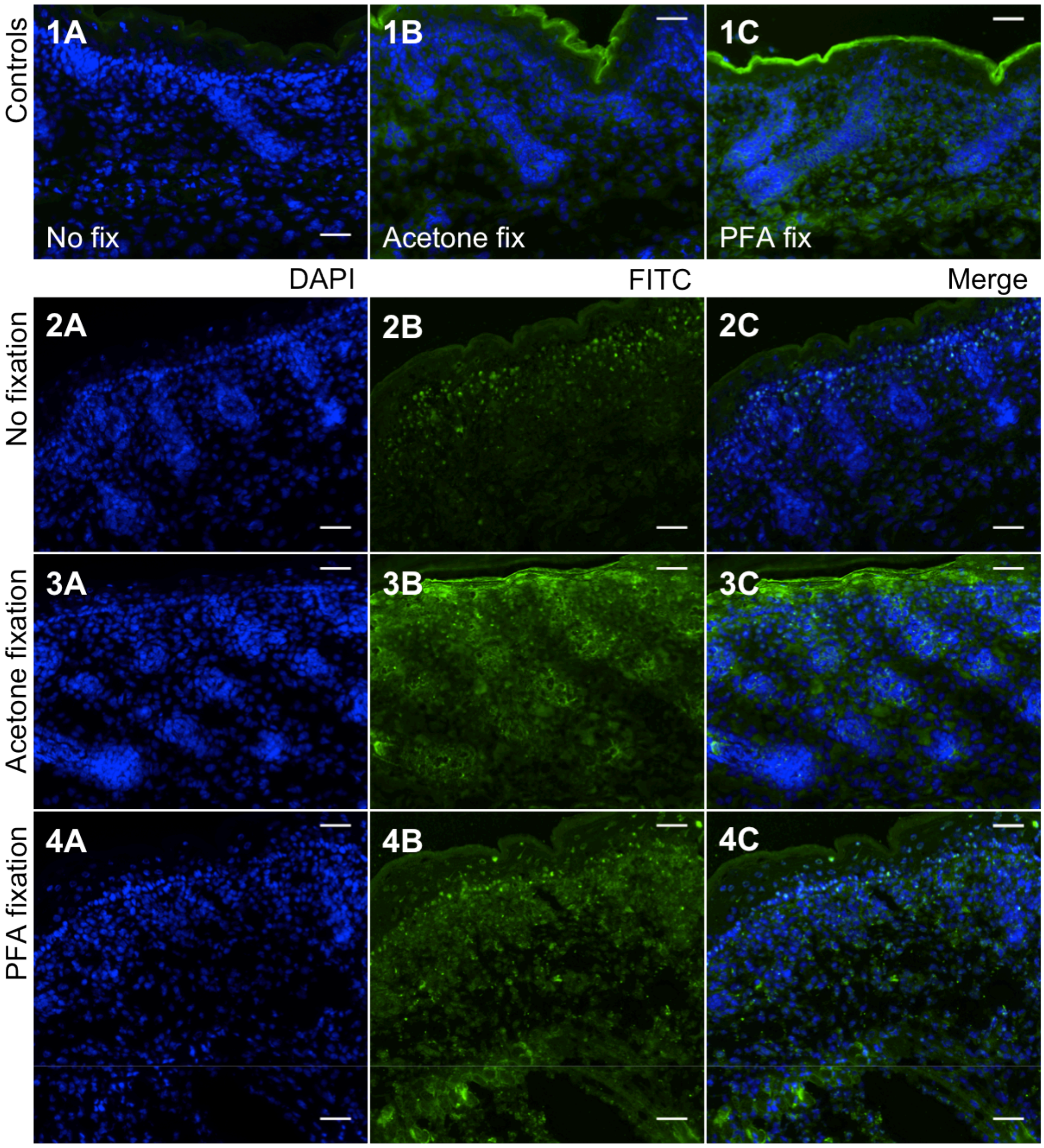

Figure 3.28: Analysis of PPARγ (Abd Serotec) expression in 18.5-day embryonic mouse back skin. Sections were cut at 7μm and stained with an antibody against PPARγ (Abd Serotec) and counterstained with DAPI. From left to right; DAPI, FITC, and merge (DAPI/FITC). FITC represents the fluorescent labelling of PPARγ. (**1A-C**) Controls showing 3 merged images with no fluorescently labelled PPARγ expression. (**1A,2**) No fixation step. (**1B,3**) Fixed in acetone. (**1C,4**) Fixed in 4% PFA. (**2-4**) labelled using PPARγ primary antibody. Fluorescent images were taken using a Zeiss Axio Imager M1. Scale bar = 40μm.

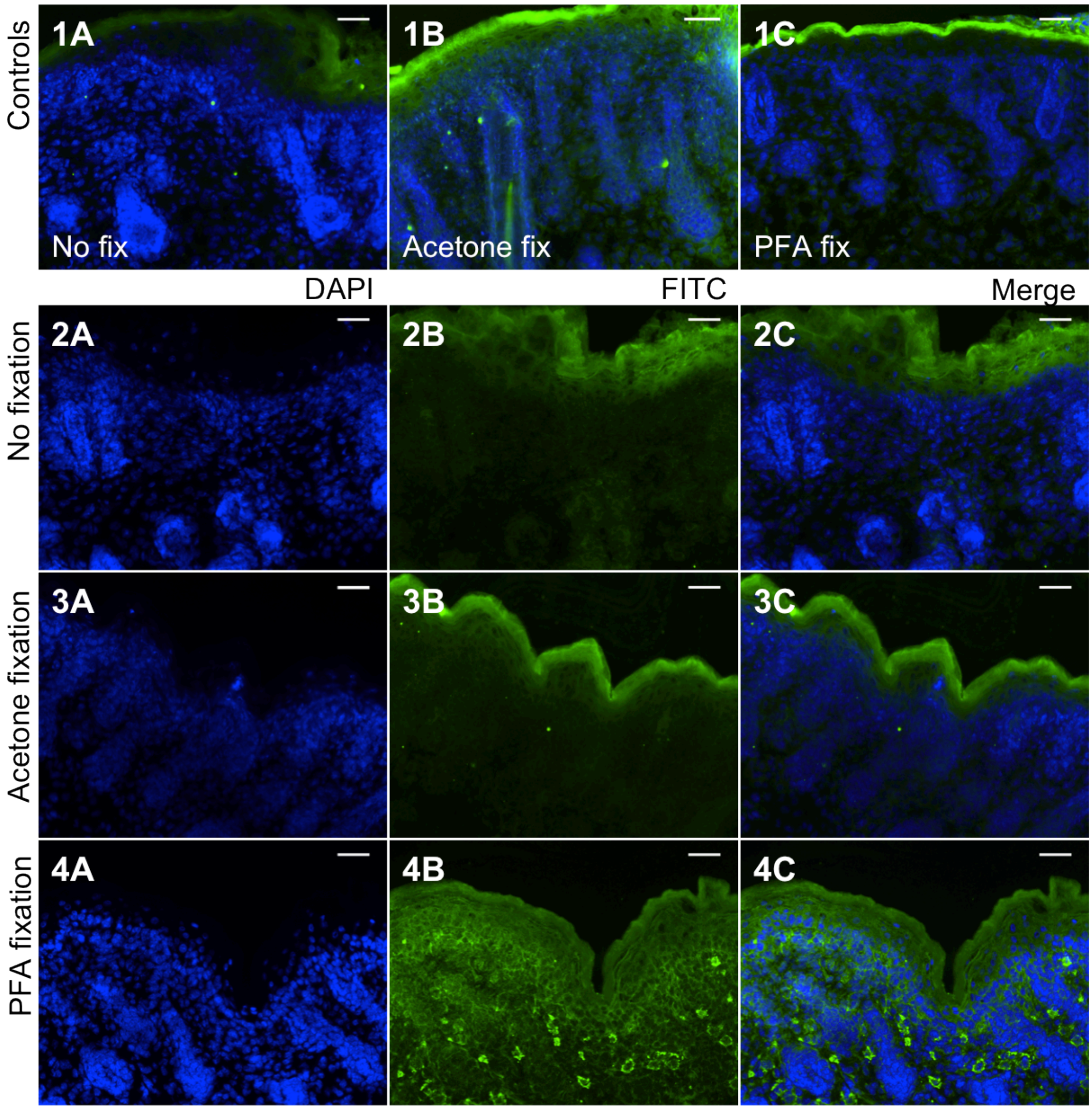

Figure 3.29: Analysis of PPARγ (Abd Serotec) expression in 1-day postnatal mouse back skin. Sections were cut at 7μm and stained with an antibody against PPARγ (Abd Serotec) and counterstained with DAPI. From left to right; DAPI, FITC, and merge (DAPI/FITC). FITC represents the fluorescent labelling of PPARγ. (**1A-C**) Controls showing 3 merged images with no fluorescently labelled PPARγ expression. (**1A,2**) No fixation step. (**1B**,**3**) Fixed in acetone. (**1C**,**4**) Fixed in 4% PFA. (**2-4**) labelled using PPARγ primary antibody. Fluorescent images were taken using a Zeiss Axio Imager M1. Scale bar = 40μm.

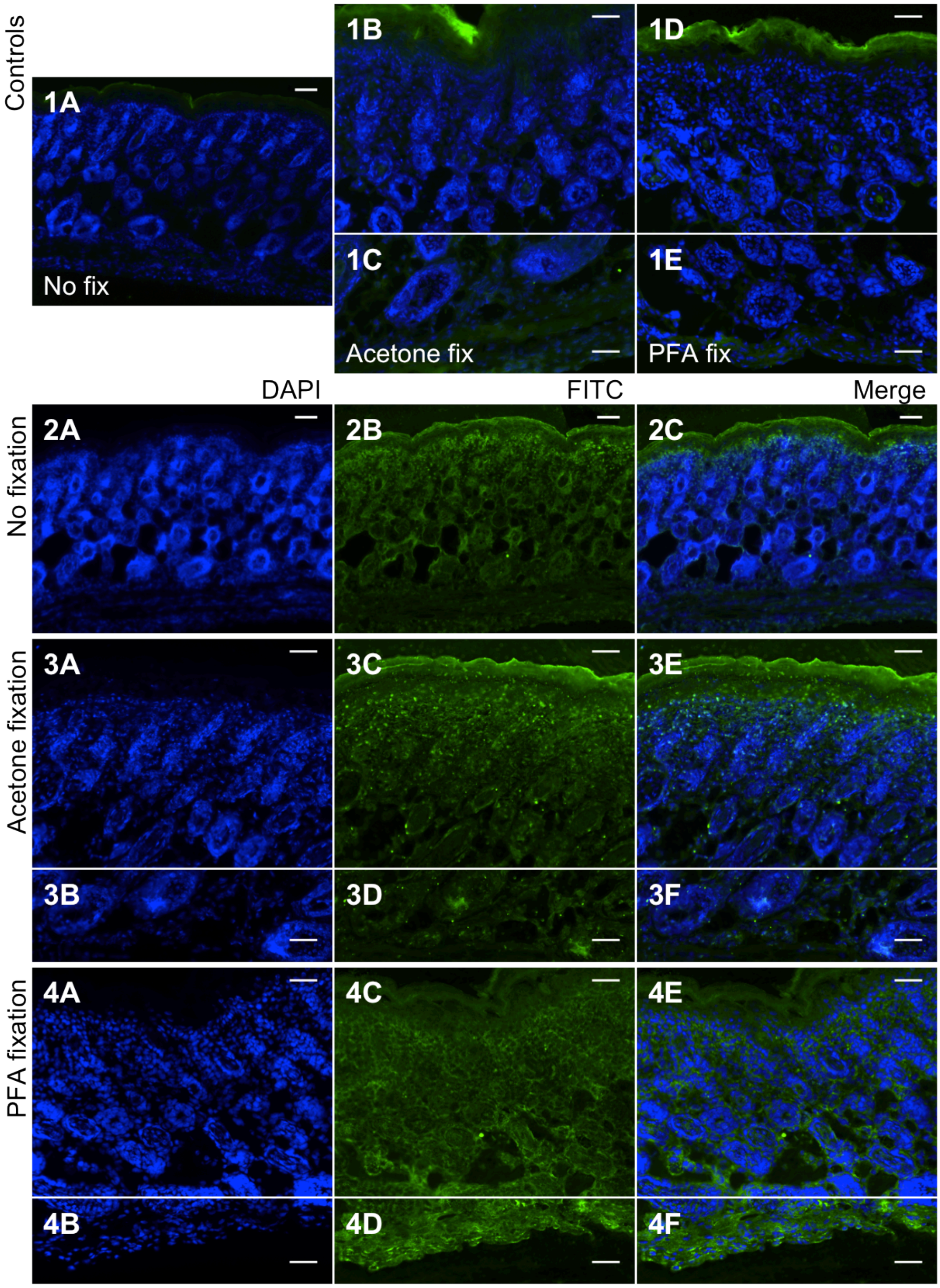

Figure 3.30: Analysis of PPARγ (Abd Serotec) expression in 3-day postnatal mouse back skin. Sections were cut at 7μm and stained with an antibody against PPARγ (Abd Serotec) and counterstained with DAPI. From left to right; DAPI, FITC, and merge (DAPI/FITC). FITC represents the fluorescent labelling of PPARγ. Images of upper and lower views of the skin shown, to give a view of the whole skin. (**1A-E**) Controls showing merged images with no fluorescently labelled PPARγ expression. (**1A,2**) No fixation step. (**1B-C**,**3**) Fixed in acetone. (**1D-E,4**) Fixed in 4% PFA. (**2-4**) labelled using PPARγ primary antibody. Fluorescent images were taken using a Zeiss Axio Imager M1. (**1A,2**) scale bar = 65μm. (**1B-E,3,4**) scale bar = 40μm.

Although the use of the Abd Serotec PPARγ antibody in frozen sections was not so successful, the protocol stated that this antibody had previously been used on paraffin wax sections. To further investigate if this antibody was capable of producing some positive nuclear labelling of where adipogenesis was taking place in the skin, specimens taken from 5-day old newborn mice were fixed, processed in paraffin wax, sectioned and stained for PPARγ using the suggested protocol. The wax sections had what looked like positive staining of slightly cuboidal shaped cells throughout the sections and in particular surrounding the follicles (Figure 3.31). However, when negative controls were examined a similar pattern of labelling was observed (Figure 3.31 1). It was therefore deduced that the staining protocol had led to non-specific labelling of cell types in the skin, possibly sebocytes or melanocytes.

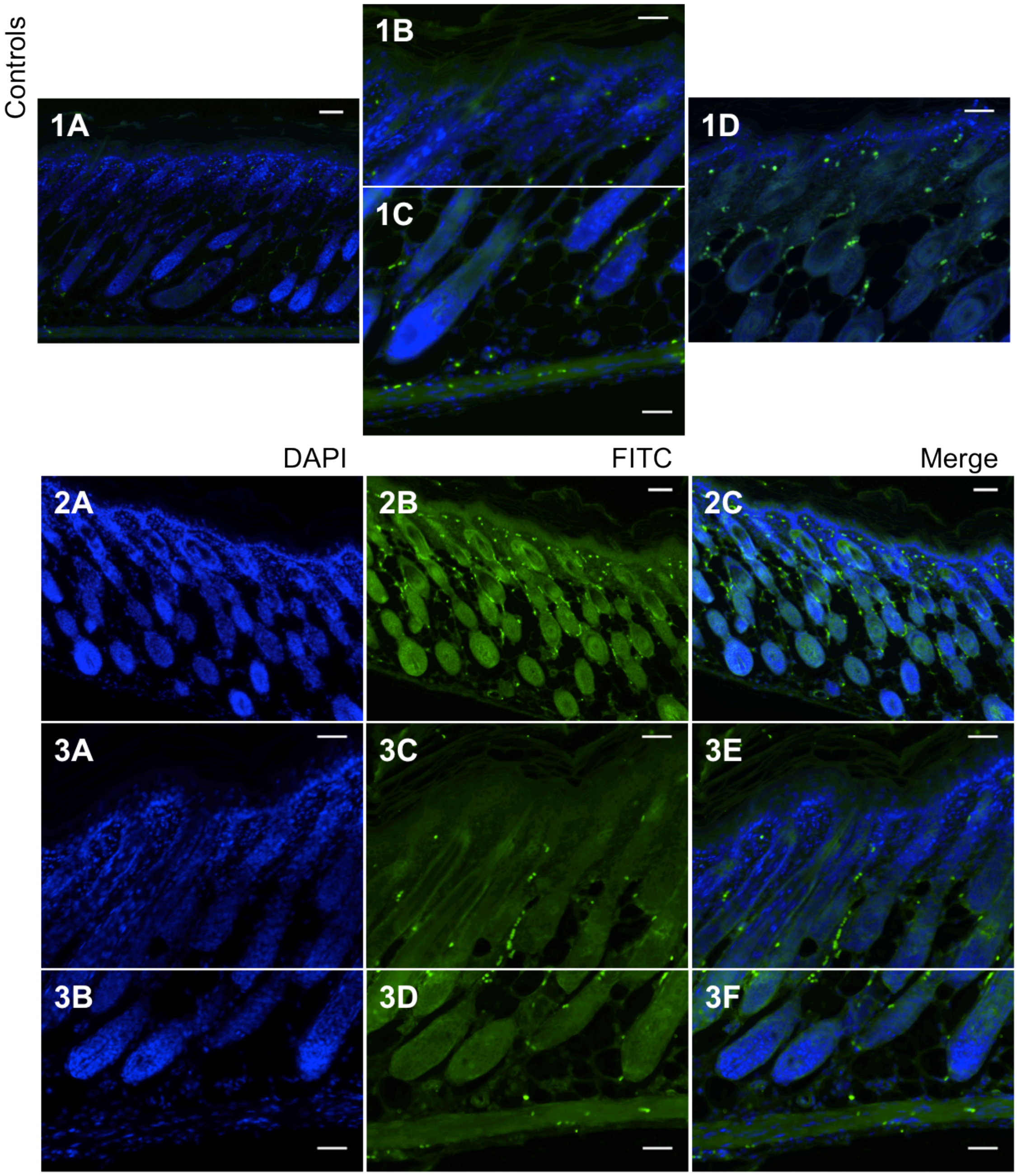

Figure 3.31: Analysis of PPARγ (Abd Serotec) expression in 5-day postnatal mouse back skin. Skin was fixed in paraffin blocks and sections were cut at 7μm, stained with an antibody against PPARγ (Abd Serotec) and counterstained with DAPI. From left to right; DAPI, FITC, and merge (DAPI/FITC). FITC represents the fluorescent labelling of PPARγ. (**1A-E**) Controls showing merged images with no fluorescently labelled PPARγ expression. (**2,3**) labelled using PPARγ primary antibody. (3) View through the whole skin shown in 2 images. Fluorescent images were taken using a Zeiss Axio Imager M1. (**1A,2**) scale bar = 65μm. (**1B-E,3**) scale bar = 40μm.

3.3.3. PPARγ Staining of Dermal Cell Spheres

To try to understand the discrepancy between PPARγ labelling in culture and in developing skin, 3-dimensional cell spheres were made using dermal cells taken from 14.5-day embryonic mouse back skin. These cells were left to cluster and then after 2, 3, 4, 5, and 6 days the spheres were frozen to stain with PPARγ. 3 different PPARγ antibodies were used: E-8 Santa Cruz, Abcam and Abd Serotec.

The spheres were stained with oil red O to detect the presence of lipids in developing adipocytes (Figure 3.32). There was red coloration present in all the sphere ages, particularly those spheres that were more densely clustered. After 5 days, the lipid droplets appeared bigger (Figure 3.32, 4a and b) and the image taken after 3 days shows the red coloration clustering in the centre of the cell sphere (Figure 3.32 2). This shows that adipose tissue is forming in the cell spheres taken from as early as e14.5.

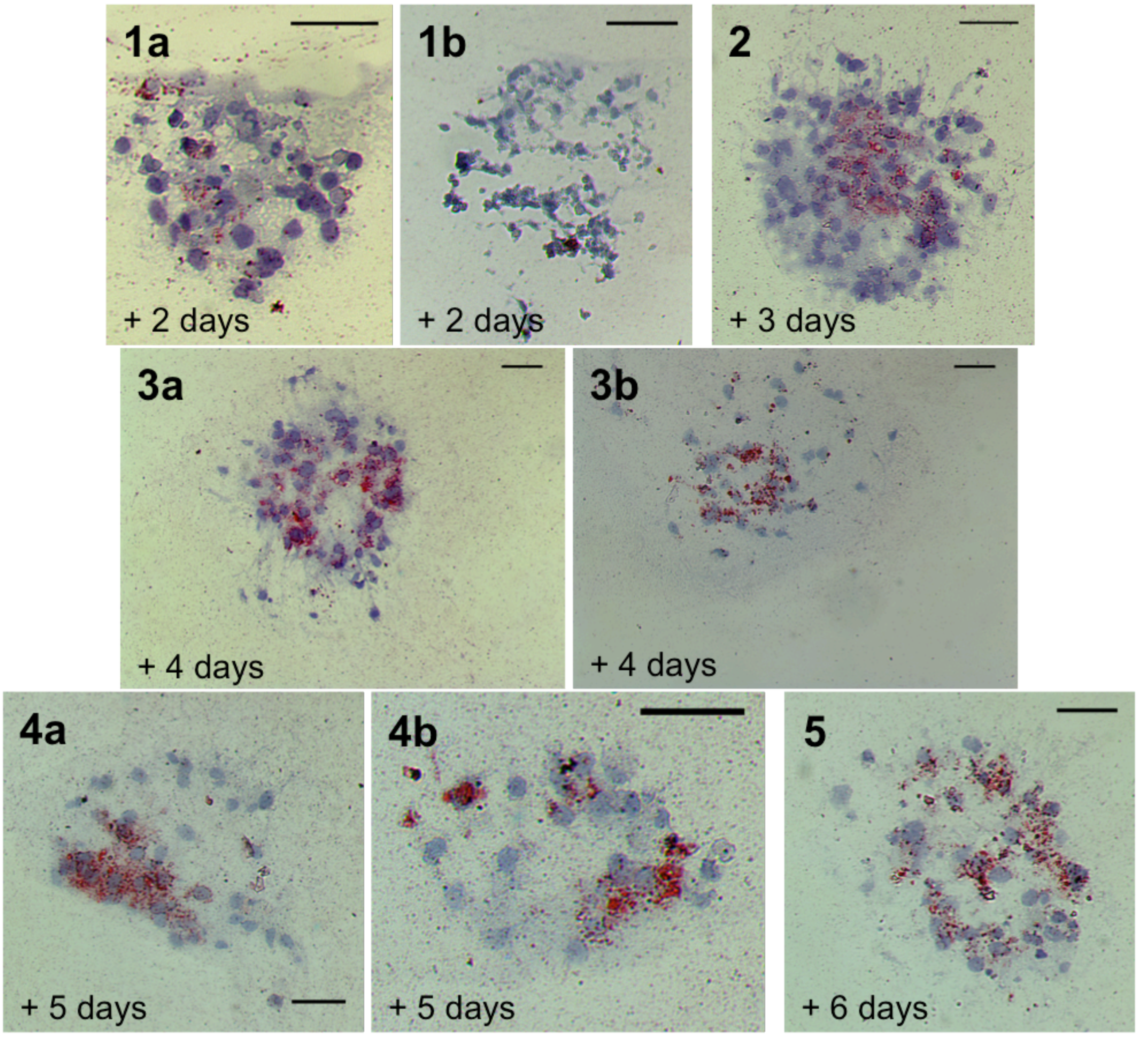

Figure 3.32: Oil red O analysis of dermal cell spheres taken from embryonic day 14.5 mouse back skin. (**1**) stained after 2 days . (**2**) stained after 3 days. (**3**) stained after 4 days. (**4**) stained after 5 days. (**5**) stained after 6 days. Fat droplets present in adipocytes visible as red coloration. Images were taken using a Zeiss Axio Imager M1. Scale bar = 40μm.

After 2 days in culture, when spheres had formed they were stained with PPARγ. For all three antibodies used and also the negative controls, a similar staining pattern was observed, though the background staining was slightly stronger using the Abcam and Abd Serotec primary antibodies (Figure 3.33). Brighter specks were seen in parts of the spheres, however when merged with the DAPI nuclear staining, the fluoresced specks did not coincide with the nuclei. In fact, the nuclei in the FITC images were not fluorescent at all, but instead registered black gaps in the staining. This suggested no PPARγ expression present after 2 days.

After 3 days in culture, the same result as 2 days was seen using the Santa Cruz antibody (Figure 3.34B). However, there was some nuclear staining of PPARγ expression found using the Abcam antibody (Figure 3.34D) and this differed from the controls where no nuclei were stained positive (Figure 3.34C). Abd Serotec was difficult to analyse due to a large amount of background staining but some of the fluoresced sections did coincide with the DAPI stained nuclei (Figure 3.34E).

After 4 days in culture, the spheres stained with Santa Cruz E-8 showed a uniform, but unexpected distribution of staining round the perimeter of each nucleus (Figure 3.35B). This differed significantly from that found using the PPARγ primary antibodies from Abcam and Abd Serotec, which showed clear nuclear expression. This was clear in the magnified sections (Figures3.35D and E). There still existed a degree of background staining, however this was also present in the negative control (Figure 3.35C).

After 5 days in culture, the spheres stained with Santa Cruz PPARγ showed more fluoresced nuclei perimeters (Figure 3.36B). This was also seen after 4 days (Figure 3.35B). However, the images obtained with the Abcam antibody differed significantly. Whereas 4-day spheres there appeared to be nuclear expression, no nuclear expression was found in 5 day spheres (Figure 3.36D). There was still a degree of nuclear staining present in the Abd Serotec stained sections, though this was less obvious due to a high level of background staining (Figure 3.36E).

After 6 days in culture, there was brighter fluorescence surrounding the nuclei peripheries present in the Santa Cruz stained spheres, suggesting the expression was cytoplasmic (Figure 3.37B). In the Abcam stained spheres, there was some cytoplasmic fluorescence and some nuclear fluorescence, suggesting that cells were differentiating at different rates (Figure 3.37D). In the Abd Serotec stained spheres after 6 days, it was difficult to deduce whether specific nuclear staining was present (Figure 3.37E). Some labelling did still appear to be nuclear, but the brighter fluorescence appears to have spread out.

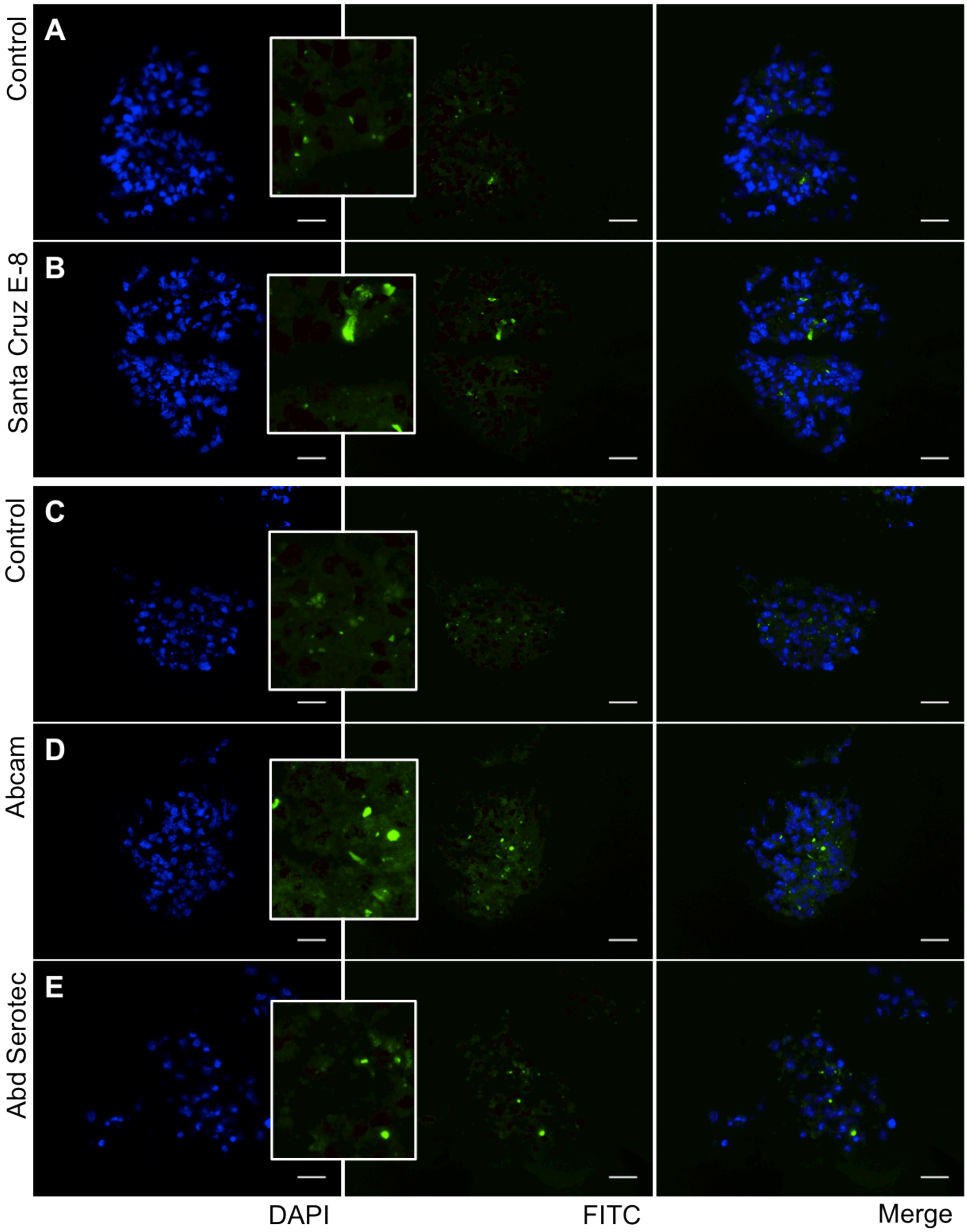

Figure 3.33: Analysis of PPARγ expression in dermal spheres taken from e14.5 mouse back skin dermis and stained after 2 days. Sections were cut at 7μm, stained with one of three antibodies against PPARγ and counterstained with DAPI. From left to right; DAPI, FITC, and merge (DAPI/FITC). FITC represents the fluorescent labelling of PPARγ. (**A**,**C**) controls showing merged images with no fluorescently labelled PPARγ expression and (**C**) is the negative control for both Abcam and Abd Serotec antibodies. (**B**,**D**,**E**) labelled using PPARγ primary antibodies. (**B**) Santa Cruz E-8. (**D**) Abcam. (**E**) Abd Serotec. Fluorescent images were taken using a Zeiss Axio Imager M1. Scale bar = 40μm.

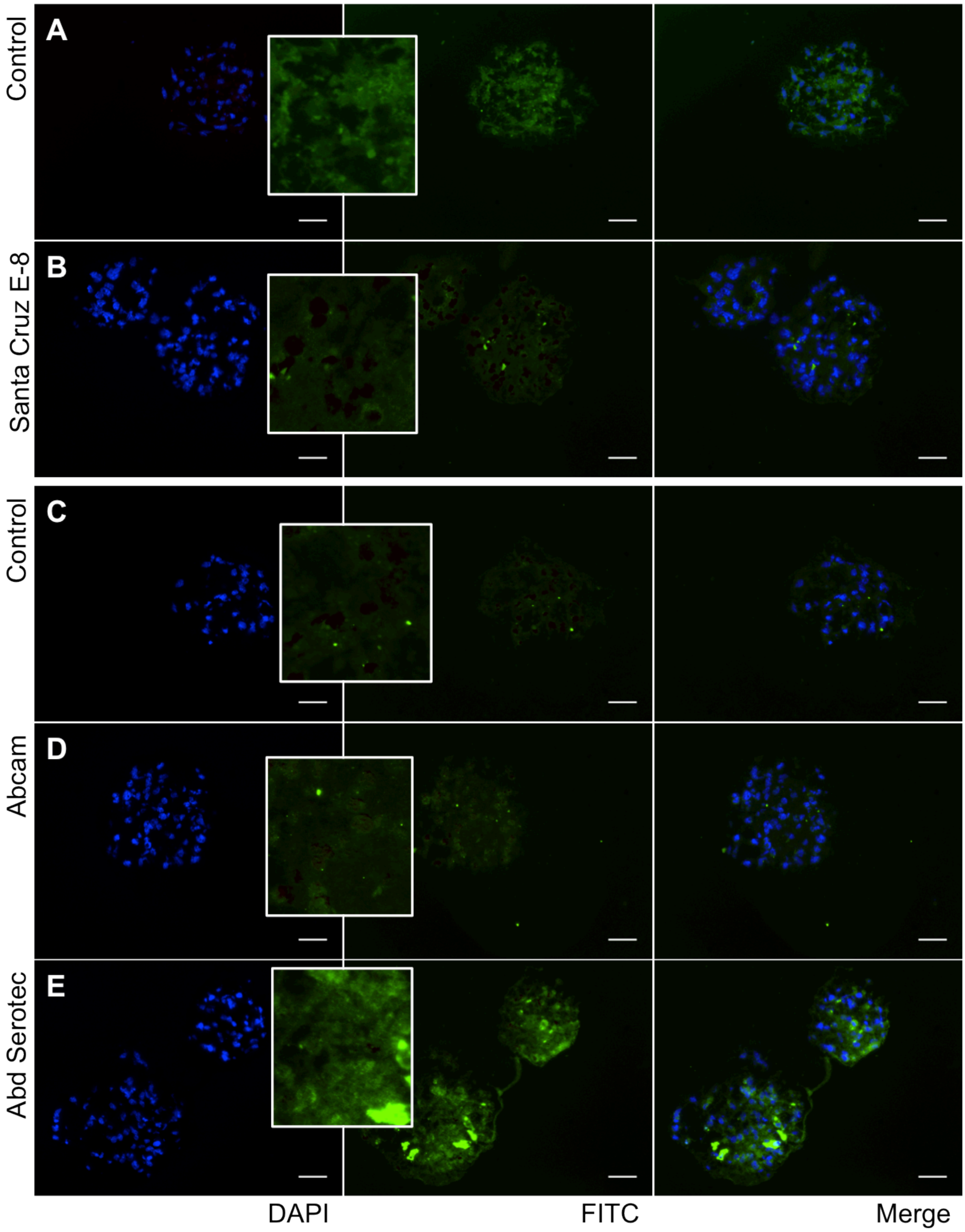

Figure 3.34: Analysis of PPARγ expression in dermal spheres taken from e14.5 mouse back skin dermis and stained after 3 day. Sections were cut at 7μm, stained with one of three antibodies against PPARγ and counterstained with DAPI. From left to right; DAPI, FITC, and merge (DAPI/FITC). FITC represents the fluorescent labelling of PPARγ. (**A,C**) controls showing merged images with no fluorescently labelled PPARγ expression and (**C**) is the negative control for both Abcam and Abd Serotec antibodies. (**B,D,E**) labelled using PPARγ primary antibodies. (**B**) Santa Cruz E-8. (**D**) Abcam. (**E**) Abd Serotec. Fluorescent images were taken using a Zeiss Axio Imager M1. Scale bar = 40μm.

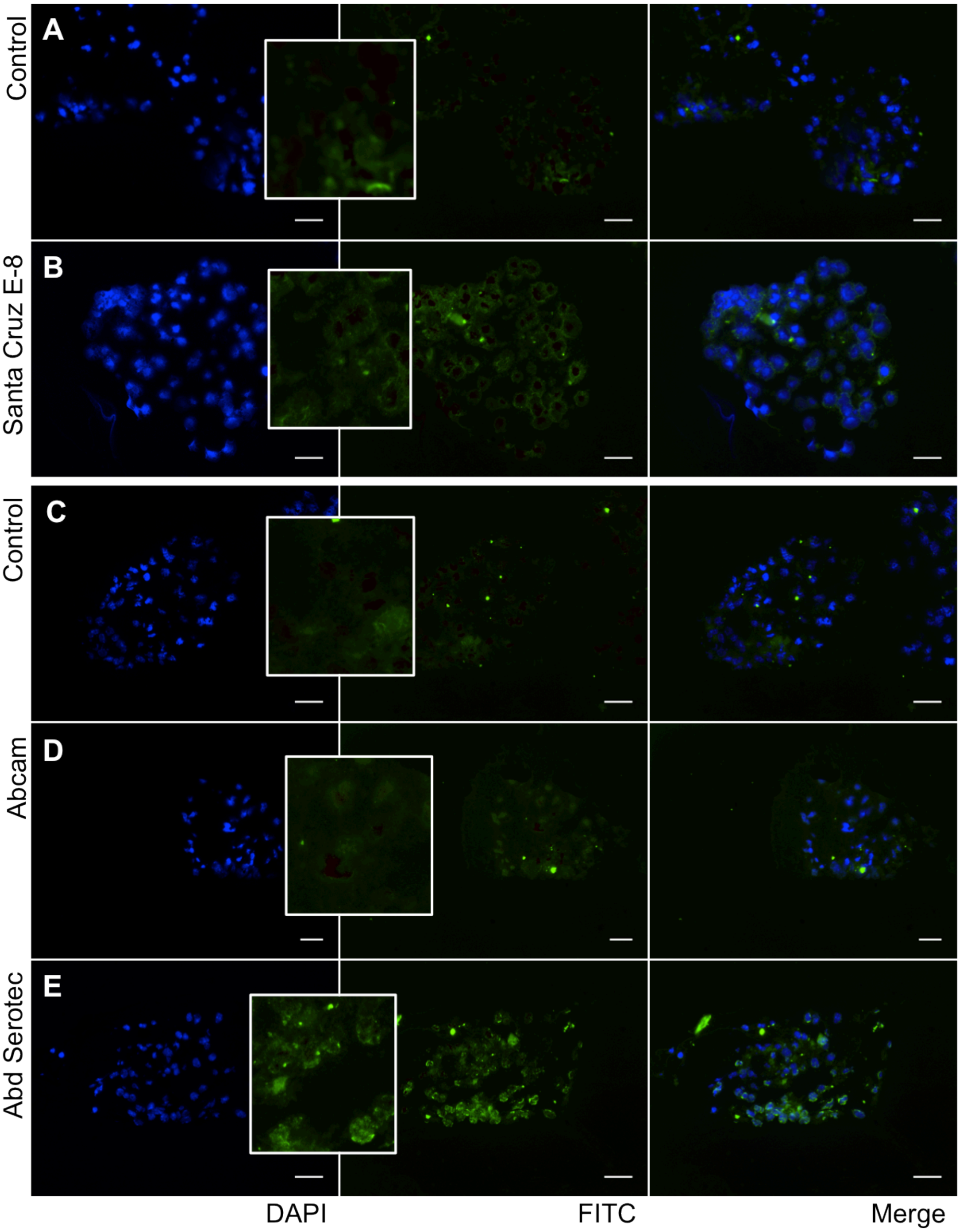

<u>Figure 3.35:</u> Analysis of PPARγ expression in dermal spheres taken from e14.5 mouse back skin dermis and stained after 4 days. Sections were cut at 7μm, stained with one of three antibodies against PPARγ and counterstained with DAPI. From left to right; DAPI, FITC, and merge (DAPI/FITC). FITC represents the fluorescent labelling of PPARγ. (**A,C**) controls showing merged images with no fluorescently labelled PPARγ expression and (**C**) is the negative control for both Abcam and Abd Serotec antibodies. (**B,D,E**) labelled using PPARγ primary antibodies. (**B**) Santa Cruz E-8. (**D**) Abcam. (**E**) Abd Serotec. Fluorescent images were taken using a Zeiss Axio Imager M1. Scale bar = 40μm.

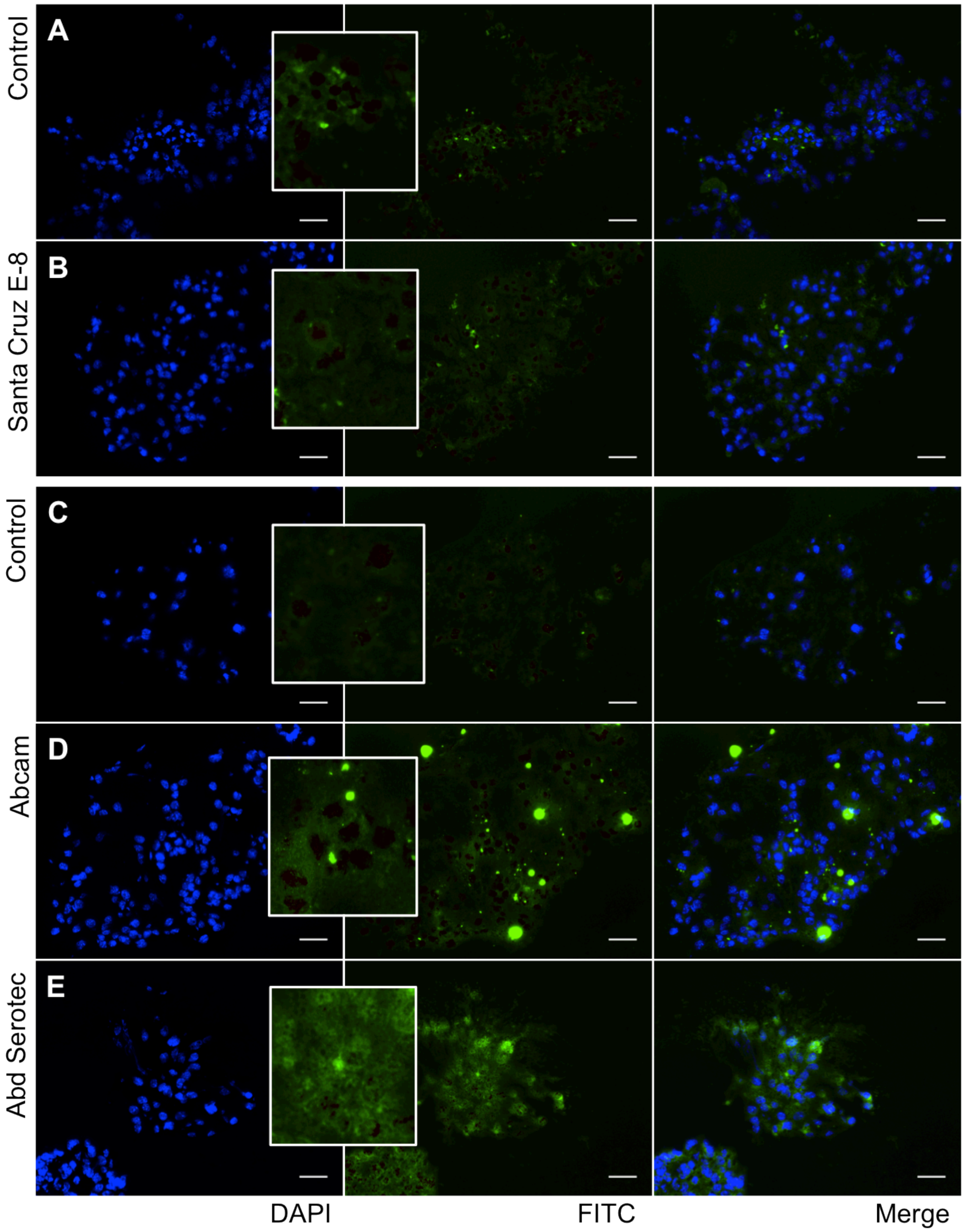

Figure 3.36: Analysis of PPARγ expression in dermal spheres taken from e14.5 mouse back skin dermis and stained after 5 days. Sections were cut at 7μm, stained with one of three antibodies against PPARγ and counterstained with DAPI. From left to right; DAPI, FITC, and merge (DAPI/FITC). FITC represents the fluorescent labelling of PPARγ. (**A,C**) controls showing merged images with no fluorescently labelled PPARγ expression and (**C**) is the negative control for both Abcam and Abd Serotec antibodies. (**B,D,E**) labelled using PPARγ primary antibodies. (**B**) Santa Cruz E-8. (**D**) Abcam. (**E**) Abd Serotec. Fluorescent images were taken using a Zeiss Axio Imager M1. Scale bar = 40μm.

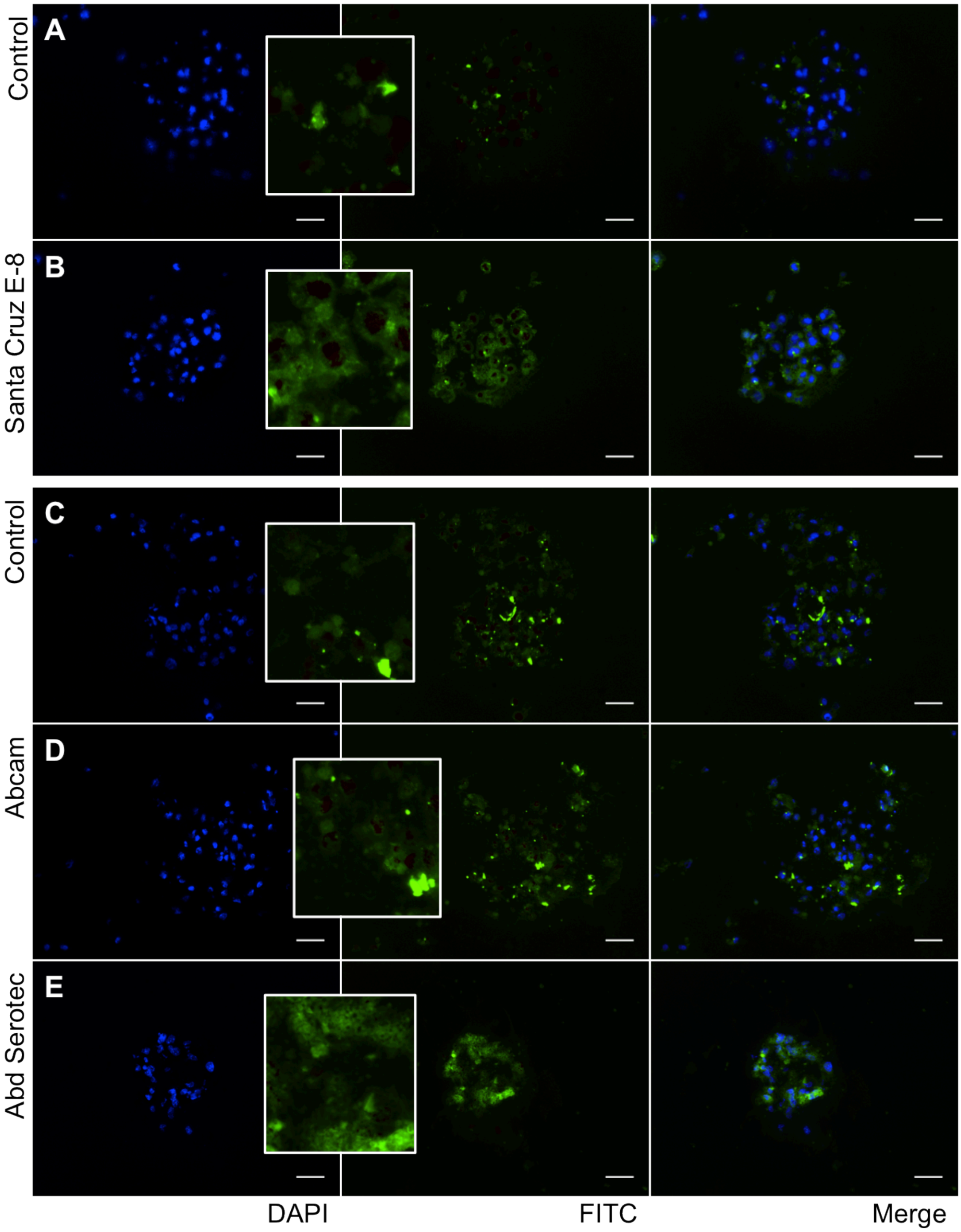

Figure 3.37: Analysis of PPARγ expression in dermal spheres taken from e14.5 mouse back skin dermis and stained after 6 days. Sections were cut at 7μm, stained with one of three antibodies against PPARγ and counterstained with DAPI. From left to right; DAPI, FITC, and merge (DAPI/FITC). FITC represents the fluorescent labelling of PPARγ. (**A,C**) controls showing merged images with no fluorescently labelled PPARγ expression and (**C**) is the negative control for both Abcam and Abd Serotec antibodies. (**B,D,E**) labelled using PPARγ primary antibodies. (**B**) Santa Cruz E-8. (**D**) Abcam. (**E**) Abd Serotec. Fluorescent images were taken using a Zeiss Axio Imager M1. Scale bar = 40μm.

3.4. Discussion

When studying the process of adipogenesis *in vivo*, preadipocyte markers are essential for locating the developing cells, in order to make accurate assessment when researching key events. PPARγ has long been recognised as the main regulator of adipogenesis from early preadipocytes right through to terminal adipocytes. However, when used as an adipogenesis marker by immunohistochemistry on mouse skin, aged e17, e18, e19 and 1 day newborn (1dN), it was not found present in the lower dermis, but instead present in the epidermis (Wojciechowicz 2012). Wojciechowicz (2012) suggested investigating the capability of the PPARγ antibody to produce positive PPARγ expression, prior to using it as a marker, since the most obvious reasons for the absence of staining where adipocytes are maturing are problems with the antibody or the staining protocols. The aim of this chapter was therefore to determine the reliability of PPARγ antibody staining using the *in vitro* 3T3 F442A cell line. 3T3 cells have been studied in depth and it is known that PPARγ expression is present 42-60 hours after being induced to differentiate (Morrison and Farmer 1999; Wojciechowicz 2012). Here, in this chapter the same antibody used (Abcam) was tested, as well as four other anti-PPARγ primary antibodies. These consisted of two Santa Cruz antibodies (B-5 and E-8) and one from Bioaffinity Reagents and another from Abd Serotec, all listed in section 3.2.

3.4.1. PPARγ in vitro using the 3T3 F442A Cell Line

When 3T3 F442A cells were grown in adherent culture, it was observed that some of the cells spontaneously differentiated into adipocytes, without the need for adipogenic-inducing medium. Proliferating 3T3 cells exhibit a fibroblast-like morphology, then after they reach confluency and growth arrest, induction media allows the cells to undergo mitotic clonal expansion needed for adipocyte differentiation (Moreno-Naverrete and Fernández-Real 2012). Growth arrest was suggested to be important for allowing cell differentiation (Pairault and Green 1979). Green and Kehinde (1976) observed that when growth arrest occurred, some 3T3 cells differentiated in culture. Therefore it is not unusual for 3T3 cells to differentiate spontaneously due to a high degree of commitment to the adipocyte lineage, more so with F442A than L1 ((Moreno-Naverrete and Fernández-Real 2012).

After inducing some of the 3T3 cells to differentiate, it was clear that the adipogenic cocktail induced a large proportion of the cells to differentiate and visibly show adipocyte features after 48 hours (Figures 3.2D-F). For example, the yellow coloration present in the images, when magnified revealed a vast quantity of lipid droplets within the cells, indicative of adipocytes (Figure 3.2). Oil red O staining of the 3T3 cells left in culture for 10 days, clearly showed that adipocytes had differentiated and expanded (Figure 3.3), because some of the red-stained lipid droplets were substantially larger from those seen in Figure 3.2.

3T3 F442A cells that were induced to differentiate were stained after 48 hours with 5 different PPARγ antibodies. Santa Cruz B-5 showed no positive staining (Figure 3.4) while Santa Cruz E-8 (Figure 3.8) and Affinity Bioreagents (Figure 3.6) showed clear nuclear expression of PPARγ. The Santa Cruz E-8 antibody appeared to be more specific and the most reliable as there was clearly less cells stained in the non induced cultures (Figure 3.9), whereas the Affinity bioreagents antibody showed a degree of background staining which was also present in the controls. The Abcam PPARγ antibody staining showed some nuclear staining in the induced cells and a degree of cytoplasmic staining, suggesting the protein had been produced and was present in the cells (Figure 3.15). When stained with the antibody from ABD Serotec and fixed in acetone, there was a degree of nuclear staining, while when fixed in 4% PFA the staining was cytoplasmic like that of Abcam (Figures 3.22 – 3.25). The Abcam antibody was that used by Wojciechowicz (2012). It was hypothesised that one of the other antibodies may be more reliable in mouse back skin, considering in the 3T3 cells Abcam was not the strongest staining antibody, though there was positive staining found.

3.4.2. PPARγ in vivo in Rodent Back Skin

Four of the PPARγ primary antibodies were investigated *in vivo* in back skin to determine if the results were similar using each antibody. The Santa Cruz B-5 antibody was not used as did not produce a positive result *in vitro*.

The affinity bioreagent antibody strongly stained the follicles in 4-day newborn mouse skin, though there was no visible staining in the lower dermis where adipocytes are known to be present (Figure 3.10). Comparatively, the Santa Cruz E-8 antibody that worked really well *in vitro*, showed what appeared to be positive staining though when compared with the negative control it was the same (Figure 3.13). The mouse-on –

mouse kit used was deemed unreliable, because when used in the same laboratory for other experiments the same results in the controls were found (unpublished). Without the MOM kit, background fluorescence of the mouse back skin was high (Figure 3.12).

The Abcam antibody was used in mouse back skin to control if the result found was the same previously conducted (Wojciechowicz 2012). The same epidermal staining at the base of the epidermis was found, with some follicular staining from e16.5 (Figure 3.20) and also present in e18.5 (3.21), 1 day and 3 day newborn (Figures 3.17 and 3.18). Interestingly this was not found at e14.5 (Figure 3.19). This could relate to the development of hair follicles. Hair follicle initiation begins around e14/14.5 and it is known that adipocytes develop around the base of the hair follicles in the lower dermis of rodent skin and also pig skin (Hausman *et al.* 1981; Hausman and Martin 1982), It could be suggested that the commitment of dermal cells to the adipogenic lineage may require the formation of the hair follicles in order to receive signals from the hair follicle end bulbs present in the lower dermis. In the skin stained from e14.5, there were no follicles visible in the lower dermis. The expression of PPARγ may in fact come from the hair follicles which signal to the preadipocytes. Hair follicle initiation may trigger the expression of PPARγ and so indirectly hair follicle formation is the cause of preadipocyte commitment.

When fixed in PFA, skin sections stained with the Abd Serotec antibody showed some staining in the upper dermis, close to the upper dermis from e18.5 (Figure 3.28) and also in the 1-day newborn skin (Figure 3.29). There is some staining of the lower dermis in the 3 day newborn samples, however when compared with the antibody control, there is the same staining which infers it to be background staining.

3.4.3. E14.5 Dermal Cell Spheres in 3-dimensional Cell Culture

The e14.5 dermal cells were put into culture in media droplets and clustered to form spheres. After 2 days, there was already a degree of lipid content present in the spheres (Figure 3.32 1a) and this developed over a further 4 days. This showed that there was successful formation of adipocytes in the spheres taken as early as e14.5. This could infer that that the dermal cells are already capable of becoming adipocytes, earlier in development than previously though, but that there is a signal from the epidermis that prevents the formation of adipocytes until a later stage (Wojciechowicz 2012). However, not all the cells in the spheres differentiate into adipocytes. This could suggest that there is already a developmental division between the upper and lower dermis, only the lower dermis requires an inhibiting signal.

The images taken from e14.5 + 3 days shows the adipocytes stained red concentrated in the centre of the sphere (Figure 3.32 2). This may be different from some of the sections depending where in the sphere the section was taken. When the cells form spheres, the dermal cells could potentially organise into upper and lower dermis with the lower dermis in the centre. E14.5 skin is very fragile and difficult to separate; therefore, there could be some epidermal contamination, from which the epidermal cells may orientate on the perimeter of the sphere.

After 3 days using the Abcam antibody (Figure 3.34D), and more clearly using the Abd Serotec antibody after 4 days (Figure 3.35E), there was nuclear expression of PPARγ present. This is respectively e18.5, which is the same time at which C/EBPα is expressed. Siersbæk and colleagues (2012) said that C/EBPα and PPARγ work together at a similar time point to initiate the cascade of adipogenic genes, sharing 35-60% co-localisation (Lefterova *et al.* 2008; Schmidt *et al.* 2011). The cells are already committed but require induction from C/EBPα and PPARγ to start differentiating. There does not appear to be a role of PPARγ in early adipogenesis and commitment, although perhaps this comes from the hair follicles.

After 6 days in culture, there was a thicker ring of fluorescence present in the Santa Cruz stained spheres, suggesting the expression was cytoplasmic and the protein was there (Figure 3.36B). This could be related to the idea that PPARγ presence is required to maintain the population of terminal adipocytes.

The spheres contain only the dermal cells and so cannot be directly contrasted with what occurs *in vivo*. The hair follicles do not develop in the spheres. However, the 3D sphere method is more beneficial than growing the dermal cells in 2D culture, because the *in vivo* environment is 3D. Culturing the dermal cells does show what these cells are capable of alone without other signals from other tissues and developing organs, which proves useful in concluding that these cells are capable of becoming adipocytes as early as e14.5.

While some of the antibody staining looks positive, each antibody produces a significantly different distribution. This does not produce reliable data for the presence of PPARγ. As well as this, no positive staining was found to coincide with the dermal fat layer. Either PPARγ is not important to the dermal adipose layer or the antibodies do not work so well using the immunofluorescence technique on frozen sections. This does not necessarily mean that PPARγ is not important for adipose development, but perhaps the dermal adipose layer is regulated in a different way, or that the signal comes from the hair follicles, or is only needed later in adipogenesis. However, other avenues need to be explored to find a marker of early adipogenesis. A dominant negative mutant of PPARγ shows what appears to be normal adipocyte development, though when looked at closer, the organ has more white adipose tissue (Gray *et al.* 2006). PPARγ may be required to produce normal adipogenesis, but precursor cells are committed prior to PPARγ expression.

Affinity bioreagents shows staining of the base of the epidermis. PPARγ may be required by hair follicles and then signals to other transcription factors down the follicle to the adipocytes around the base of the hair follicles.

3.4.4. Further Work

This is by no means conclusive evidence. While some of the antibodies appear to work very well i*n vitro*, there is such a degree of difference in the staining *in vitro* and vivo, between the antibodies, even though all of them are staining for PPARγ. The immunofluorescence method is maybe not reliably accurate enough. In line with what the literature states, that expression in 3T3 cells is 42 to 60 hours after induction (Morrison and Farmer 1999), it would be beneficial to confirm using Western blot analysis that the PPARγ protein is present around this time in the cells and then also use in the skin to confirm the presence of PPARγ in the skin. Western blot analysis may be more effective use of the antibodies. A good control would be to make spheres with the 3T3 cells. This would show whether the difference in the staining were due to the 2D vs. 3D environment or were tissue specific differences.

The cells don't cluster uniformly across all the spheres. A reason for the differential staining i*n vitro* could be that when there is less cell-to-cell interaction the signalling is different. The density of the spheres could be calculated and the density compared with the degree of PPARγ expression and adipocyte formation.

The e14.5 spheres have not been influenced by the waves of hair follicle formation and it is thought that there is interaction between adipogenesis and hair follicle formation. Spheres from different ages could be put into culture in the same way and the level of expression and oil red O staining should be analysed. However, most importantly, the first step is to confirm an effective PPARγ antibody or method of detecting PPARγ for use in this investigation. 3T3 cells are developed from 3T3 mouse embryos and may be already committed so they are not as reliable as *in vivo*. However, they are useful for studying the effectiveness of the antibodies.

CHAPTER 4:

Establishing the Models; Experimenting with Organ and Cell Culture using both 2-Dimensional and 3-Dimensional Methods

4.1. Introduction

As introduced in chapter 1, a dermal adipose layer has recently been found to exist in the skin. The overall aim of this thesis is to investigate the role of key signalling pathways in dermal adipogenesis. To do so, a suitable experimental model is required. Many different types of model system have been used to study the process of development. Three main types of model are discussed in this chapter; mouse models, organ culture models and cell culture models.

4.1.1. Mouse Models

Model systems have been deemed appropriate ways of studying many biological processes, both by i*n vitro* and *in vivo* means. In response to the fact that it is difficult to fully understand what is going on during development in a normally functioning organism, knockout and other transgenic mouse models, including those with silenced or mutated genes are found throughout research. For example, a C/EBPβ-C/EBPδ double knockout mouse was created by Tanaka and colleagues (1997) using gene targeting and led to the conclusion that these genes are needed for terminal differentiation. Another is example is that when Caveolin-1 (Cav-1) was knocked out and caused abnormal adipocytes with irregular lipid metabolism and prevented diet-induced obesity (Razani *et al.* 2002). Mice have been deemed appropriate for studies throughout research as they are small and manageable and their gestation cycle is relatively short at 19-21 days long (Green, 2013). By observing what happens when normal development is disrupted, the role of certain genes at different timings and localisations can be used to infer what is occurring during normal development. For example in the study of adipogenesis, by knocking out C/EBPα, brown and white adipocytes cannot accumulate and the mice die shortly after birth (Wang *et al.* 1995) This also occurred with PPARγ null mice, which were embryonic lethal (Barak *et al.* 1999).

Mouse models are useful to infer the effects of certain genes during development, e.g. the C/EBPβ-C/EBPδ double knockout mouse (Tanaka *et al.* 1997) or Cav-1 knockout mice (Razani *et al.* 2002). However, they also have their limitations e.g. short-term survival, and there is not enough known about the molecular basis of development of the dermis to produce a mouse model for this project. What would be used as the driver in the dermis to create a transgenic mouse? Mouse models are also too expensive and there is not enough time available on this project.

4.1.2. Organ Culture Models

An alternative to mouse models is to use organ culture and perform experiments of these cultures. Many different research groups have used similar methods of culturing skin. Whatever the research question, the basic requirements of these organ culture models are the same, including the ability of the skin to survive and be metabolically active. Additionally the isolated skin contains all the cell types present that could be influencing the development and/or growth of the structure.

Kao *et al.* (1983) focused on developing a short-term organ culture model of skin from 7 to 8 week old mice to investigate cutaneous toxicity. Yasuoka *et al.* (2008) used a similar technique with human skin. Organ cultures have also proved beneficial as a way of replicating *in vivo* activities, *ex vivo* for developing skin. Kashiwagi *et al.* (1997) used whole back skin of embryos grown on filters coated with type 1 collagen in a medium containing 1% foetal bovine serum. A similar substrate organ culture model was employed by Richardson *et al.* (2009) to investigate the influence of KGF and FGF pathways on follicle development. This method involved the microdissection of small pieces of dorsolateral skin around e14 and the skin was normally maintained for 72 hours. A similar technique was initiated by Wojciechowicz (2012) with older (e16.5) skin to investigate adipogenesis.

4.1.3. Cell Culture Models

Cell cultures can also be used to study adipogenesis In fact, most of what is known about the cellular and molecular basis of adipogenesis originally comes from 3T3 cell lines. These include, the 3T3-F442A and 3T3-L1 cell lines. These lines were generated from embryos of Swiss mice (Todaro and Green 1963). Lipid accumulation was found to occur in these cells after they had reached 100% confluency (Green and Kehinde 1974). Factors can be added to these cells to induce or inhibit adipogenesis, which makes them useful for studying what effects different growth factors might be having on the ability of the cells to differentiate.

These cell lines are cost effective as they can provide an unlimited number of cells of a pure population and differentiate efficiently without the ethical restrictions that come with using animal or human tissue (Kaur and Dufour 2012; Siersbæk *et al.*

2012). While there are many advantages to using cell lines as opposed to primary cells, with their usage also comes a number of disadvantages. Since they have been genetically altered, they may not be as similar to primary cells as desired and passaging the cells may cause further genotypic and phenotypic alterations (Kaur and Dufour 2012). Confirmation should always be done with primary cell and the findings associated with cultured cell lines are not definitive. As well as this, in comparison with cells *in vivo*, the two-dimensional environment that the cells are cultured in does not reflect that of the three-dimensional environment of tissues in the body.

Other cell lines have been produced from adult adipose tissue. For example, the preadipocyte cell line AP-18, which was created from an adult C3H/HeM mouse, subepidermal layer of ear skin (Doi *et al*. 2005). Primary cultures are better and have also been produced from adult tissues of many species including rodents.

Primary cells, in this case cells taken from the dermis of the skin, can be used to study development through cell culture. Both two-dimensional and three-dimensional culture techniques can be used. In the Jahoda group, the 3D spheroid cell culture technique has been used extensively (Higgins *et al.* 2009; Wojciechowicz 2012). This technique is used in this project to create a model system to study adipogenesis.

Adipogenesis has been much more extensively studied *in vitro* using cell lines compared with *in vivo*. This is partly because *in vitro* methods are more accessible. They are also less likely to be influenced by other cell types and developmental processes occurring alongside adipogenesis (adipocyte formation). Due to full genome microarray analysis studies, however, Wojciechowicz (2012) as well as others have shown that there are many fundamental differences between *in vitro* and *in vivo*, including those associated with gene expression. For example, *Cebpβ, Cebpδ* and *Stat5* were not found *in vivo*, but were found *in vitro* (Wojciechowicz 2012). This has encouraged the need for more *in vivo* and *in-vivo* like methods of investigation and cell culture methods are largely artificial.

The aim of this chapter was to establish a model with which to study and be able to manipulate adipogenesis *in vitro*. The initial approach was the development of a whole skin organ culture model. I replicated Wojciechowicz's (2012) organ culture of foetal mouse skin in order to develop a method of investigating the effects of altering specific signalling pathways on the development of adipocytes and lipid accumulation in the dermis. The aim was, to generate an *in vivo*-like environment *ex vivo*, so that, different factors involved in signalling pathways could be applied directly to the culture to examine their influences on adipogenesis at key time points. This reduces the influences of other developmental events that occurring at around the right time, while still leaving the skin in its correct *in vivo*-like organisation. Within the general protocol, a number of different variables were experimented with, including medium type, serum concentration and length of culture. When considerable inconsistency was encountered, a different strategy was employed. This involved the establishment of primary dermal cultures from embryonic skin and the development of a novel 3D spheroid model using hanging drop techniques. Adipogenesis in these structures were compared with that of the same cells in regular 2D monolayer culture. The results suggest that the 3D model is a relatively robust representation of adipogenic activities in the dermis.

4.2. Material and Methods

4.2.1. Origin, Maintenance and Breeding of Mice

Mouse back skin aged from e14.5 to e18.5 was taken from the FVB strain from the Durham University Life Sciences Support Unit (LSSU). Mice were kept at 21°C, 55% humidity on a 12 hour light/dark cycle. They were fed on the Harlan Teklad 2013 Rodent Maintenance diet and watered *ad libitum*.

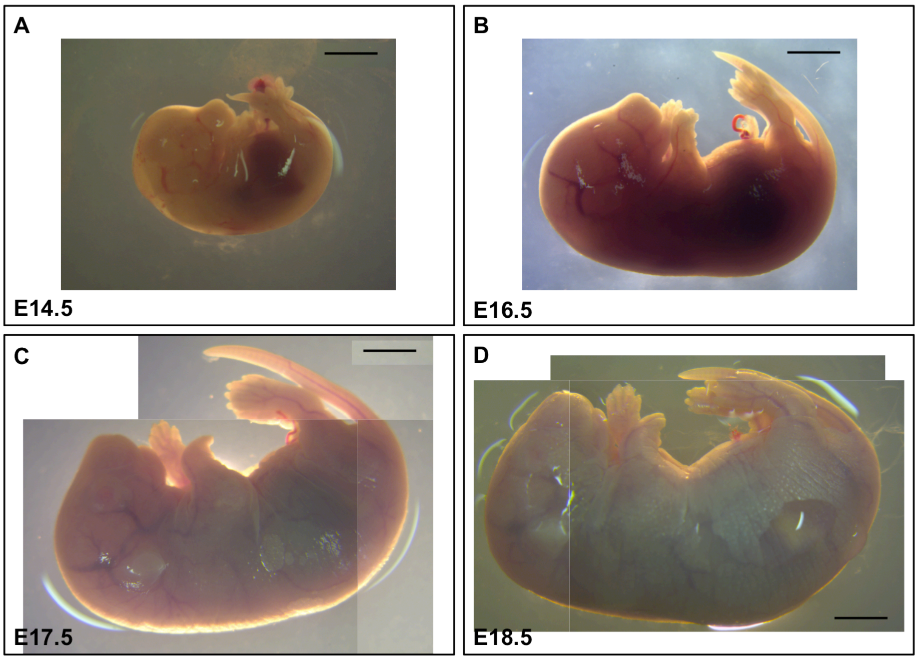

<u>Figure 4.1:</u> Images of whole embryos taken from FVB mice at specific time points. Embryos photographed before manipulation. (A) 14.5 day embryo. (**B**) 16.5 day embryo. (**C**) 17.5 day embryo. (**D**) 18.5 day embryo. Images were taken in dark field using a Zeiss Stemi SV 11. Scale bar = 3mm.

Vaginal plug analysis was used to obtain skin from embryos at specific ages. The presence of a vaginal plug the morning after breeding pairs had been kept together was used as an indication of a successful mating and the embryos were noted at 0.5 days gestation at this point. Animals were killed using CO_2/cervical dislocation.

4.2.2. Isolation of Skin Samples

Skin samples were taken from FVB embryos between 14.5 and 18.5 days, mainly 16.5-day-old embryos (e16.5). The skin along the back of the embryos was held taut by two pins before two longitudinal incisions were made as shown below in Figure 3.2. The skin was then carefully separated from the underlying muscle layer using a circular motion to detach it. Three or four transverse cuts were made to divide the piece into two or three depending on the size of the embryo in relation to its age. This process was repeated on the other side.

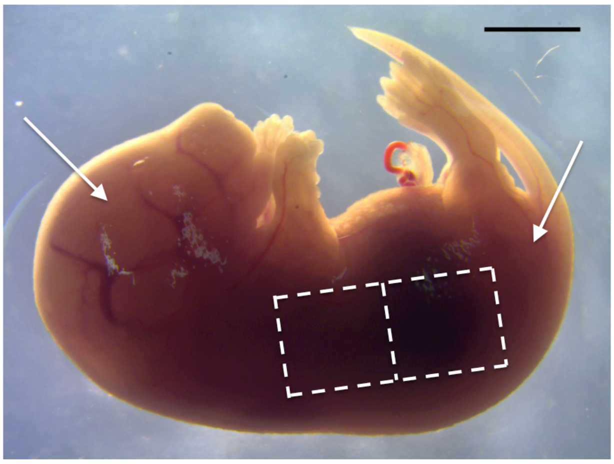

<u>Figure 4.2:</u> Diagram depicting where the mouse skin was taken from. 16.5 day old embryo. Arrows show where pins were placed. Dotted line shows where the skin was cut. Scale bar = 3mm

4.2.3.1. Establishment of Organ Cultures

Collagen coated filters were first prepared. Nucleopore filters (Whatman) were coated with rat tail collagen (Sigma) (Appendix III). These were then placed on the lid of a petri dish before being left under UV overnight and then kept in the fridge.

A drop of media was placed in a 35mm dish on which a collagen-coated filter was placed with the shiny surface facing upwards. This was then lifted to the surface by carefully pipetting 2ml of media underneath it. Different serum concentrations and types of media were trialled to determine whether any of them were more successful than the others in allowing healthy and consistent culture results. Both Modified Eagle's Medium (MEM: Gibco, Paisley UK) and William's E Medium (Gibco, Paisley UK) were used and supplemented with 0%, 1% and 2% foetal bovine serum (Sigma, MO USA).

The skin pieces were carefully transferred to these filters with the epidermis facing upwards and the dermis in contact with the filter. Approximately 5 pieces were placed on each filter in each dish. Images were taken (Zeiss Stemi SVII microscope with AxioCam ERc5s and Axiovision software) before the dishes were transferred to an incubator at 37°C, 5% CO_2. Alongside this, some skin pieces were suspended in hanging drops of media to experiment with different methods of culturing the skin pieces.

After three days the skin pieces were put into Tissue-Tek® O.C.T.™ compound (Sakura, Agar Scientific, Netherlands) and orientated flat using fine tweezers so sections can be cut right through the skin (see figure 4.3). These were snap frozen in liquid nitrogen and kept at −80°C. Skin sections (7µm and 10µm), were cut on a cryostat (LEICA CM 3050S) and attached to ColorFrost®Plus slides (Thermo Shandon Ltd, Cheshire, UK). The slides were dried for 2 hours at room temperature, and then either used immediately or frozen before immunofluorescence staining, oil Red O lipid detection or haematoxylin and eosin (H&E) staining. Frozen slides, were defrosted before staining.

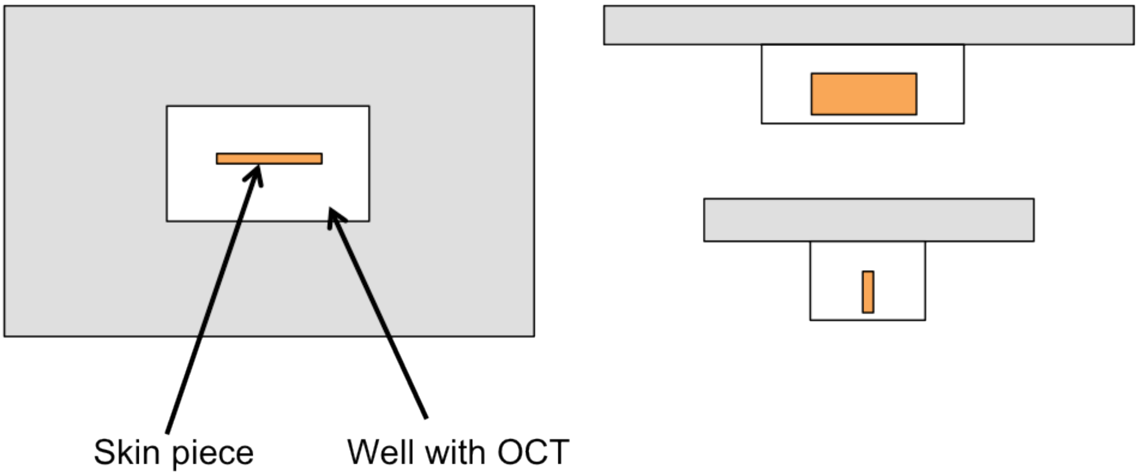

Figure 4.3: Schematic showing the orientation of the skin pieces in the freezing boats in preparation for sectioning. 3 different views are shown. Left is an aerial view from above and Right shows both side views.

4.2.3.2. Establishment of the Cell Culture System

Throughout the cell culture, the cells were cultured in a culture medium, referred to as the “basic medium”. This consisted of modified essential medium (MEM) (Gibco) with 10% foetal bovine serum (Sigma) and antibiotics; 10U/ml penicillin, 100μg/ml streptomycin (Gibco) and 2μg/ml fungizone (Sigma).

4.2.3.2.1. Production of Single Cell Suspensions from Mouse Dermis

Skin pieces obtained from foetal mouse back skin were put in a 6% Pancreatin/5% Trypsin cocktail in Earle's solution (1:1:2) (Appendix III)) at 4ºC for between 30-90 minutes according to age. Fine tweezers were then used to carefully prise apart the dermis from the epidermis. Dermal pieces were transferred to sterile Earle's solution before being incubated in a warm working solution of DNase I (Sigma)/Collagenase II (Appendix III) at 37ºC for 15-20 minutes. Mechanical dissociation was carried out with a 1ml pipette to form a single cell suspension of the dermis. The suspension was diluted with 2ml of 10% FBS-MEM and filtered through a cell strainer (70μm nylon mesh; Fisherbrand), before being centrifuged at 1000rpm for 5 minutes. The supernatant was carefully poured off leaving a cell pellet which was resuspended in 1ml of the basic medium.

A haemocytometer was used to count the number of cells collected (appendix IV). This was to ensure consistency in cell number across each experiment and between 2D and 3D culture methods.

4.2.3.2.1.1. Density Separation using Ficoll PM400 (Dermis purification)

To try to reduce the chance of contamination of the dermal cells with epidermal cells, Ficoll PM400 (GE Healthcare, Life Sciences) was used to separate the densities of the cells (keratinocytes and fibroblasts). Two ficoll fraction mixtures were created. For the density of fibroblasts, 1.05 grams of Ficoll was added to 1ml sterile PBS. For the density of keratinocytes, 1.06 grams of Ficoll was added to 1ml sterile PBS. These were left to mix overnight at 4C. The 1.05g solution was then pipetted on top of the 1.06g solution and left for 1 hour at room temperature before use (Figure 4.4). All processes were conducted in a microbiological safety cabinet to reduce the risk of contamination.

In order to separate the cell densities, the single cell suspensions described in section 4.2.3.2.1 were pipetted in the 1ml basic medium into the prepared Ficoll. This was then centrifuged at 8000g/rcf for 1 hour. The cell pellet present in the top fraction was then taken off and resuspended in 1ml basic medium, before being put into cell culture.

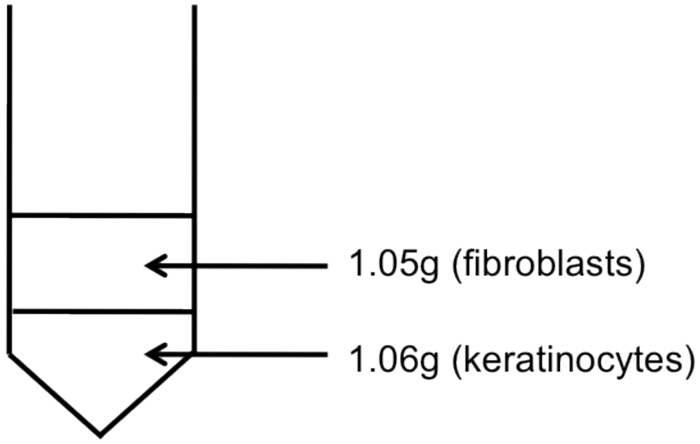

Figure 4.4: Schematic showing FICOLL set-up. 2 different fractions were used: 1.05 grams of Ficoll in 1ml PBS and 1.06 grams Ficoll in 1ml PBS.

4.2.3.2.2. Two-dimensional and 3-dimensional Culture Techniques

2D and 3D culture techniques were used and at specific time-points. 3D was also transferred to 2D. Different incubation times were experimented with to reach what was considered the optimum for the survival of the cells and successful formation of the spheres. Originally the 3D spheres were put into 2D to adhere for just 24 hours, but this was extended to two days. Table 4.1 illustrates the finalized timings used for these procedures.

Table 4.1: The final incubation times for cells in the cell culture model

Embryonic Age (Days)	Incubation Time (Days)		
	2D	3D	3D to 2D
15.5	7	5	2
16.5	6	4	2
17.5	5	3	2
18.5	4	2	2

As well as the length of time, other variables were experimented with, including the size of the well, number of cells and whether to use coverslips or not.

To show clearly the methodology of the cell culture model experimented with, in this chapter and chapter 5, a schematic diagram was made. 2D, 3D and 3D to 2D culture was combined to establish the model system (Figure 4.5).

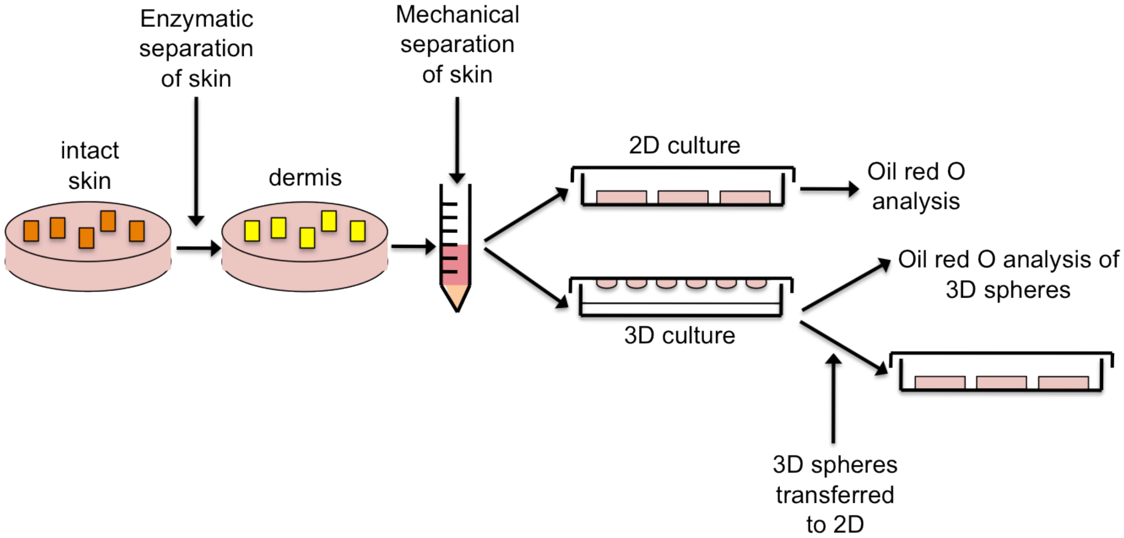

Figure 4.5: Schematic showing the cell culture model system used in this chapter. Skin pieces taken from the mouse embryos were separate to produce dermal pieces. Dermis pieces were mechanically separated to produce a single cell suspension. This was put into 2D and 3D culture and then analysed. Some 3D spheres were transferred to 2D and then analysed.

4.2.3.2.2.1 Two-Dimensional Cell Culture

Many different cell numbers (from 6000 to 600,000 cells) were tried to determine an optimum experimental method. Finally 24,000 cells were settled on so that numbers could be kept relatively consistent with the 3D culture methods.

To each well of a 6-well plate (Bio-weiner, Sigma) or 35mm dish (Nunc), 24000 cells were added in 2ml of basic medium. These were then incubated at 37°C, 5% CO_2. When first establishing the models, media was changed every two days though this was found to have more of a negative effect than leaving the media for the duration of the incubation and reducing infection/contamination risk. While 6-well plates were used for the final experiments, 24-well plates were also experimented with. As well as this, in an attempt to use the cells for immunofluorescence analysis, coverslips were placed in the bottom of the wells before pipetting the cells on top.

After the respective durations in culture, representative pictures were taken of the cells (Zeiss Axiovert 10 with AxioCam ERc5s) before being washed in PBS (3x5mins) in preparation for analysis (e.g. Oil Red O or immunofluorescence analysis).

4.2.3.2.2.2. Three-Dimensional Cell Culture

Spheres were created by pipetting 10µl drops containing 3000 or 6000 cells onto the petri dish lids, evenly spaced and not too close to the edge. Control dishes using the original (much higher) cell density suspensions were also set up, termed "concentrated spheres". 25ml of sterile distilled H_20 was put into each petri dish and the drops were suspended over this to prevent them from drying out (Figure 4.5). Petri dishes containing 25ml of sterile distilled H_20 but no spheres were placed above and below before being transferred to the incubator (37C, 5% CO_2).

After the respective durations in culture as described in table 4.1, representative images were taken of the spheres (Zeiss Stemi SVII). 10-15 spheres were embedded in Tissue-Tek® O.C.T.™ compound (Sakura, Agar Scientific, Netherlands), snap frozen in liquid nitrogen and kept at −80°C.

4.2.3.2.2.3. Three-Dimensional to Two-Dimensional Cell Culture Transfer

Images were taken of the spheres (Zeiss Stemi SVII) before being transferred to 2D culture. Different experiments transferred different number of spheres from 1 sphere per well of a 24 well plate to pipetting all the spheres into one 35mm dish. However, for comparison with dishes containing 24,000 cells in 2D culture, the method used consistently was that four spheres (4x 6000 cells) were plated in 200ul of the basic medium in the centre of each well of a plate. These were allowed to adhere and grow out for 1-2 days. Spheres were also transferred onto coverslips for one of the experimental repetitions and left to adhere for a couple of hours in an incubator before more media was added.

After the durations in culture listed in table 4.1, representative pictures were taken of the spheres having grown out and adhered, before being washed in PBS (3x 5 minutes) in preparation for analysis (e.g. Oil Red O or immunofluorescence analysis).

4.2.3.2.2.4. Whole Skin Cultures

To observe the effects of contamination, the cell culture model system was set up with whole skin. To do so, both the epidermis and dermis pieces were made into a single cell suspension and cultured together. The dermis and epidermis was still separated to make it easier to break up the cells. The cells were then put into 2D and 3D culture in the same way as the dermal cells as described above (section 4.2.3.2.2).

4.2.4. Oil Red O Analysis

Slightly different staining protocols were used depending on the type of sample being analysed. The organ culture frozen skin sections were stained in the same way as the frozen sphere sections cut from the frozen blocks (see sections 4.2.3.1 and 4.2.3.2.2.2).

4.2.4.1. Frozen Skin and Sphere Sections

Following incubation for the required period, spheres were either put into 2D cell culture in 6 well plates or frozen in OCT for subsequent analysis. Sections (10µm) were cut on a cryostat (LEICA CM 3050S) and attached to ColorFrost®Plus slides (Thermo Shandon Ltd, Cheshire, UK). Slides were left to dry at room temperature for 1hour 30 minutes and then washed in PBS (3x 5 minutes) followed by fixation in calcium formal (Appendix I) for 1 hour. They were then incubated with 60% isopropanol (Sigma) for 15 minutes and stained with a working solution of oil red O (Appendix 1) for 15 minutes. Slides were briefly washed in 60% isopropanol to remove excess oil red O and then rinsed in water. They were counterstained by dipping each slide in Shandon instant haematoxylin (Thermo Scientific, Cheshire, UK) and then rinsing in water. Slides were mounted in pre-warmed glycergel (DakoCytomation Inc. California, USA) and coverslipped. Images were taken on a Zeiss Axio Imager (M1) microscope using Volocity software.

4.2.4.2. 2D Cell Oil Red O Staining Method

A shortened staining protocol was used for the cells. After cell culture and pictures had been taken on a Zeiss Axiovert 10 microscope using Axiovision software and a Zeiss AxioCam ERc5s camera (put earlier), the cells adhered to 6 well plates grown in 2D and those transferred from 3D-2D were washed in PBS and then fixed in calcium formal for 10 minutes. The wells were then immediately stained or stored in PBS at 4°C prior to staining.

An incubation with 60% isopropanol was followed by 10 minutes with a working solution of oil red O. A short wash in 60% isopropanol was then used to remove any excess oil red O followed by two careful washes in PBS to make sure the spheres remained adhered to the plastic. The cells were then stored in PBS at 4°C before pictures were taken.

4.2.4.3. Oil Red O Quantification

While in most cases, the images in these experiments clearly showed a difference in the amount of lipid detected in the cells subjected to different experimental conditions (2D vs. 3D), another aim was to establish a means of quantifying the level of oil red O to support these visual assessments. A number of experimental variables were adapted as the best potential method of quantification was experimented with.

Wells had been stained with oil red O (Sigma) and stored in PBS at 4°C. Before quantification, the PBS was pipetted off and the wells were allowed to dry out for several minutes. 100% isopropanol was added to each well or 35mm dish. Varying amounts were experimented with - from 100μl to 1ml. A cell scraper (Greiner bio-one) was also used at one point to detach and dissociate the cells and spheres from the base of the wells. This was to ensure all oil red O was picked up. The wells were then fairly vigorously shaken for 10 minutes to take off any oil red O present in the cells. Serial sampling was conducted across 3 wells. The 100ml of isopropanol in each well was collected and added together with that from 2 other wells to create one sample.

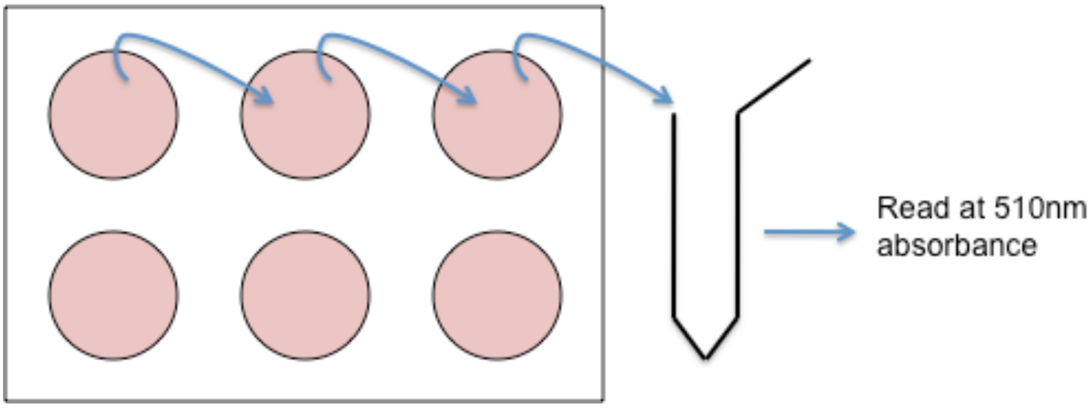

Figure 4.6: Diagram depicting serial sampling of oil red O for quantification. 100% isopropanol with the oil red O from the cultured cells was collected to together from 3 wells of the 6-well experiment plate and read at 510nm on a nanodrop using UV-Vis software.

Using a nanodrop and UV-Vis software, the absorbance values of oil red O from each well were read at 510nm. A spectrophotometer was also tried, whereby the volume of isopropanol collected was made up to 1ml and measured. Each reading was repeated three times to make sure the results were consistent and generate an average. 100% isopropanol was used as a blank and each solution was vortexed, before reading to evenly distribute the oil red O.

4.2.5. Immunofluorescence Analysis

Table 4.2: Summary of primary antibodies, fluorescent secondary antibodies and conditions used for immunofluorescent staining

Antibody/ Factor Name	Manufacturer	Raised in	Clonality (P/M*)	Dilution	Secondary antibody used
C/EBPα	Santa Cruz	Rabbit	P	1:100	Goat anti rabbit (FITC)
					Goat anti rabbit (594)
FABP4	R&D Systems	Goat	P	1:50	Goat anti mouse (FITC)
Pan-keratin	Zymed	Mouse		1:100	Goat anti mouse (FITC)
PECAM1	DSHB	Mouse		1:100	Goat anti mouse (FITC)

* P - polyclonal; M – monoclonal

Table 4.3: Details of the corresponding secondary antibodies used for immunofluorescence

Secondary Antibody		Manufacturer	Dilution
Donkey anti rabbit (FITC)	AlexaFluor^{R} 488 AlexaFluor 594	Invitrogen	1:500
Goat anti rabbit (FITC)	AlexaFluor^{R} 488	Invitrogen	1:500
Goat anti mouse (FITC)	AlexaFluor^{R} 488	Invitrogen	1:500

4.2.5.1. Indirect Immunofluorescence

Approximately six sections cut at 7μm were attached to the slides and then allowed to dry (see section 4.2.4.1). Slides were then fixed, blocked and stained for the specific factors described below. During staining, slides were kept in a humidity chamber in the dark to prevent the sections from drying out and the fluorescence fading. After staining, the slides were mounted in anti-fade Mowiol (or Vectashield to counterstain with DAPI if they had not been incubated with DAPI. Slides were stored at 4°C in the dark.

Immunofluorescence analysis was performed on a Zeiss Axio Imager M1 microscope with Volocity software. For each age, negative controls were produced whereby there was no incubation with the primary incubation but 1% goat (or donkey serum/PBS overnight. The same secondary antibodies were used to observe non-specific staining.

4.2.5.1.1. Preadipocyte Marker – C/EBPα

In order to determine whether cells were committed to the adipocyte lineage before morphological changes occurred the preadipocyte marker, C/EBPα was stained for using indirect immunofluorescence.

While originally slides with skin sections were not fixed but first washed in PBS (3 x 5 minutes), 2D cells on coverslips and 3D sphere sections were fixed prior to C/EBPα staining using 4% PFA for 15 minutes followed by permeabilisation for 5 minutes in 0.5% Triton-X (Appendix I). Sections were then blocked in 20% goat serum (Sigma, MO, USA) for 30 minutes and washed in PBS for a couple of minutes. The slides were incubated with C/EBPα (1:100, Santa Cruz) in 1% goat serum/PBS overnight at 4°C or left at room temperature for 2 hours. The slides were washed three times in PBS for 5 minutes and incubated with a goat anti-rabbit fluorescent secondary antibody (Invitrogen, 1:500) for 1 hour at room temperature. After 55 minutes of incubation with the secondary antibody, 4′,6-diamidine-2′-phenylindole, dihydrochloride (DAPI) (KPL, Maryland, USA) was added to the slides for 5 minutes. Three more 5-minute washes in PBS were conducted before being coverslipped and mounted.

4.2.5.1.2. Pan keratin

To determine the degree of epidermal contamination, if any, in the dermal cell spheres a pan-keratin antibody also known as cytokeratin was used to stain for epidermal cells. Sections were washed in PBS (3x 5min) and fixed in ice-cold methanol for 15 minutes followed by ice-cold acetone for 5 minutes. They were then blocked in 10% goat serum for 1 hour or 20% goat serum for 30 minutes at room temperature. Slides were incubated with the pan-keratin primary antibody (Zymed, 1:100) overnight at 4C. 3 x 5 minute PBS washes were then conducted prior to incubation with a goat anti-mouse secondary antibody for 1 hour at room temperature. To this, DAPI (1:5000) was added for 5 minutes. 3 x 5 minute PBS washes were undertaken before slides were mounted in Mowiol and coverslipped.

4.2.5.1.3. PECAM1

A PECAM antibody was used to detect if blood vessels were developing. The slides were fixed in ice-cold methanol for 15 minutes and then ice-cold acetone for 5 minutes, followed by 2, 2 minute washes in PBS. The sections were then blocked in 20% goat serum for 30 minutes and washes 3 x 5 minutes in PBS before being incubated with the PECAM antibody overnight. 3 x 5 minutes PBS washes were conducted and then the slides were incubated with the goat anti-mouse secondary antibody for 1 hour at RT. Slides were mounted and coverslipped.

4.2.6. Haematoxylin and Eosin (H&E) Staining

This was used to recognize the structure of the skin/spheres in particular to determine whether the sections were healthy and thus determine the reliability of the culture systems.

The slides were washed in distilled water for 5 minutes and then incubated for 5 minutes in haematoxylin (Haematoxylin prepared according to Gills; Sigma). They were rinsed in distilled water and then washed for 5 minutes in tap water. The slides were then dipped in acid ethanol 6-8 times before being washed in tap water twice for one minute and once for 2 minutes in distilled water. The sections were then counterstained with eosin (Sigma, Egham, UK) for less than 30 seconds. A series of washes were then conducted; 3 x 1 minutes washes in 75% ethanol, 2 x 2 minute washes in 100% ethanol and 2 x 2 minute washes in histoclear (National Diagnostics, Hull, UK). Coverslips were mounted in DPX (Agar Scientific Ltd., Stansted, UK) and left to dry for 2 hours in a fume cupboard.

4.2.7. Toluidine Blue Staining

Slides were dried and then stained with a solution of 1g toluidine blue in 100ml 70% ethanol for 3 minutes. Excess stain was washed off using water and slides were mounted in DPX and coverslipped.

4.3. Results

4.3.1. Organ Culture Model

Many stages and varying techniques were undergone to develop this model. While in general the results from this model were not consistent and therefore the organ culture method was not deemed reliable enough to put to further use in this project, it did show some interesting results. The skin was observed during the course of the experiment and repeats of it to become familiar with the system. Eventually skin taken from embryonic day 16.5 aged embryos (e16.5) was focused on for the establishment of these models, though often other ages were readily available and were useful for investigating certain variables of the models. As well as this it was originally thought more appropriate to look later, though more recently it has been considered that commitment to the adipocyte and lineage and process of development actually starts much earlier. Part of this hypothesis comes from the fact that fat can still form from dermal cells separated from the epidermis as early as e14.5 as shown in the spheres in chapter 3.

In this section, the many stages of establishing this organ culture model are described. The model was persisted with, with several avenues being explored and many repeats conducted as not only was it deemed a promising way of looking at development in terms of it being closer to in vivo than in vitro cell line studies but it was also a manageable way of creating in vivo-like conditions ex vivo. It had also been used before in Jahoda's lab.

4.3.1.1. Morphology of Mouse Back Skin in Organ Culture

One of the defining characteristics, after three days incubation, was the ridge that formed around the edge of the skin sections, thought to be a wound healing response. This was used as a positive indication that the skin was alive and developing and therefore potentially healthy. As well as this, the formation of follicles, visible as raised bumps on the surface of the skin, was suggested to show that the skin is developing in culture (Figures 4.7C and D). An example of both the ridge and the follicles are shown in figures 4.7C and D. A visible difference exists between the skin before and after culture. Conversely, the darker coloration of some skin pieces was considered a negative indication of its physical condition (Figure 4.8C).

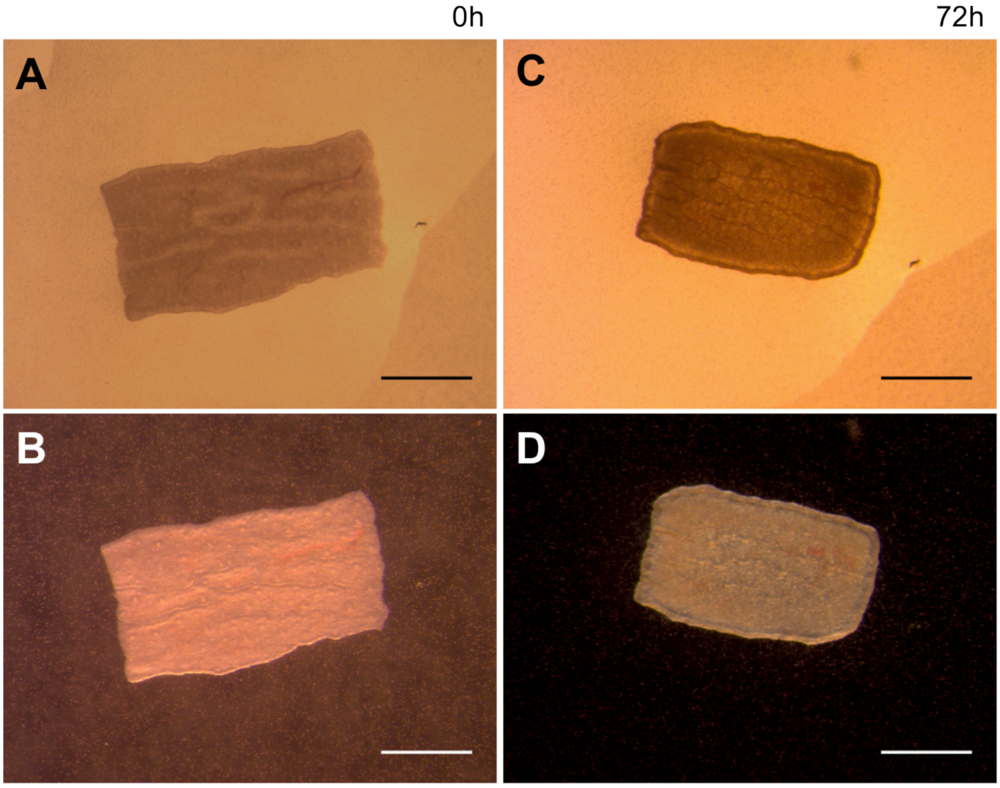

Figure 4.7: **Organ culture of 16.5 embryonic day mouse back skin.** (**A,B**) Skin on collagen filters prior to incubation. (**C,D**) Skin on collagen filters are 72h incubation period. Images were taken using a Zeiss Axiovert 10 microscope. (**A,C**) bright field. (**B,D**) dark field. Scale bar = 1mm.

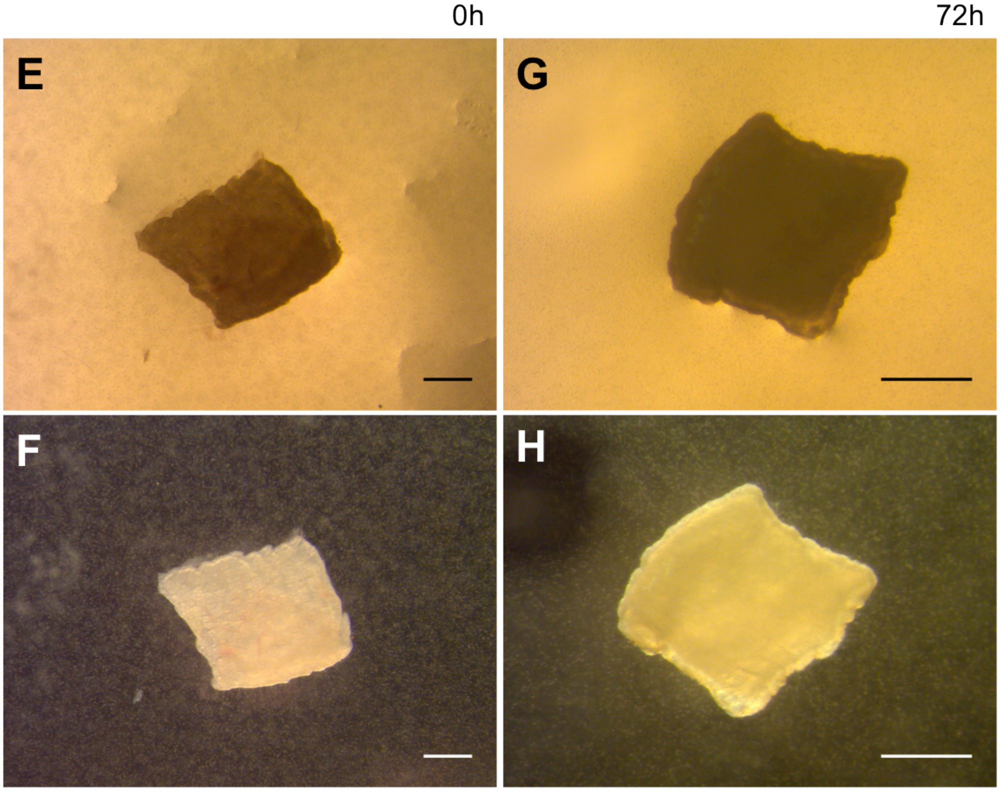

Figure 4.8: **Organ culture of 16.5 embryonic day mouse back skin.** (**A,B**) Skin on collagen filters prior to incubation. (**C,D**) Skin on collagen filters are 72h incubation period. Images were taken using a Zeiss Axiovert 10 microscope. (**A,C**) bright field. (**B,D**) dark field. Scale bar = 1mm.

While originally oil red O analysis was going to be conducted on the skin sections after 3-day incubations to determine what level of fat development was occurring (Wojciechowicz 2012), H&E staining was focused on while the model was in the process of development. This was to look at the quality of skin pieces rather than purely examining their fat content. This was because the skin pieces were found to vary and some were pathological or had formed a gap in the dermis of the sections. This gap was thought to be in response to the staining protocol (Figures 4.9D and E). Upon repetition of the staining, however, and use of a quick, less harsh toluidine blue staining, the gap in the dermis was still visible in some sections.

Some of the sections exhibited follicles with darkened nuclei that had become concentrated circles rather than growing down from the epidermis and forming extended hair follicles, hence they had become pathological (Figures 4.9A-C). Therefore, developing the culture model to produce consistently healthy, developing skin pieces was the focus of the experiments, rather than the degree of red staining of the adipocytes at this stage.

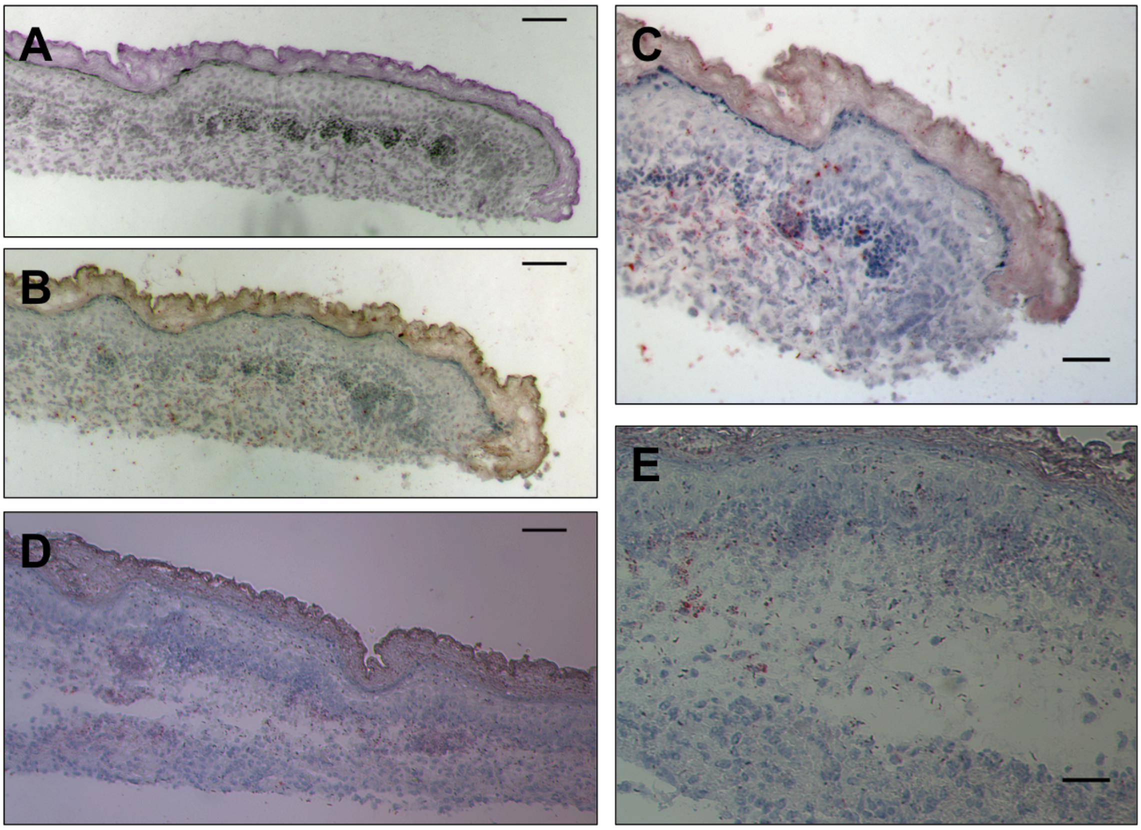

<u>Figure 4.9:</u> Oil red O analysis of organ cultured 16.5 embryonic day mouse back skin. Fat droplets present in adipocytes visible as red coloration. Images were taken using a Zeiss Axio Imager M1. (**A,B,D**) scale bar = 65μm. (**C,E**) scale bar = 40μm.

One day older skin aged 17.5 day embryonic was put into organ culture (Figure 4.10) to elicit if perhaps the age of the skin was an impeding factor on why some of the skin pieces were not developing properly. It was found that younger skin was more responsive in culture than the older skin and the older pieces were darker in coloration (Figure 4.10 1E). As well as e17.5, skin left in culture for 4 days appeared darker as well.

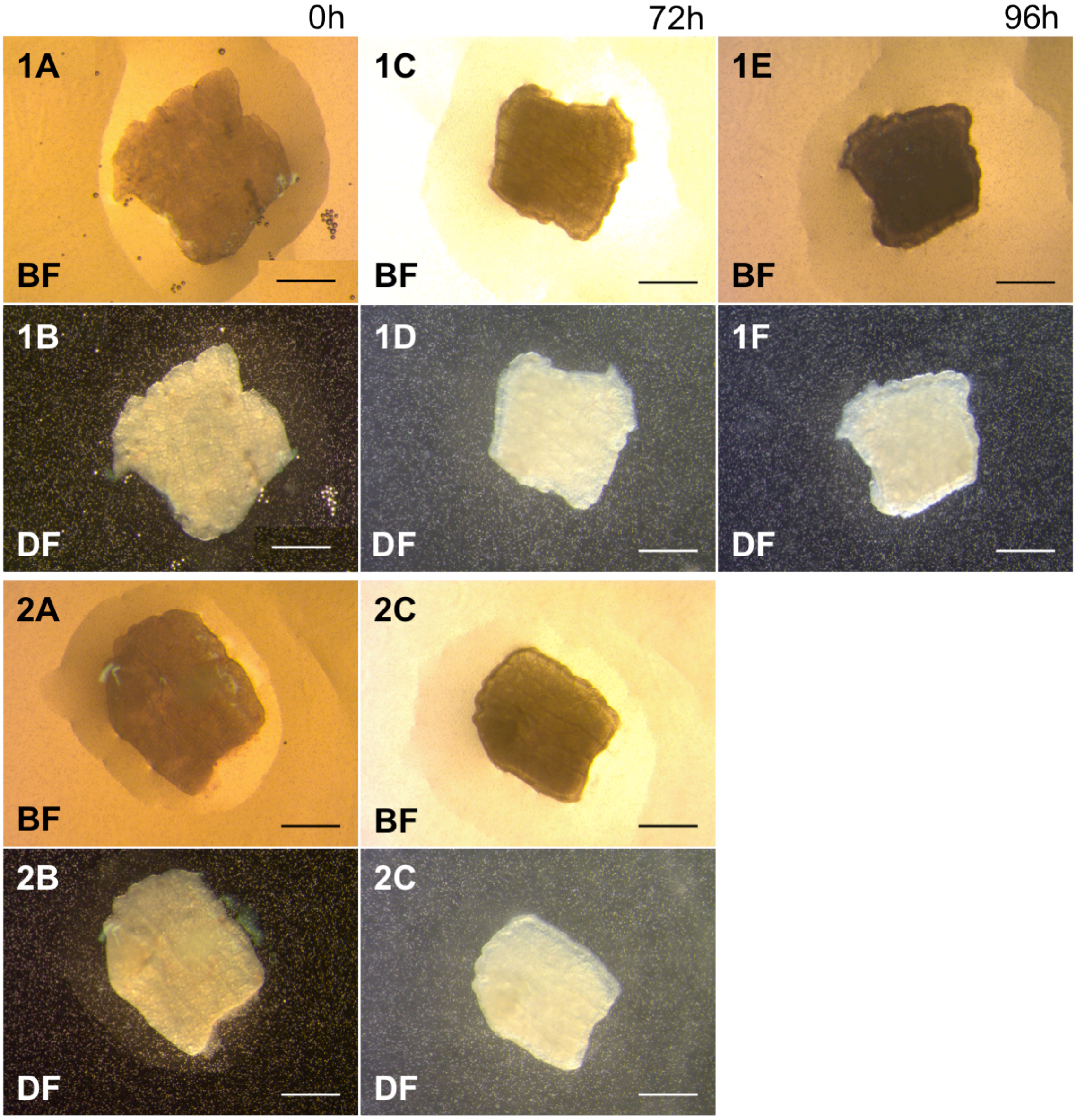

<u>Figure 4.10:</u> Organ culture of 17.5 embryonic day mouse back skin. (**1A,B, 2A,B**) Skin on collagen filters prior to incubation. (**1C,D, 2C,D**) Skin on collagen filters are 72h incubation period. (**1E, F**) Skin on collage filters after 4 days/96 hours incubation. Images were taken using a Zeiss Axiovert 10 microscope. (**A,C**) bright field. (**B,D**) dark field. Scale bar = 1mm.

Skin pieces, with the muscle layer and some of the subcutaneous layer, termed 'thick skin', were put into culture to determine if perhaps the skin wasn't surviving, because it needed the tissue layers beneath the skin for maintenance. This was of no increased benefit as follicular growth was not clearly visible and the piece looked particularly dark after 72 hours in culture (Figure 4.11C).

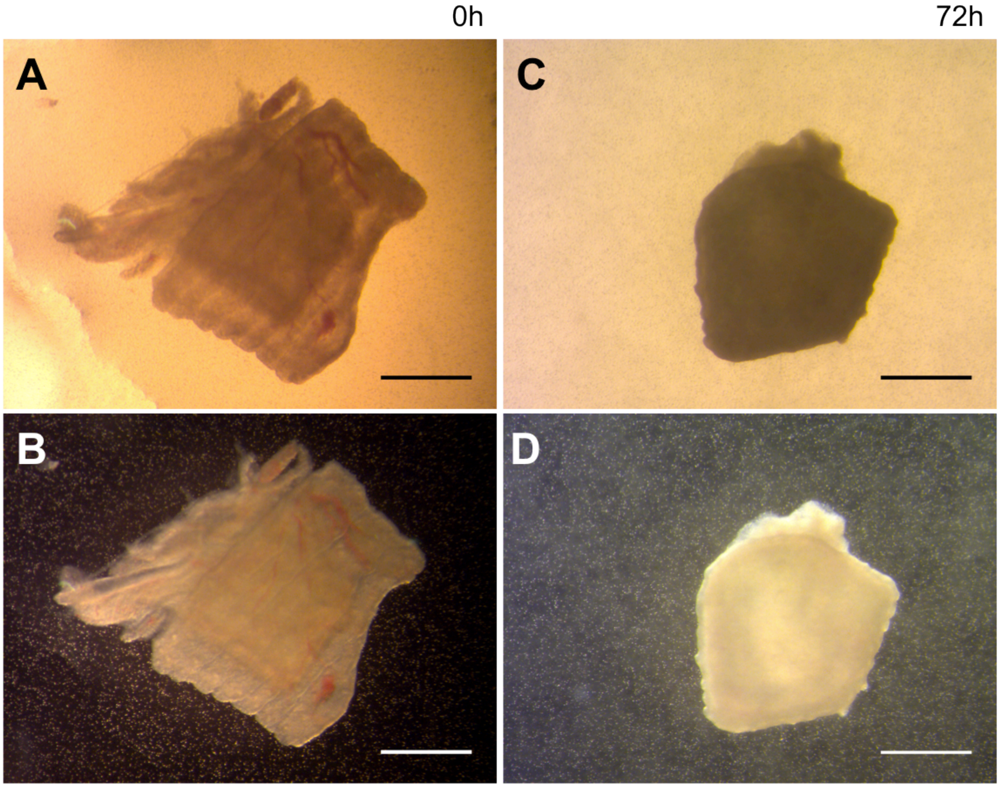

Figure 4.11: Organ culture of 17.5 embryonic day mouse thick skin pieces. (**A,B**) skin on collagen filters prior to incubation. (**C,D**) skin on collagen filters are 72h incubation period. Images were taken using a Zeiss Axiovert 10 microscope. (**A,C**) bright field. (**B,D**) dark field. Scale bar = 1mm.

4.3.1.2. Use of Different Serum Concentrations

This preliminary organ culture experiment was repeated with little positive advancement in the physical appearance of the skin, therefore different serum concentrations were experimented with. Figures 4.12-14 show representative pieces from these experiments and their repeats that produced similar results. It was considered that the factors in the serum may be helping or hindering the skin's development thus, as well as the 1% serum, organ culture dishes were set up with 0% serum and 2% serum. This revealed not much difference between the pieces. In general, follicle growth was present in many of the skin pieces and the pieces cut were of a more uniform shape. While not much overall difference was exhibited, the pieces were not consistent under each condition. For example, two separate pieces supplied with 0% FBS/MEM were different in that while piece 1 (Figures 4.12a-h) showed developing follicles, piece 2 (Figures 4.12i-p) developed less well with a split in the skin's dermis. In 1% FBS/MEM, the wound healing response at the edge of the skin pieces occurred though the dermis did have a split in both pieces (Figure 4.8o). Those subjected to 2% FBS/MEM showed clear expansion of the epidermis but different follicular development (Figure 4.14).

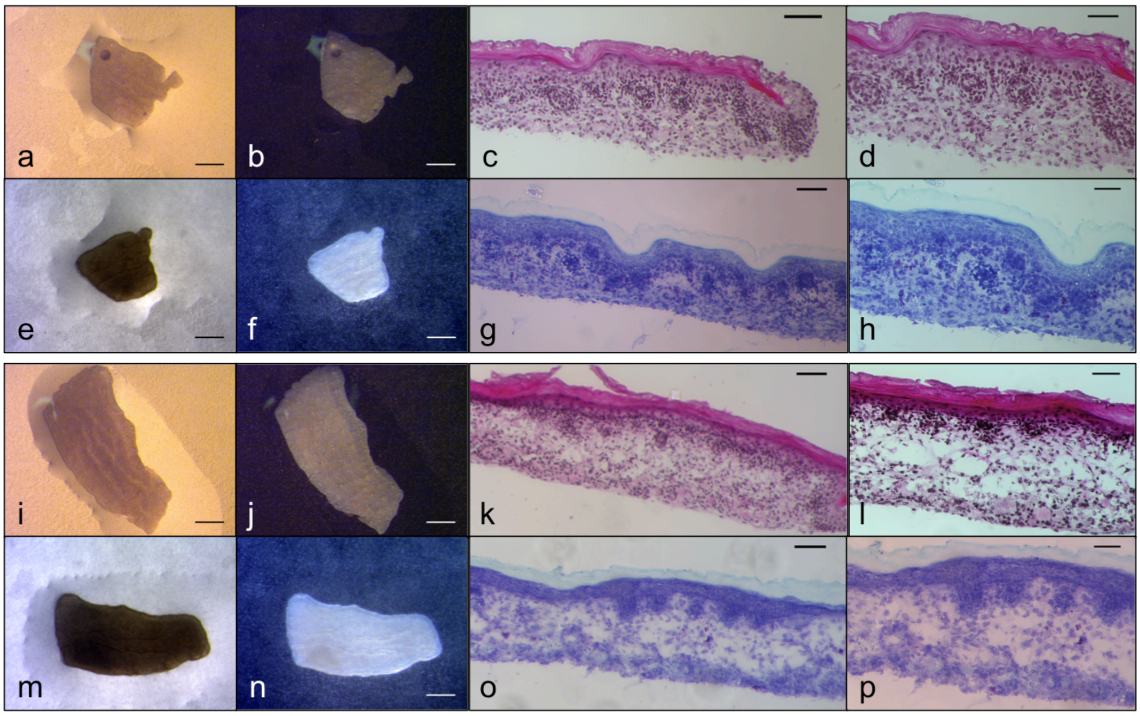

Figure 4.12: 16.5 embryonic day organ cultured skin in 0% FBS/MEM. (**a-h**) piece 1. (**i-p**) piece 2. (**a,e,i,m**) bright field images and (**b,f,j,n**) dark field images, taken on Zeiss Axiovert 10. (**c-h** and **k-p**) after 72 hours in culture. (**c,d,k,l**) H&E staining and (**g,h,o,p**) toluidine blue staining, images were taken using a Zeiss Axio Imager M1. (**a,b,e,f,I,j,m,n**) scale bar = 1mm. (**c,g,k,o**) scale bar = 65µm. (**d,h,l,p**) scale bar = 40µm.

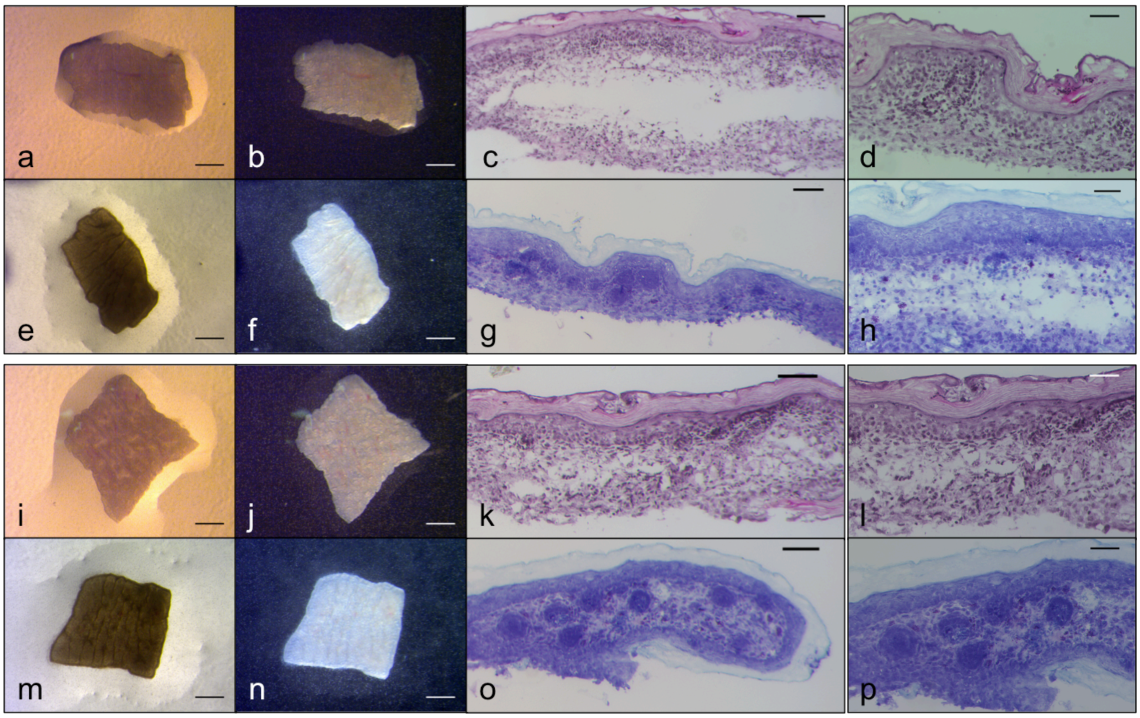

Figure 4.13: **16.5 embryonic day organ cultured skin in 1% FBS/MEM.** (**a-h**) piece 1. (**i-p**) piece 2. (**a,e,i,m**) bright field images and (**b,f,j,n**) dark field images, taken on Zeiss Axiovert 10. (**c-h** and **k-p**) after 72 hours in culture. (**c,d,k,l**) H&E staining and (**g,h,o,p**) toluidine blue staining, images were taken using a Zeiss Axio Imager M1. (**a,b,e,f,I,j,m,n**) scale bar = 1mm. (**c,g,k,o**) scale bar = 65μm. (**d,h,l,p**) scale bar = 40μm.

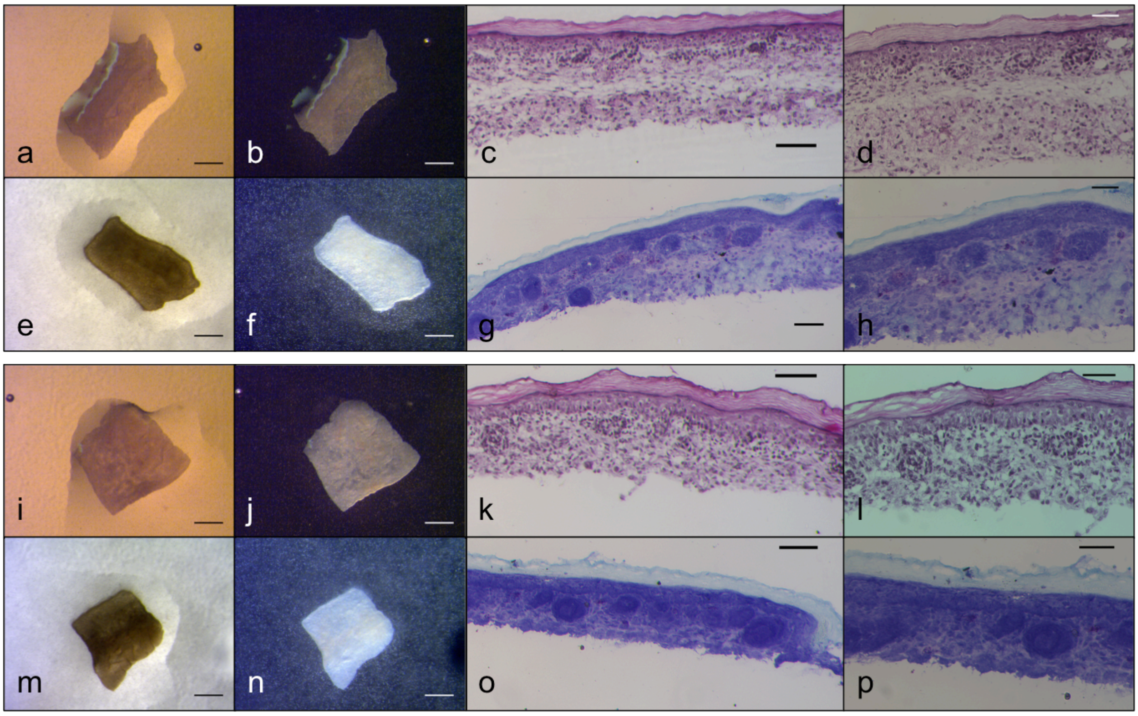

Figure 4.14: **16.5 embryonic day organ cultured skin in 2%FBS/MEM.** (**a-h**) piece 1. (**i-p**) piece 2. (**a,e,i,m**) bright field images and (**b,f,j,n**) dark field images, taken on Zeiss Axiovert 10. (**c-h** and **k-p**) after 72 hours in culture. (**c,d,k,l**) H&E staining and (**g,h,o,p**) toluidine blue staining, images were taken using a Zeiss Axio Imager M1. (**a,b,e,f,I,j,m,n**) scale bar = 1mm. (**c,g,k,o**) scale bar = 65μm. (**d,h,l,p**) scale bar = 40μm.

4.3.1.3. Changing from MEM to William's Medium

The organ culture method was then tried with a different type of media, known as William's media; the higher glucose concentration could potentially aid the survival and better growth of the skin in culture. Alongside this, organ culture dishes with modified essential medium (MEM) were also set up as a direct comparison, the results of which are discussed previously in section 4.3.1.2. For both types of media, 0%, 1% and 2% serum concentrations were investigated. H&E staining was then conducted to determine whether any one combination of conditions was behaving optimally. When provided with no serum, clear follicle down growth occurred, especially in one of the pieces (Figure 4.15f). The skin pieces were more regularly shaped. It can be suggested that perhaps the more regular, even shaped skin pieces are more capable of healthy and realistic development. This was also the case with those supplemented with 1% FBS/William's E media, whereby the even shaped piece (Figure 4.16a-h) had grown a lot healthier than piece 2 (Figure 4.16i-p). With 2% foetal bovine, while one piece appeared to have lost all evidence of follicular down growth, a second piece had visible follicle down growth, expansion of the epidermis and presence of a wound healing response clearly illustrated by epidermal growth round the edge of the skin piece (Figure 4.17k).

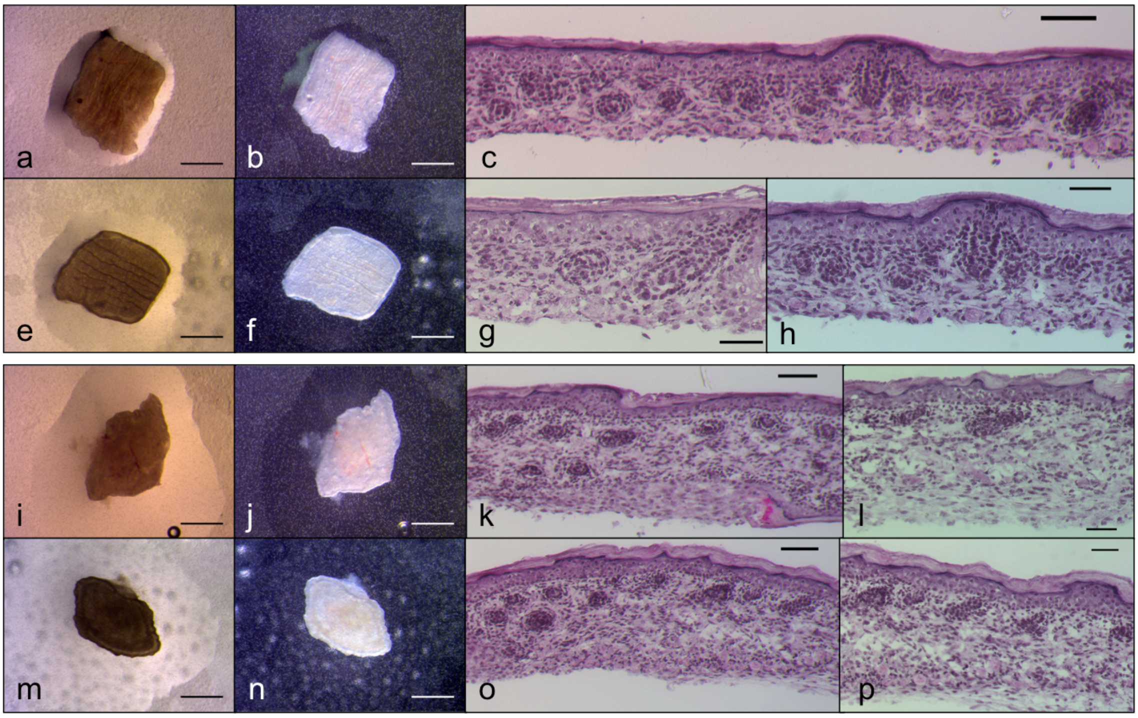

Figure 4.15: **16.5 embryonic day organ cultured skin in 0%FBS/William's E.** (**a-g**) piece 1. (**h-o**) piece 2. (**a,d,h,l**) bright field images and (**b,e,i,m**) dark field images, taken on Zeiss Axiovert 10. (**c-g** and **j-o**) after 72 hours in culture. (**c,f,g,j,k,n,o**) H&E staining, images were taken using a Zeiss Axio Imager M1. (**a,b,d,e,h,i,I,m**) scale bar = 1mm. (**c,j,n**) scale bar = 65μm. (**f,g,k,o**) scale bar = 40μm.

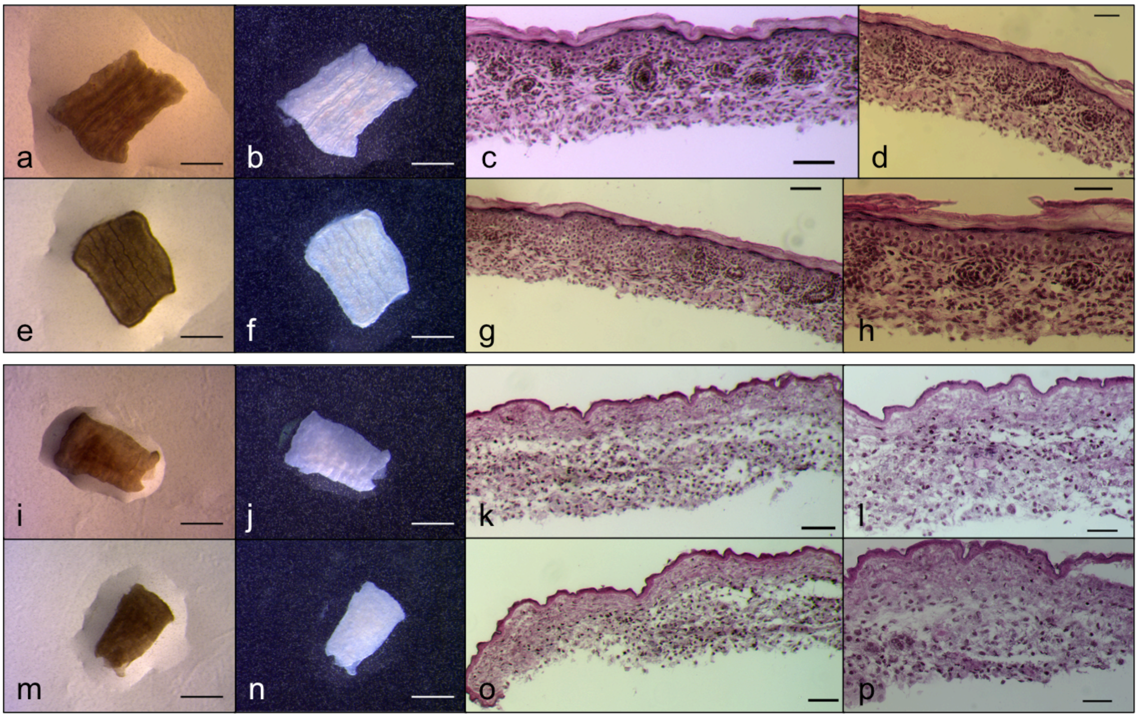

Figure 4.16: **16.5 embryonic day organ cultured skin in 1% FBS/William's E.** (**a-h**) piece 1. (**i-p**) piece 2. (**a,e,i,m**) bright field images and (**b,f,j,n**) dark field images, taken on Zeiss Axiovert 10. (**c-h** and **k-p**) after 72 hours in culture. (**c,d,g,h,k,l,o,p**) H&E staining, images were taken using a Zeiss Axio Imager M1. (**a,b,e,f,I,j,m,n**) scale bar = 1mm. (**c,g,k,o**) scale bar = 65μm. (**d,h,l,p**) scale bar = 40μm.

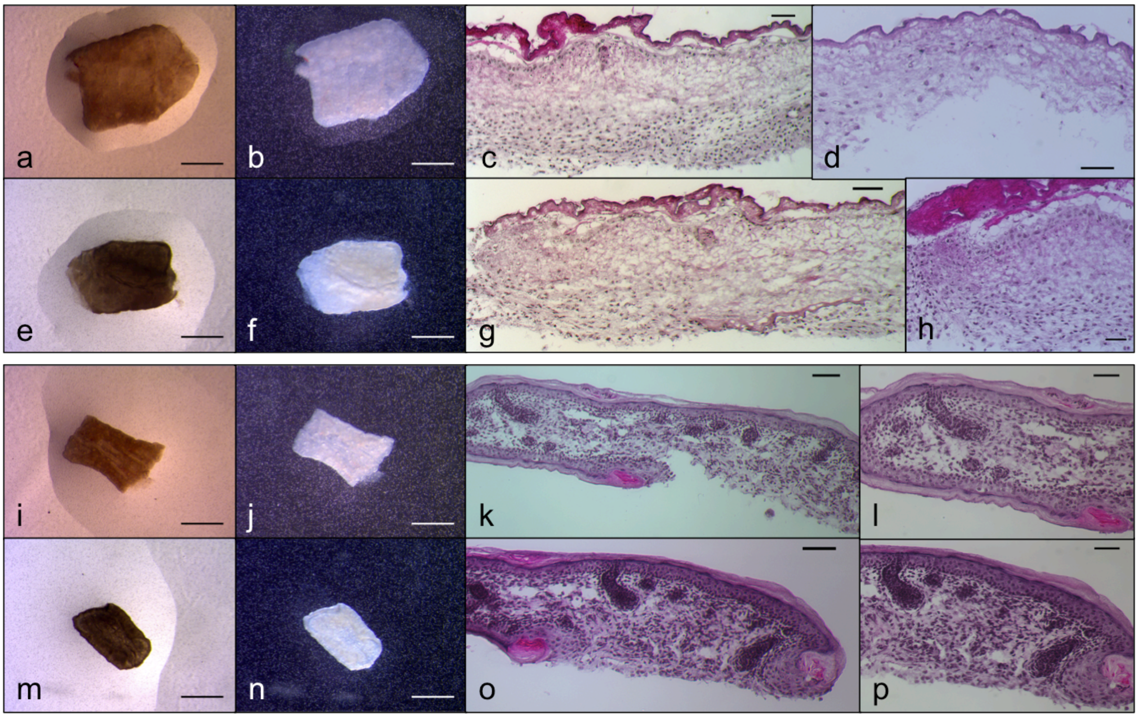

Figure 4.17: **16.5 embryonic day organ cultured skin in 2% FBS/William's E.** (**a-h**) piece 1. (**i-p**) piece 2. (**a,e,i,m**) bright field images and (**b,f,j,n**) dark field images, taken on Zeiss Axiovert 10. (**c-h** and **k-p**) after 72 hours in culture. (**c,d,g,h,k,l,o,p**) H&E staining, images were taken using a Zeiss Axio Imager M1. (**a,b,e,f,I,j,m,n**) scale bar = 1mm. (**c,g,k,o**) scale bar = 65μm. (**d,h,l,p**) scale bar = 40μm.

4.3.1.4. Oil Red O Analysis of Organ-cultured Skin

While H&E staining (and often the quick toluidine blue staining) became the primary focus in comparing the different pieces, it was of interest to see if the difference in the quality of the skin was having an effect on adipocyte formation in the lower dermis. Organ-cultured skin pieces that had been frozen down were later stained with oil red O. Culture supplied with MEM and supplemented with either 0%, 1% or 2% FBS (Figure 4.18) exhibited skin pieces that were not as well developed and appeared to show more red staining (Figures 4.18 2a and 2c) than those which evidence would suggest were healthier (Figure 4.18 1b). Comparatively with William's E media, the degree of healthy development did not relate to the level of oil red O staining visible (Figure 4.19). There was evidence of variety across the pieces, which is reason in itself that the culture system is currently not successful enough to use as a suitable model for further investigation. Ideally, with respect to the fact that all the skin pieces here were of the same age, the level of adipocyte development interpreted by the degree of red coloration from the oil red O should have been relatively similar.

The follicles have already started to form by e16.5, once initiated around e14/14.5 (Figures 4.20 1a-c), therefore, one would expect to see apparent follicles 3 days after organ culture. Comparatively, however, the oil red O stained skin (Figure 4.20.2) illustrated that the follicles became pathological. This was an indication that the model was not appropriate to further study adipogenesis at this stage.

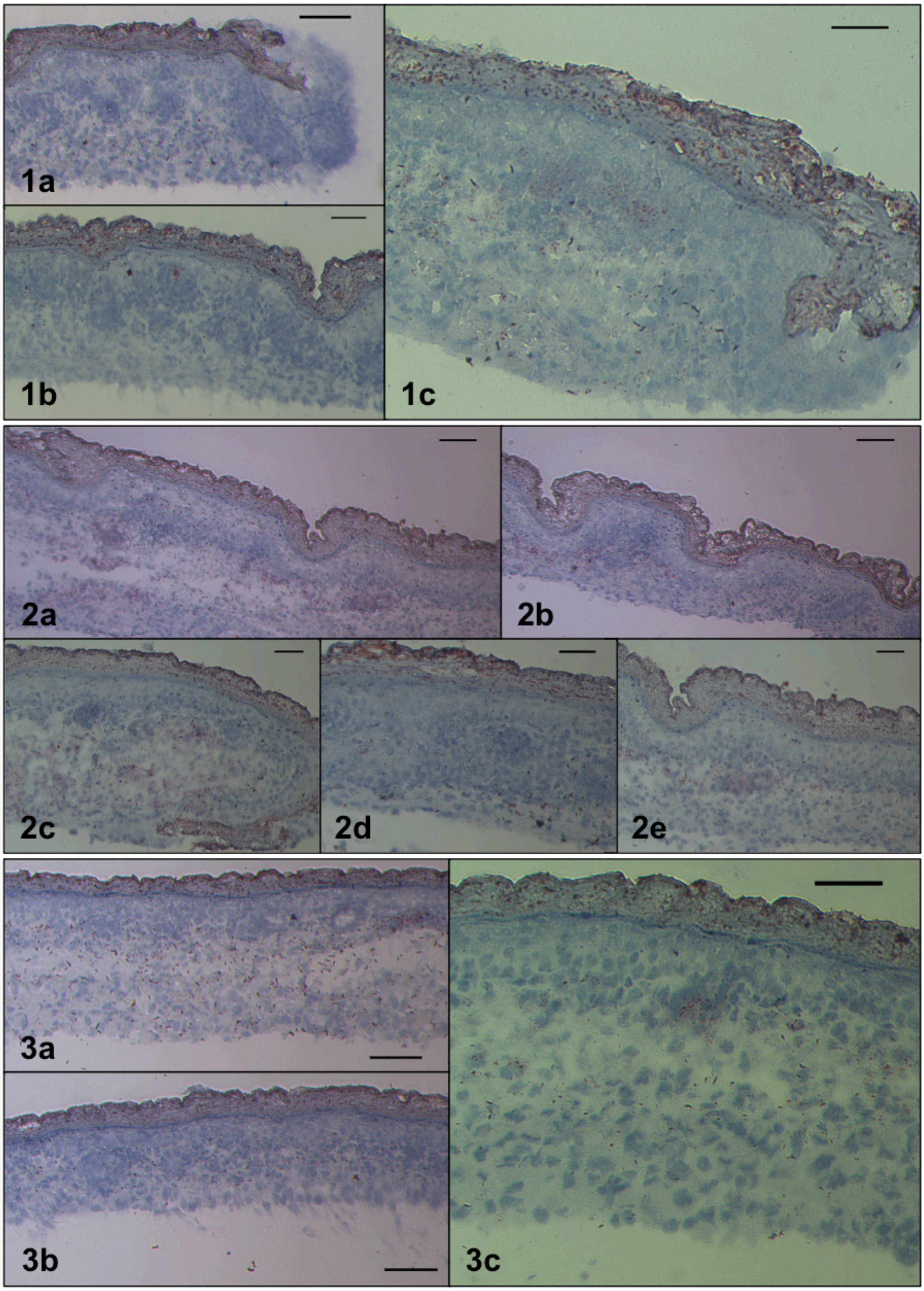

Figure 4.18: Oil red O analysis of organ cultured 16.5 embryonic day skin in MEM. (**1**) no serum. (**2**) 1% FBS. (**3**) 2% FBS. Fat droplets present in adipocytes visible as red coloration. Images were taken using a Zeiss Axio Imager M1. (**1a,2a/b,3a/b**) scale bar = 65μm. (**1b/c,2c-e,3c**) scale bar = 40μm.

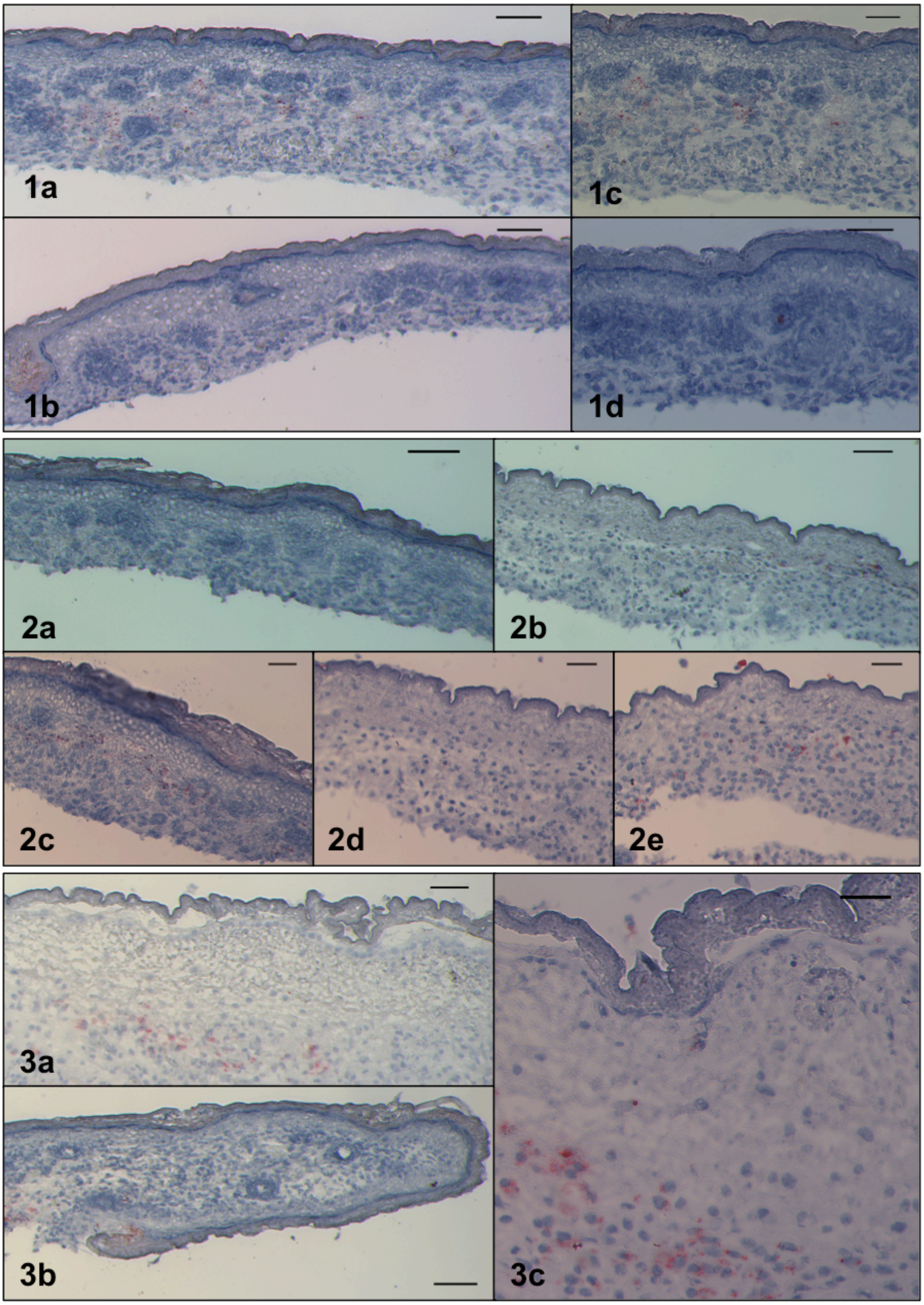

Figure 4.19: Oil red O analysis of organ cultured 16.5 embryonic day skin in William's E. (**1**) no serum. (**2**) 1% FBS. (**3**) 2% FBS. Fat droplets present in adipocytes visible as red coloration. Images were taken using a Zeiss Axio Imager M1. (**1a/b,2a/b,3a/b**) scale bar = 65μm. (**1c/d,2c-e,3c**) scale bar = 40μm.

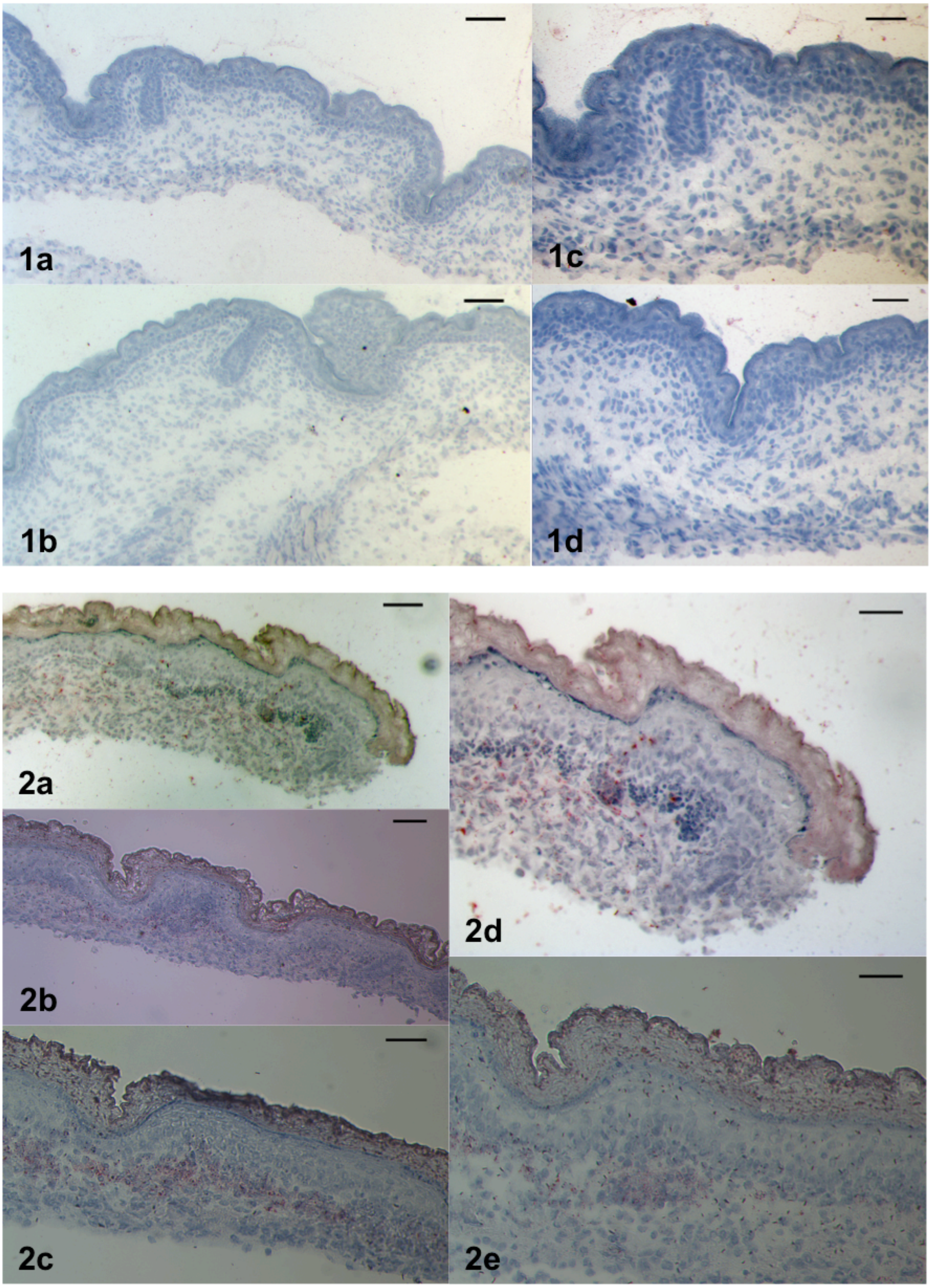

Figure 4.20: Oil red O analysis of 16.5 embryonic day skin before and after 72h organ culture in 1% FBS/MEM. (**1**) e16.5 normal skin (**2**) e16.5 skin post 72h organ culture. Fat droplets present in adipocytes visible as red coloration. Images were taken using a Zeiss Axio Imager M1. (**1a/b,2a/b**) scale bar = 65μm. (**1c/d,2c-e**) scale bar = 40μm.

4.3.2. The Cell Culture Model

Next, the potential of creating a cell culture model, closer to reality than using cell lines was investigated. Firstly, cells taken from the dermis of e16.5 mouse embryos were plated into a 35mm dish to determine if this was a viable way of developing a potential model (Figure 4.21). After 7 days, the cells were confluent and split. One dish was left unsplit as a control (Figure 4.21E and F). There were some dark granular shapes within the cells, which suggested lipid droplets had formed, thus adipocytes developed in culture. These cells were later stained with oil red O (Figure 4.21D and F).

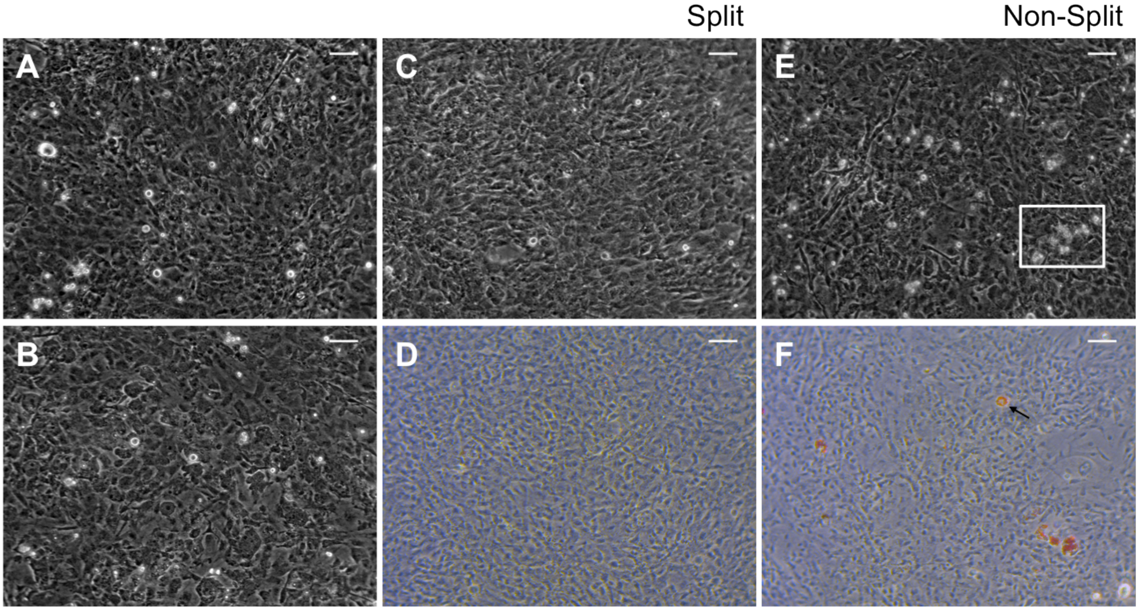

<u>Figure 4.21:</u> Cell culture of 16.5 embryonic day mouse back skin. (**A-C,E**) unstained in culture images. (**A**) after 3 days. (**B**) after 6 days. (**C,D**) Cells split. (**E,F**) Cells not split (**D,F**) Oil red O staining. Fat droplets present in adipocytes visible as red coloration. Images were taken using a Zeiss Axiovert 10. Scale bar = 65μm.

Dermal cells were then again put in culture for 10 days and one dish for 14 days. This proved to be too long: the fibroblasts took over the culture and any early adipocytes or preadipocytes that may have been present were unable to thrive and were instead outcompeted. It was therefore deduced from this, that in order to develop the model in terms of optimizing the variables, potentially both the cell number and number of days in culture should be reduced. This was repeated and the cells were fixed and stained with oil red O after 5-7 days, which was determined better than 10 days.

Upon showing that the dermal cells can successfully thrive in 2D culture, the cells were also put into 3D culture as spheres in hanging media drops. These were first taken from e17.5 skin alongside the organ culture model and seeded at 3000 cells per sphere. Control spheres using the concentrated cell suspension were also set up at

150,000 cells per sphere (Figure 4.22A-D). It was found that a high proportion of the 3000 cell spheres did not aggregate particularly well, however, the concentrated spheres aggregated well, so it may be that the cell count in the 3000 cell spheres was not high enough. The hanging drops containing the 3000-cell spheres were collected and put into two-dimensional culture in 35mm dishes. The cells coped well when transferred from 3D to 2D culture and adipocytes formed (Figure 4.22). This had positive implications for improving the cell culture model.

Spheres transferred from 3D to 2D culture were originally spun down at 1000rpm for 5 minutes and resuspended. Some of the cells clumped and others grew in a 2D manner. This may be why there were clusters of adipocytes (Figure 4.22). It was found more advantageous to pipette the spheres straight into 2D (Figure 4.24) and allow the spheres to adhere to the substrate as this way they were still to some extent in 3D culture and allowed less manipulation of the cells, preventing/reducing any changes or stress-related responses upon disturbance.

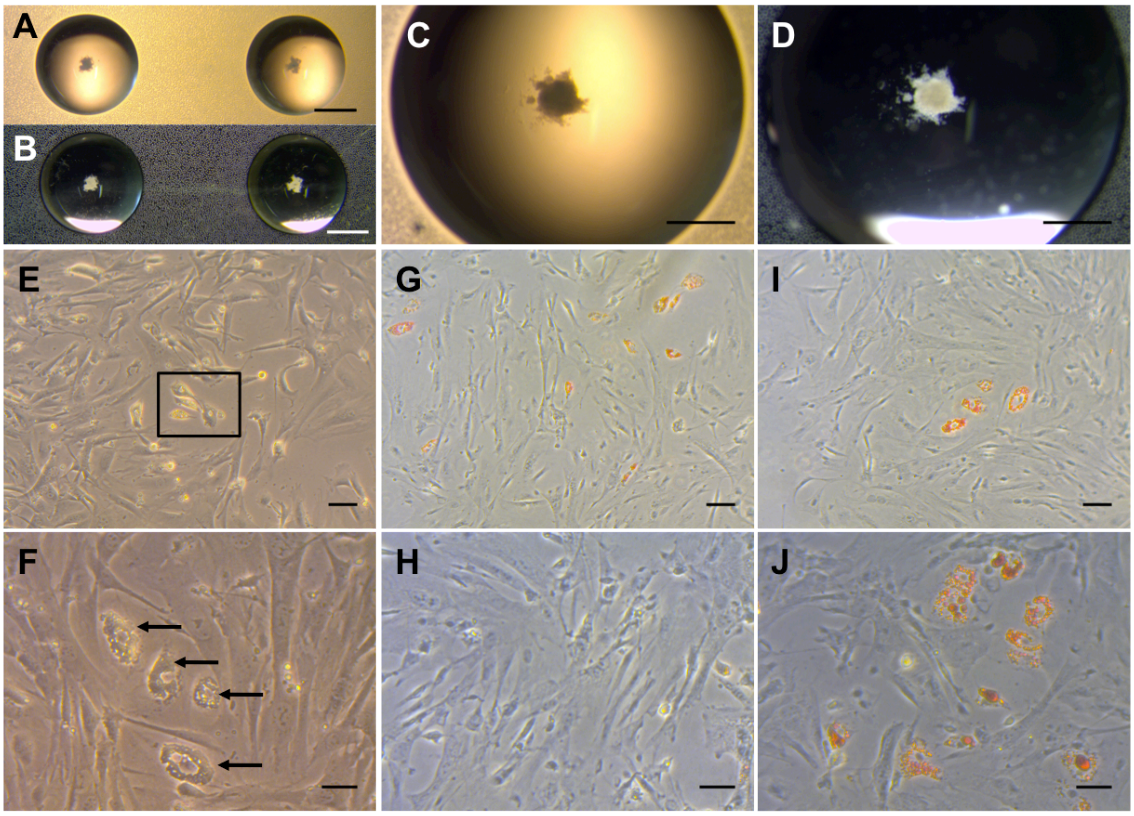

Figure 4.22: 3-dimensional spheres put into 2-dimensional culture. (**A-D**) concentrated 3D spheres. Images taken on Zeiss Stemi SV11. (**E-J**) 3D to 2D culture. Images taken on Zeiss Axiovert 10. (**G-J**) Oil red O staining of fat droplets. Arrows label adipocytes. (**A,B**) scale bar = 2mm. (**C,D**) scale bar = 1mm. (**E,G,I**) scale bar = 65μm. (**F,H,J**) scale bar = 40μm.

The next experiment and available e18.5 mice were used to determine what numbers of cells were most appropriate in both 2D and 3D culture for this model to be improved and reliably usable. Both 3000 and 6000 cells were seeded in each well of both 24 well plates and 6 well plates (Figure 4.23). Spheres were also formed with both 3000 and 6000 cell drops in 10ul of 10% FBS/MEM (Figure 4.25).

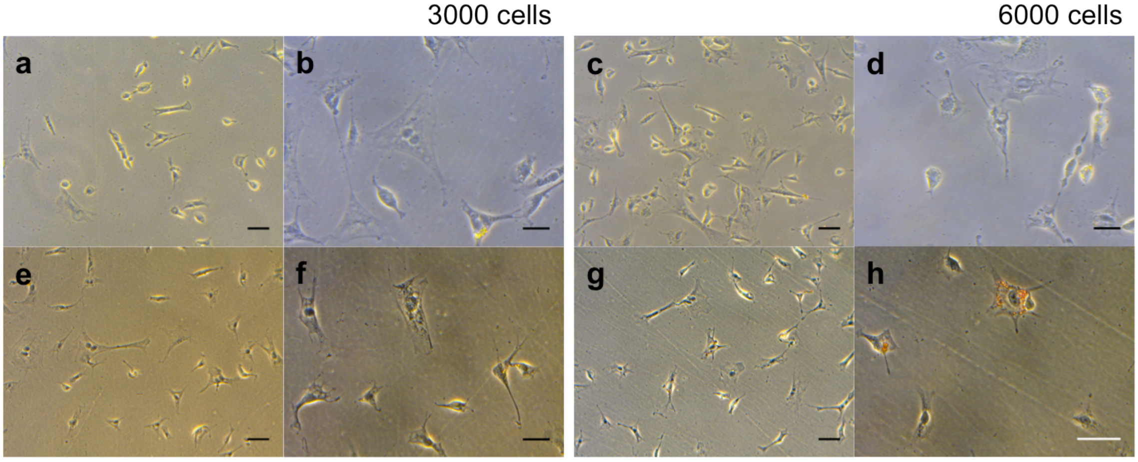

Figure 4.23: **2-dimensional cell culture of 18.5-day embryonic mouse dermis.** (**a-d**) images taken of both 3000 and 6000 cells in culture after 4 days. (**e-h**) oil red O staining of fat droplets. Images taken on a Zeiss Axiovert 10. (**a,e,c,g**) scale bar = 65μm. (**b,f,d,h**) scale bar = 40μm.

After 3 days, the spheres were transferred into 2D culture. Both the 3000 and 6000 cell spheres were put into 35mm dishes (Figure 4.24e-h) and individual 3000-cell spheres were put in wells of a 24 well plate (Figure 4.24i-j). The spheres did not adhere well and the cultures were not clean. It was considered that the cells should be filtered through a cell strainer to prevent contaminants being present after the skin separation process. There was variation in the levels of successful adherence and outgrowth of the spheres, meaning results in terms of quantifying the level of oil red O and thus lipid content in the spheres would not be consistently reliable. It was decided that 6000 cell spheres would be used in future as 3000 dermal cells were not sufficient to form defined aggregations. Putting 3000 or 6000 cells into 2D culture was not sufficient as the cell were unable to communicate and did not proliferate and develop particularly well (Figure 4.23). As well as this the spheres grew better in 6 well plates (Figures 4.24a-h) and when there were other spheres nearby, compared with isolating each sphere (Figures 4.24i and j). To keep it consistent 6 well plates were then used.

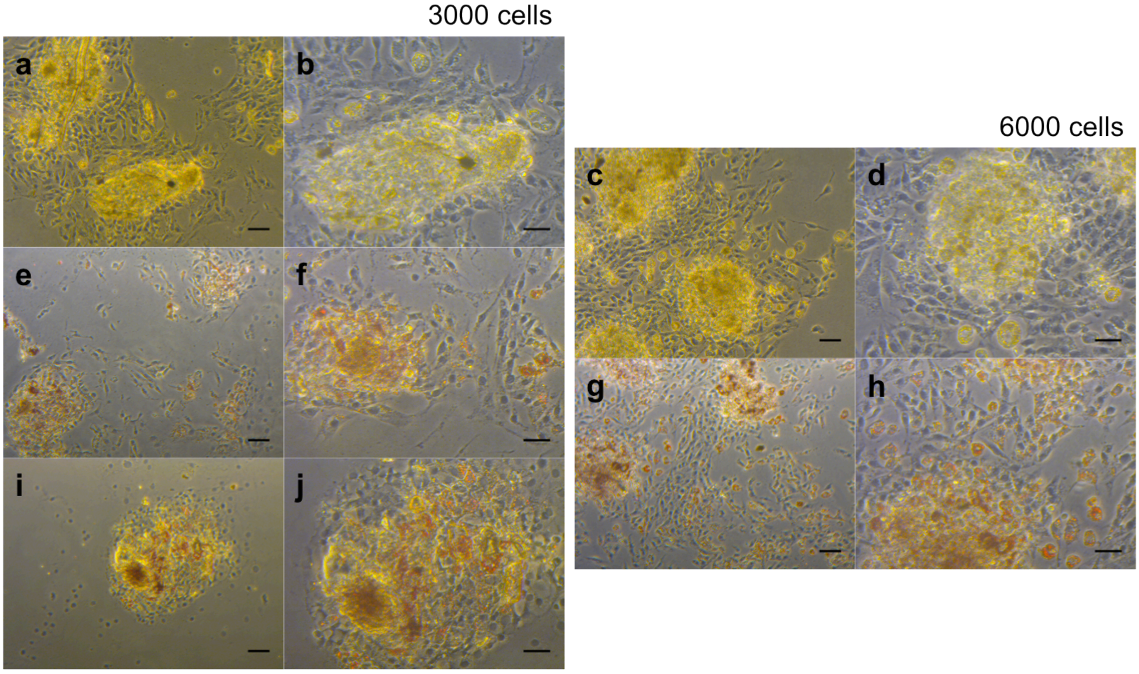

<u>Figure 4.24:</u> 3-dimensional to 2-dimensional cell culture of 18.5-day embryonic mouse dermis. (**a-d**) images taken of both 3000 and 6000 cell spheres in 2D culture after 1 day. (**e-l**) oil red O staining of fat droplets. (**e-h**) 6-well plates. (**i-l**) 24-well plates. Images taken on a Zeiss Axiovert 10. (**a,e,c,g,I,k**) scale bar = 65μm. (**b,f,d,h,j,l**) scale bar = 40μm.

While 3000 seemed to form better spheres with e18.5 (Figure 4.25) than e16.5, it was still clear 6000 cells were less of a risk as more consistently aggregated better. There was a high level of red staining in the spheres from e18.5, showing they have differentiated into adipocytes (Figure 4.25).

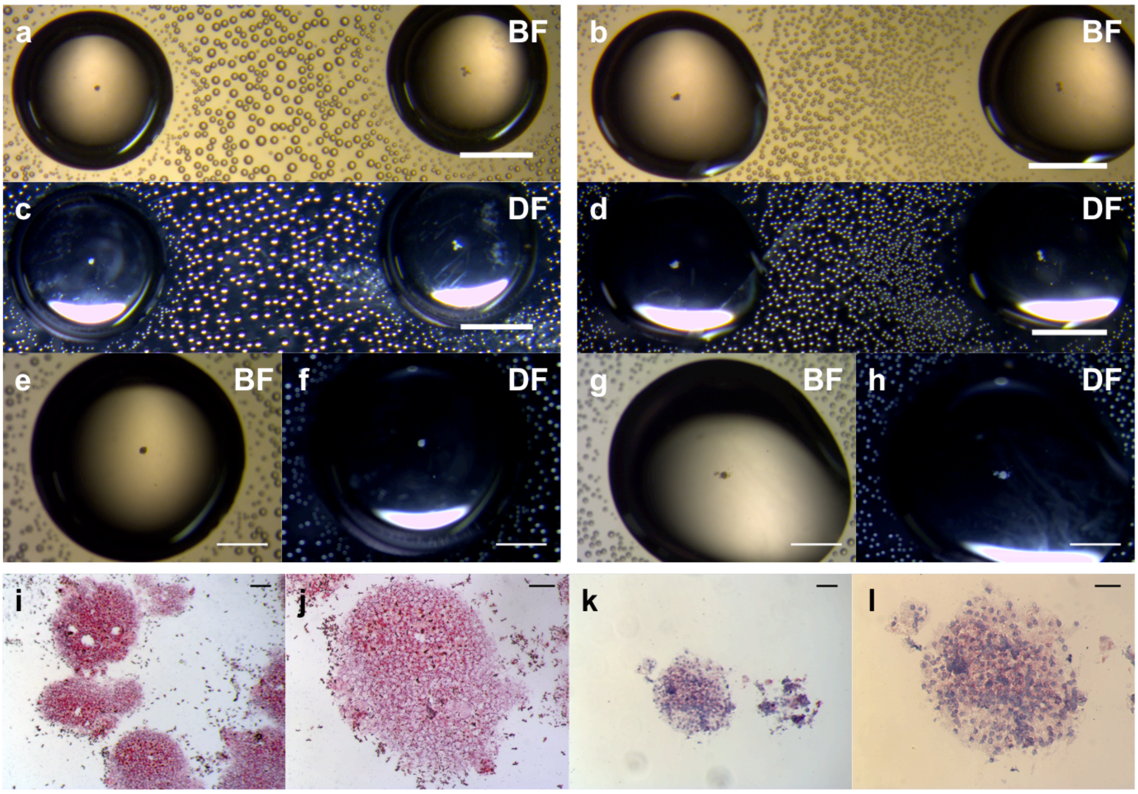

__Figure 4.25:__ **3-dimensional cell culture of 18.5-day embryonic mouse dermis.** (**a-h**) images taken after 3 days in culture on a Zeiss Stemi SVII. (**a,c,e,f**) 3000 cell spheres. (**b,d,g,h**) 6000 cell spheres. (**I,j,k,l**) oil red O staining of fat droplets in spheres. Images taken on a Zeiss Imager, M1. (**i,j**) without counterstain. (**k,l**) with haematoxylin counterstain. (**a-d**) scale bar = 2mm. (**e-h**) scale bar = 1mm. (**i,k**) scale bar = 65μm. (**,j,l**) scale bar = 40μm. BF = bright field, DF = dark field.

In order to increase reliability and uniformity across the experimental variables, the next step was to balance out the cell numbers between 2D and 3D culture. With 6000 cells being put into drops for spheres, it was decided that four spheres should be transferred into each well for 2D culture. This would increase the chances of at least one sphere adhering and growing out successfully in each well. Therefore, 24000 cells were seeded into each well for the 2D comparison to even the original cell numbers.

In further development of the model, both e15.5 and e16.5 were next looked at. In order to conduct immunofluorescence analysis and potentially remove chances of excess oil red O inflicting on any potential quantification results, placing circular coverslips at the bottom of each well before transferring the spheres to 2D was trialled. However, the spheres did not adhere as well to the glass coverslip substrate, particularly those from cells of the younger age, e15.5 (Figures 4.26g-i). Many of the spheres were lost during the staining procedure with oil red o (Figures 4.26d-f), leaving only the outgrowth cells. While some of the e16.5 spheres did adhere, this was very few and some of them had slipped to the edge of the coverslip before attaching (Figure 4.26B). This environment was less advantageous for growth than closer to the centre of the coverslip or indeed the well, because the cells grew better in the centre than at the edges.

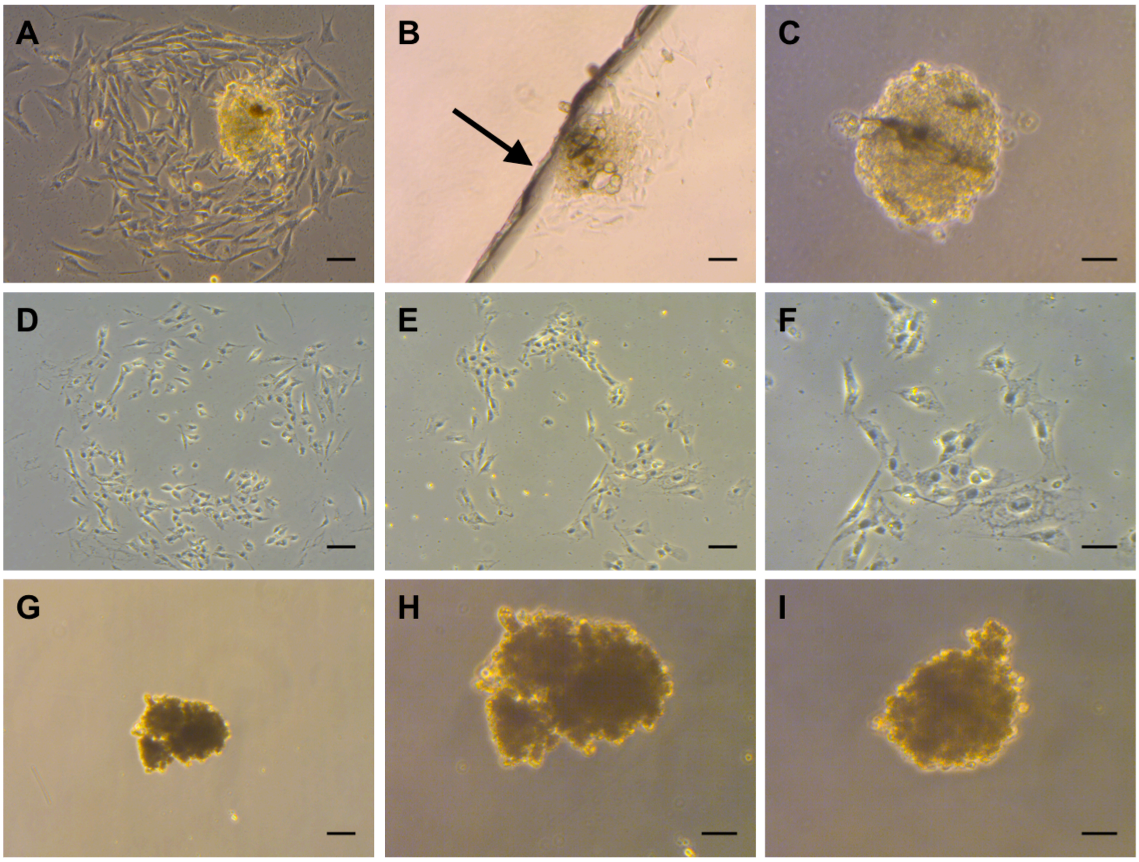

Figure 4.26: 3-dimensional to 2-dimensional cell culture of 15.5- and 16.5-day embryonic mouse dermis. (**A-C,G-I**) Images taken 1 day after transfer to 2D. (**A-F**) e16.5. (**G-I**) e15.5. (**D-F**) Oil red O staining, The main part of the sphere has undetached. (**A**) Adhered sphere. (**B**) Sphere adhered to edge of coverslip. (**C, G-I**) Unstuck spheres. Images taken on a Zeiss Axiovert 10. (**A,B,D,E,G**) scale bar = 65µm. (**C,F,H,I**) scale bar = 40µm.

There was little evidence of fat development in 2D culture (Figures 4.27c-e) compared with the 3D spheres (Figure 4.29). Cells taken from e16.5 dermis successfully produced cell spheres while e15.5 did less so (Figure 4.28). When stained with oil red O these spheres showed clear development of adipocytes in culture (Figure 4.29). More red coloration in the e15.5 spheres after 7 days (Figures 4.29A and B) appears to be observed compared with the e16.5 spheres after 6 days (Figures 4.29C and D). It was deemed appropriate to leave the cells in culture for a certain number of days in relation with their age. This was to keep the age of the cells consistent; 6 days for e16.5 and 7 days for e15.5. Some of the spheres were transferred to 2D for the last day of culture, i.e. 5+1 or 6+1 (Figure 4.26).

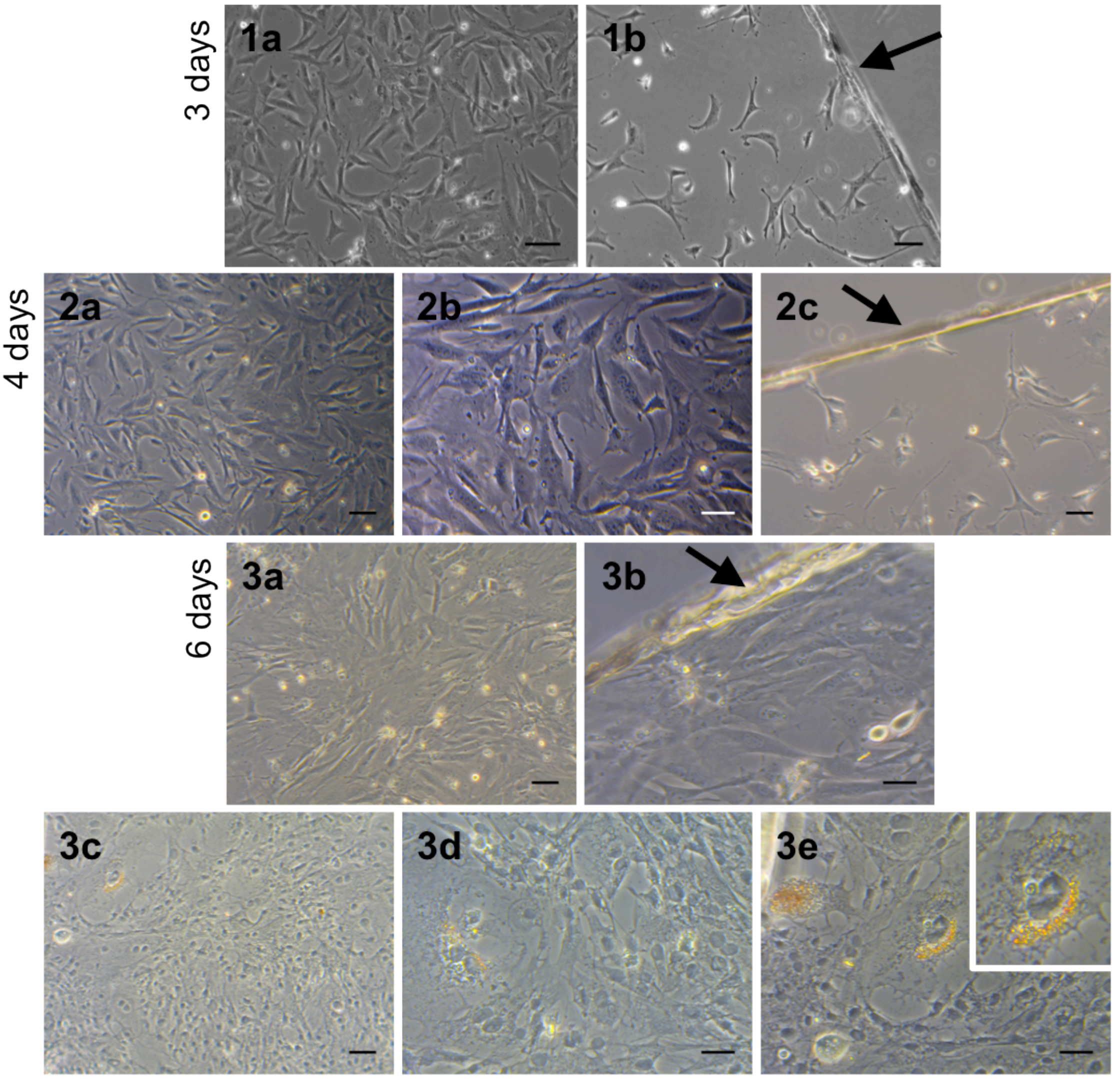

Figure 4.27: **2-dimensional cell culture of 16.5-day embryonic mouse dermis.** (**1,2,3**) Images taken of culture after 3, 4 and 6 days respectively. **(3c-e**) Oil red O staining. Images taken on a Zeiss Axiovert 10. The arrows point to the edge of the coverslips. (**1a/b,2a/c,3a/c**) scale bar = 65μm. (**2b,3b/d/e**) scale bar = 40μm.

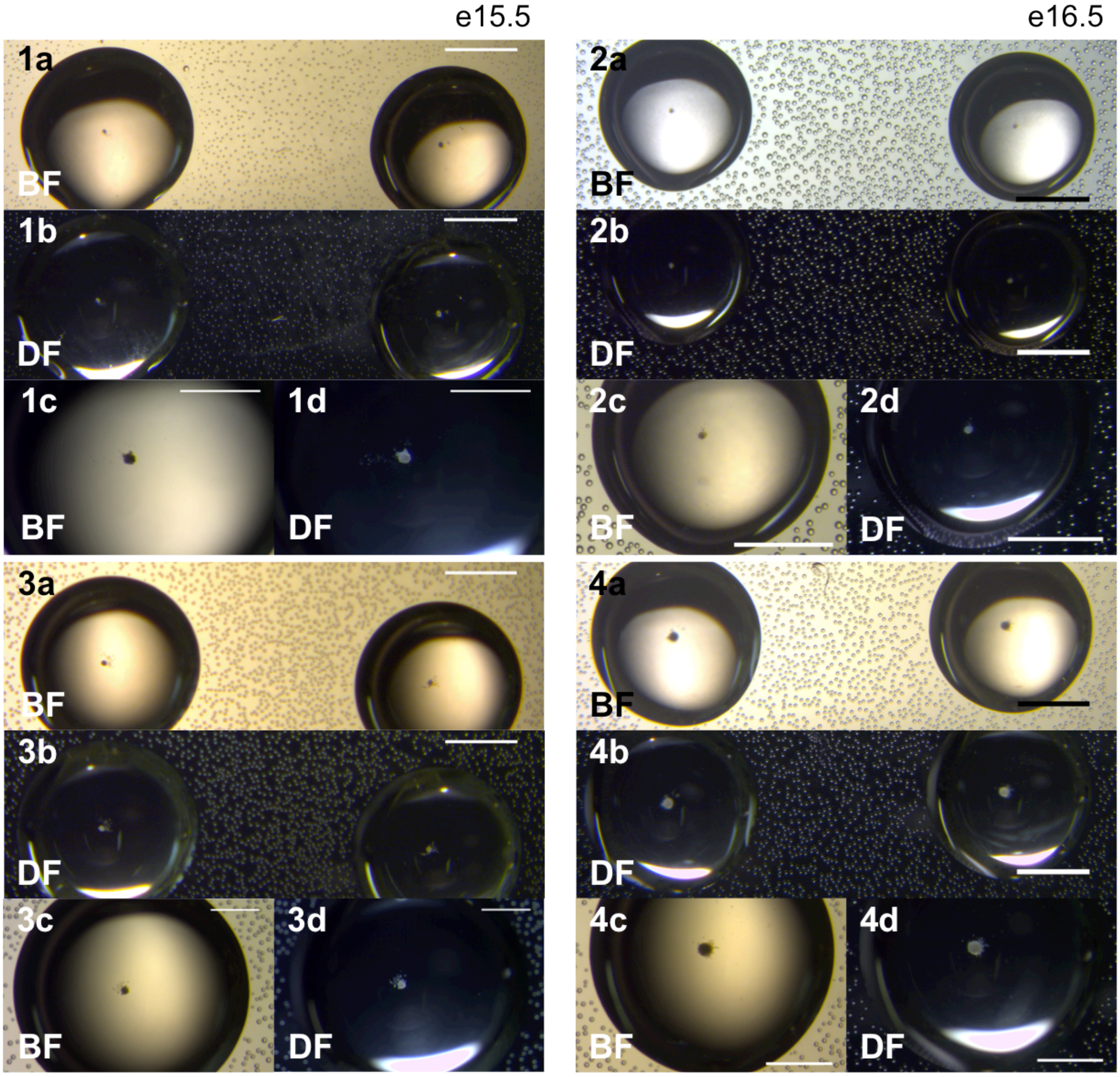

Figure 4.28: **3-dimensional cell culture of 15.5- and 16.5-day embryonic mouse dermis.** Images taken of e15.5 (Left) and e16.5 (Right) spheres. (**1,2**) 6000 cell spheres. (**3,4**) Concentrated cell spheres. Pictures taken of the 6000 cell spheres before transferring to 2D. Pictures taken of concentrated spheres after 6 days. Pictures taken on a Zeiss Stemi SVII. (**1a/b,2a/b,3a/b,4a/b)** scale bar = 2mm. (**1c/d,2c/d,3c/d,4c/d**) scale bar = 1mm. BF = bright field, DF = dark field.

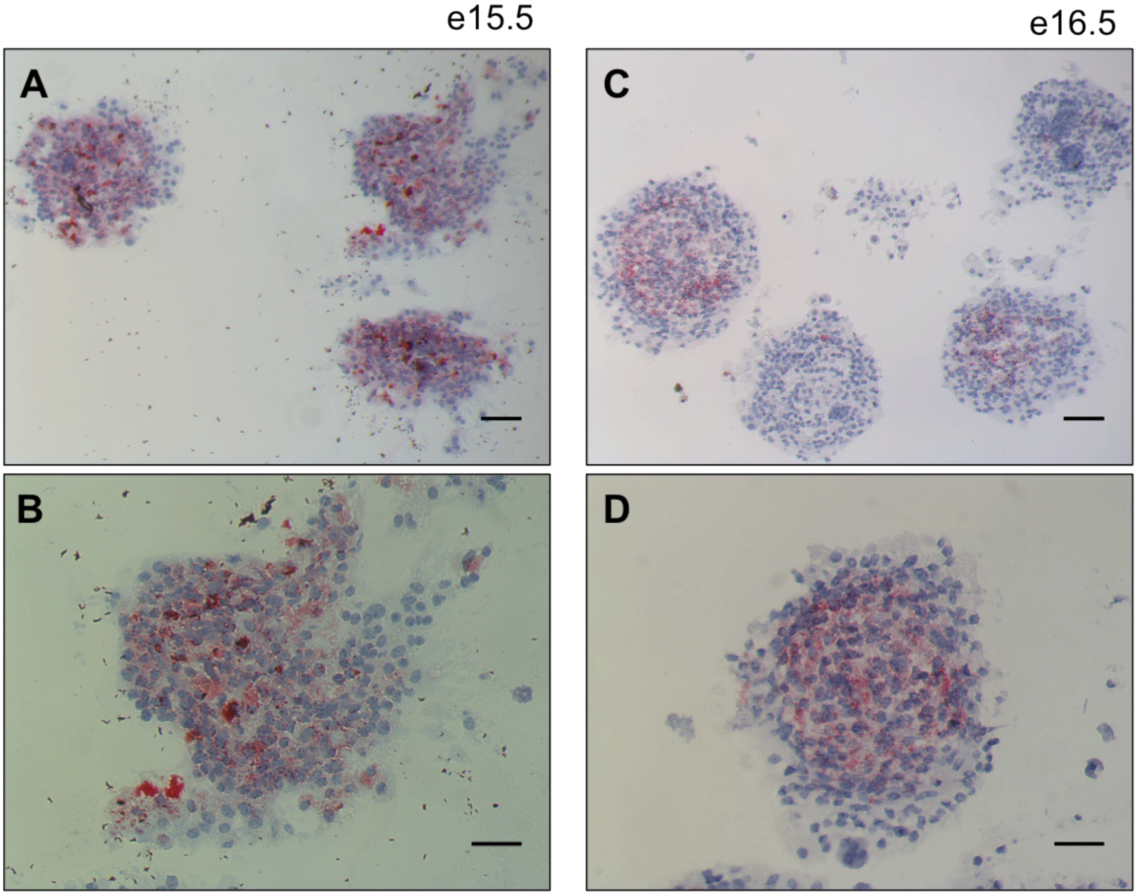

Figure 4.29: **Oil red O analysis of 15.5- and 16.5-day embryonic mouse dermal spheres.** Spheres stained with oil red O and images taken on a Zeiss Imager M1. (**A,C**) scale bar = 65μm. (**B,D**) scale bar = 40μm.

The experiment was conducted twice with e15.5 and e16.5 cell cultures, to make sure contamination wasn’t influencing the experiment. Coverslips were not used and when transferring the spheres to 2D 6 well plates, they were still allowed to adhered for several hours before adding more media. Many of the spheres, however, still became unstuck when the rest of the media was added or during oil red O staining and the cells shrunk after fixation (Figure 4.30).

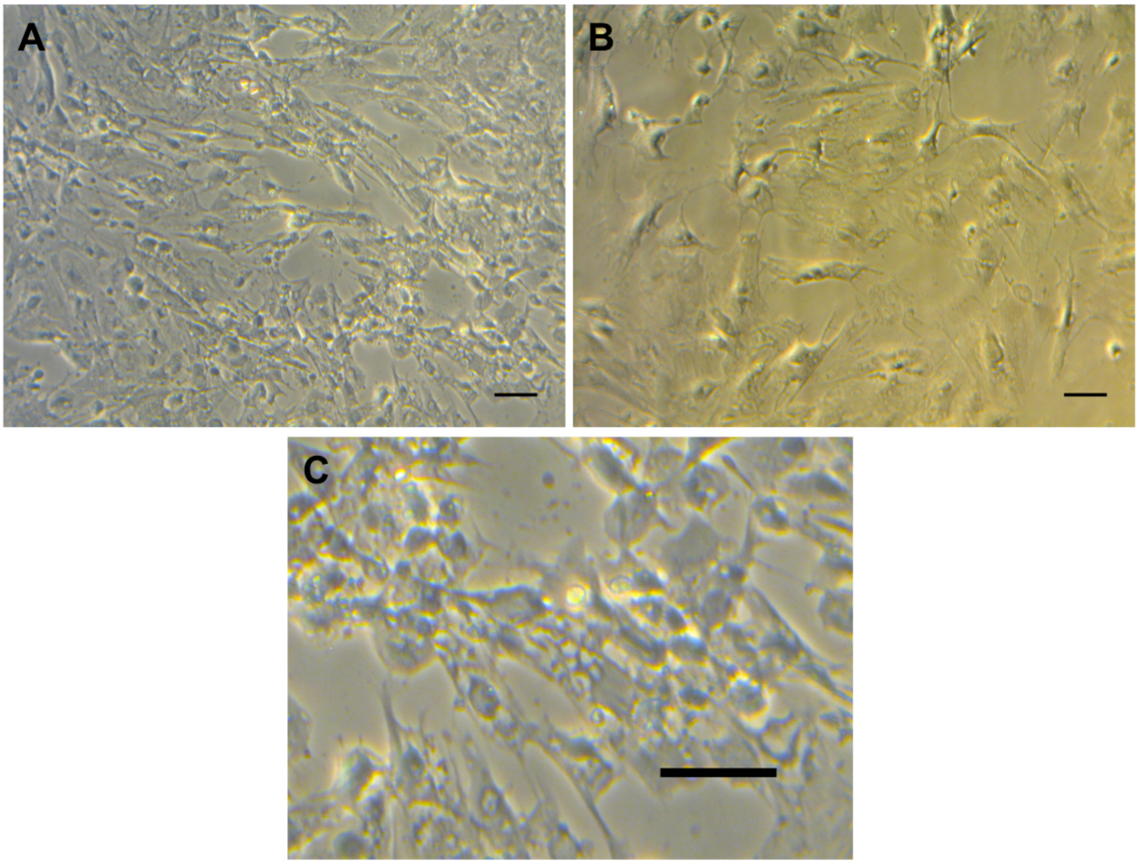

<u>Figure 4.30:</u> 2-dimensional cell culture of 15.5-day embryonic mouse dermis. Images showing shrunken cells after fixation. Images taken on a Zeiss Axiovert 10. Scale bar = 65μm.

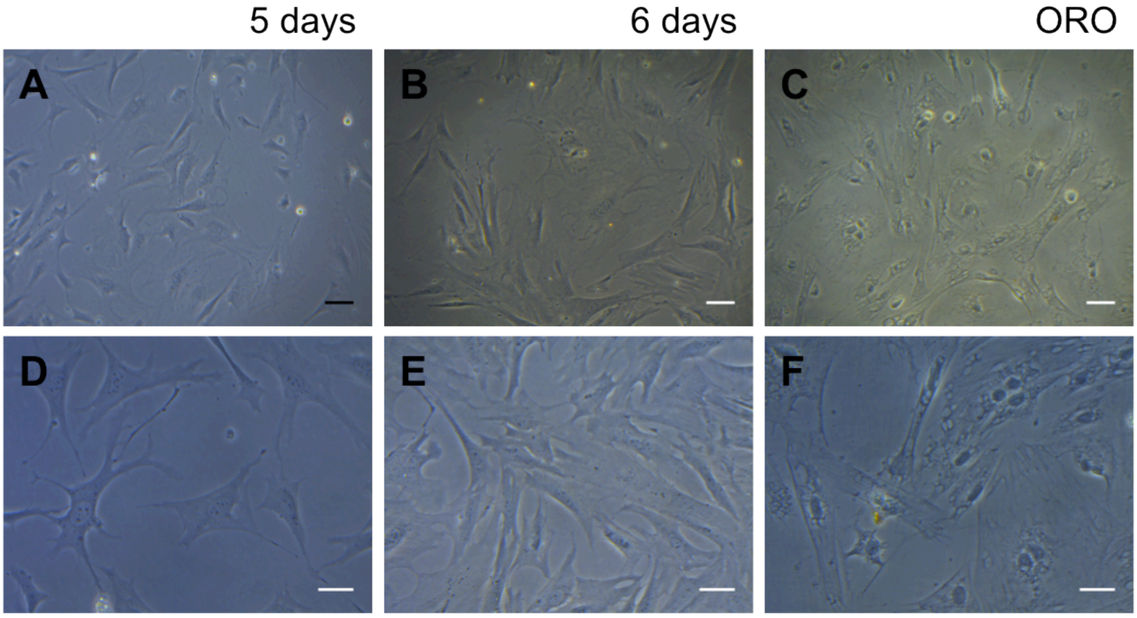

Figure 4.31: **2-dimensional cell culture of 16.5-day embryonic mouse dermis.** Images from 5 and 6 days in culture. **(C,F)** Oil red O staining after 6 days. Images taken on a Zeiss Axiovert 10. (**A-C**) scale bar = 65µm. (**D-F**) scale bar = 40µm.

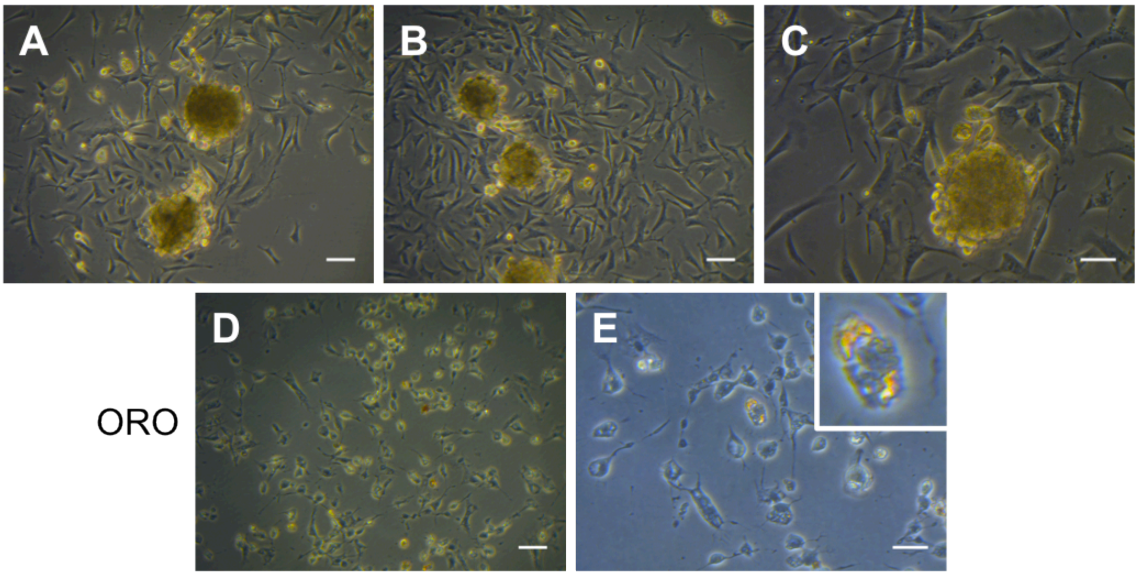

Figure 4.32: **3-dimensional to 2-dimensional cell culture of 16.5-day embryonic mouse dermis.** Images taken 1 day after transfer to 2D. (**D,E**) Oil red O staining, The spheres have adhered and grown out in 6-well plates in culture. Images taken on a Zeiss Axiovert 10. (**A,B,D**) scale bar = 65µm. (**C,E**) scale bar = 40µm.

When repeated, the spheres adhered and grew out better without the coverslips, though the main part of the spheres still became unstuck after oil red O staining (Figures 4.32D and E).

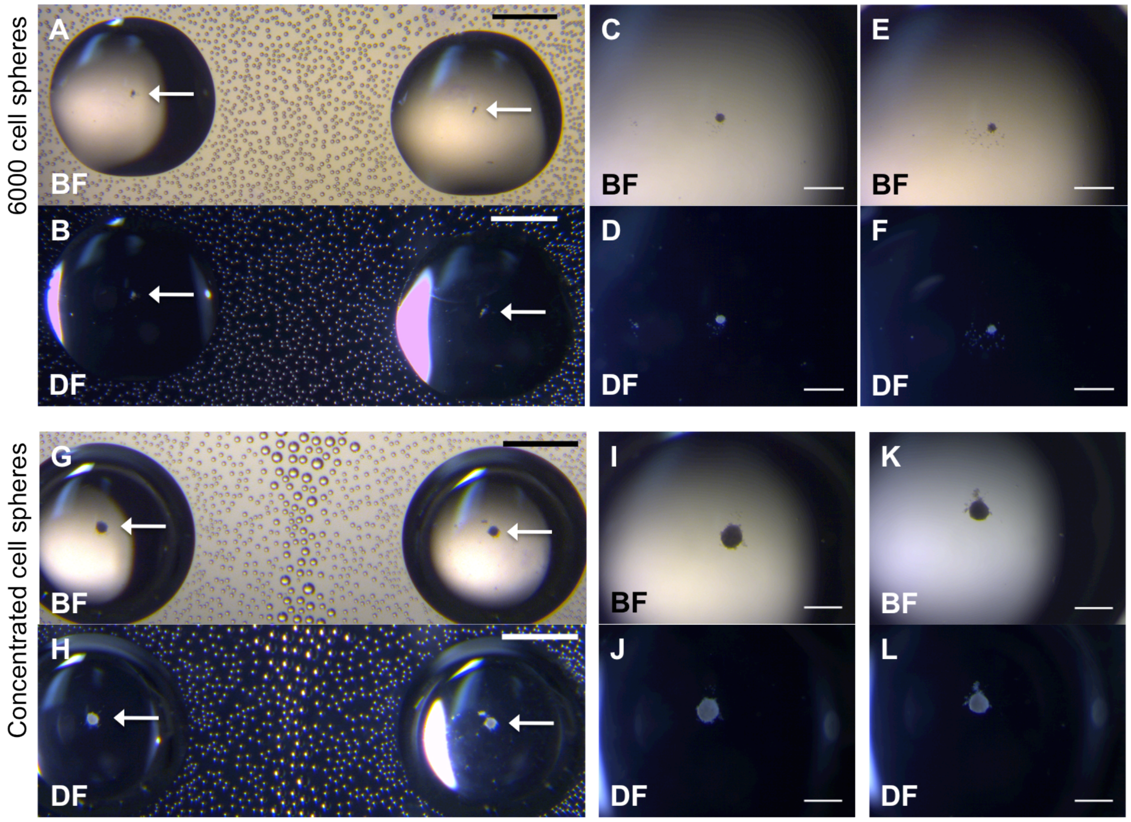

Figure 4.33: **3-dimensional cell culture 16.5-day embryonic mouse dermal cells.** Images taken after 5 days in culture. (**A-F**) 6000 cell spheres. (**G-L**) Concentrated cell spheres. Pictures taken on a Zeiss Stemi SVII. (**A,B,G,H**) scale bar = 2mm. (**C-F,I-L**) scale bar = 0.5mm. BF = bright field, DF = dark field.

Two factors were adapted to improve the adherence of the spheres and thus the quality of the analysis. The spheres were put into 2D culture for 2 days instead of one, by removing a day off the 3D culture time, e.g. instead of 5+1, 4+2 was used (Figure 4.35). As well as this, allowing the spheres to adhere in just 200μl of media in the middle of the well was trialled and it was found that the cells still grew well as well as adhering much better. Due to incubation only being needed for 1 or 2 days, using 200μl of media was not a problem as the cells still thrived. Length of calcium formal fixation was also decreased for 7 minutes, though this proved an insignificant change.

The 2 dimensional cell culture was carried out in the same way. In comparison with the 3D into 2D cell culture, there was less fat development in 2D as shown not only in the representative culture images but the analysis with the lipid stain oil red O (Figure 4.34 and 4.35).

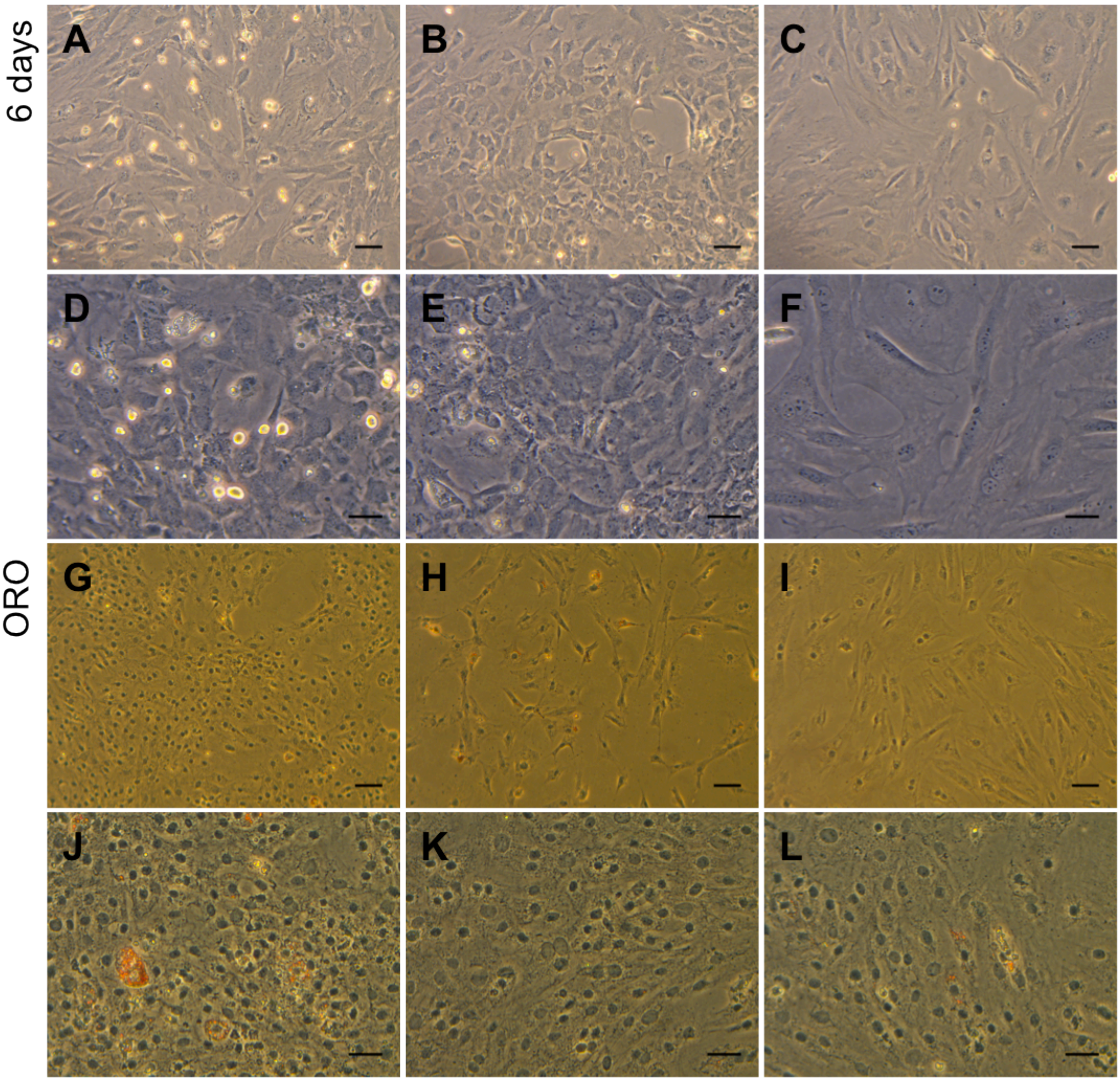

Figure 4.34: 2-dimensional cell culture of 16.5-day embryonic mouse dermis. Representative images from 6 days in culture, (**C,F,I,L**) taken closer to the edge of the substrate. **(G-L**) Oil red O staining after 6 days. Images taken on a Zeiss Axiovert 10. (**A-C,G-I**) scale bar = 65μm. (**D-F,J-L**) scale bar = 40μm.

The spheres had aggregated well (Figure 4.36) and when stained with oil red O for lipid detection, there was some red staining visible, though this was less than that found with e18.5 (Figure 4.25). Putting the spheres into 2D for two days rather than solely one meant the main body of the sphere as well as the outgrown cells remained stuck and successfully stained with oil red O (Figures 4.35G-L). Clear shapes of adipocytes were seen in the dense aggregations and some of the cells spread out from the spheres. Not all the cells differentiated into adipocytes. This was a positive correlation with the fact that only part of the dermis forms adipose tissue.

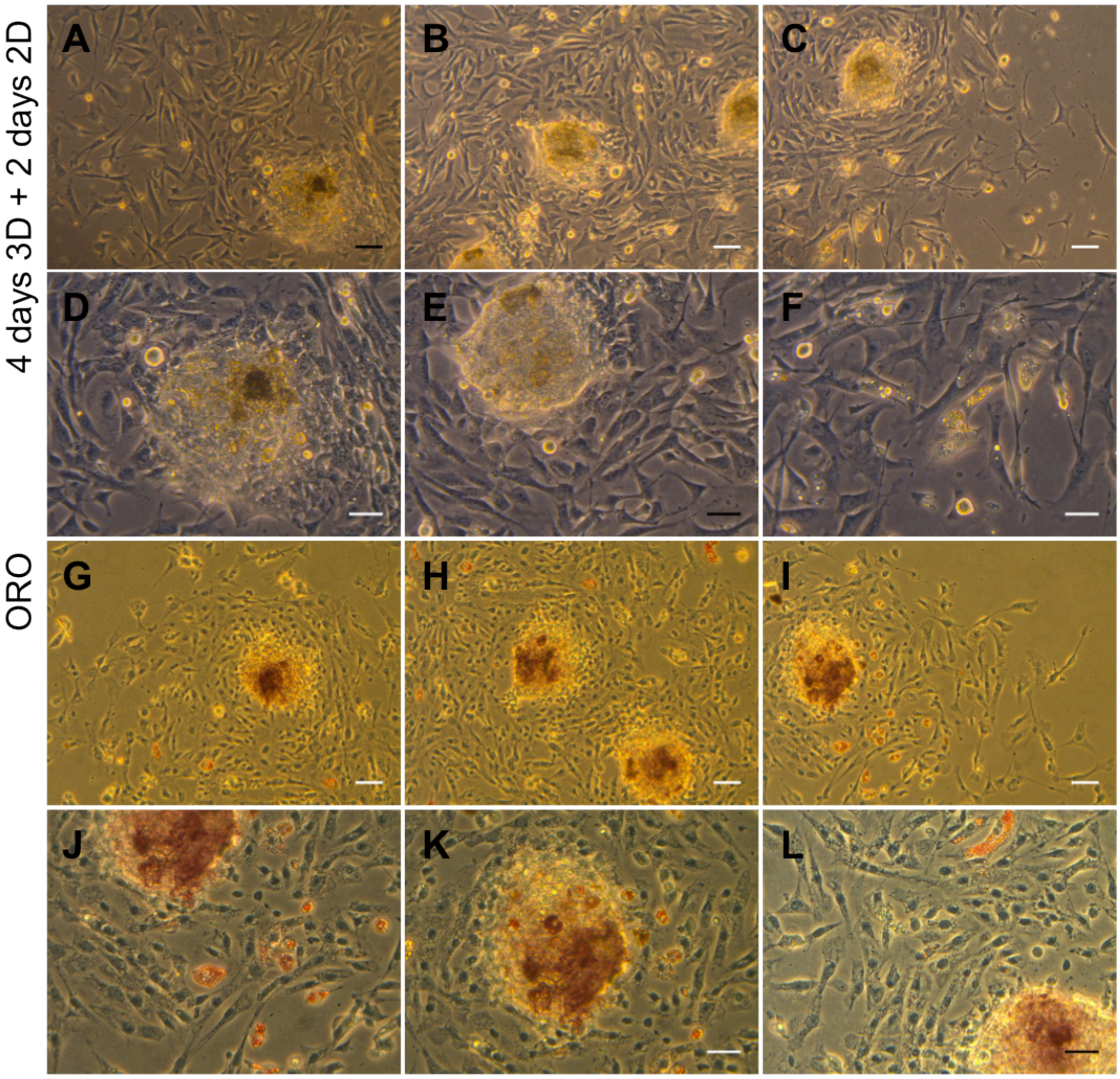

<u>Figure 4.35:</u> 3-dimensional to 2-dimensional cell culture of 16.5-day embryonic mouse dermis. Images taken 2 days after transfer to 2D. (**G-L**) Oil red O staining, The spheres have adhered and grown out in 6-well plates in culture. Images taken on a Zeiss Axiovert 10. (**A-C,G-I**) scale bar = 65µm. (**D-E,J-L**) scale bar = 40µm.

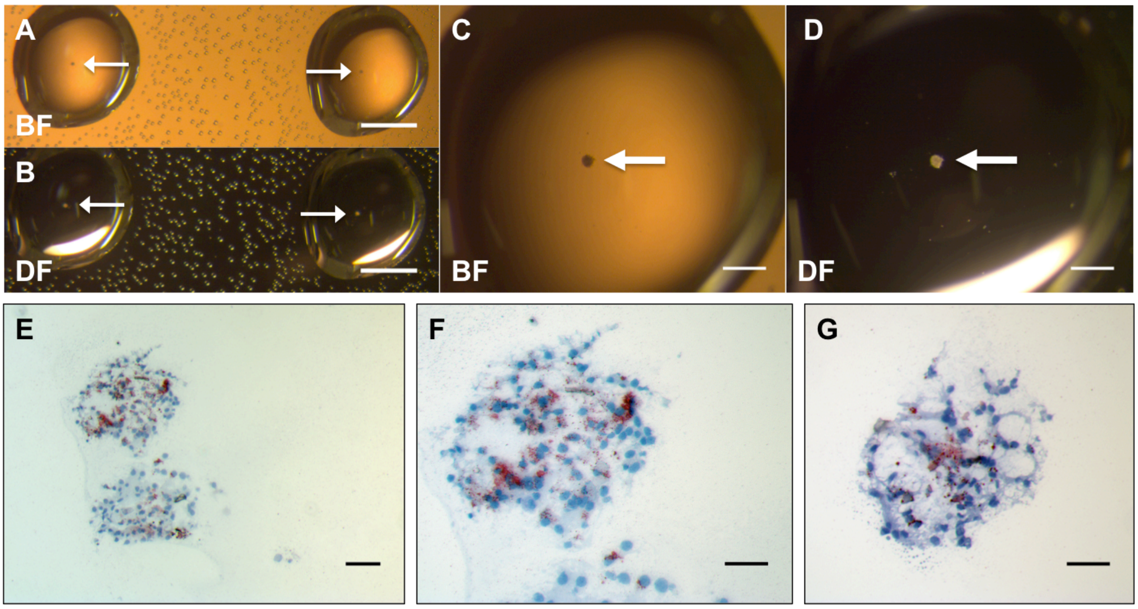

Figure 4.36: 3-dimensional cell culture of 16.5-day embryonic mouse dermal cells. Images taken after 6 days in culture. (**A-D,G**) 6000 cell spheres. (**E,F**) Concentrated cell spheres. (**A-D**) Images taken on a Zeiss Stemi SVII. (**E-G**) Images taken on a Zeiss Imager, M1. (**A,B**) scale bar = 2mm. (**C,D**) scale bar = 0.5mm. (**E**) scale bar = 65µm. (**F,G**) scale bar = 40µm. BF = bright field, DF = dark field.

4.3.2.1. Epidermal Contamination

Alongside the 2D versus 3D comparison and 3D to 2D sphere transfer, some of the spheres were frozen down directly after the full incubation period decided upon, e.g. 6 days for dermal cells taken from e16.5 skin. These were then stained with oil red O to investigate the degree of fat development occurring in the spheres in 3D to ensure that which develops when transferred to 2D isn't due to the change in environment. This was conducted across all the ages experimented with and some interesting and somewhat unexpected results were found.

It was noticed that some of the spheres appeared to have dense clusters of cells in them, visible from the haematoxylin nuclear staining (Figure 4.37). This was queried as epithelial contamination from the epidermal-dermal separation step, i.e. the epidermal cells (keratinocytes) were clustering together separate from the dermal content of the spheres. While there was contamination, there was also evidence of increased adipocyte formation in the spheres from e16.5 to e18.5 (Figure 4.37).

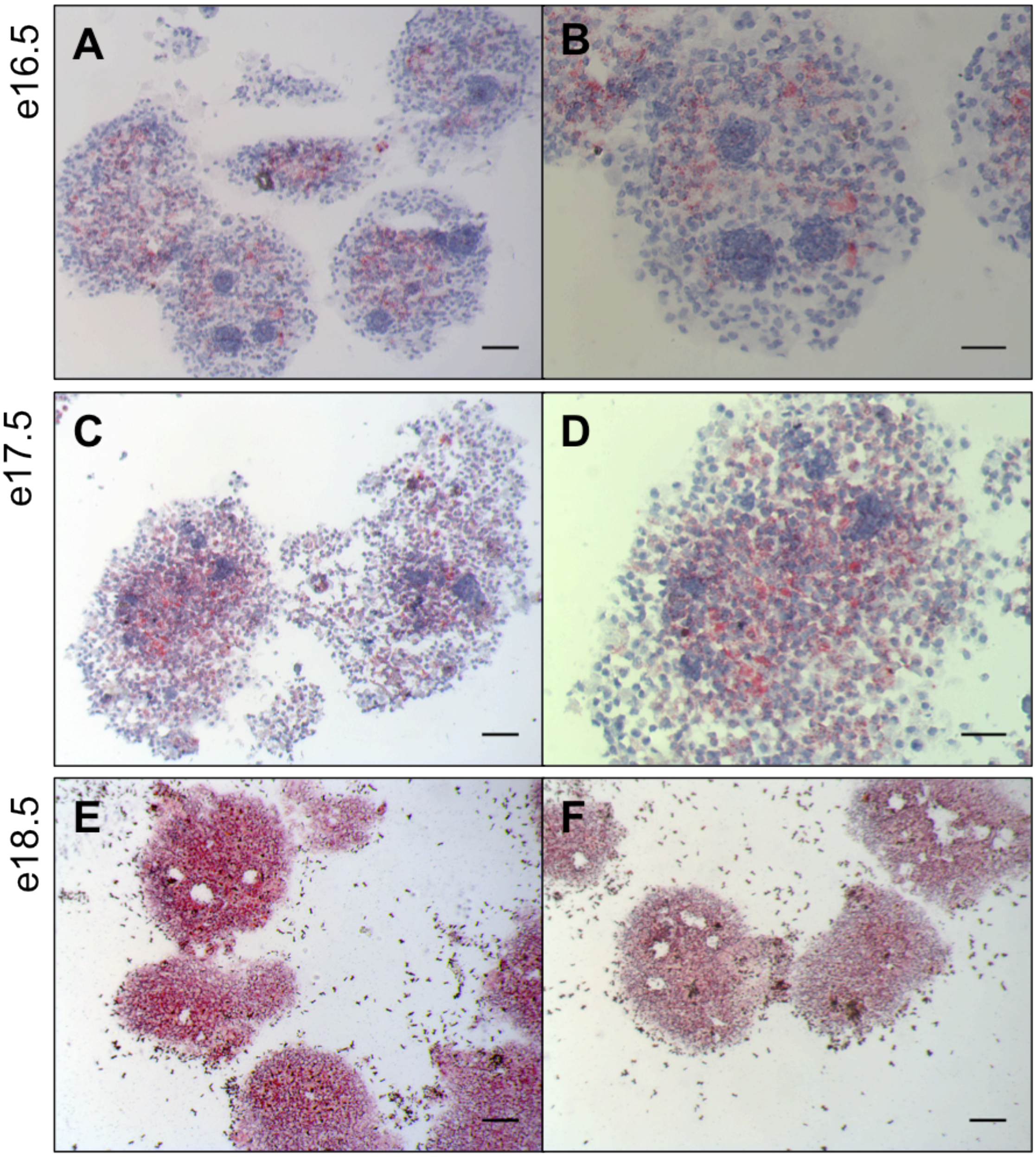

Figure 4.37: Oil red O stained spheres of 15.5-, 16.5- and 17.5-day embryonic mouse dermis showing dense clusters. Spheres stained with oil red O and images taken on a Zeiss Imager M1. (**A-D**) Haematoxylin counterstain. (**E,F**) No counterstain. (**A,C,E,F**) scale bar = 65μm. (**B,D**) scale bar = 40μm.

A pan-keratin epithelial marker was used with immunofluorescence analysis. This showed that some but not all of the clusters corresponded to epithelial cells. There was a degree of contamination present shown by specific green staining using pan-keratin (Figure 4.38). The arrows label those clusters that correspond to fluorescent staining in the FITC and merge images, while all the clusters have been labelled in the DAPI images to show that it is not all of them.

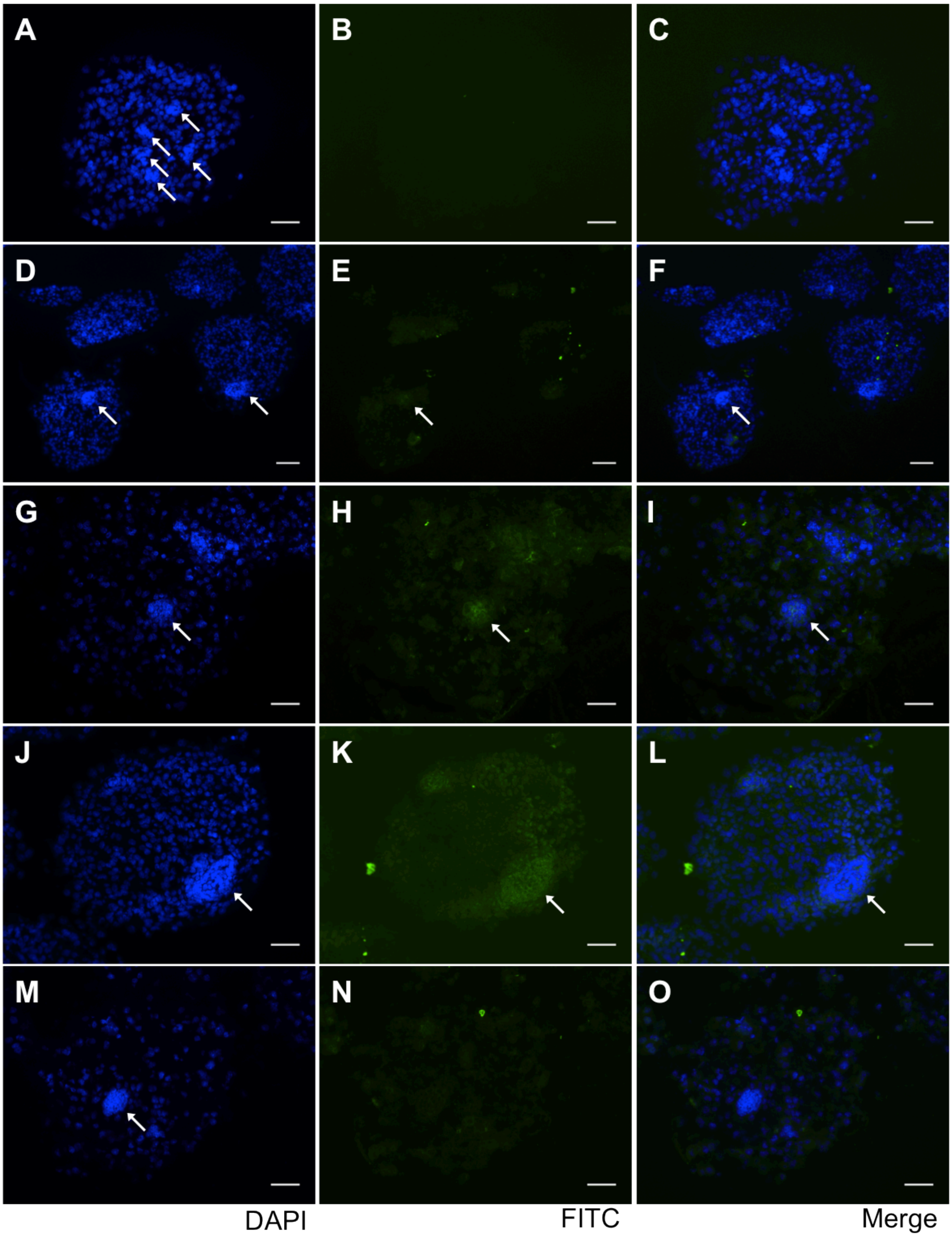

Figure 4.38: Analysis of Cytokeratin expression in 16.5-day embryonic dermal spheres. Sections were cut at 7μm, stained with an antibody against cytokeratin and counterstained with DAPI. From left to right; DAPI, FITC, and merge (DAPI/FITC). FITC represents the fluorescent labelling of cytokeratin. (**A-C**) Control showing no fluorescently labelled cytokeratin expression. (**D-O**) labelled using Cytokeratin primary antibody. Fluorescent images were taken using a Zeiss Axio Imager M1. (**D-F**) scale bar = 65μm. (**A-C,G-O**) scale bar = 40μm. Arrows label dense clusters of cells. In DAPI images all clusters labelled. In FITC/Merge images, only those which correspond to positive fluorescence are labelled.

The potential of ficoll to separate the densities of the two cell types – keratinocytes and fibroblasts – was explored in order to improve the purity of the dermal cell suspension prior to culture. A direct comparison of cultures using ficoll with those not using ficoll was conducted and the spheres were stained with pan keratin. This was first tried using the age e17.5 as the contamination if any would be more obvious by this age. It was expected that two fractions would be produced after centrifugation, however, only one layer (fibroblast layer) was seen (Figure 4.39C). This may have been because there were only a few epidermal cells which were not clearly visible as a distinct layer or that in fact the cells were too similarly dense for the separation to occur. The cell density generated was not sufficient to conduct a full experiment. Ficoll was then used in an e16.5 experiment to determine whether the separation of densities was easier at a younger age. Similarly one distinct cell layer in the form of a pellet formed on the surface of the ficoll (Figures 4.39A and B).

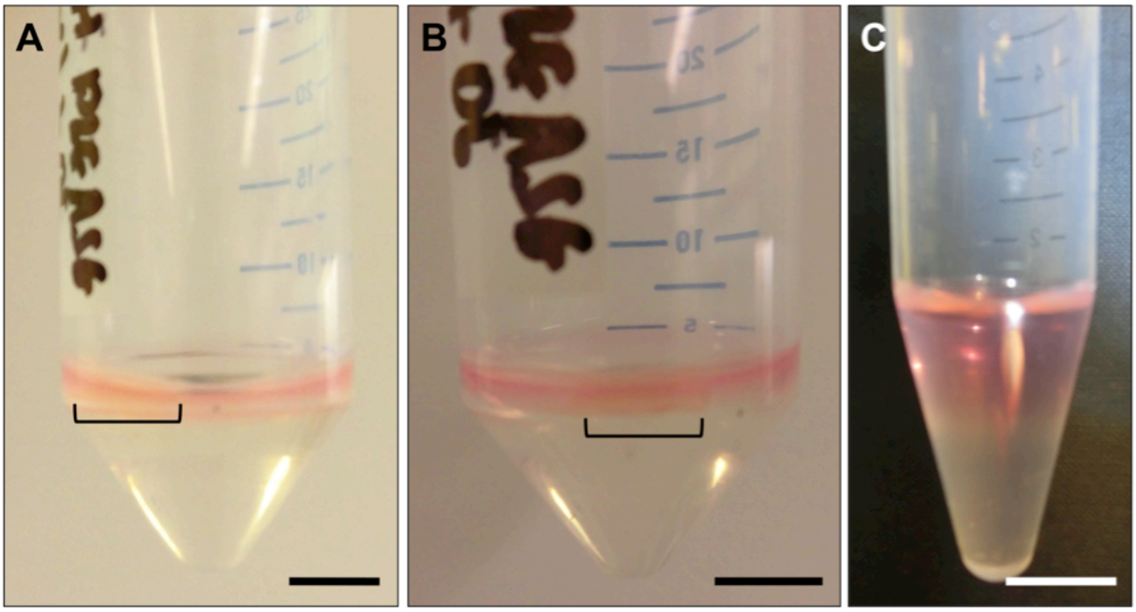

Figure 4.39: Photographs of Density Centrifugation using Ficoll PM400. Two fractions were used, 1.05g/ml and 1.06g/ml. (**A,B**) Embryonic day 16.5; 50ml falcons, formation of cell pellets in one layer of the top fraction shown by the black bar. (**C**) Embryonic day 17.5; 15ml falcon; no cell layer/s visible. Scale bar = 1mm.

Images of the spheres in hanging drops were taken of both 6000 cell spheres and concentrated cell spheres, this time of 40,000 cells per sphere (Figure 4.40). There was not a significant difference, between cells separated by ficoll and those not separated, in the morphology of the spheres.

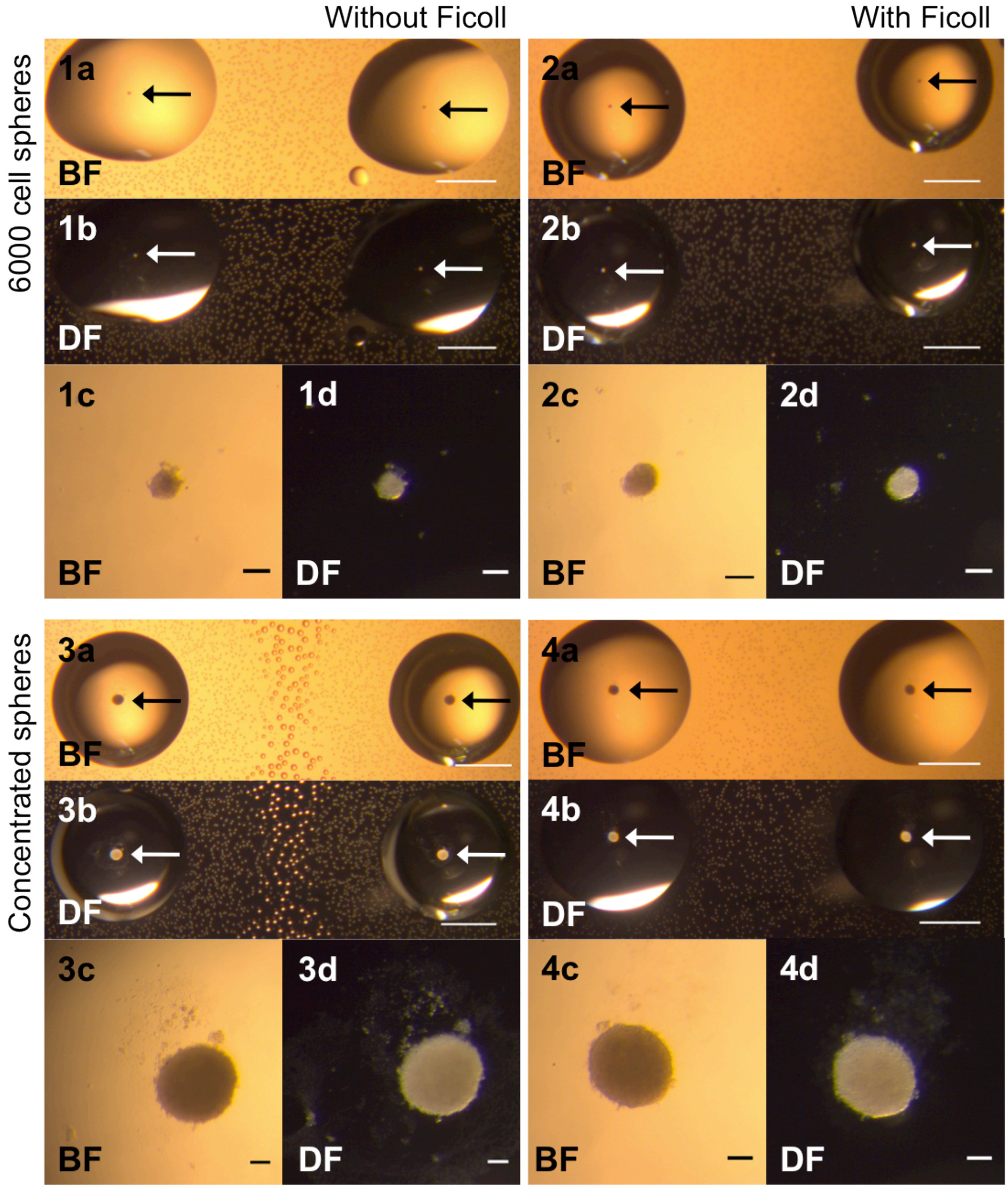

Figure 4.40: 3-dimensional cell culture of 16.5-day embryonic mouse dermal cells with and without FICOLL. Images taken after 6 days in culture. (**1,3**) Without Ficoll density separation. (**2,4**) With Ficoll density separation. (**1,2**) 6000 cell spheres. (**3,4**) Concentrated cell spheres. Images taken on a Zeiss Stemi SVII. (**a,b)** scale bar = 2mm. (**c,d**) scale bar = 0.1mm. BF = bright field, DF = dark field.

The spheres were stained immunofluorescently with the cytokeratin antibody previously used (Figures 4.41 and 4.42). There was still epidermal contamination in the spheres with ficoll, shown by the brighter fluorescence of densely clustered sections in the spheres (Figure 4.42), though there were fewer clusters.

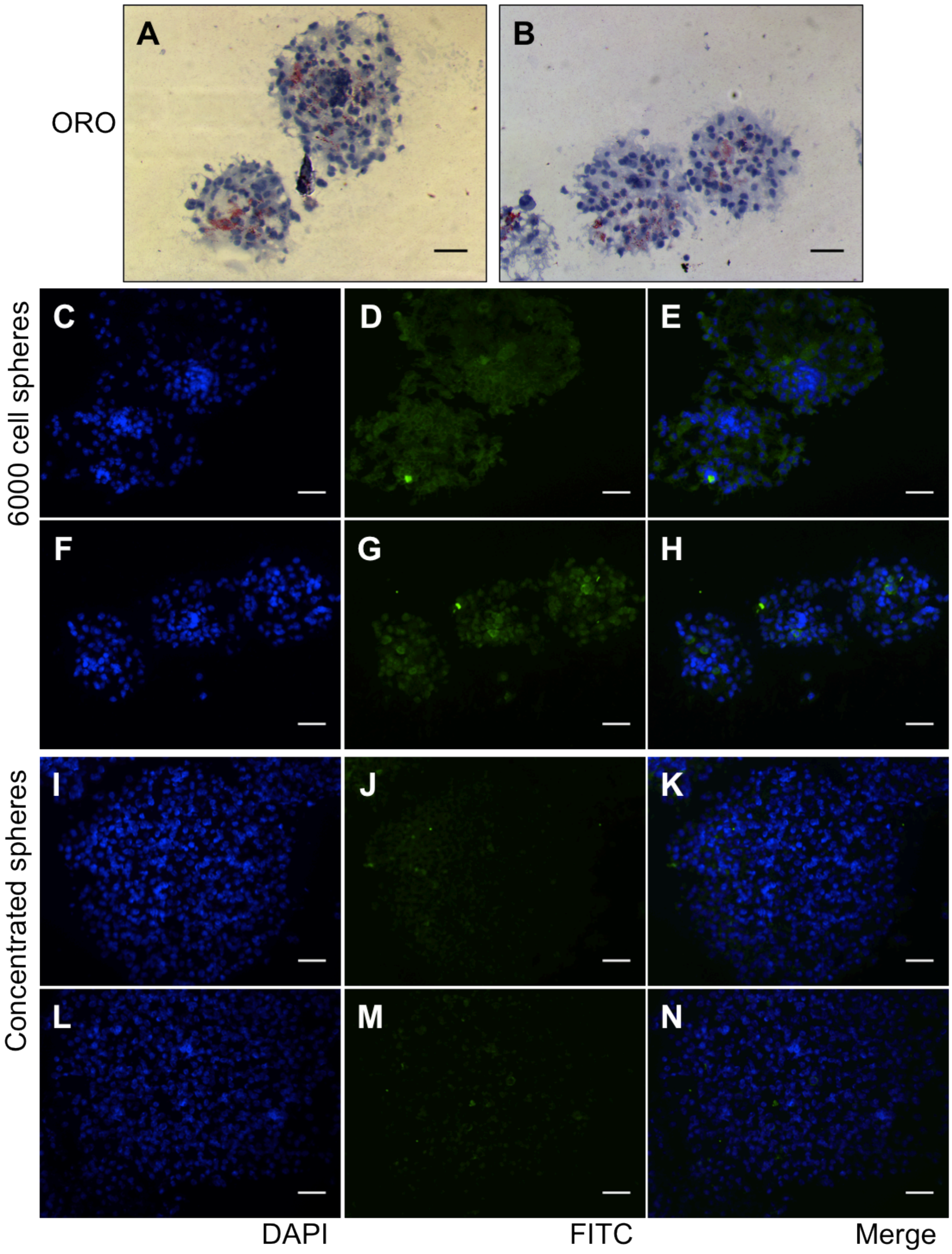

__Figure 4.41:__ **Analysis of 16.5-day embryonic dermal spheres, without Ficoll fractionation.** (**A,B**) Sections cut at 10mm were stained with oil red O to detect presence of fat. (**C-N**) Sections were cut at 7mm, stained with an antibody against cytokeratin and counterstained with DAPI. From left to right; DAPI, FITC, and merge (DAPI/FITC). FITC represents the fluorescent labelling of cytokeratin. (**C-H**) 6000 cell spheres. (**I-N**) Concentrated cell spheres. (**C-E,I-K**) Control showing no fluorescently labelled cytokeratin expression. (**F-H,L-N**) labelled using Cytokeratin primary antibody. Images were taken using a Zeiss Axio Imager M1. (**D-F**) Scale bar = 40μm.

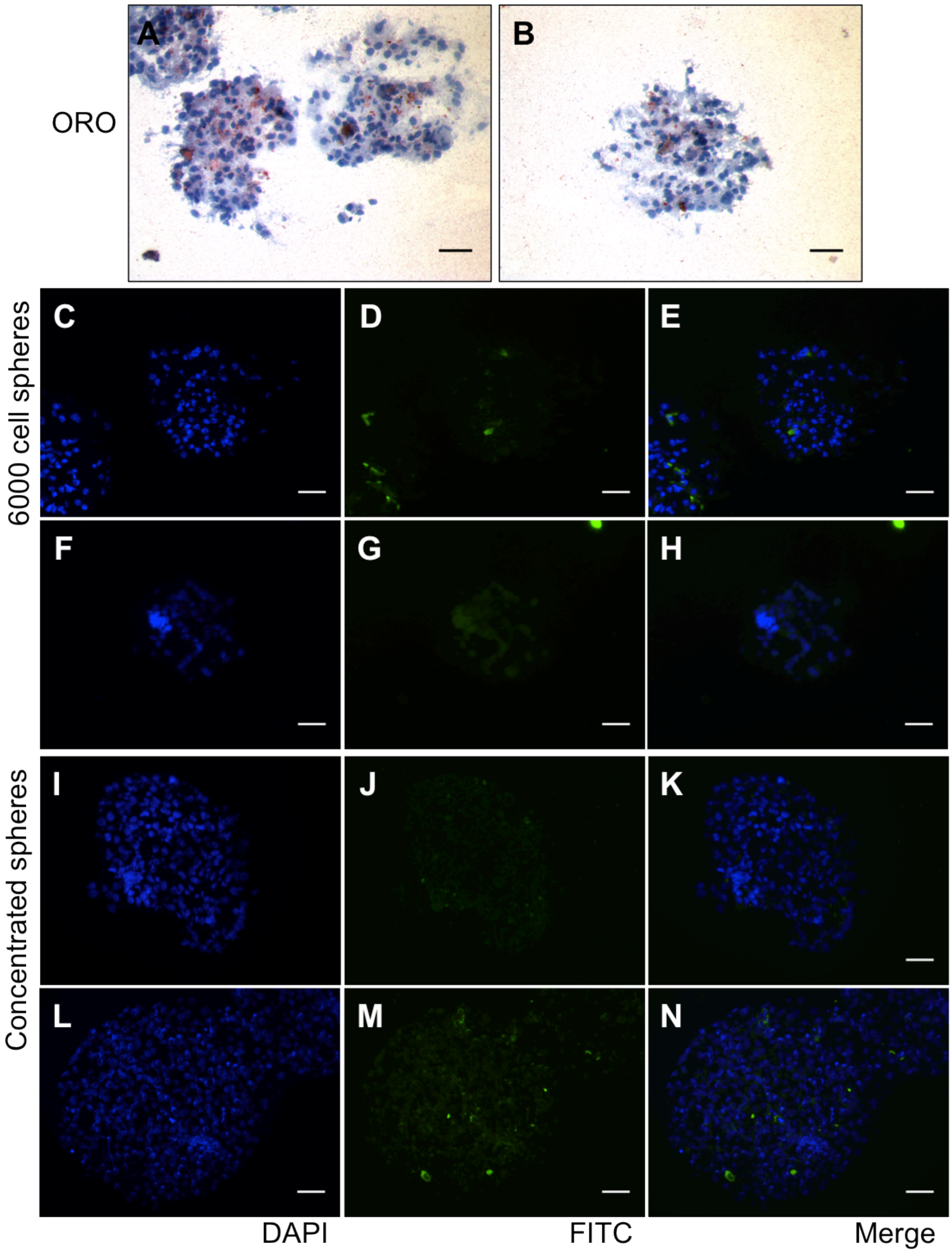

Figure 4.42: Analysis of 16.5-day embryonic dermal spheres, with Ficoll fractionation. (**A,B**) Sections cut at 10mm were stained with oil red O to detect presence of fat. (**C-N**) Sections were cut at 7mm, stained with an antibody against cytokeratin and counterstained with DAPI. From left to right; DAPI, FITC, and merge (DAPI/FITC). FITC represents the fluorescent labelling of cytokeratin. (**C-H**) 6000 cell spheres. (**I-N**) Concentrated cell spheres. (**C-E,I-K**) Control showing no fluorescently labelled cytokeratin expression. (**F-H,L-N**) labelled using Cytokeratin primary antibody. Images were taken using a Zeiss Axio Imager M1. Scale bar = 40μm.

Some of the spheres from both sets of conditions were put into 2D culture after 4 days (Figure 4.44) and some of the cells were also incubated for 6 days in 2D culture (Figure 4.43). In both cases, little difference was found between the two, though in general the level of contamination appeared to be significantly reduced. As previously found, more adipose development occurred in 3D than 2D. It was decided that Ficoll would not be used in the model as it was a time-consuming step that ran the risk of reducing the cell numbers available for cell culture.

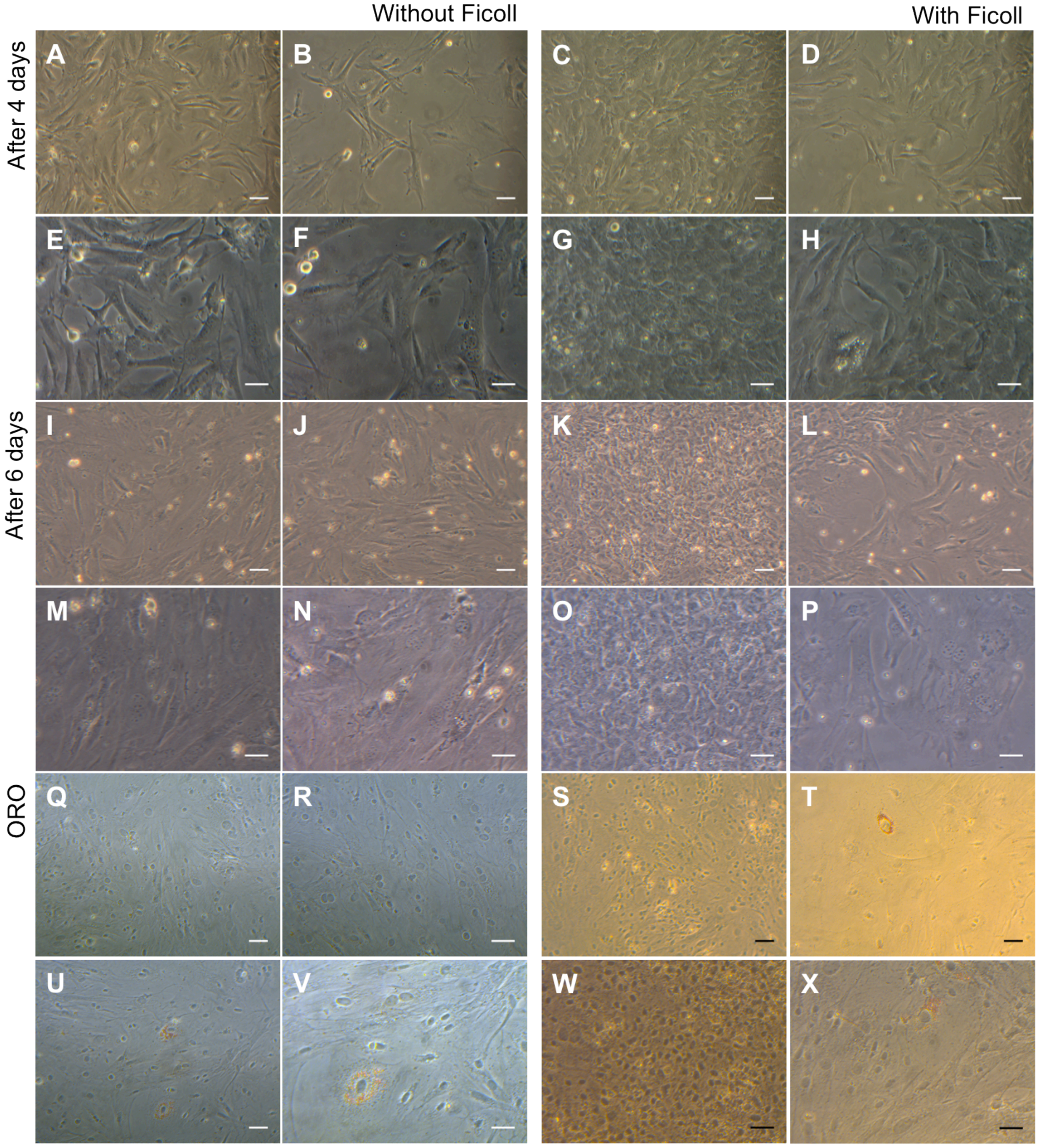

Figure 4.43: 2-dimensional cell culture of 16.5-day embryonic mouse dermis with and without FICOLL. (**A-H**) After 4 days in culture. (**I-X**) After 6 days in culture, (**Q-X**) Oil red O staining after 6 days. Representative images taken on a Zeiss Axiovert 10. (**A-D,I-L,Q-T**) scale bar = 65μm. (**E-H,M-P,U-X**) scale bar = 40μm.

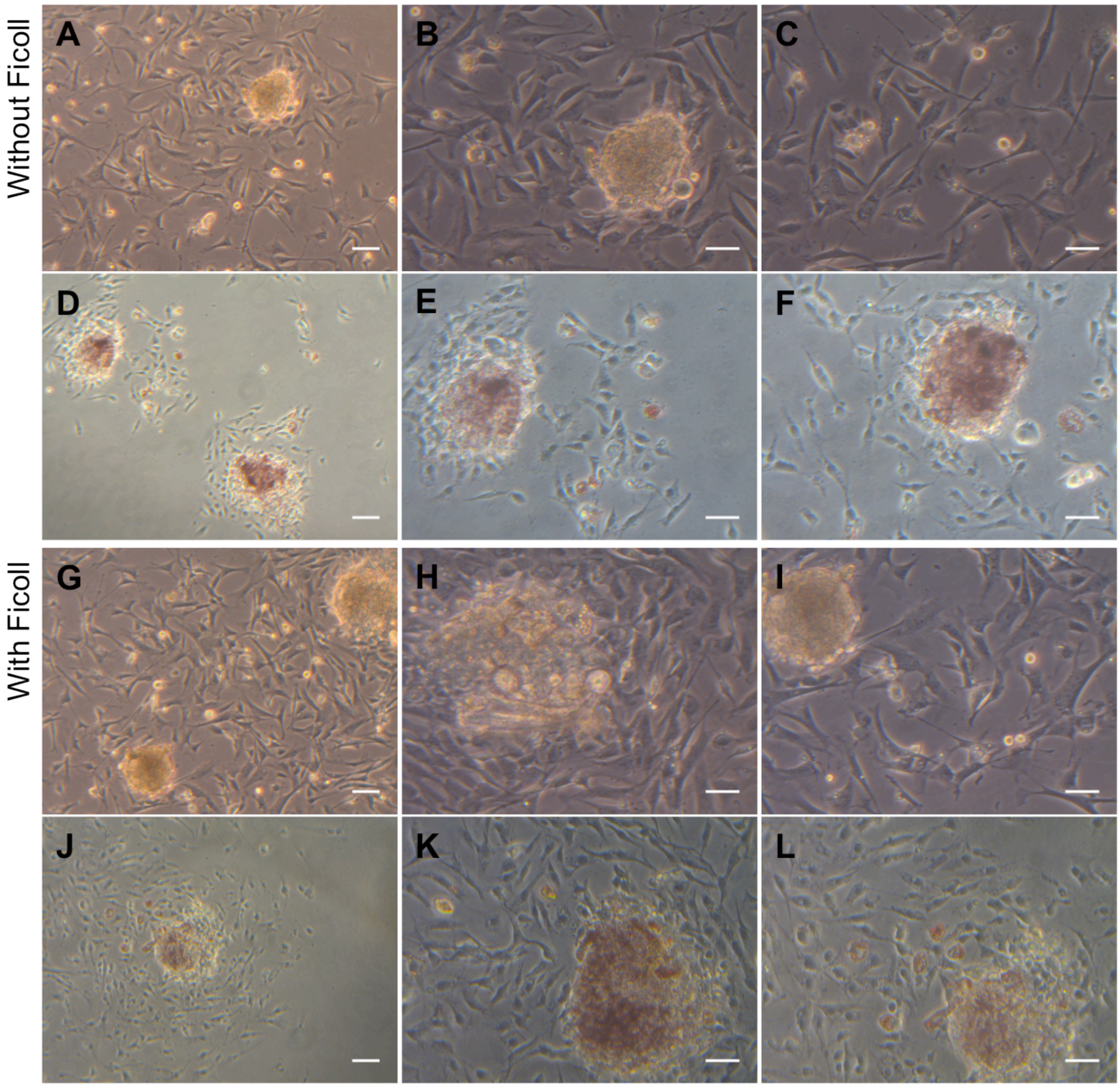

Figure 4.44: 3 dimensional to 2-dimensional cell culture of 16.5-day embryonic mouse dermis with and without Ficoll separation. (**A-F**) Without ficoll (**G-L**) With ficoll (**D-F,J-L**) Oil red O staining after 4 days in 3D and 2 days in 2D. Representative images taken on a Zeiss Axiovert 10. (**A,D,G,J**) scale bar = 65μm. (**B,C,E,F,H,I,K,L**) scale bar = 40μm.

'Whole skin cell' whereby a single cell suspension was generated from the whole skin (epidermal and dermal) was cultured alongside dermal cultures to determine if the epidermal content was having a dramatic influence on the results gained and the success of the model (Figures 4.45-4.48). Results of the e17.5 experiment are shown. There were epidermal cells present in the mixed cultures (Figures 4.45C and G), comparatively with normal dermal cell cultures. The epidermal content did not seem to affect the fat content of the cultures (Figures 4.45D,H,L and P).

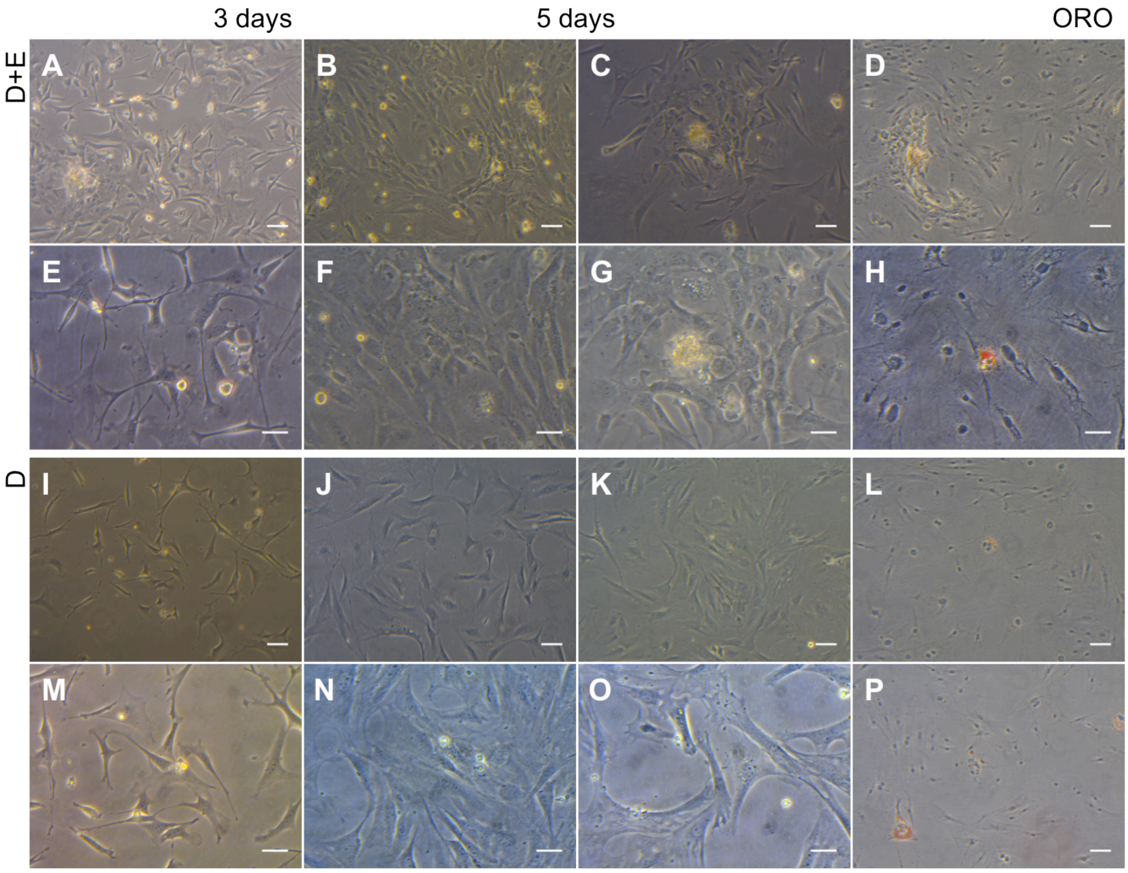

<u>Figure 4.45:</u> 2-dimensional cell culture of 17.5-day embryonic mouse skin. Both (**A-H**) combined dermal and epidermal cells, and (**I-P**) dermal cells. (**A-M**) After 3 days in culture. (**B_D,F-H,J-L,N-P**) After 5 days in culture, (**D,H,L,P**) Oil red O staining. Representative images taken on a Zeiss Axiovert 10. (**A-D,I-L**) scale bar = 65μm. (**E-H,M-P**) scale bar = 40μm.

In relation to the 3D spheres put into 2D culture (Figure 4.46), it could be inferred that there was slightly more fat development in the cultures of solely dermal cells in comparison with the cultures of dermal and epidermal cells. This, however, was a minute difference and so was unlikely that, when in cell culture, the epidermal content was having a dramatic effect on any adipogenesis that occurred.

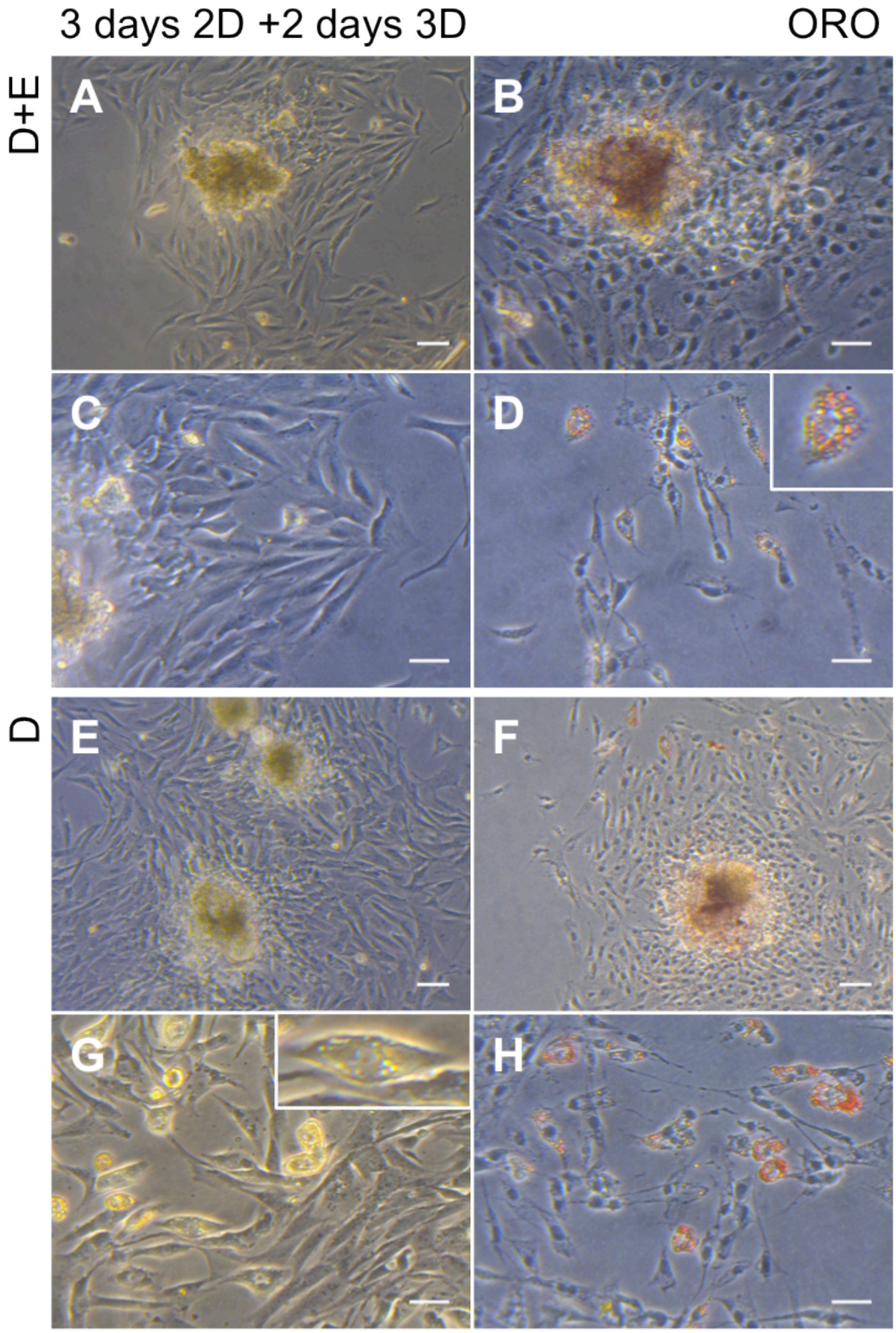

Figure 4.46: **3 dimensional to 2-dimensional cell culture of 17.5-day embryonic mouse skin.** (**A-D**) Combined dermal and epidermal cells (**E-H**) Dermal cells. (**B,D,F,H**) Oil red O staining after 3 days in 3D and 2 days in 2D. Representative images taken on a Zeiss Axiovert 10. (**A,B,E,F**) scale bar = 65µm. (**C,D,G,H**) scale bar = 40µm.

There were significantly more epithelial cells in the spheres generated from dermal and epidermal cells combined (Figures 4.47J-O) in relation to those spheres from the dermis (Figures 4.47J-L). This was demonstrated by fluorescent labelling of the epithelial cells with a cytokeratin antibody. As with the 2D and 3D-2D cultures, there was little difference in the level of oil red O staining and therefore lipid content of the spheres between dermal plus epidermal spheres (Figures 4.47E and F) and just dermal spheres (Figures 4.48E and F).

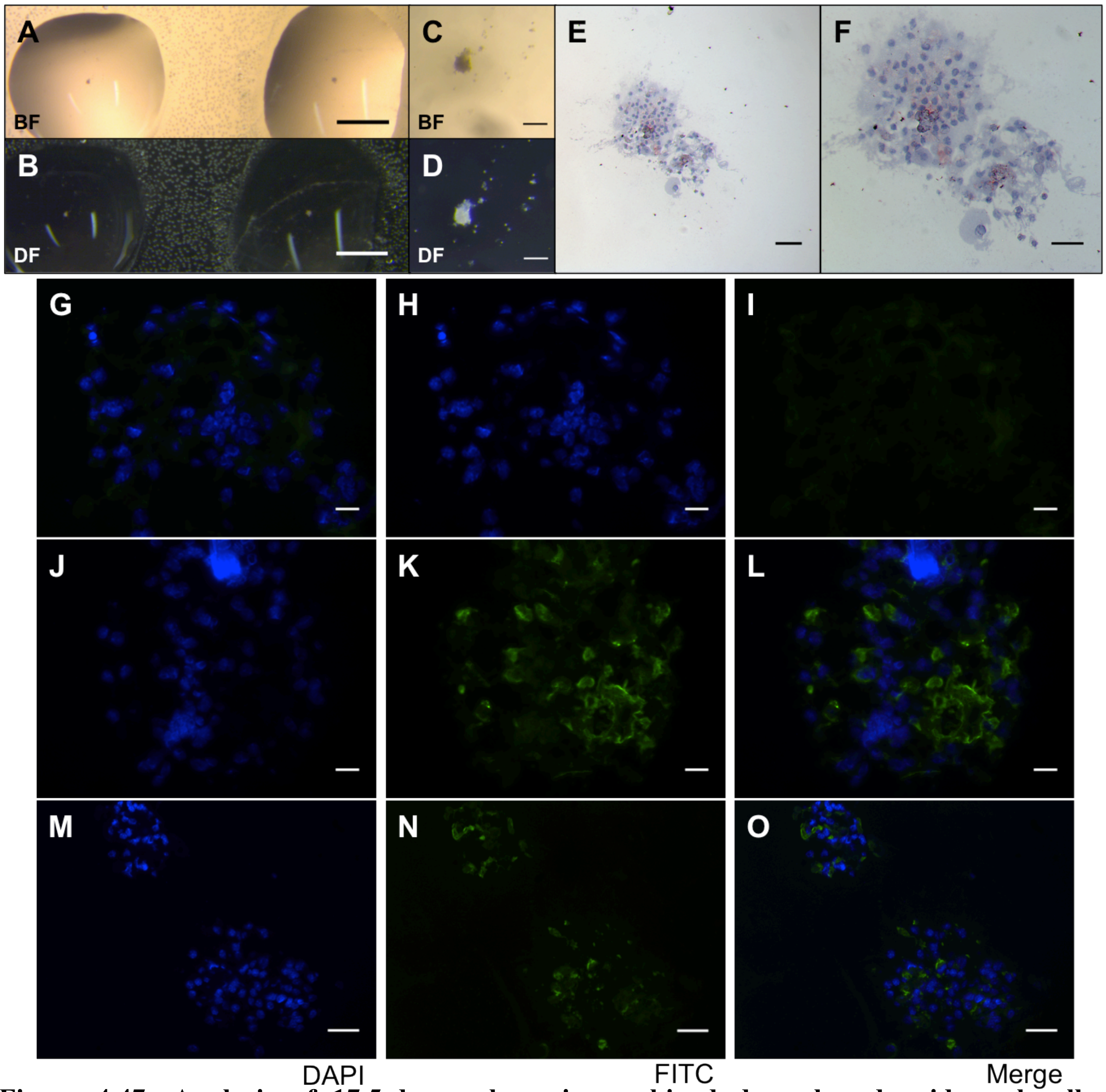

Figure 4.47: **Analysis of 17.5-day embryonic combined dermal and epidermal cell spheres.** (**A-D**) Images taken of 6000 cell spheres on Zeiss Stemi SVII. (**E,F**) Sections cut at 10μm were stained with oil red O to detect presence of fat. (**G-O**) Sections were cut at 7μm, stained with an antibody against cytokeratin and counterstained with DAPI. From left to right; DAPI, FITC, and merge (DAPI/FITC). FITC represents the fluorescent labelling of cytokeratin. (**G-I**) Control showing no fluorescently labelled cytokeratin expression. (**J-O**) labelled using Cytokeratin primary antibody. Images were taken using a Zeiss Axio Imager M1. (**A,B**) scale bar = 2mm. (**C,D**) scale bar = 0.2mm. (**M-O**) scale bar = 40μm. (**G-L**) scale bar = 15μm.

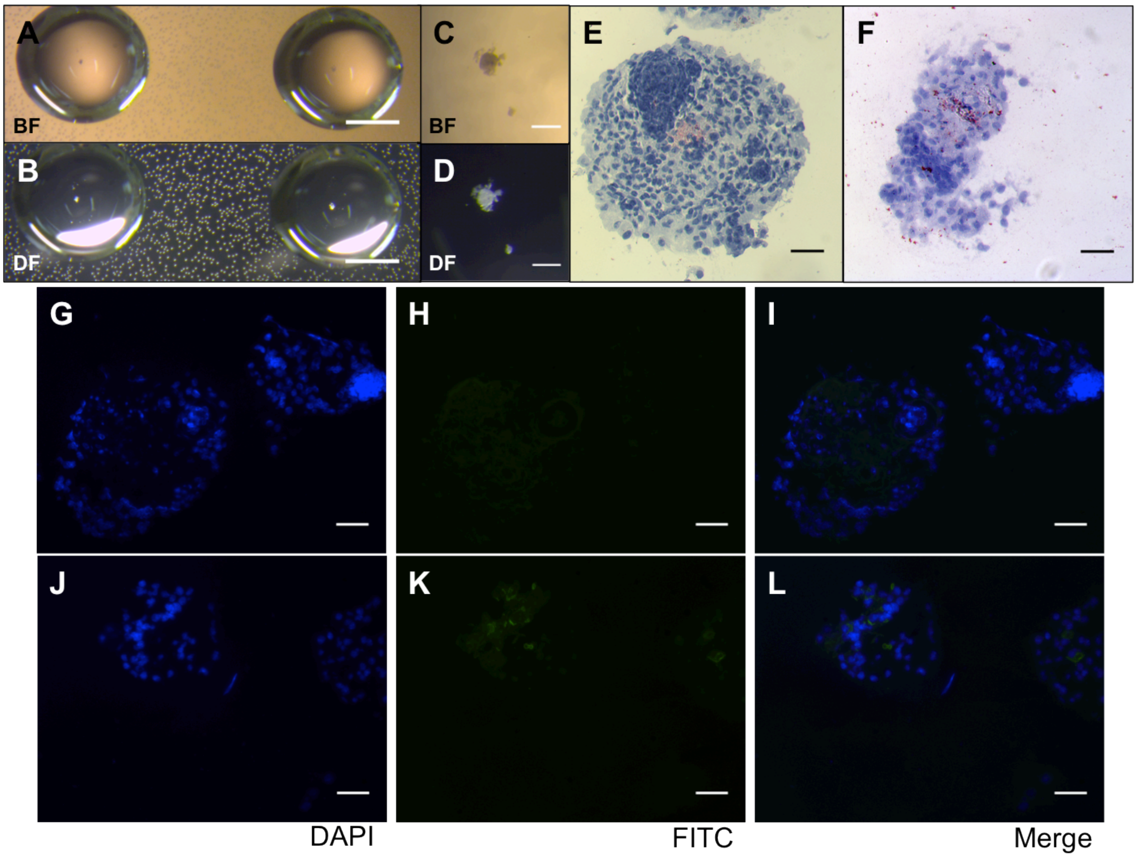

Figure 4.48: Analysis of 17.5-day embryonic dermal cell spheres. (**A-D**) Images taken of cell spheres on Zeiss Stemi SVII. (**E,F**) Sections cut at 10µm were stained with oil red O to detect presence of fat. (**G-L**) Sections were cut at 7µm, stained with an antibody against cytokeratin and counterstained with DAPI. From left to right; DAPI, FITC, and merge (DAPI/FITC). FITC represents the fluorescent labelling of cytokeratin. (**G-I**) Control showing no fluorescently labelled cytokeratin expression. (**J-L**) labelled using cytokeratin primary antibody. Images were taken using a Zeiss Axio Imager M1. (**A,B**) scale bar = 2mm. (**C,D**) scale bar = 0.2mm. (**G-L**) scale bar = 15µm.

4.3.2.2. The Culture Model with E14.5 Dermal Cells

It was thought that adipogenesis might start even earlier, around the timing of hair follicle development initiation. One experiment was conducted using dermal cells taken from e14.5 mouse back skin, when there is less risk of contamination. The e14.5 spheres showed lots of defined lipid droplets demonstrating that the cells of the dermis were capable of differentiating into adipocytes earlier (Figure 4.49). When transferred to 2D culture, there was visible formation of adipocytes, though most of them remained in the spheres and did not spread out (Figure 4.50).

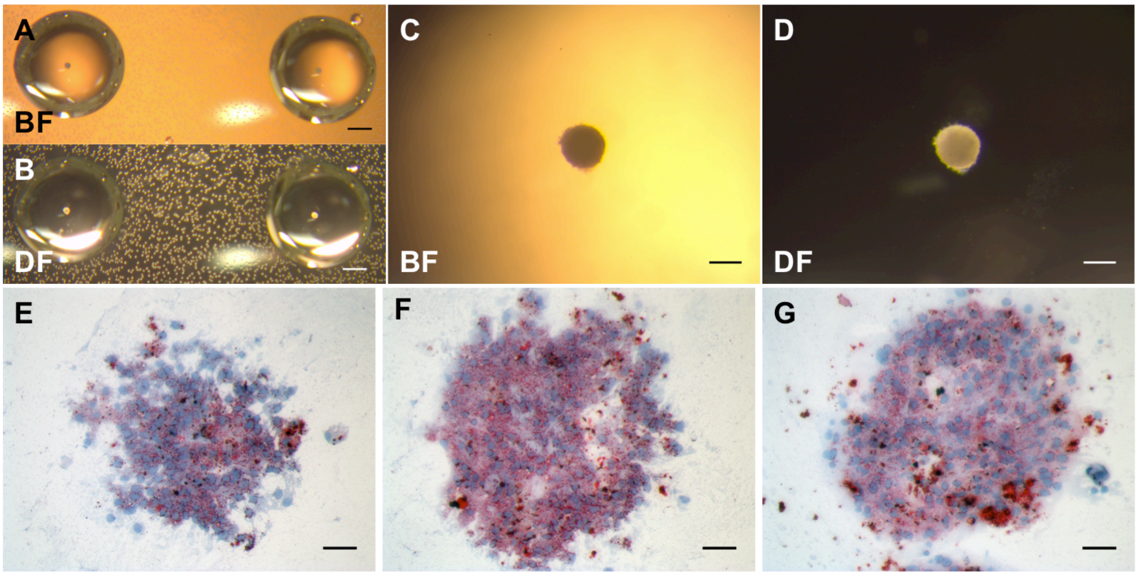

Figure 4.49: **3-dimensional cell culture of 14.5-day embryonic mouse dermal cells.** Images taken after 8 days in culture of concentrated cell spheres. (**A-D**) Images taken on a Zeiss Stemi SVII. (**E-G**) Images taken on a Zeiss Imager, M1. (**A,B)** scale bar = 2mm. (**C,D**) scale bar = 0.2mm. (**E**) scale bar = 65µm. (**F,G**) scale bar = 40µm. BF = bright field, DF = dark field.

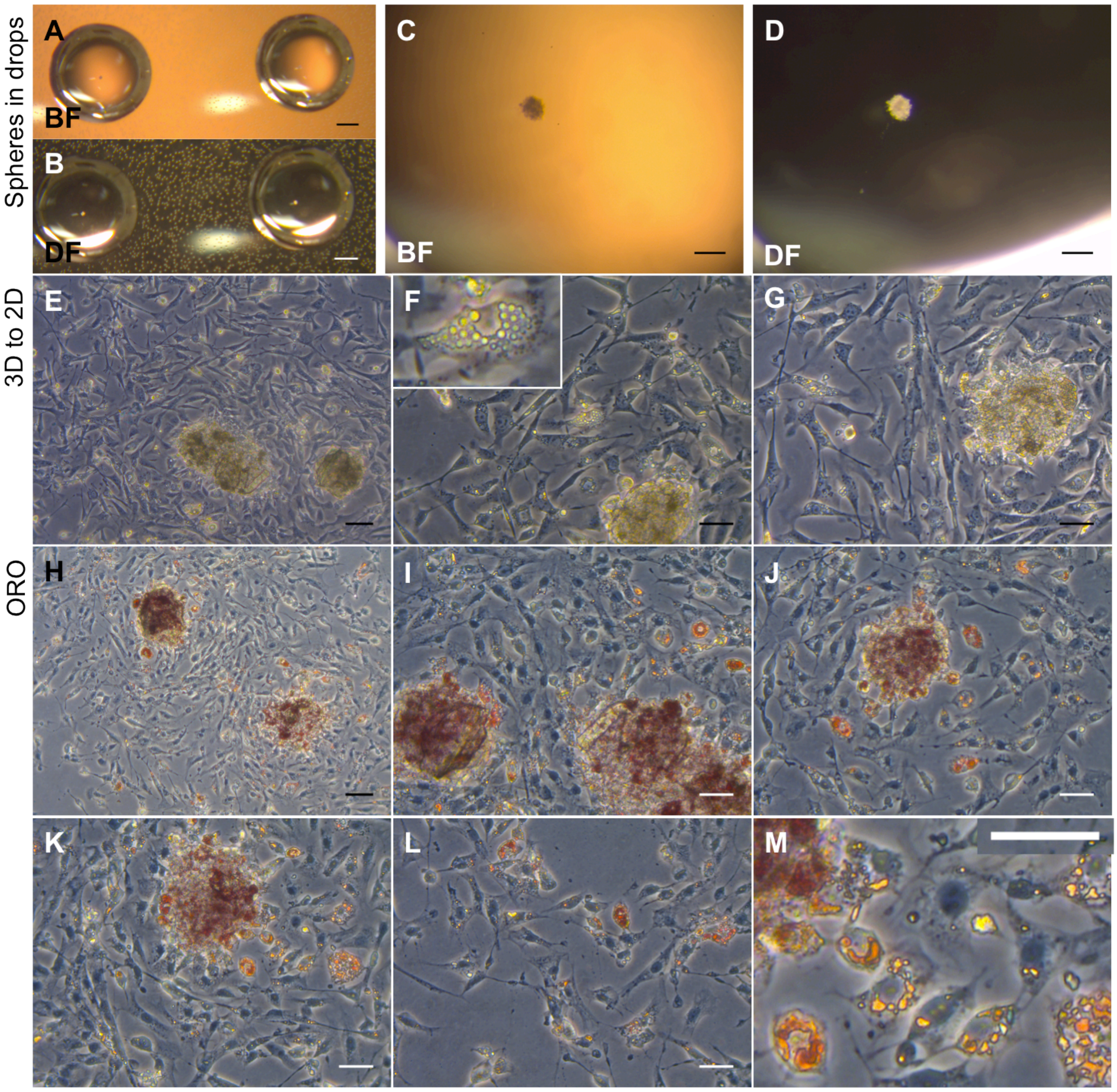

Figure 4.50: 3-dimensional to 2 dimensional cell culture of 14.5-day embryonic mouse dermal cells. Images taken after 2 days in 3D culture of 6000 cell spheres. (**A-D**) and after 6 days in 2D culture (**E-G**). Cells stained with oil red O (**H-M**). (**A-D**) Images taken on a Zeiss Stemi SVII. (**E-M**) Images taken on a Zeiss Axiovert 10. (**A,B**) scale bar = 2mm. (**C,D**) scale bar = 0.2mm. (**E,H**) scale bar = 65µm. (**F,G, I-M**) scale bar = 40µm. BF = bright field, DF = dark field.

4.3.2.3. Epidermal-Dermal Separation

The older skin was found to separate much more easily into epidermis and dermis than the younger embryonic skin. For example, e18.5 skin needed only 30 minutes in the trypsin/pancreatin solution, while e14.5 skin required 1 hour 30 minutes. It was found that it was more advantageous to be patient to minimise the chance of damaging the epidermis and therefore, epidermal contamination. Smaller pieces were easier to manipulate, so 3 pieces were more often cut from each side instead of two, particularly for larger embryos.

4.3.2.4. Oil Red O Quantification

The images in the experiments showed a difference between adipocytes differentiated, however, a way of quantifying the cells could support the observations. In the 3 dimensional hanging drop culture method, cells are known not to divide, whereas in 2-dimension, they do. Quantification of oil red O was used to investigate if even though there were less 3D cells there was still a higher number of red staining and therefore adipocytes because it is suspected that a 3D environment allows better differentiation. It proved difficult to quantify the oil red O.

A serial sampling method was trialled, to collect enough oil red O to detect a result to compare 2D with 3D. For the 3D result, the 3D to 2D samples were collected. Firstly the samples were taken from the embryonic day 18.5 experiment.

Table 4.4: Results of oil red O absorbance from 2D and 3D cultures of embryonic day 18.5 mouse back skin dermal cells, read at 510nm on both a nanodrop and spectrophotometer

	2D plate		3D plate	
	Nanodrop	Spectrophotometer	Nanodrop	Spectrophotometer
1	0.035	0.051	0.044	0.043
2	0.033	0.039	0.044	0.050
3	0.028	0.026	0.036	0.044
4	0.040	0.041		
5	0.045	0.047		
6	0.023	0.047		
7	0.045	0.056		
8	0.078	0.078		
Mean	0.041	0.048	0.041	0.046

Only the wells that contained spheres adhered were selected for quantification. However, with the e18.5 experiment, there were few spheres stuck and so there were only 3 samples (Table 4.4). There was variation in the values collected from both the nanodrop and the spectrophotometer, though the average means were similar for both 2D and 3D to 2D. It was thought that the oil red O may have not completely dissolved, therefore some of the results would detect higher than others and so the samples were filtered using a syringe filter twice before reading off the values.

Next, using the results from the e17.5 experiment, samples were made and absorbances measured on the nanodrop which measured smaller amounts so was more reliable than the spectrophotometer. The samples were filtered twice and three readings were taken from each sample to account for the level of variance found across different samples (Table 4.5). A control was also conducted to test the reliability, whereby empty wells containing no cells were stained with oil red O and then serially sampled for reading. This showed the level of background red staining that adhered to the wells.

Table 4.5: Results of oil red O absorbance from 2D and 3D cultures of embryonic day 17.5 mouse back skin dermal cells, read at 510nm on a nanodrop using UV-Vis software.

					Mean	Mean - Control
	Control	0.016	0.014	0.010	0.013	-
2D	**1**	0.039	0.027	0.037	0.034	0.021
	2	0.026	0.022	0.025	0.028	0.015
	3	0.065*	0.035	0.029	0.032	0.019
3D to 2D	**1**	0.042	0.041	0.041	0.041	0.028
	2	0.045	0.044	0.044	0.044	0.031
	3	0.042	0.053	0.046	0.047	0.034

*discarded from the mean.

One value (0.065*) was significantly higher and so discarded from the mean (Table 4.5). While the samples for 2D were generally lower than 3D (more than 5 times lower) there was still a lot of variability across both the samples and the readings for each sample. When control wells were stained, they read a lower absorbance, which suggested that the nanodrop readings were accurate to some extent, but that residual oil red O stuck to the wells during staining.

With the next experiment with 16.5-day embryonic back skin dermal cells, the samples were vortexed to mix the oil red O evenly within the isopropanol and a 100% isopropanol blank was measured at 0.002. A cell scraper was used to detach the cells and break them up in order to collect the entire sample and prevent the spheres from clumping together. This was compared with not using a cell scraper on the same experiment.

The values were higher using the cell scraper (Table 4.6) which suggested that it was helping to break up the cells so all the oil red O so more of the oil red O is released. There was an anomaly (Table 4.6, with cell scraper 4), which was lower than the other values. This was compared with 2D with an average mean of 0.062 across the 12 samples (Table 4.7). The values were more similar to those found using a cell scraper on 3D spheres with an average mean of 0.065 (not including the 0.027 value). Overall, using this technique there was no significant difference in the level of oil red O quantified between 2D and 3D cultures, though variation across the samples did exist.

Table 4.6: Result of oil red O absorbance of 3D cultures transferred to 2D from embryonic day 16.5 mouse back skin dermal cells.

					Mean	Mean - Blank
No cell scraper	**1**	0.051	0.042	0.042	0.045	0.043
	2	0.048	0.046	0.045	0.046	0.044
	3	0.043	0.050	0.043	0.044	0.042
	4	0.067	0.060	0.057	0.061	0.059
	5	0.064	0.061	0.064	0.063	0.061
	6	0.030	0.032	0.035	0.032	0.030
With cell scraper	**1**	0.067	0.069	0.066	0.067	0.065
	2	0.065	0.064	0.066	0.065	0.063
	3	0.070	0.069	0.068	0.069	0.067
	4	0.028	0.031	0.028	0.029	0.027
	5	0.066	0.063	0.060	0.063	0.061
	6	0.067	0.072	0.077	0.072	0.070

Samples were collected both using a cell scraper and not using a cell scraper and average means were calculated before subtracting the isopropanol blank.

Table 4.7: Result of oil red O absorbance of 2D cultures from embryonic day 16.5 mouse back skin dermal cells.

				Mean	Mean - Blank
1	0.063	0.065	0.066	0.065	0.063
2	0.061	0.063	0.062	0.062	0.060
3	0.061	0.061	0.059	0.060	0.058
4	0.057	0.056	0.057	0.057	0.055
5	0.057	0.060	0.062	0.060	0.058
6	0.065	0.066	0.065	0.065	0.063
7	0.064	0.063	0.061	0.063	0.061
8	0.075	0.074	0.074	0.074	0.072
9	0.065	0.066	0.065	0.065	0.063
10	0.061	0.060	0.063	0.061	0.059
11	0.053	0.051	0.051	0.052	0.050
12	0.073	0.081	0.098	0.084	0.082

Average means were calculated before subtracting the isopropanol blank.

4.3.3. Immunofluorescence Labelling of Markers

4.3.3.1. C/EBPα

C/EBPα was first looked at in normal embryonic day 18.5 mouse back skin to detect the antibody's presence, which had previously been found to be nuclear around e18 (Wojciechowicz 2012). The labelling was found nuclear in the lower dermis, but also throughout the whole skin sample from this age; it was not localised around hair follicle end bulbs (Figure 4.51).

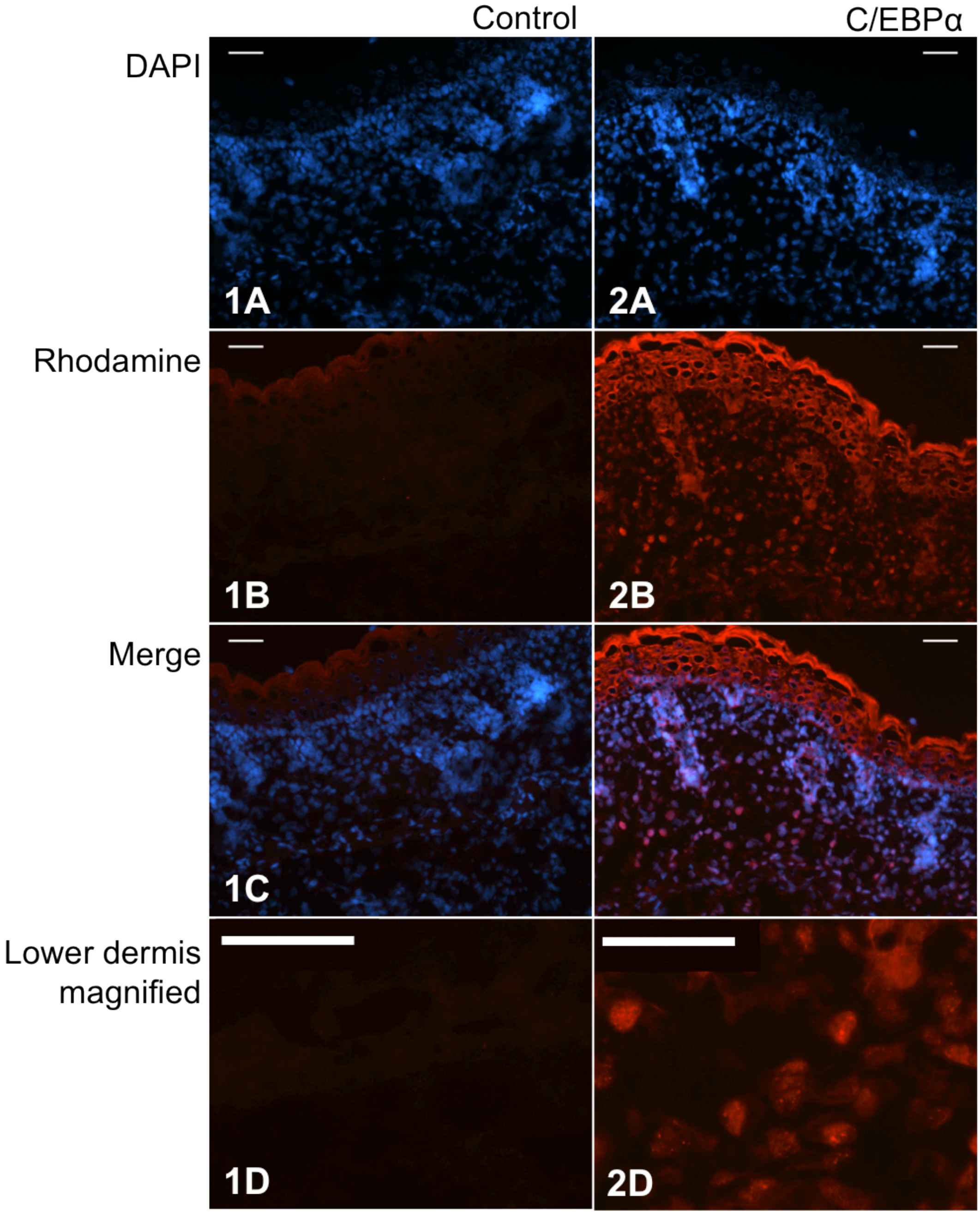

Figure 4.51: Analysis of C/EBPα presence in embryonic day 18.5 mouse back skin. Sections were cut at 7μm, stained with an antibody against C/EBPα and counterstained with DAPI. From top to bottom, DAPI, Rhodamine, and merge (DAPI/Rhodamine). Rhodamine 594 represents the fluorescent labelling of C/EBPα. (**1**) Control showing no fluorescently labelled C/EBPα expression. (**2**) labelled using C/EBPα primary antibody.(**1D** & **2D**) magnified images to show nuclear staining. Images were taken using a Zeiss Axio Imager M1. Scale bar = 40μm.

C/EBPα was then used on spheres to test its effectiveness for the model. The fluorescence adhered to the outside of the spheres (Figure 4.52) and did not appear positive reliable staining.

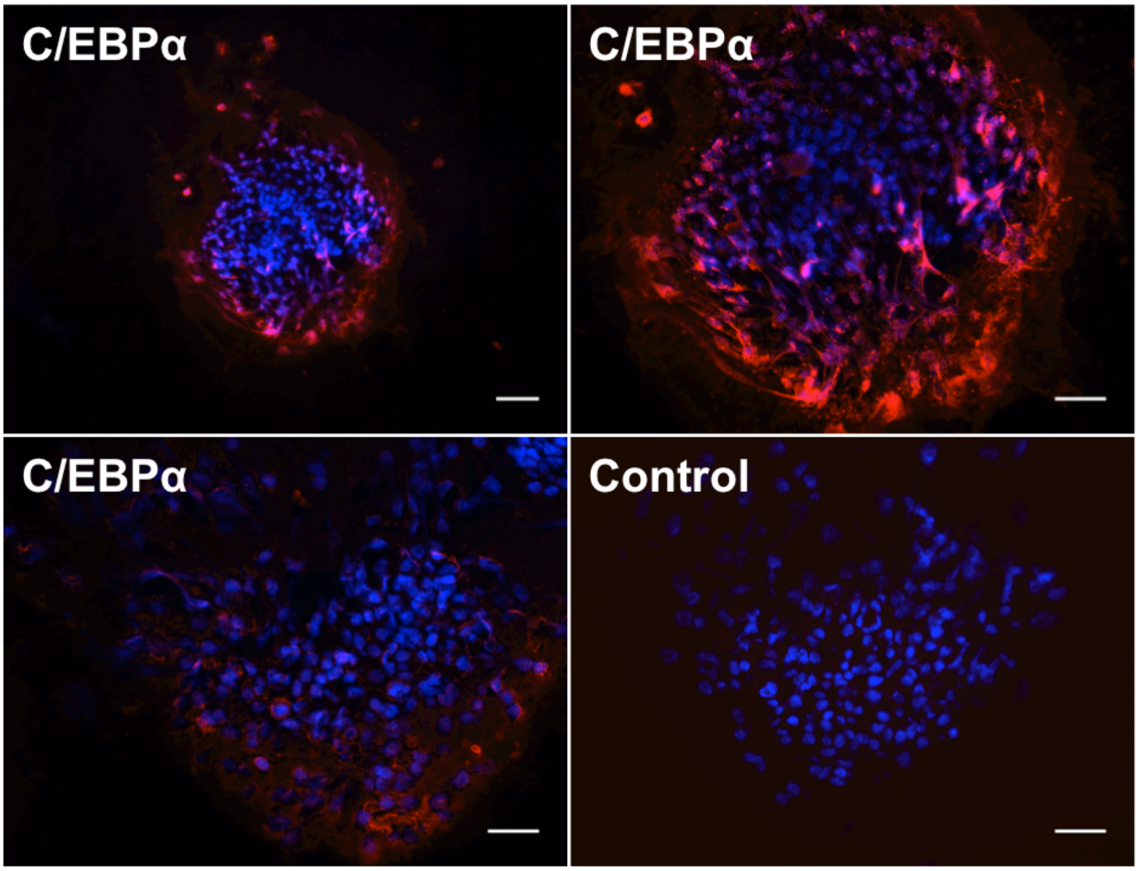

Figure 4.52: Analysis of C/EBPα presence in dermal cell spheres taken from embryonic day 16.5. Sections were cut at 7μm, stained with an antibody against C/EBPα and counterstained with DAPI. Control shows no fluorescently labelled C/EBPα expression. Images were taken using a Zeiss Axio Imager M1. (**upper left**) scale bar = 65μm. (**upper right, lower left & right)** scale bar = 40μm.

It was thought that considering C/EBPα nuclear expression had previously been found around e18 that spheres around this age should be labelled with C/EBPα. Therefore, spheres from e15.5 plus 3 days (Figure 4.53) and e16.5 plus 2 days (Figure 4.54) were stained for C/EBPα. Spheres at the end of the experiment, e.g. e15.5 plus 7 days and e16.5 plus 6 days were also investigated for a comparison. A different secondary antibody was also used. In the e15.5 spheres after 3 and 7 days there was still fluorescence round the periphery of the spheres (Figure 4.53). In the spheres taken from e16.5 dermal cells, there was a high degree of nuclear expression found after 2 days and by 6 days there was a less even distribution with a higher amount of fluorescence around the sphere periphery (Figure 4.54).

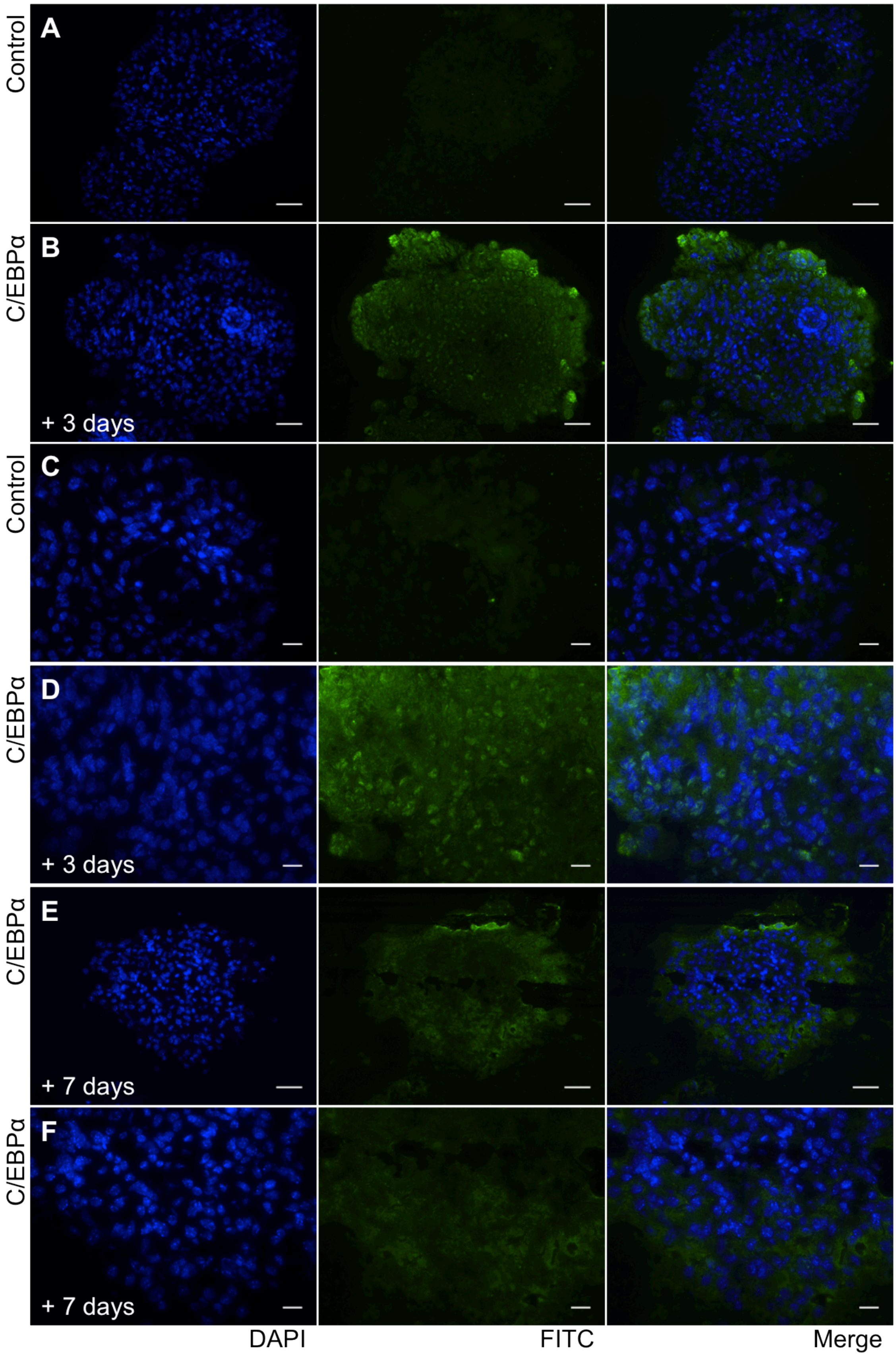

Figure 4.53: Analysis of C/EBPα presence in dermal cell spheres taken from embryonic day 15.5 after 3 and 7 days. Sections were cut at 7μm, stained with an antibody against C/EBPα and counterstained with DAPI. From left to right, DAPI, FITC, Merge (DAPI/FITC). Control shows no fluorescently labelled C/EBPα expression. Images were taken using a Zeiss Axio Imager M1. (**A,B,E**) scale bar = 65μm. **(C,D,F)** scale bar = 40μm.

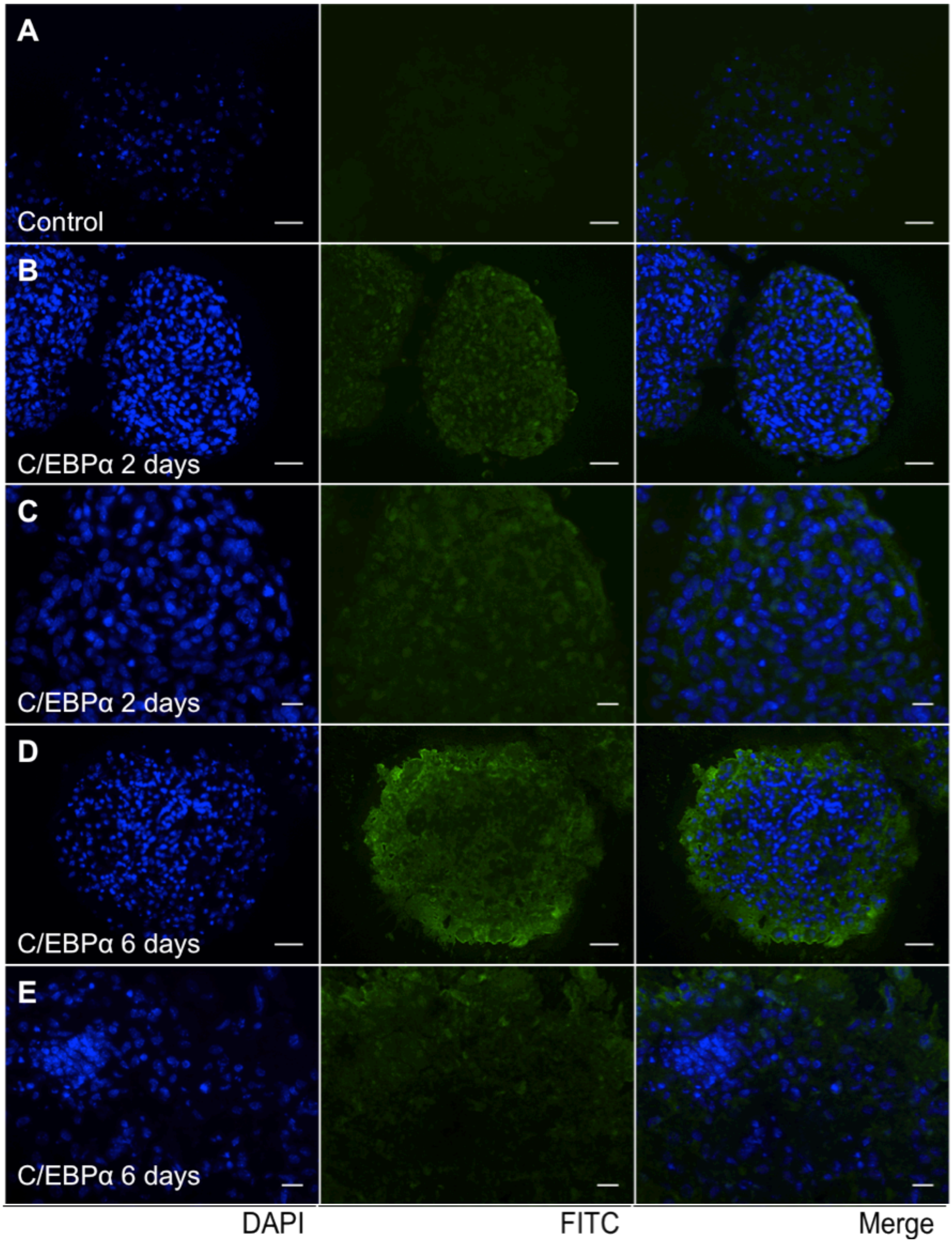

Figure 4.54: **Analysis of C/EBPα presence in dermal cell spheres taken from embryonic day 16.5 after 2 and 6 days.** Sections were cut at 7μm, stained with an antibody against C/EBPα and counterstained with DAPI. From left to right, DAPI, FITC, Merge (DAPI/FITC). Control shows no fluorescently labelled C/EBPα expression. Images were taken using a Zeiss Axio Imager M1. (**A,B,D**) scale bar = 40μm. (**C,E)** scale bar = 15μm.

Spheres created from e14.5 dermal cells were stained for C/EBPα and most of the cells showed nuclear expression of C/EBPα (Figure 4.55). However, whether this was a reliable result or not is unclear, considering the labelling on mouse back skin was unsuccessful and not all the dermal cells differentiate into adipocytes.

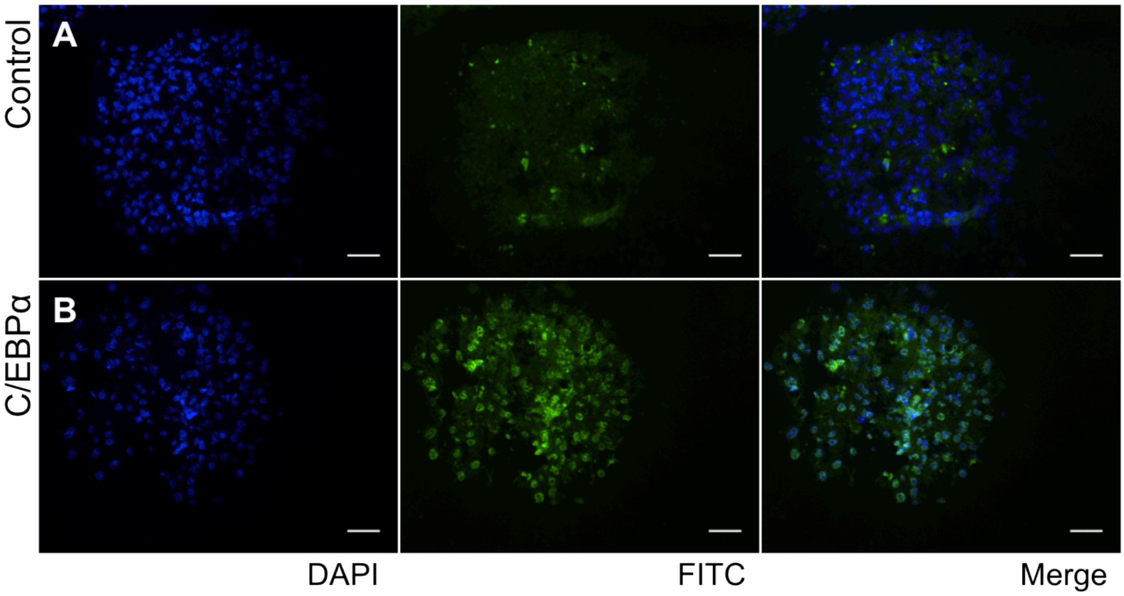

<u>Figure 4.55:</u> Analysis of C/EBPα presence in dermal cell spheres taken from embryonic day 14.5 after 4 days. Sections were cut at 7μm, stained with an antibody against C/EBPα and counterstained with DAPI. From left to right, DAPI, FITC, Merge (DAPI/FITC). Control shows no fluorescently labelled C/EBPα expression. Images were taken using a Zeiss Axio Imager M1. (**A,B,D**) scale bar = 40μm. (**C,E)** scale bar = 15μm.

4.3.3.2. PECAM1

Spheres from e14.5 dermal cells were also stained for PECAM1/CD31 to detect the presence of developing blood vessels. There was some labelling found in the spheres to suggest blood vessels were capable of developing alongside adipocytes, though there was a little staining in the control spheres, which could mean the fluorescence was picking up background between the cells (Figure 4.56).

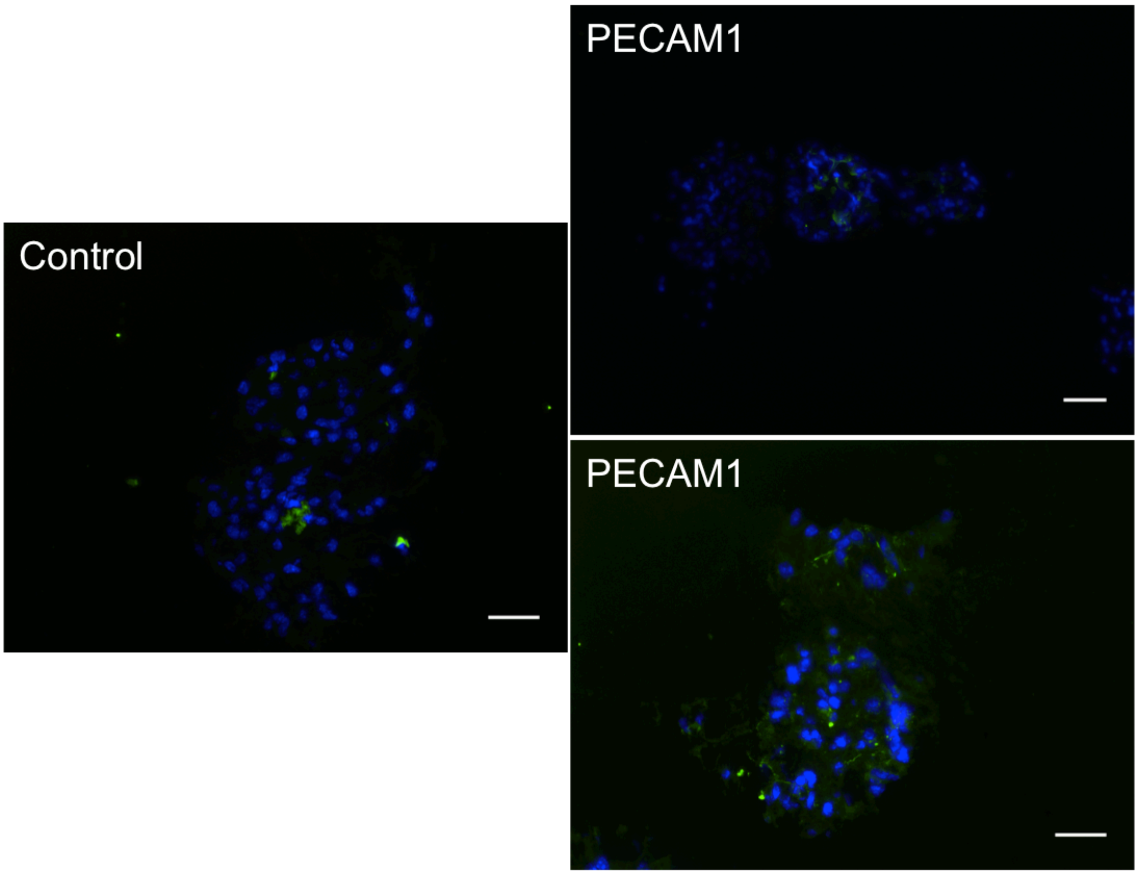

Figure 4.56: Analysis of PECAM1 presence in dermal cell spheres taken from embryonic day 16.5. Sections were cut at 7μm, stained with an antibody against PECAM and counterstained with DAPI. Control shows no fluorescently labelled PECAM1 expression. Images were taken using a Zeiss Axio Imager M1. (**Upper right**) scale bar = 65μm. (**Left & Lower right)** scale bar = 40μm.

4.4. Discussion

4.4.1. Organ Culture Model

In the majority of the experiments, embryos aged 16.5 day could be used. This was considered the best age to look at, as by this point the development of the hair follicles had been initiated and it was therefore considered that their effects would not be as major. While it would be beneficial to eliminate the effects of the developing hair follicles on adipogenesis, this would be unrealistic in terms of normal adipocyte development. Since the development of hair follicles and adipocytes are thought to interact, it may in fact be of use to eliminate the hair follicles and observe how adipogenesis proceeds.

It was found that the results across the different experiments were not consistent. Certain morphological features of the skin were used to assess the quality of the cultured pieces. These include follicle downgrowth, expansion of the epidermis and/ or dermis, darkness of the skin and wound healing response around the perimeter of the skin pieces. All these were thought to be positive indications of the skin's quality, except the darkness of the skin, which was considered an indication of the skin turning pathological. Due to many of the pieces appearing pathological, different variables of the culture system were altered to determine if a more successful organ culture method could be created. Since this method had been used successfully before, though it was time-consuming the model was persisted with.

The media and substrate for the skin to be cultured in needed to be as close to realistic conditions as possible. Serum, the most commonly used being foetal bovine serum, was added to the media. This contains hormones and growth factors amongst other things which help to stimulate growth and cell proliferation. Serum also provides binding and transport proteins and is involved in detoxification and maintaining the pH, allowing the cells to survive and grow healthily (Gstraunthaler 2003). While universally used as a media supplement for successful cell culture, serum use comes with its disadvantages. In particular, the precise contents of serum is not defined therefore some of its functions in culture are unknown (Bjare 1992; Gstraunthaler 2003). Serum can also vary from batch to batch so its effects many not be consistent. It is largely an unknown variable therefore for some of the experiments in this chapter, as well as using different concentrations, serum was omitted. Two different types of media were also experimented with to look for the optimum conditions. Modified Eagle's Media, the standard media used for culture of skin was compared with using William's E media (Section 4.3.1.3). William's E media has been supplemented with amino acids and increased levels of glucose, which allows skin and hair follicles to grow in organ culture without the need for serum and was found to reduce cell death (Lu *et al.* 2007). William's Media has been used in the organ culture of human hair follicles (Philpott *et al.* 1994). However, changing the media from MEM to William's which contained Vitamin E, as well as removing the serum or increasing the percentage did not appear to have a positive more consistent effect on the cultured skin. It was therefore decided that an alternative more manipulative model should be looked into as while further developing this organ culture-type model would be beneficial to our understanding of adipogenesis in the lower dermis, there was limited time available.

4.4.2. Cell Culture Model

The results show that in general there is a higher proportion of adipocytes produced in 3D culture compared with 2D culture. This may be because 3D represents a more life-like environment since the cells are not in contact with a plastic or glass substrate and do not grow in monolayers.

Often the adipocytes grouped in clusters. This would suggest that there is signalling between neighbouring cells. The red staining was often found in the centre of the spheres. Perhaps the cells organise into the upper and lower dermis. Oxygen pressure is not reliable in the spheres and varies throughout, which may be why fat forms in the middle of the spheres. Hypoxia has been found to exist in cell spheres (Liu et al. 2013). Hypoxia in 3D spheroid cell cultures exists 200 microns from the surface of the spheres (Allison, 2014). As well as this, proliferation occurs more easily at the surface of the spheres.

Adipocytes formed from cells as early as e14.5 and in fact in a greater density than e16.5. This implies that the mesenchymal stem cells are committed to the adipocyte lineage a lot earlier than previously thought. Perhaps there is a process of inhibition at a later stage that prevents all of the cells becoming adipocytes. There are many mechanisms by which this could occur. The fact that the epidermis has been removed and is therefore not able to influence the development of the dermal cells could be a reason, i.e. the epidermis may have an inhibitory influence on the degree of adipocyte differentiation. As an alternative theory, the upper and lower dermis might be signalling to each other to prevent the upper dermis from developing fat. The cells may be capable of doing so, but a signal is required to prevent differentiation from occurring. The cell culture model is a mixture of upper and lower dermal cells, which are not in distinct layers, thus no signalling between the layers is possible. A possible hypothesis is that without a negative signal, all the dermal cells are capable of turning into adipocytes.

In some of the earlier cell cultures, there was evidence of epidermal contamination. A Pan keratin antibody was used to detect the degree of contamination in the spheres. While more careful experimentation reduced the degree of contamination there were still some epidermal cells found in some of the cultures. The presence of these cells may have an impact on the degree of adipogenesis occurring in the cells taken from the dermis. Keratinocytes can proliferate rapidly. Ficoll was then used to separate the cell types by density. The cell densities for keratinocytes and fibroblasts was taken from Reiners and Slaga (1983). The aim was to remove any keratinocytes from the fibroblast populations that had got into the cell suspension before the cells were put into culture. It was expected that two distinct layers would be seen in the Ficoll fractions, but in fact both times, a cell pellet was found floating on the top layer of Ficoll. This could be because the cells were actually less dense than expected, or that there were two layers, but the numbers of keratinocytes were so small they were difficult to see. One density was used for keratinocytes, while in actual fact they vary in density throughout the epidermis and the basal keratinocytes overlap with fibroblasts in terms of density (Reiners and Slaga 1983). When comparing the results found using Ficoll from not using Ficoll, the difference in both adipocyte formation and the number of cells stained with the pan keratin antibody did not appear to be significantly different. Therefore due to time constraints and the need for a high number of cells for the use of Ficoll, it was not used in the final model protocol to look at the signalling pathways. Epidermal contamination while considered an issue, would not render the model useless for looking at signalling pathways as it would still be looking at the effect they can have on the skin adipogenesis. Pan keratin was still used to monitor the levels of contamination across the experiments. This way, any anomalous results could be considered in relation to contamination. To observe what effects the epidermis might be having on the dermis in culture, whole skin cultures were also performed, whereby the whole skin was put into cell culture. There was less fat production. This may be because the cells have been dissociated and are not in a normal organisation.

Not only is the epidermis thought to influence adipogenesis in the lower dermis, but blood vessel development (angiogenesis) has been implicated (Neels *et al.* 2004; Cao 2007). It occurs prior and during adipogenesis (Fukumura 2003; Hausman and Richardson 2004; Hausman and Hausman 2006; Wang *et al.* 2006) and has been previously suggested to be the reason for many of the genes found in the adipose microarrays. The microarray values depend on the location in the dermis selected, thus a blood vessel could be located. The antibody, PECAM1, was used to look for blood vessel formation in the spheres. These spheres showed blood vessel like structures in the spheres after 2 days which was around embryonic day 18.5. Thus, angiogenesis could be influencing adipogenesis.

It was originally thought that if the later dermal cells were put into culture 50% of them would differentiate into adipocytes. Often the spheres showed a high degree of red staining and it was inferred that there must be a degree of cell-to-cell signalling.

Interactions between cells are important for development and aid the organisation of tissues and structures (Cooper 2000).

The sphere model, initially looked like it was showing how the dermis alone behaved autonomously, however epithelial "contamination" was then found, so from e15 onwards, dermal cells plus epidermal influences were investigated. Comparing with 2D was difficult since one of the differences between the 2D and 3D cultures was that the 3D have retained an epithelial influence. This being said the fact that the e14.5 3D spheres which have no epithelial cells still showed the same 3D vs. 2D difference suggested that at least a positive epithelial influence is not required from this point on.

4.3.3. Oil Red O Quantification

Establishing a method of quantifying the oil red O proved difficult. While originally it was thought that it would be appropriate to use 100% isopropanol to collect the oil red O from the wells and read the absorbance on a nanodrop, this method was found to be unreliable. One of the problems encountered was images showed that the oil red O had stained the lipid droplets within the cells; it had also adhered to the sides of the well where there were no cells. This meant that the oil red O collected included inconsistent excess from the sides of the wells. Secondly, staining the 3D spheres, which had been transferred to 2D culture was challenging. Often the spheres detached from the wells and it wasn't certain that all the staining from inside the spheres had been collected. In order to make sure that all the cells were collected, a cell scraper was used on some of the wells to detach all the cells and therefore collect all possible oil red O. The results were inconsistent between the wells containing the same treatment. As well as this, some of the spheres disintegrated in the 100% isopropanol, which led to the chance that the absorbance readings could be wrong if particles were registered instead of a solution. In order to prevent this from being the case, some of the mixtures were briefly centrifuged so the cells that had been picked up in the isopropanol settled at the bottom of the eppendorf. This did not prevent anomalous results from being produced. While the method was found largely unreliable, there were some improvements in the consistency of the results found when three readings were taken from each data set, compared with the earlier attempts. However often the results also varied for the same samples.

4.4.4. Further Work

Oil red O quantification could really aid defining the visual results. A potential method of quantifying could involve counting the red stained cells in proportion to how many cells in a frame. Several frames could then be added together to create an average. This technique relies upon the images showing an overall representation of the cells growing in the wells. Another method could be conducted by staining the cells with lipid red and using flow cytometry to measure the level of fluorescence present. It should show that even though there are less 3D cells as proliferation does not occur like 2D, there is still more red staining, thus 3D allows for better differentiation.

In order to conduct the organ culture model without the influence of hair follicle formation, a mouse model that does not develop follicles could be used. If it is an epidermal mutation, could potentially recombine with another mouse dermis to observe if adipocyte development is inhibited. Conversely adult follicles could be cultured with the embryonic skin in co-culture. As well as hair follicle presence, the use of Ficoll to separate the epidermis from the dermis cell densities was found difficult, most likely because the densities can be very similar as keratinocytes have varying densities (Reiners and Slaga 1983). In order to better purify the dermal cell suspension, an experiment could be conducted using fluorescence-activated cell sorting (FACs) to separate the upper and lower dermis by detection of CD36.

In all the skin ages (e14.5, e15.5, e16.5, e17.5 and e18.5), after culture, there was evidence of adipose development. In order to show that adipogenesis can also be inhibited and there find at which age it is too late to inhibit, SPARC (Secreted protein acidic and rich in cysteine) could be used as a control. Without SPARC (-/-) mice produce more adipose tissue, but *in vitro*, SPARC can inhibit adipogenesis (Nie and Sage 2009). In order to show inhibition of adipogenesis, isolate the SPARC protein and transfect the cells using siRNAto block transcription, causing gene knockdown. This can either be transient so that the effects of adipogenesis inhibition at certain time points can be observed, or permanent by inserting a vector.

In order to track the development, a marker of early adipogenesis is needed. C/EBPα was immunfluorescently stained for, but seemed to show inconclusive results. The periphery of the spheres fluoresced and when the skin was stained, there was no specificity; all the cells were labelled. Perhaps the antibody, like that of PPARγ (Chapter 3) is not suitable for immunofluorescence analysis on frozen sections. A future experiment could involve the use of Western blot analysis.

Potentially, if both models were working, they could be used in conjunction with each other to investigate adipogenesis. Why the skin organ culture model was not able to be recreated was questionable. However, if it were working perfectly would allow how specific influences affected adipogenesis at key times to be asked, in the context of all other influences being present – including hair follicles. The sphere model if taken from e14 or even earlier could look at the specific influences dermal cells have on each other. Embryonic day 16.5 was focused on, though as it is becoming increasingly more likely that adipogenesis starts earlier than the ages the microarray data was collected from (Wojciechowicz 2012), getting the model reproducible at a variety of ages so that it can be pushed back earlier would be beneficial. There are different stages of regulation during adipogenesis; therefore, it is still valuable to look at e16.5, after the establishment of the hair follicles. As well as this, some pathway signals influence hair follicle initiation and so by investigating later, follicles are already forming. It can be concluded that many different methods of studying development should be combined and no one such model can be accepted as identical to that found in a normal environment. While both models could be beneficial to the study of adipogenesis, in this case in terms of the role of particular signalling pathways, due to time constraints the cell culture model established here was used. Further investigation into the organ culture model may enable it to be developed for future work. While the organ culture model would be considered a more realistic model system, when testing factors, the signal is unspecific signal as both the epidermis and dermis receive it so in this case, perhaps the cell culture model would actually be better.

CHAPTER 5:

The Signalling Pathway Question; Investigation into the Effects of Pathway Activators and Inhibitors of Three Signalling Pathways on Adipocyte Development

5.1. Introduction

As well as those considered as the master regulators of adipogenesis, e.g. PPARγ and C/EBP family members, other factors have been found having positive or negative regulatory effects on the development (Lefterova and Lazar 2009).

Signalling, including extracellular and intercellular signalling, is fundamental to the organisation of embryonic (and post-natal) development, involving differentiation and the growth of different cell types in the skin (Figure 5.1). A number of conserved families of signalling molecules orchestrate embryogenesis and similarly tissue regeneration (Hogan 1996). Microarray analysis data has shown that there are many factors linked in a number of signalling pathways. These interact with each other through both activating and inhibiting effects, which regulate development, including the development of fat (adipogenesis). Signalling pathways generally involve ligands, e.g. growth factors binding to receptors and triggering a signalling cascade and a number of cellular responses. Adipogenesis involves the induction of factors with cause the cells to commit to adipogenesis and the activation of a number of transcription factors downstream of signalling pathways that allow or prevent differentiation from occurring (Rosen and MacDougald 2006). Not only this, but these factors can also have different influences at different locations, timings and doses. For example, it is known that bone morphogenetic protein 4 (BMP4) has a concentration-dependent effect on the development of the dorso-ventral patterning of the neural tube with an opposing gradient of Sonic hedgehog (Shh) signalling. Cell-to-cell interactions, vasculature and innervations are also influential as to the effects signals and signalling pathways have (Gesta *et al.* 2007).

The type of signalling can help to explain what sort of role a pathway can have on development. Different modes of signalling occur over different distances. For example, juxtacrine and autocrine signalling requires close cell to cell contact, while paracrine signalling can occur over short distances and intracrine signalling occurs within a cell. Epidermal growth factor (EGF) acts in an autocrine manner, while keratinocyte growth factor is thought to act in a paracrine manner. This means they signal between members of the same cell type by binding to receptors on the surface of these cells (autocrine) (EMBL-EBI 2013) or the cell releases the signal to affect nearby cells (paracrine). How these different types of signalling work together and cross-talk is important for understanding cell signalling networks. These ligands, e.g. EGF, as mentioned previously, bind to specific receptors and this triggers a signalling cascade to control many processes within a cell. This includes changes in size and shape or transcriptional activity (Millar 2005).

Transgenic and knockout mouse models can be used to understand the roles of these growth factors and pathways in development, as described in sections 3.1.1. While useful to a certain degree, these can impact other tissues and organogenesis across the body so there is a need to look at different methods to isolate the study to their effects on the skin (dermal fat in particular). As the dermal adipose (fat) layer has only recently been recognised as distinct from the subcutaneous adipose layer beneath the skin and also of separate developmental origin, it could be thought that these signalling pathways may be acting differently from those already studied.

Most fundamental cellular signalling pathways have an effect on adipogenesis with several of them having both positive and negative controls. Many different signalling pathways have been shown to influence adipogenesis *in vitro*, e.g. EGF/EGFR and Wnt pathways, but their effects i*n vivo* are not as well known. Highly conserved signalling pathways including BMP, EGF/EGFR and more recently KGF/KGFR have been implicated as some of the important signalling pathways in hair follicle morphogenesis (Richardson *et al*. 2009) and more recently for their association with adipocytes and potential role in adipogenesis in the dermis of the skin. Activation and inhibition of these pathways at certain times and in certain locations is key to the successful development adipocytes and the committed precursor cells. A network of transcription factors and events involved in the signalling cascade can be seen expressed in microarrays. These can all interact to create a balance of activating and inhibitory effects, of which is largely unknown. A link has been suggested between hair follicle and adipose tissue development, thus further implicating these pathways in adipogenesis (Festa *et al.* 2011). The exact roles and effects these pathways play in adipogenic development is largely unknown (Gesta *et al.* 2007). The aim is to improve our understanding of the roles these signalling pathways have on adipogenesis. It is important to note that while these three pathways are looked at in more detail there are other pathways and signals implicated in adipogenesis, e.g. Wnt, Notch, Hedgehog and other FGF pathways other than FGF-7/KGF (Zehentner *et al.* 2000; Rosen and MacDougald 2006).

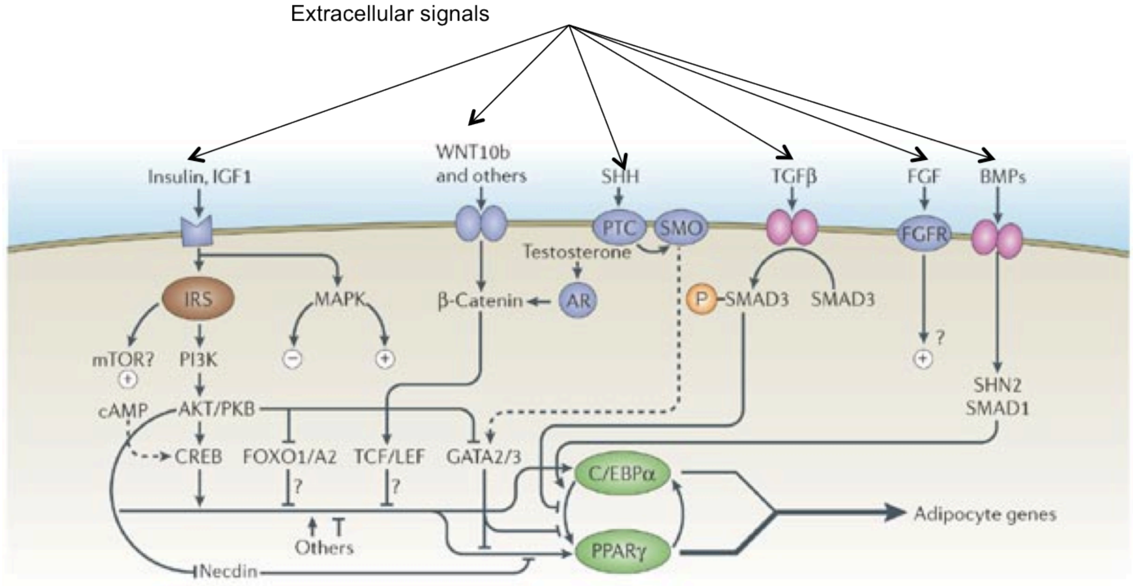

Copyright © 2006 Nature Publishing Group
Nature Reviews | Molecular Cell Biology

<u>Figure 5.1:</u> Extracellular activators and inhibitors regulate adipogenesis. Many factors influence adipogenesis and induce signalling pathways. KGF is a more recent extracellular signal. Adapted from Rosen and MacDougald (2006).

5.1.1. The EGF/EGFR Signalling Pathway

Epidermal growth factor (EGF) is a member of the epidermal growth factor superfamily. This is a growth factor involved in growth, proliferation and differentiation of many different cell types. It acts as a ligand to the epidermal growth factor receptor (EGFR), which signals to the nucleus through a signalling cascade. EGFRs (EGFR/ErbB1, HER2/ErbB2, Her3/ErbB3 and HER4/Erb4) are a family of transmembrane receptors and are important in regulating cell behaviour, e.g. proliferation and differentiation (Huang *et al.* 1999; Massutí 2003; Sugawara *et al.* 2010). These receptors have an extracellular ligand-binding domain and a cytoplasmic domain with tyrosine-kinase activity. EGFR can be received by several activating ligands including EGF, TGFα, heparin-binding EGF (HBEGF), betacellulin and amphiregulin (Massagué and Pandiella 1993; Yamanishi 1998). It is expressed in basal keratinocytes, sebocytes, outer root sheath (ORS) cells and in the dermal ducts of eccrine sweat glands (Nanney *et al.* 1986; Yamanishi 1998).

The signalling pathway involves these ligands inducing dimerization and autophosphorylation of the receptors. Homodimers (with EGFR) or heterodimers (with ERBB2,3 or 4) form (Massutí 2003; Sugawara *et al.* 2010). Phosphorylated tyrosine residues become the binding sites for Src-homology 2 (SH2) parts of Grb-2, Shc proteins and phospholipase C-g which lead to downstream signalling cascades and a number of cellular responses (Yamanishi 1998; Yarden *et al.* 2007; Sugawara *et al.* 2010). The downstream modification of enzymes, adaptor proteins, second messengers and transcription factors involved in this signalling cascade can induce a number of different signal transduction cascades including Ras-Raf-MEK-MAPK and PI3-kinase.

Many pathways cross-talk to each other, e.g. the EGF/EGFR pathway with the MAP kinase pathway. MAP kinase is activated by EGF and also insulin through Ras (Suga *et al*. 1997). In EGF signalling, the EGF receptor binds to growth factor receptor-bound protein 2 (Grb-2)/son of sevenless (Sos) to activate Ras. Alternatively EGF and insulin phosphorylate Shc forming Shc/Grb-2/Sos complex, which activates Ras. As well as MAP kinase, Raf-1 kinases and MEKs are activated. Not only does the MAP kinase interact with the EGF signalling cascade, but also phosphatidylinositol 3 (PI3)-kinase binds to Ras (Rodriguez-Viciana *et al.* 1994; Suga *et al.* 1997) and can consequently activate Raf-1 kinase. In EGF signalling, Cbl and ErbB3 proteins recruit PI3-kinase to the EGF receptor and are phosphorylated and thus become docking proteins between EGFR and PI3-kinase. (Soltoff *et al.* 1994; Fukazawa *et al.* 1996; Suga *et al.* 1997).

This pathway is fundamental to the correct development of hair and skin (Sugawara *et al.* 2010). The ligands that bind to EGFR have been found to inhibit developing hair follicles but the mechanisms by which this occurs are largely unknown (Richardson *et al.* 2009). A number of mouse models have been created to understand the role of EGFR in the skin. EGF plays an important role in control of adipocyte differentiation (Serrero and Mills 1991). Waved-2, which has a mutated *Egfr* gene has wavy hairs and curled whiskers (Keeler 1935; Sugawara *et al.* 2010). However, these mice only show a mild abnormal phenotype, but targeted gene disruption results in mortality either embryonically or post-natally with the latest survival being approximately three weeks (Sugawara *et al.* 2010). Premature hair follicle differentiation, epidermal atrophy and decreased keratinocyte proliferation is exhibited by these mice (Threadgill *et al.* 1995; Sugawara *et al*. 2010). EGFR is also thought to be involved in the inflammatory response as demonstrated by replacing *Egfr* with the human EGFR cDNA as the hair follicles experience inflammation and degrade over time (Sibilia *et al.* 2003; Sugawara *et al.* 2010). Waved-5 mice (Lee *et al.* 2004), also named Velvet (Du *et al.* 2004) with the *Egfrwa5* allele that codes for a dominant negative receptor, show a heterozygous phenotype unlike Waved-2 mice. These mice have defective wavy hairs and curled whiskers as does the mutant Dsk5 mouse, which also has a thickened epidermis (Fitch *et al.* 2003; Sugawara *et al.* 2010).

EGFR knockout mice have been created from a number of different mouse strains, while some of these are lethal, e.g. CF-1; others survive but with a thin stratified epithelium and reduced numbers of disorientated follicles (Yamanishi 1998). In these mice, the appearance of irregular epithelial tissues is not limited to the skin but can also be found in other organs and tissues including the lung. EGFR knockout mice died early on and so effective studies are limited. Disrupting the EGF receptor has resulted in malfunctions during late follicle development, which would suggest that EGF signalling has a positive influence on hair follicle formation (Murillas *et al.* 1995; Richardson *et al.* 2009). It also had no adipocytes between the hair follicles (Murillas et al. 1995). In contrast others suggest it has a negative effect; Hair follicle formation is inhibited in terms of both timing and dose when supplied with EGFR ligands (HBEGF and amphiregulin), but epidermal differentiation does occur as shown by analysis of downstream molecular markers and microarray profiling (Kashiwagi *et al.* 1997; Richardson *et al.* 2009). It can therefore be suggested that when investigating this pathway the timings at which it is studied are crucial to the role it plays.

Microarray analysis has shown epidermal growth factor receptor (EGFR) to be upregulated in the lower dermis of embryonic mouse skin, which provoked interest in its role in adipogenesis (Wojciechowicz 2012). It was found that EGFR presented opposite effects during the process of adipocyte development, i.e. if the cells were differentiated EGF promoted this, whereas if the cells were not yet committed, adipocyte differentiation was inhibited (Wojciechowicz, 2012). This receptor interacts with EGF and has been found to play a role in adipogenesis *in vitro* (Adachi *et al.* 1994; Wojciechowicz 2012) though the point during development at which EGF is supplied is important.

Wojciechowicz (2012) developed an organ culture model as described in Chapter 4 in which to study the effects of this pathway on adipocyte development. Skin in culture was supplied with an EGF activator or inhibitor. Embryonic day 15/15.5 skin did not show any adipocytes while by e16-17 those supplied with the activator showed adipocyte staining. By e18/19 adipocytes were clearly visible, particular in the lower dermis and surrounding the hair follicles. Their development was not impeded by the presence of an inhibitor. This shows that the timing of the activation of the pathway is crucial to localised development of fat and the commitment of the precursor cells. This model was repeated in the current study prior to experimenting with the cell culture model, the development of which is described in chapter 4. From this previous work, it can be hypothesised that EGF induces adipocyte development, but does not have an effect on cell commitment. EGF is also not the only activating ligand of EGFR. It is therefore important when looking at the pathway to inhibit the receptor rather that purely the growth factor. An EGF inhibitor (AG1478) was used to contrast the effects of EGF.

5.1.2. The TGFβ/BMP Signalling Pathway

Within the transforming growth factor-β (TGFβ) superfamily, one of the largest families of signalling molecules, are grouped the bone morphogenetic proteins (BMPs), whose functions are more diverse than this name suggests (Massagué and Chen 2000; Gesta *et al.* 2007). They are known not only for their involvement in bone formation but also for being multifunctional through vertebrate development, involved in cell proliferation, differentiation and also apoptosis throughout the body, including the skin (Hogan 1996; Botchkarev 2003). BMP signalling receptors are transmembrane serine-threonine kinases of which two types exhibit, I and II (Massagué and Weis-Garcia 1996; Hogan 1996; Botchkarev 2003). Individually these receptors have a low affinity for BMP but in a heterotetrameric complex of types I (BMPR-IA and BMPR-IB) and II (BMPR-II), BMP dimers can bind with high affinity (Botchkarev 2003). The type I receptor is transphosphorylated by the type II kinase at the GS box region of the cytoplasmic domain. In mammalian cells *in vitro*, one BMP can recognise several type II receptors and therefore phosphorylate different type I receptors, which then causes a downstream signalling cascades (Hogan 1996).

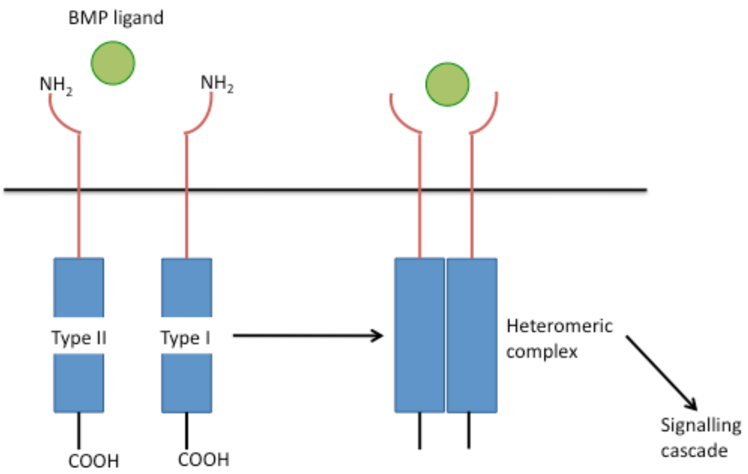

<u>Figure 5.2:</u> The BMP receptor. Type I and type II serine threonine kinase receptors form a heteromeric complex. Based on Hogan 1996 (adapted from Massagué and Weis-Garcia 1996).

Characterization of downstream signalling of BMP is limited; though *Drosophila* are thought to have similar signalling cascades and has been used for much of the research into this pathway. BMPR-IA also known as activin-like kinase-3 (ALK-3) and has been found to induce adipocyte differentiation whereas BMPR-IB induces osteogenesis. It is therefore important to clarify which aspects are experimented with, as the BMP pathway can have both positive and negative influences on adipocyte development. The BMP pathway is particularly complex because opposing effects have been found in almost every situation.

The BMP signalling pathway can occur and be regulated at many different levels from the cell surface, to the cytoplasm and in the nucleus. The pathway mechanisms can be "canonical" which is SMAD-dependent or "noncanonical", SMAD-independent (Botchkarev 2003; Rosen and MacDougald 2006). In the "canonical" pathway, the binding of BMP to the receptor complex is regulated by SMADS. Smad1, Smad5 and Smad 8 are phosphorylated by BMPR-I kinases, which cause complexes to form with Smad4. These heteromeric complexes are then translocated to the nucleus to induce transcription of target genes (Botchkarev 2003; Rosen and MacDougald 2006). This pathway is somewhat more complex with some Smads inhibiting this process, e.g. Smad 6 and Smad 7 and the involvement of other regulatory proteins e.g. AMSH and Smurf1 (Zhu *et al.* 1999; Botchkarev 2003). The effects of BMP binding are further regulated in the nucleus where the binding of cofactors to the Smad complex can have positive or negative effects on the target genes (Botchkarev 2003). The "noncanonical" pathway involves binding to BMPR-IA and then joining with BMPR-II with subsequent activation of the mitogen-activated protein (MAP)-kinase pathway (Nohe *et al.* 2002; Botchkarev 2003). Once activated, the receptor complex interacts with intracellular adaptor protein XIAP. This triggers the binding of TAK1 binding protein (TAB1) leading to the activation of the MAPK family member, TGFβ activated kinase 1 (TAKI) (Yamaguchi *et al.* 1999).

While it is well known that BMPs are involved in body patterning, including neural patterning, it has also been shown that they are involved in other aspects of development. Evidence has been found that BMPs can induce both proliferation and differentiation for different cell types. It may therefore be that BMPs can cause different effects in different cell types and depending on the concentrations the cells are exposed to (Hogan 1996). Not only can the function of BMPS differ in relation to their concentration, but also in relation to the type of mesenchymal cell and what other regulatory factors are present (Rosen and MacDougald 2006).

Members of the TGFβ family, including BMPs, have been found to have an influence on adipogenesis and be involved in differentiation of adipocytes (Zamani and Brown 2011; Siersbæk *et al.* 2012)). TGFβ and elements of its signalling pathway are expressed in cultured adipocytes, but it has previously been shown to inhibit differentiation *in vitro* pre-adipocytes and transgenic overexpression of TGFβ causes adipose development to fail (Rahimi *et al.* 1998; Rosen and MacDougald 2006). Conversely blocking TGFβ, by using dominant-negative TGFβ receptor expression or SMAD inhibition, causes increased adipocyte development (Choy *et al.* 2003; Rosen and MacDougald 2006). Commitment to the adipocytes lineage of mesenchymal cells has been found to involve BMP4 (Tang *et al.* 2004). BMP2 is also thought to influence adipogenesis but requires other signalling molecules e.g. TGFβ to interact and acts in a concentration-dependent manner. For example, at low concentrations it can stimulate cells *in vitro* to undergo adipogenesis (zur Nieden *et al.* 2005), while at higher concentrations osteogenesis and chondrogenesis is more likely to occur (Wang *et al.* 1993; Rosen and MacDougald 2006). BMP2 was also found to inhibit adipogenesis when supplemented with retinoic acid in the 3T3-F442A cell line. The consensus could be that the presence of BMP2 is to direct cells away from the adipocytes lineage, but it cannot act alone. As well as BMP2, BMP7 has been found to direct cells away from the adipogenic lineage and down the osteogenic lineage from MSCs, though this is concentration-dependent (Gesta *et al.* 2007). The cells experimented with however, are *in vitro* cell lines, therefore it is of interest to see what occurs *in vivo* mesenchymal cells. Some knockout mouse models i*n vivo* die prior to adipocyte development limiting *in vivo* studies. For example, BMP4 knockout mice die early in embryogenesis because of defects in gastrulation and the mesoderm (Winnier *et al.* 1995). The Schnurri2-2 (SHN2) gene downstream of BMP2 has however been found to interact with PPARγ and C/EBPα expression and is necessary for adipogenesis *in vivo* as well as *in vitro* (Jin *et al.* 2006; Gesta *et al.* 2007). SHN2 is translocated to the nucleus upon induction by BMP2 and joins the SMAD proteins SMAD1, SMAD4 as wells as CEBPα on the PPARγ2 promoter (Jin *et al.* 2006; Rosen and MacDougald 2006).

BMP antagonists e.g. noggin or follistatin regulate the pathway by binding to BMPs with a higher affinity that the receptors (Botchkarev 2003). Smad6 and Smad7 are also antagonists because they prevent Smad1, Smad5 and Smad8 from being phosphorylated (Botchkarev 2003). Therefore, looking at the effects of inhibiting BMP is important, because BMP may in reality in this situation be being blocked during certain stages of adipogenesis. Looking at both the effects of BMP and an inhibitor of BMP can therefore give a better understanding of what might be happening in the dermis in relation to the BMP pathway at this point in development. In this project an inhibitor of BMPR1A, also referred to as DMH1 is used to do so.

BMPs, BMP antagonists, BMP receptors and Smad proteins work together to produce spatio-temporal patterns of expression to regulate development throughout the body, including in the skin epithelium and mesenchyme (Botchkarev and Sharov 2004). As well as this, similarly to the EGF/EGFR pathway, the BMP pathway interacts with a number of different pathways to create the overall regulatory and developmental effects. For example, EDA and its receptor EDAR as part of the Wnt pathway are crucial to hair follicle morphogenesis and interact with BMP to determine patterning of the follicles (Richardson et al. 2009).

BMP signalling has been found crucial to many stages of development of the skin epidermis and hair follicle formation. At induction of the hair follicles, BMP-2 and BMPR-IA are expressed at the placode, and BMP-4 and noggin are expressed on the mesenchymal condensation cells. Noggin-knockout mice lack all secondary follicles, while overexpressing Noggin increased the density of follicles (Botchkarev *et al.* 1999; Botchkarev and Sharov 2004). In general BMP-2 has been found to be expressed more in the epithelium while BMP-4 is expressed more prominently in the mesenchyme, which works in conjunction with EGF to control hair follicle development. In this project, BMP-4 is the chosen BMP for its implication in adipogenesis (Rosen and MacDougald 2006). Mice that lack BMP2 or BMP4 die prior to adipocyte development, therefore *in vivo* studies have been limited.

5.1.3. The KGF/KGFR Signalling Pathway

Keratinocyte growth factor (KGF) is part of the fibroblast growth factor (FGF) family and is also known as fibroblast growth factor 7 (FGF7) (Finch *et al.* 1989; Aaronson *et al.* 1991; Guo *et al.* 1993; Guo *et al.* 1996). KGF is a 194 amino acid protein and is capable of secretion by encompassing a signal peptide (Finch *et al.* 1989; Rubin *et al.* 1995). FGFs control a number of cellular responses, critically by regulating cell proliferation, differentiation and migration in embryogenesis, though they are also involved in control in the adult organism (Eswarakumar *et al.* 2005). It is produced by stromal fibroblasts, though its mitogenic activity is on keratinocytes in the skin (Guo *et al.* 1993; Rubin *et al.* 1995; Guo *et al.* 1996). It has, therefore, been suggested that it might mediate mesenchymal-epithelial communication (Rubin *et al.* 1995).

Fibroblast growth factor receptors, FGFRs are tyrosine kinase receptors (RTKs), which have an extracellular ligand-binding domain with immunoglobulin-like (Ig) domains, a transmembrane domain and a cytoplasmic domain, which contains a catalytic protein tyrosine kinase core and regulatory sequences (Hunter 2000; Eswarakumar *et al.* 2005). Isoforms have been isolated from both mouse and human cells with three Ig loops though originally thought to only have two and bind KGF with the same affinity (Miki *et al.* 1992; Rubin *et al.* 1995). FGFR isoforms are formed by alternative splicing. KGF (FGF7) is received by an alternatively spliced variant of FGFR2 (Peters *et al.* 1992; Johnson and Williams 1993; Guo *et al.* 1996). This is created by alternative splicing in the third Ig-like domain of the extracellular domain called D3. This alters the ligand-binding, thus specifically FGFR2b binds FGF7 as well as FGF10 (Eswarakumar *et al.* 2005). By creating molecules with different combinations of the second and third Ig loops it was found that the third Ig loop is responsible for the majority of KGF's affinity for KGFR (Cheon *et al.* 1994; Rubin *et al.* 1995) FGFR2b is also referred to as KGFR and is only expressed in epithelial cells (Guo *et al.* 1993).

KGF/KGFR pathway is a paracrine pathway. KGFR binds both KGF and aFGF (Rubin *et al.* 1995). These signalling molecules bind to the receptor's tyrosine auto-phosphorylation sites and the associated docking proteins (FRS2α and FRS2β) become tyrosine phosphorylated and induce the formation of other complexes with additional signalling proteins, Gab1 and the effector proteins, Grb2/Sos complexes and Shp2. Shp2 is phosphorylated in response to FGF stimulation and also complexes with Grb2 molecules. This leads to activation of MAP kinase, PI-3 kinase, chemotaxis and cell proliferation. This was found by isolating fibroblasts from FRS2α-/- embryos (Hadari *et al.* 2001; Eswarakumar *et al.* 2005).

A number of procedures and mouse models have been used to determine the roles of KGF. Homologous recombination shows that alongside other FGFs, KGF is fundamental to the majority of mouse development stages and organogenesis (Eswarakumar *et al.* 2005). Targeted disruption of FGF7 results in hair follicle and kidney deficiency (Guo *et al.* 1996; Eswarakumar *et al.* 2005). When transgenic mice are created with KGF expression targeted to the basal epidermal layer, controlled by the human K14 promoter, the function is altered from paracrine to autocrine and epidermal thickening and proliferation occurs (Guo *et al.* 1993). Not only this, but there is noticeable suppression of both hair follicles and adipogenesis (Guo *et al.* 1993). Even very low levels of KGF blocked fat formation, which suggested that adipose tissue is particularly sensitive to KGF. These mice are very frail and as adults exhibit hypersalivation with abnormal differentiation of the salivary glands (Guo *et al.* 1993; Yamanishi 1998).

Guo *et al.* (1996) used embryonic stem cell technology to knockout KGF. This resulted in defects in the hair shaft, making the fur appear matted due to KGF influencing the matrix cells. Epidermal growth and morphology appear normal, as does the wound healing response. Contrastingly, when KGFR is truncated, wound healing cannot occur correctly (Werner *et al.* 1994), which would suggest KGF is important for wound healing or perhaps the receptors can be influenced by other factors/ligands other than KGF (e.g. aFGF) (Guo *et al*. 1993).

Richardson *et al.* (2009) also show that KGF can inhibit hair follicle formation in a time and dose-dependent manner but epidermal differentiation does occur. Mouse model work has also shown that when the FGFR2(IIIb) receptor is inhibited, hair follicle density decreases and development is negatively impacted (Petiot *et al.* 2003; Richardson *et al.* 2009). Over expression of FGFR2 dominant negative also inhibits hair follicle formation (Werner *et al.* 1994), while over expression of KGF in the epidermis inhibits follicle development (Guo *et al.* 1993).

While it is known to be important in epidermal growth and regeneration, its role in adipose tissue is not as well known. Adipogenesis can be described as preadipocyte proliferation and differentiation and is fundamental to adipose tissue growth, which can lead to obesity. KGF has been found upregulated in rat models subjected to maternal protein restriction (MPR), where foetal nutrition has been limited and so overcompensation occurs (Zhang *et al*. 2010). Individuals subjected to MPR exhibit increased adipose tissue growth and obesity risk, which may correlate with the upregulation of KGF. Zhang *et al.* (2010) used *in vitro* models e.g. 3T3-L1 and rat primary preadipocytes to look at the role of KGF in adipogenesis. KGF was found to stimulate preadipocyte proliferation in an autocrine fashion controlled by the PI3 kinase signalling pathway. This was demonstrated by the activation of the PI3 kinase downstream target, protein kinase Akt (Zhang *et al.* 2010). While proliferation is stimulated, differentiation of adipocytes is not: as shown by no change in lipid accumulation or expression levels of adipocyte markers, aP2 and PPARγ. This differs from the paracrine role of KGF in the epidermis (Finch and Rubin 2004). Having shown the importance of KGF in adipogenesis *in vitro*, there is now a need to reliably test its role *in vivo*. (Zhang *et al.* 2010). KGF has therefore been shown to be able to affect differentiation and development and not just proliferation and is necessary for mesenchymal-epithelial interactions (Yamanashi 1998). It is involved in the development of a number of organs including the skin, lungs, kidneys and salivary glands (Rubin *et al.* 1995; Yamanishi 1998). KGF is known for stimulating keratinocyte proliferation but more recently has been found to be involved in preadipocyte proliferation (Zhang *et al.* 2010). This activity is stronger than EGF *in vitro* (Yamanishi 1998). The effect on mesenchymal tissues including adipose tissue may be mediated through the effects KGF has on the epidermis and hair follicles as an indirect effect. Can KGF actually have a direct influence on dermal cells or is it mediated through signals from the epidermis?

The role of the KGFR pathway in epidermal growth and wound healing as well as associated processes including hair follicle formation and adipogenesis is largely unknown. While more is known in relation to the epidermis, the fact that the FGFR2 receptor is expressed at the point at which epidermal-mesenchymal interactions may be influencing development (Peters *et al.* 1992; Guo *et al.* 1993) suggests that KGF may have a wider impact on a number of cell types and tissues, including dermal tissues. There is, therefore, a need for ways of investigating the influences this pathway has and this is one reason KGF and its respective pathway may be a suitable candidate to study to further our understanding of adipogenesis, particularly in the skin.

While there is currently limited evidence on the importance KGF might be having on adipogenesis in the skin, there was however an experiment conducted in Jahoda's lab, which prompted further analysis to be done with respect to it. Here immunofluorescence showed that there was positive labelling of KGF in the lower dermis in relation to the H&E stained skin. It was just above the muscle layer, as early as embryonic day 13. This would suggest that KGF may be more important than originally thought, thus not just involved in keratinocyte development but also in the dermis, in particular the lower dermis where adipocyte development is taking place.

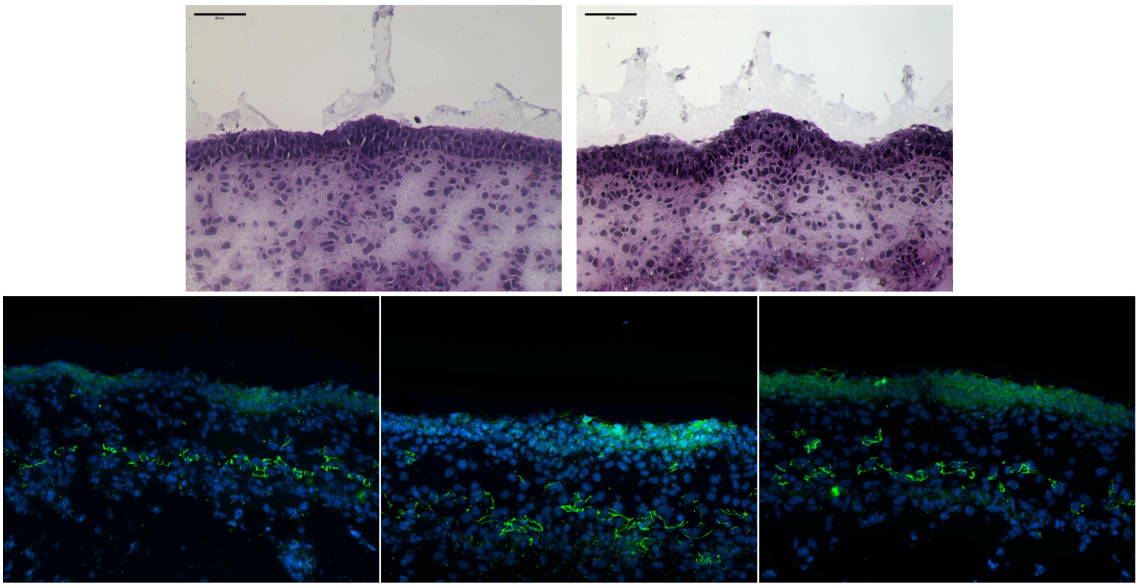

Figure 5.3: KGF expression in the lower dermis at e13. H&E staining of the skin at embryonic day 13 and immunofluorescence labelling of KGF. Images taken from an experiment conducted in Jahoda C.A.B.'s research group (Richardson and Jahoda, accessed August 2013).

5.1.4. Aims of the Chapter

Prior to Wojciechowicz's work there was no evidence of an *in vivo* experiment to look at the EGF-EGFR signalling pathways' involvement in differentiation in the lower dermis during late mouse embryonic development. Her results act as a control in terms of how the models respond to this pathway. Both the organ culture model that was previously used, and a novel cell culture model were used to look at this pathway. The aim of these models is to act in a manner, which closely resembles that *found in vivo*. An inhibitor and an activator of EGFR were used and the accumulation of lipids in the cells was examined using Oil Red O staining. This cell culture technique was then used to test the roles of two other pathways in adipogenesis: the TGFβ/BMP and KGF/KGFR pathways.

5.2. Materials and Methods

First, the organ culture model, which was previously used by Wojciechowicz (2012) and experimented with as described in section 4.2 was applied to look at the EGF/EGFR pathway. Four to five pieces of skin were placed on collagen filters in each 35mm dish. To investigate this pathway, the media was supplemented with an activator of EGFR or an inhibitor. EGF/amphiregulin or InSolution^{TM} AG1478 (Calbiochem) respectively (Appendix III). Table 5.1 shows the concentrations used. A control dish was set up alongside with normal 1% FBS/MEM. This experiment was repeated 4 times.

Due to time constraints, since the organ culture model was deemed unreliable, due to the lack of consistency shown between repeats, it was not used to investigate the other pathways. However, the 2D/3D cell culture model described in section 4.2 was used to investigate all three pathways; EGF/EGFR, BMP and KGF/KGFR.

Sets of 2-dimensional cultures in 6-well plates were set up alongside plates of 3-dimensional spheres. One was supplemented with an activator (EGF, BMP4 or KGF), one with the inhibitor (AG1478 or DMH1) and one acted as control with 10% FBS-MEM (Appendix III). No KGF inhibitor was used. Controls containing 100ng/ml of DMSO were also established, as this was the maximum concentration, which the growth factors had been dissolved in. 6000 cell spheres were made in 10ul drops. For each experiment, an extra dish of spheres with much higher cell numbers was made from the original 1ml cell suspension. This was conducted on embryos from day 16.5 and at least two repeats were made for each pathway.

After pilot experimentation it was decided not to disturb the cells and therefore not change the media during the culture period. After 5 days, 4 spheres were put into each well of a 6 well plate, suspended in 200ul of 10%FBS/MEM, for each activator and inhibitor. After a further two days, images were taken and the cells were then fixed in calcium formal for 10 minutes and stored in PBS at 4ºC prior to oil red O analysis. This was conducted on both the 2D cultures, 3D spheres put into 2D and the 3D spheres frozen in OCT as described in section 4.2.4.

Table 5.1. The concentrations of the activation and inhibition factors used to test each pathway.

Factor	Concentration		
EGF/EGFR Pathway			
EGF^{+}	100ng/ml		
Amphiregulin^{+}	1ug/ml		
AG1478^{-}	50uM		
BMP Pathway			
BMP4^{+}	1ng/ml	10ng/ml	100ng/ml
DMH1^{-}	19ng/ml	190ng/ml	1.9ug/ml
KGF/KGFR Pathway			
KGF^{+}	1ng/ml	10ng/ml	100ng/ml

*All factors were added to the 10% FBS-MEM with antibiotics before the required cell densities were added.

$^{+}$ Activation; $^{-}$ Inhibition

5.2.1. Oil Red O Quantification

The oil red O quantifying method, described in chapter 4.2 was used to quantify the volume of lipids and therefore adipocytes by measuring the level of red coloration present. E16.5 mouse back skin dermal cells cultured in 2D and in 3D spheres that were then transferred to 2D culture were investigated. Both the EGF/EGFR pathway and TGFβ/BMP pathways were quantified.

5.2.2. EDU Treatment of KGF Spheres

In addition to the model established with cells from e16.5 skin, spheres were set up from e14.5 dermal cells and treated with 10ng/ml or 100ng/ml of recombinant KGF. After three days, the spheres had aggregated and were pulsed with EDU (Click-IT® EDU Imaging Kit: Invitrogen, Oregon, USA) for four hours to look at rates of proliferation. To do this, new drops of 10% FBS/MEM with 2.5μg/ml of EDU were created and the each sphere was transferred to a new drop. Only the spheres treated with 10ng/ml of KGF had aggregated so only these were given EDU. Alongside this, as a control, untreated spheres of the same age were also pulsed with EDU. After 4 hours, the spheres were snap frozen in liquid nitrogen and stored at -80ºC prior to staining.

Immunofluorescence analysis of the EDU was then carried out on the spheres. Sections were cut at 7μm and adhered to ColorFrost slides. These were left to dry for 1 hour 30 minutes before being fixed in 4% PFA for 15 minutes. After rinsing in 1x PBS the slides were permeabilised in 0.1% Triton X for a further 15 minutes and then washed for 5 minutes in PBS. The slides were then incubated in an EDU reaction cocktail (Appendix III) for 30 minutes at room temperature in the dark. Three PBS washes for 5 minutes were then followed by mounting the slides in Mowiol with DAPI. Slides were kept in the dark at 4°C prior to images being taken on the Zeiss Imager, M1.

5.3. Results

5.3.1 EGF/EGFR Pathway

5.3.1.1. Organ Culture Model

Firstly, the organ culture model system was replicated. Chapter 4 demonstrates that it was tried with both MEM and William's media and 1%, 2% or no serum and still no reliably consistent results were produced. Section 4.2.1 shows the different controls produced for this. While this was the case, in the early stages of developing the model, skin was also supplemented with the EGF activator, amphiregulin or inhibitor, AG1478) to show whether the results found were consistent with those published by Wojciechowicz (2012) in Jahoda's lab. There was variability in the skin pieces cultured in 1% FBS/MEM as a control and how they developed in organ culture (Figure 5.4), which limited the reliability of that seen with the inhibitor (EGF-) and activator (EGF+). For example, EGF+ (Figure 5.5) and the controls (Figure 5.4) were darker in coloration compared with EGF- (Figure 5.6).

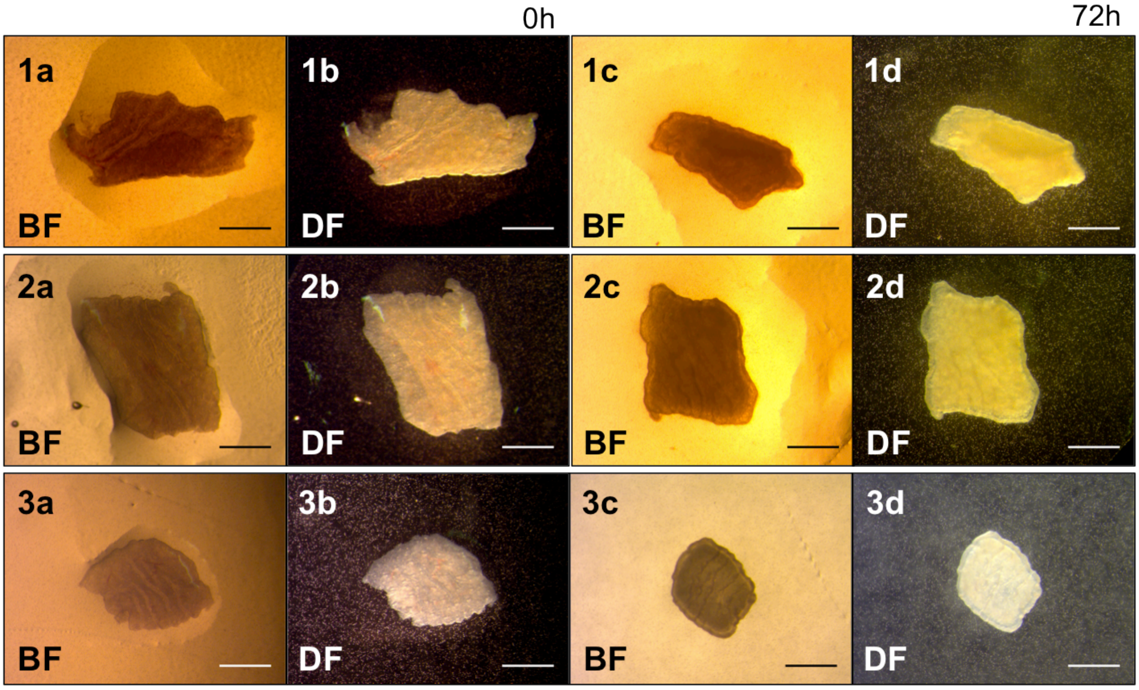

<u>Figure 5.4:</u> Organ culture of 16.5 embryonic day mouse back skin in 1% FBS/MEM. Three separate skin pieces are shown (1,2,3) both before (a,b) and after incubation for 3 days (c,d). Images were taken using a Zeiss Axiovert 10 microscope. BF = bright field. DF = dark field. Scale bar = 1mm.

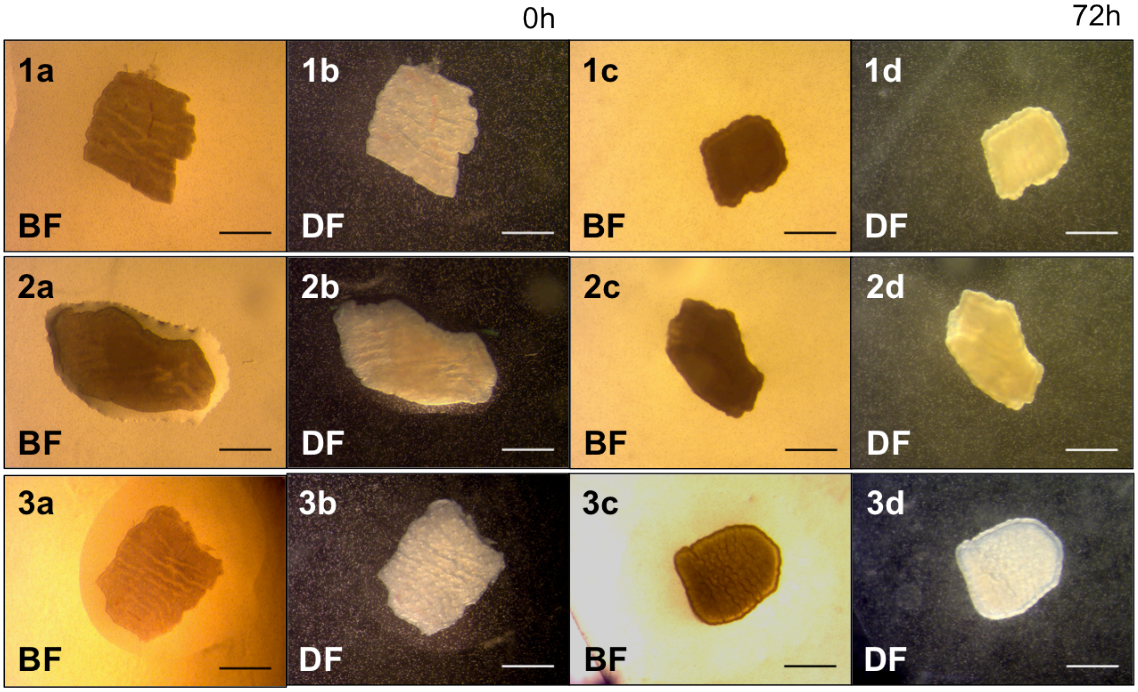

Figure 5.5: Organ culture of 16.5 embryonic day mouse back skin in 1% FBS/MEM supplemented with the EGF activator (EGF+). Three separate skin pieces are shown (1,2,3) both before (a,b) and after incubation for 3 days (c,d). Images were taken using a Zeiss Axiovert 10 microscope. BF = bright field. DF = dark field. Scale bar = 1mm.

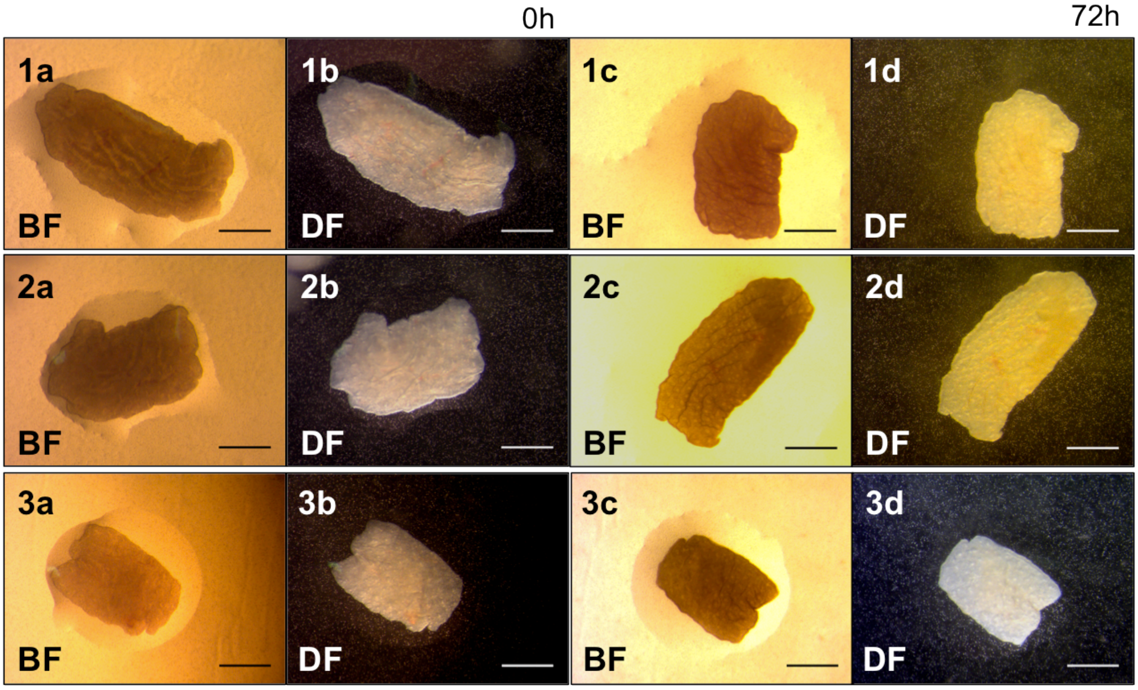

Figure 5.6: Organ culture of 16.5 embryonic day mouse back skin in 1% FBS/MEM supplemented with the EGF inhibitor (EGF-). Three separate skin pieces are shown (1,2,3) both before (a,b) and after incubation for 3 days (c,d). Images were taken using a Zeiss Axiovert 10 microscope. BF = bright field. DF = dark field. Scale bar = 1mm.

The skin pieces treated with EGF- exhibited significant follicle bumps and no clear ridge round the edge of the skin after 3 days incubation (Figure 5.6c,d), compared with the skin treated with EGF+. EGF may play a role in the wound healing response as well. The control pieces (Figure 5.4) and those supplemented with the EGF activator (Figure 5.5) had defined ridges around the edge of the skin pieces.

H&E and toluidine blue staining was conducted on the sections cut from the incubated skin pieces, represented in figures 5.7 and 5.8. Control results produced from the same experiment were analysed in chapter 4 (Figure 4.13). EGF+ and EGF- culture was set up alongside to attempt to replicate the method (Wojciechowicz 2012). While some follicular development occurred with EGF+ (Figure 5.7), they were not as well developed as those in the skin treated with the inhibitor (Figure 5.8).

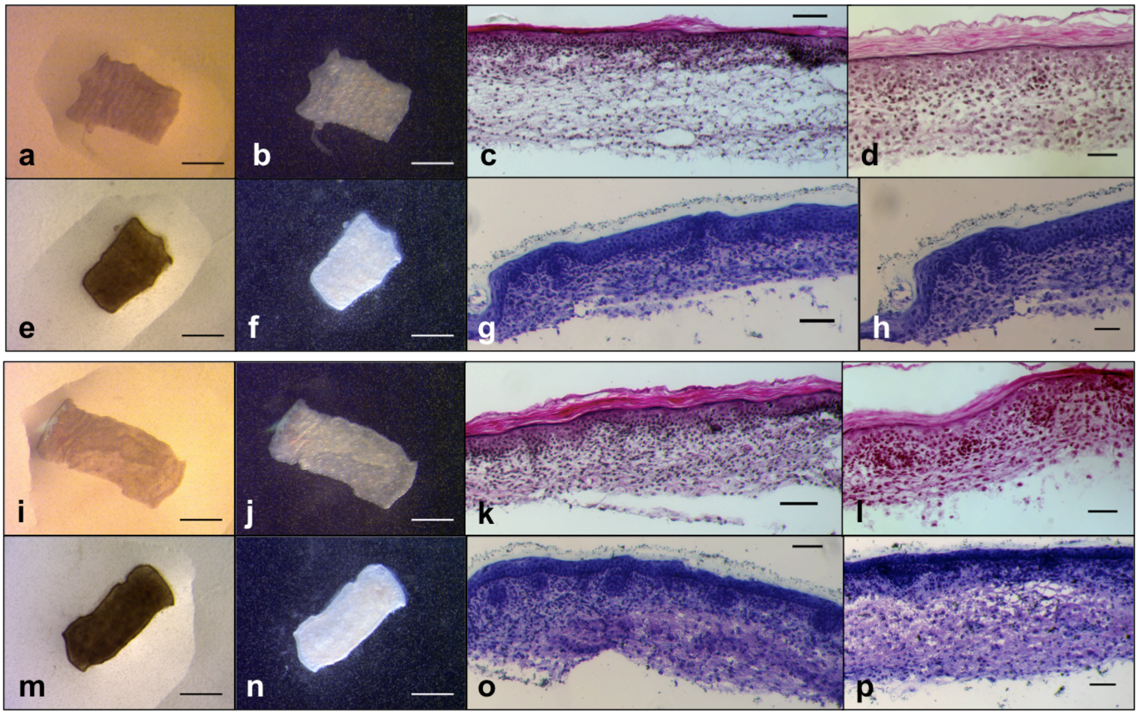

Figure 5.7: 16.5 embryonic day organ cultured skin in 1% FBS/MEM supplemented with the EGF activator (EGF+). (**a-h**) piece 1. (**i-p**) piece 2. (**a,e,i,m**) bright field and (**b,f,j,n**) dark field, taken on Zeiss Axiovert 10. (**c-h** and **k-p**) after 72 hours in culture. (**c,d,k,l**) H&E staining and (**g,h,o,p**) toluidine blue staining, images were taken using a Zeiss Axio Imager M1. (**a,b,e,f,I,j,m,n**) scale bar = 1mm. (**c,g,k**) scale bar = 65μm. (**d,h,l,o,p**) scale bar = 40μm.

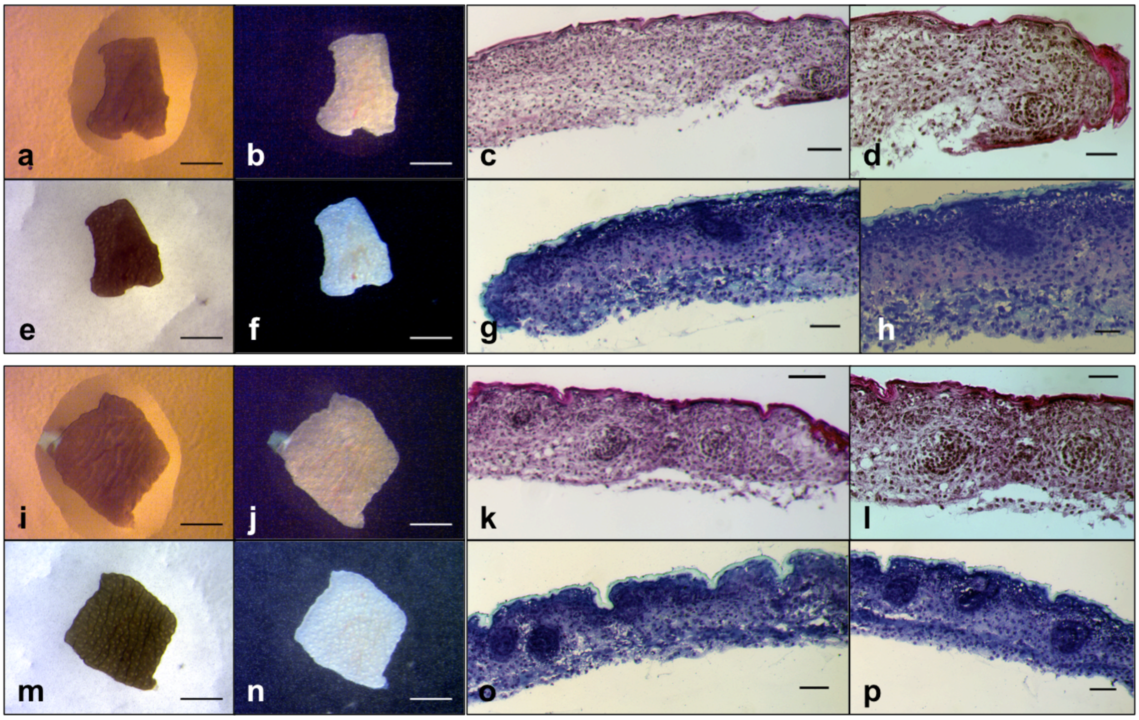

Figure 5.8: 16.5 embryonic day organ cultured skin in 1% FBS/MEM supplemented with the EGF inhibitor (EGF-). (**a-h**) piece 1. (**i-p**) piece 2. (**a,e,i,m**) bright field and (**b,f,j,n**) dark field taken on Zeiss Axiovert 10. (**c-h** and **k-p**) after 72 hours in culture. (**c,d,k,l**) H&E staining and (**g,h,o,p**) toluidine blue staining, images were taken using a Zeiss Axio Imager M1. (**a,b,e,f,I,j,m,n**) scale bar = 1mm. (**c,g,k,o,p**) scale bar = 65µm. (**d,h,l**) scale bar = 40µm.

This experiment was repeated twice more with the EGF+ and EGF- variables. Sections cut from the cultured skin pieces under all 3 conditions (control, EGF+ and EGF-) were stained with oil red O staining to determine the adipocyte content. Those pieces cultured in 1%FBS/MEM (Figure 5.9) appeared healthy with a clear defined ridge round the perimeter of the skin pieces, raised follicular bumps and the skin was not dark in colour (Figures 5.9C and D). However, when stained with oil red O and counterstained with a haematoxylin nuclear stain, the follicles had formed dark concentrated circles which looked pathological and there was limited oil red O staining (Figures 5.9E-H). The pieces cultured with the EGF activator, amphiregulin, had developed fat in the skin dermis. The skin also expanded, though the red staining was visible in original location of the lower dermis in a line across the skin (Figure 5.10). There was little evidence of developing follicles in the EGF+ skin. Comparatively, the EGF inhibitor appeared to impede on fat development, as there was no clear red staining in the dermis of the skin (Figures 5.11E-H). Some follicular down growth, however, was seen stained with haematoxylin (Figure 5.11F).

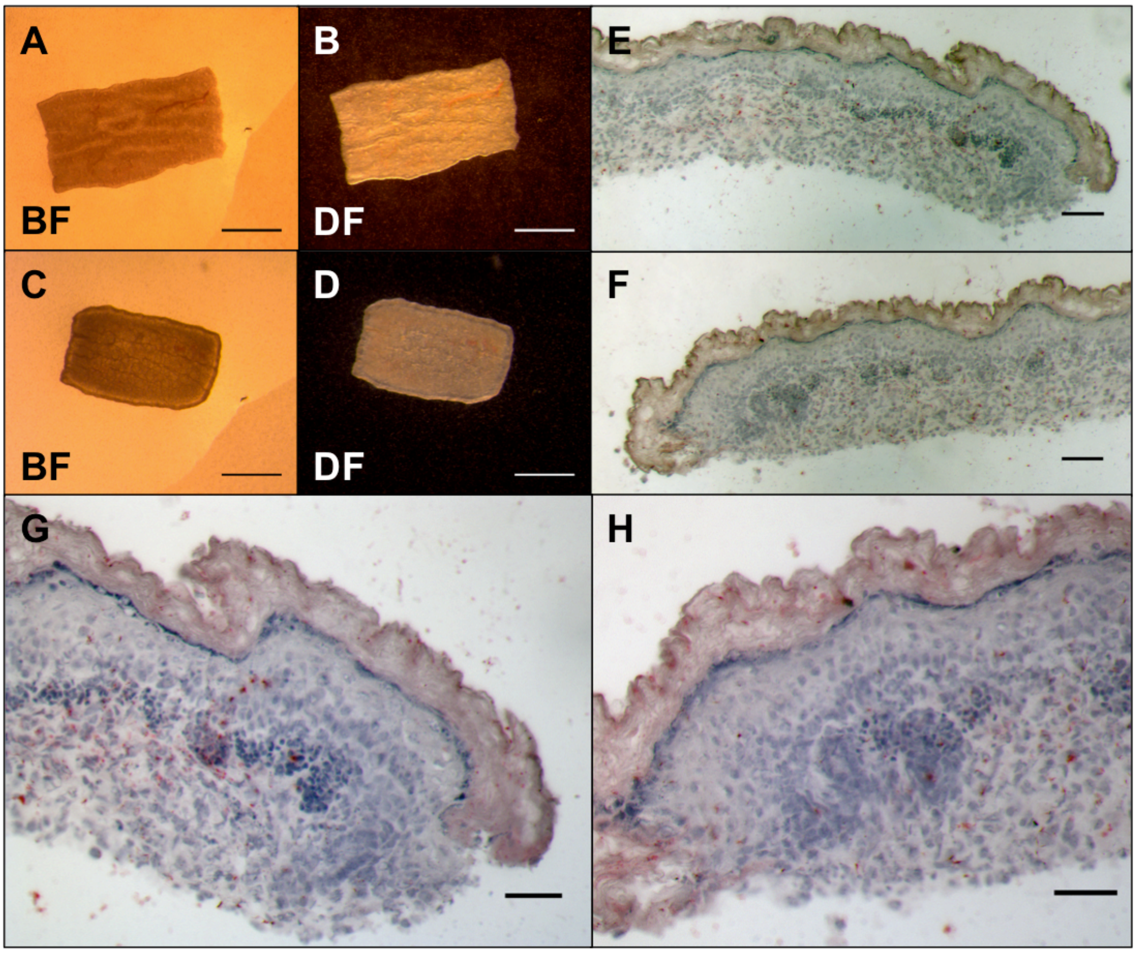

Figure 5.9: Oil red O analysis of organ cultured 16.5 embryonic day mouse back skin in 1% FBS/MEM. (**A,B**) Skin prior to incubation. (**C,D**) Skin after 72 hours in culture. (**E-F**) Fat droplets present in adipocytes visible as red coloration. Images were taken using a Zeiss Stemi SVII and oil red O images were taken using a Zeiss Axio Imager M1. (**A-D**) scale bar = 1mm. (**E,F**) scale bar = 65µm. (**G,H**) scale bar = 40µm.

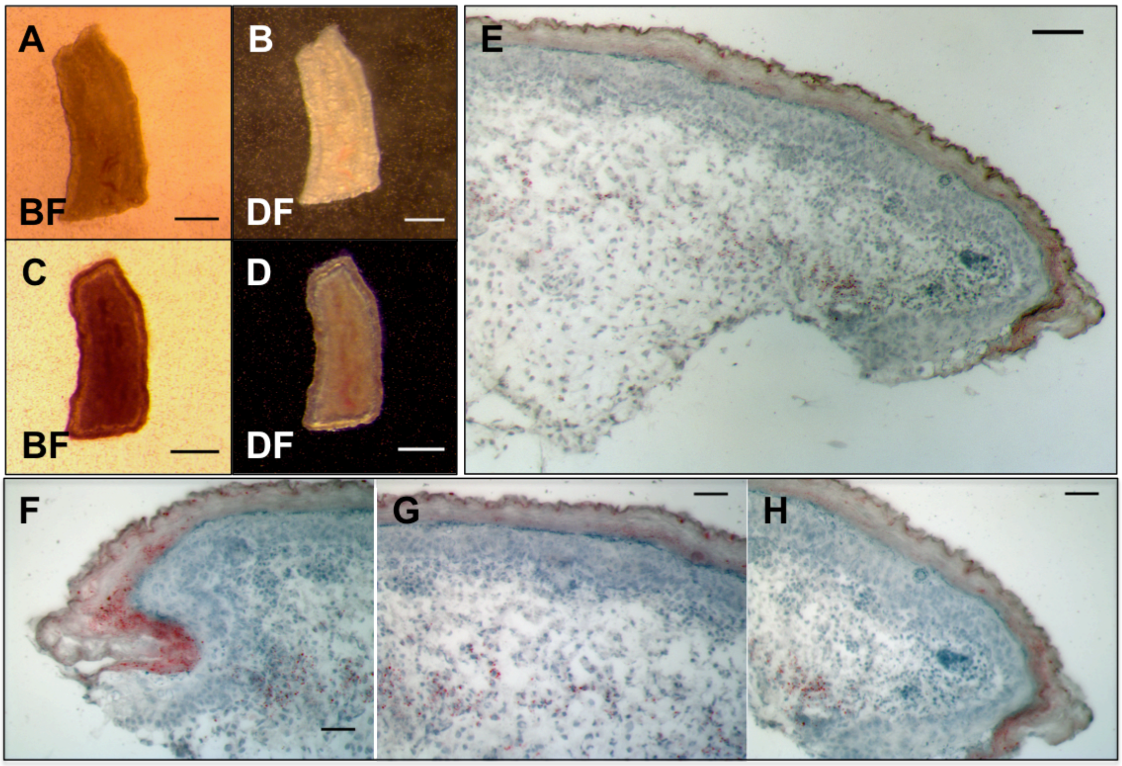

Figure 5.10: Oil red O analysis of organ cultured 16.5 embryonic day mouse back skin in 1% FBS/MEM with the EGF activator (EGF+). (**A,B**) Skin prior to incubation. (**C,D**) Skin after 72 hours in culture. (**E-F**) Fat droplets present in adipocytes visible as red coloration. Images were taken using a Zeiss Stemi SVII and oil red O images were taken using a Zeiss Axio Imager M1. (**A-D**) scale bar = 1mm. (**E**) scale bar = 65μm. (**F-H**) scale bar = 40μm.

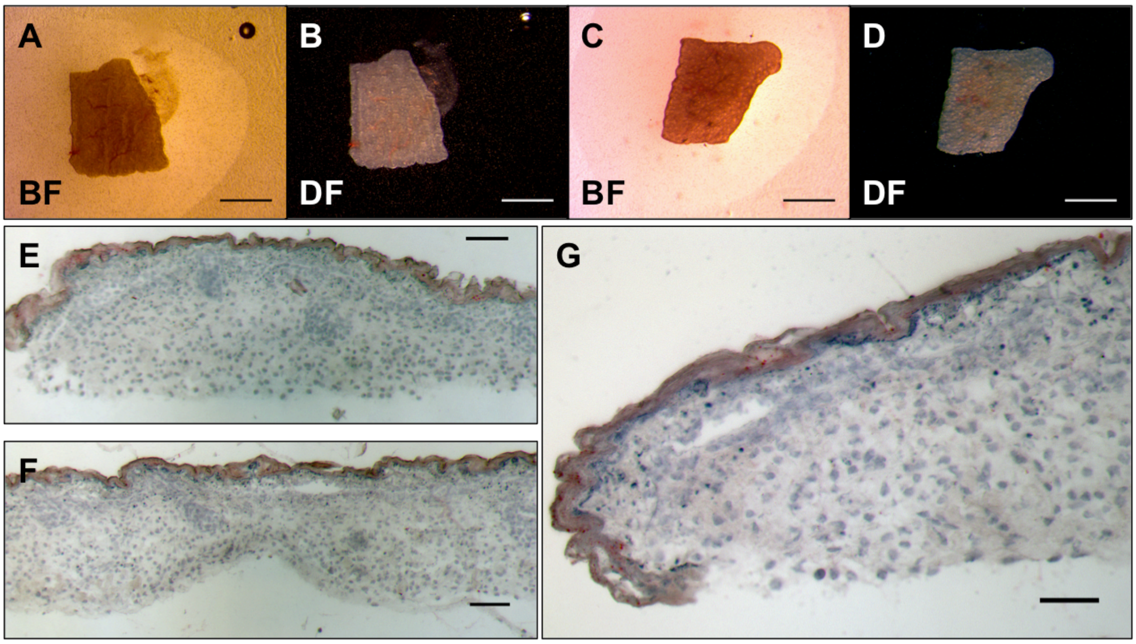

Figure 5.11: Oil red O analysis of organ cultured 16.5 embryonic day mouse back skin in 1% FBS/MEM with the EGF inhibitor (EGF-). (**A,B**) Skin prior to incubation. (**C,D**) Skin after 72 hours in culture. (**E-F**) Fat droplets present in adipocytes visible as red coloration. Images were taken using a Zeiss Stemi SVII and oil red O images were taken using a Zeiss Axio Imager M1. (**A-D**) scale bar = 1mm. (**E,F**) scale bar = 65μm. (**G**) scale bar = 40μm.

While some of the results were similar to those previously found they were not consistent and by no means conclusive. Simultaneously, a potential cell culture model was being developed, the process of which was explained in chapter 4. This proved much more successful and so was also used to look at the EGF/EGFR pathway as well as the two other pathways investigated.

5.3.1.2. Cell Culture Model

The EGF/EGFR pathway was then investigated using this cell culture model. The cells taken from 16.5-day embryos were put into two-dimensional culture to show that the environment in which the cells are grown is important to their growth and development. The experiment was repeated several times as summarised in figure 5.12. It was observed that the cells grown as a control in 10% FBS-MEM proliferate and develop and to a similar extent to those supplemented with EGF (Figures 5.12 column 1 and 2). Comparatively, the cells taken from the dermis and supplemented with the inhibitor AG1478 did not cope so well in 2-dimensional culture. A few cells survived after 4 days (Figures 5.12C,F and I) similarly to that found after 6 days with no further growth (Figures 5.12L,O and R).

Cells were also grown in 3-dimensional spheres and then put into 2-dimensional culture, at the same density (Figure 5.13). These cells flourished under the influence of the EGF inhibitor. In fact, the majority of the cells developed into adipocytes after a further two days in culture, which was visible prior to staining with oil red O (Figures 5.13M-R). On the other hand, the spheres supplied with the EGF activator and allowed to adhere and grow out for two days showed little development of fat and formation of adipocytes (Figure 5.13). There is a significant replicable difference between these two treatments as shown by repeating the experiment several times. The EGF inhibitor produced distinctly more adipocytes than the control treatments without supplements.

After 4 days, the control spheres (Figures 5.14B,E,H,K) were had a smaller average diameter of 0.09mm compared with both the EGF+ (0.20mm) and EGF- (0.15mm) treated spheres-. This could be used to infer that the factors are having some effect on the cells. After 6 days, the spheres under all three conditions were smaller in diameter, by 0.05mm (Figure 5.14). The average diameters of these spheres were measured using Image J.

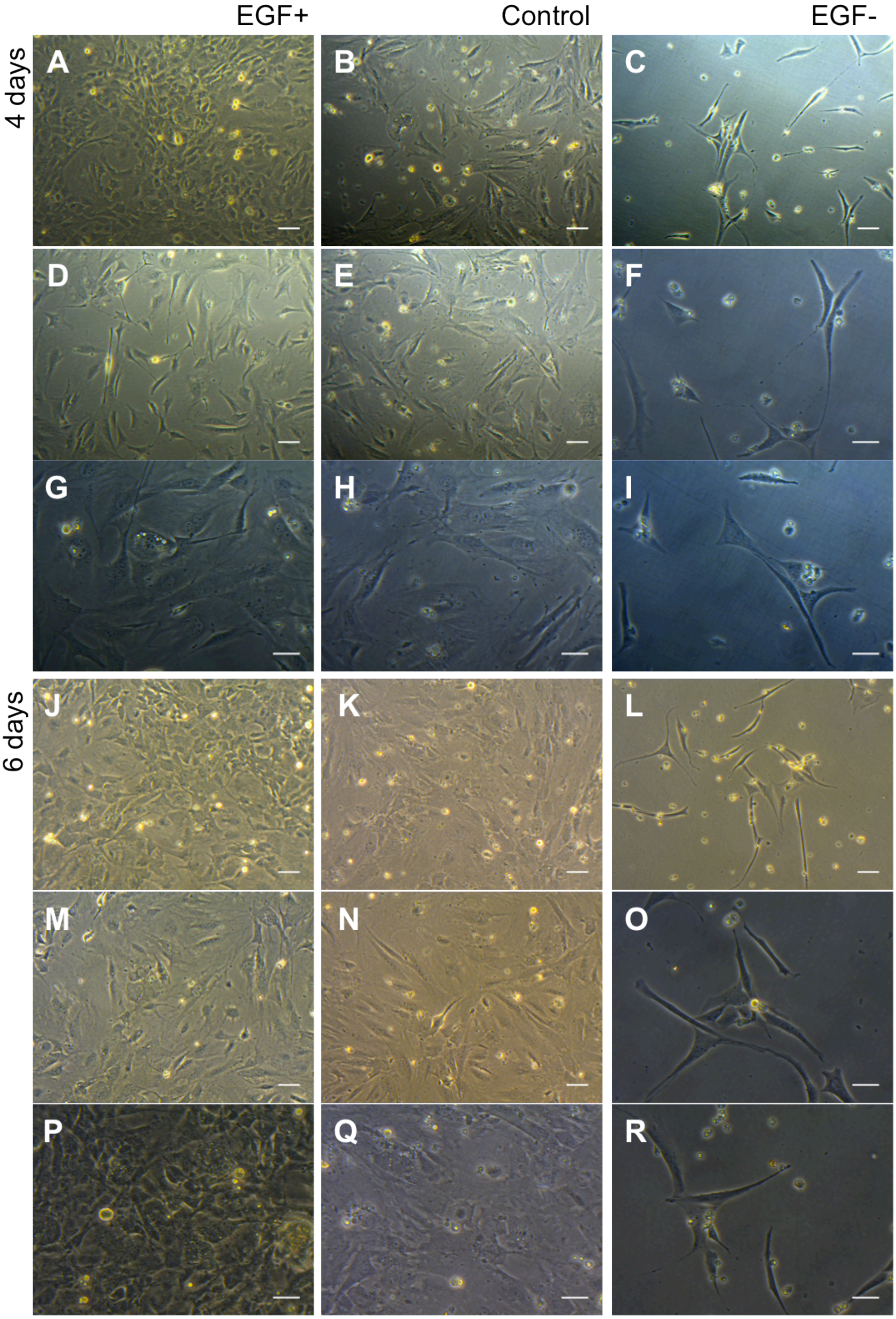

<u>Figure 5.12:</u> 2-dimensional cell culture of 16.5-day embryonic mouse dermis. (**1,2,3**) From left to right, EGF+, Control with DMSO and EGF-. Images taken of culture after 4 days (A-I) and 6 days (J-R). Images taken on a Zeiss Axiovert 10. (**A-E,J-N**) scale bar = 65μm. (**F-I,O-R**) scale bar = 40μm.

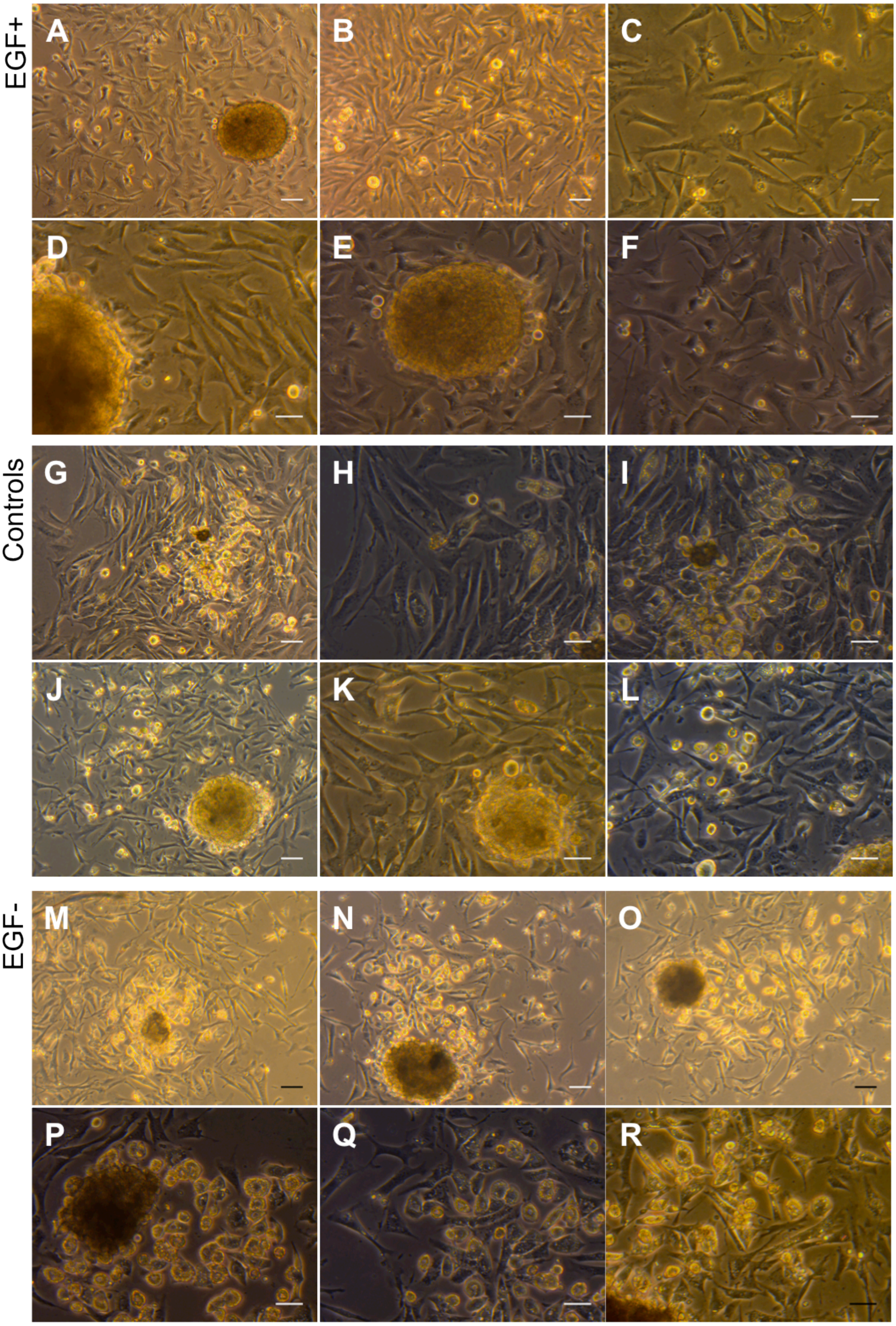

Figure 5.13: 3 dimensional into 2-dimensional cell culture of 16.5-day embryonic mouse dermis. (**A-F**) EGF+ with the EGF activator. (G-I) Control with DMSO. (J-L) Control without DMSO. (M-R) EGF-with EGF inhibitor. Images taken of culture after 4 days in 3D and 2 days in 2D. Images taken on a Zeiss Axiovert 10. (**A,B,G,J,M-O**) scale bar = 65μm. (**C-F,H,I,K,L,P-R**) scale bar = 40μm.

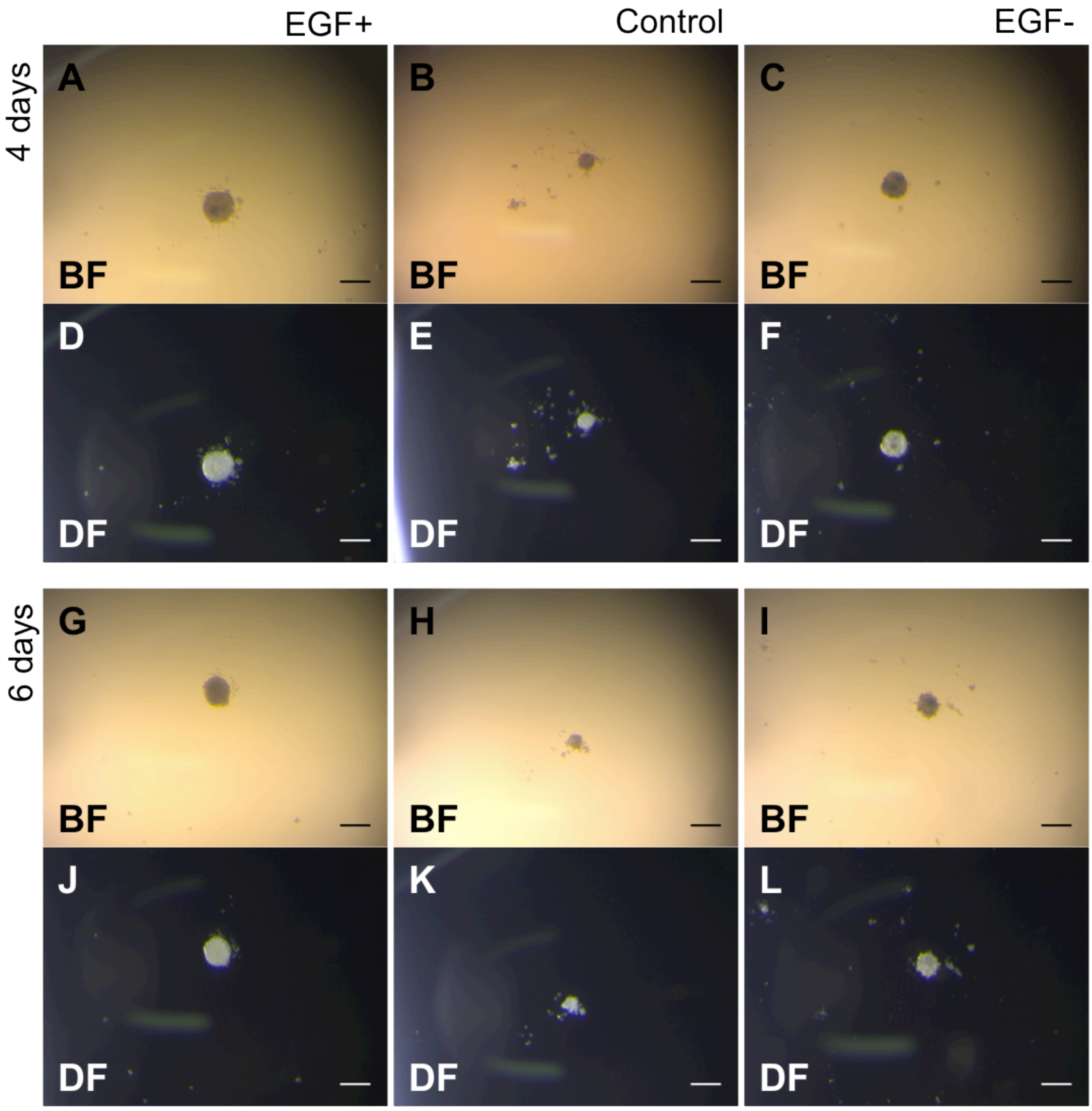

<u>Figure 5.14:</u> 3 dimensional cell culture of 16.5-day embryonic mouse dermis. From left to right, spheres grown under the conditions, EGF+, EGF-. Images taken of culture after 4 days (A-F) and 6 days (G-L). Images taken on a Zeiss Stemi SVII. Scale bar = 0.2mm. BF = bright field. DF = dark field.

While some of the cells were damaged to some extent under oil red O staining (Figures 5.15 and 5.16), there was a greater degree of red staining visible in the 3D to 2D culture compared with 2D. Not only this, but also more cells contained red staining in the AG1478 treated cells than any of the other treatments. It could even be said that when supplied with the EGF activator, there was even less adipocyte development than the controls.

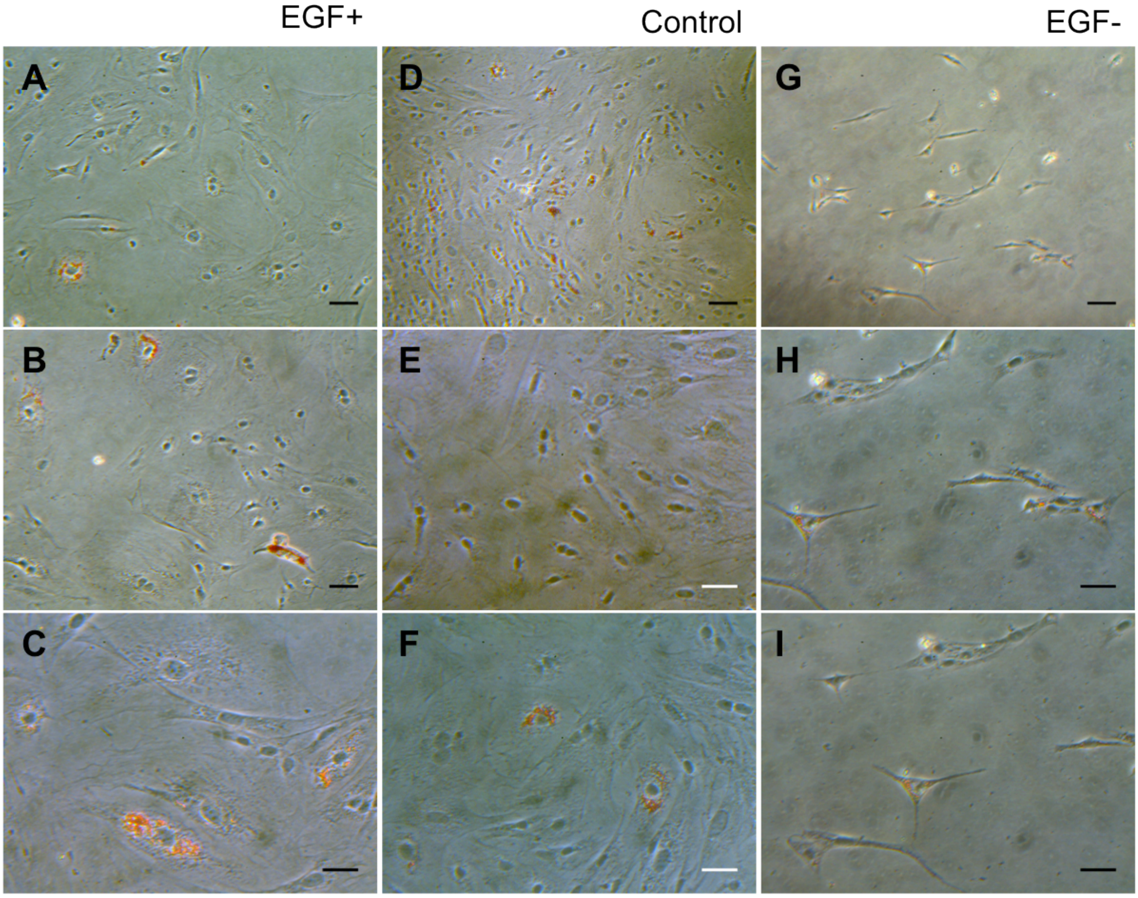

<u>Figure 5.15:</u> Oil red O analysis of 2-dimensional cell culture of 16.5-day embryonic mouse dermis. From left to right, EGF+, Control and EGF-. Images taken of culture after 6 days (J-R). Images taken on a Zeiss Axiovert 10. (**A,B,D,G**) scale bar = 65µm. (**C,E,F,H,I**) scale bar = 40µm.

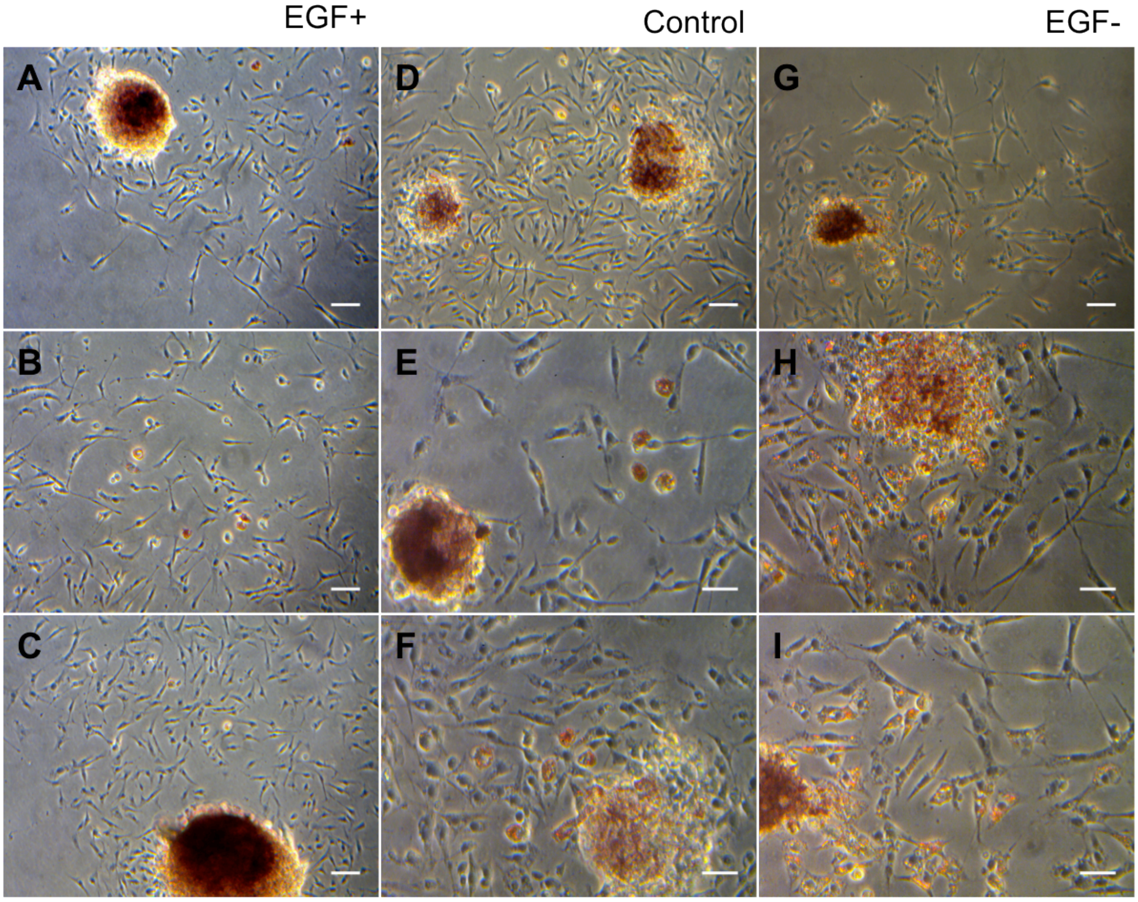

Figure 5.16: Oil red O analysis of 3-dimensional into 2-dimensional cell culture of 16.5-day embryonic mouse dermis. From left to right, EGF+, Control and EGF-. Images taken of culture after 4 days in 3D and 2 days in 2D. Images taken on a Zeiss Axiovert 10. (**A-D,G**) scale bar = 65μm. (**E,F,H,I**) scale bar = 40μm.

To further the analysis of 3D culture through the formation of dermal cell spheres, which worked well, cells that were left to develop in spheres for the full 6 days prior to freezing, were stained with oil red O (Figure 5.17). The EGF+ spheres had more densely packed nuclei illustrated by the blue haematoxylin stain (Figures 5.17A-C) compared with the control and EGF-. This packing structure, correlated with the larger size of the EGF+ spheres (Figure 5.14). While it was difficult to determine cell numbers in the spheres due to not knowing at which point through the sphere the cross sections were taken, it could be suggested that there was more proliferation in the positive spheres.

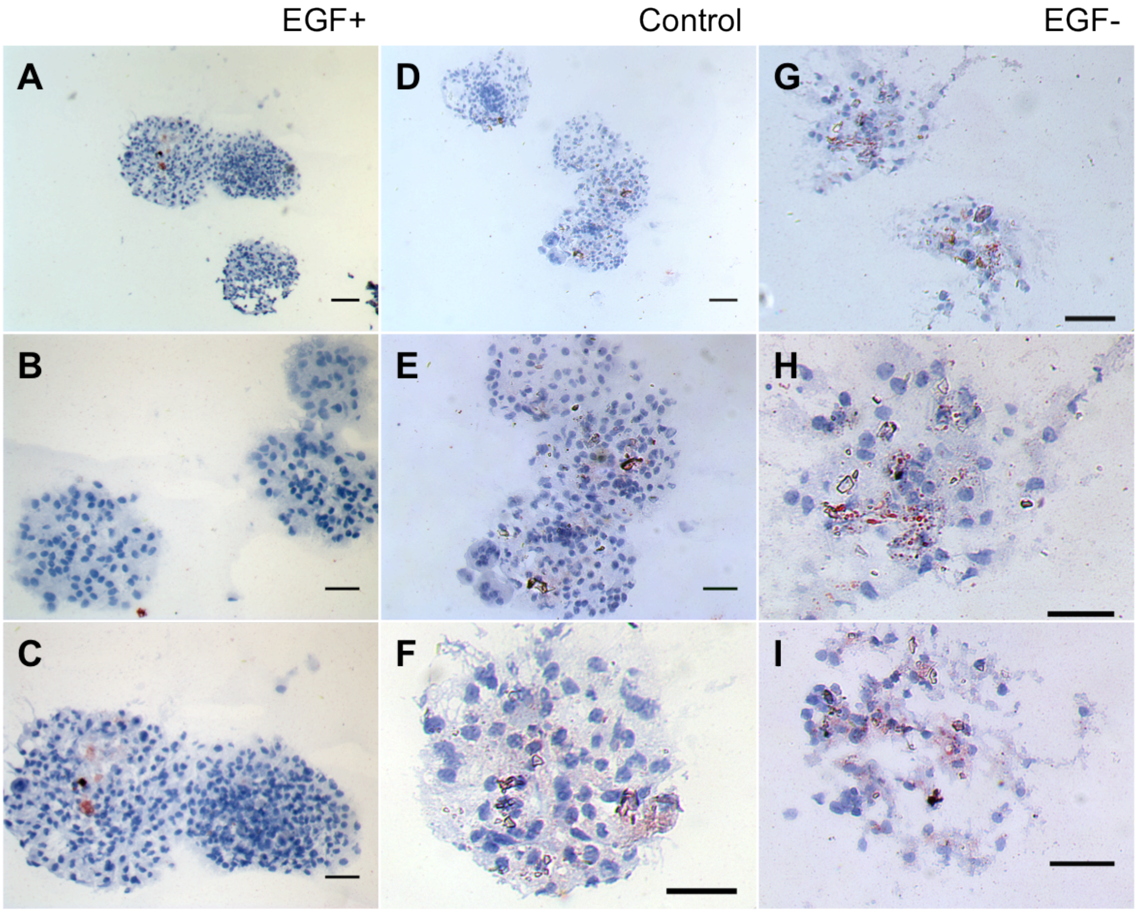

Figure 5.17: Oil red O analysis of 3-dimensional cell spheres of 16.5-day embryonic mouse dermis. Sections cut at 10μm and stained with Oil red O and counterstained with haematoxylin. From left to right, EGF+, Control and EGF-. Images taken of culture after 6 days in 3D. Images taken on a Zeiss Axiovert 10. (**A,D,G**) scale bar = 65μm. (**B,C,E,F,H,I**) scale bar = 40μm.

The experiment was also conducted with a slightly different protocol while the model was being established. This included investigating the effects of EGF at embryonic day 15.5 and leaving the spheres in culture for 5 days and 1 day in 2D culture. This was less effective because the spheres did not adhere and grow out as well and therefore oil red O staining was not good quality. While dermal cells taken from e15.5 were more fragile when it came to staining, it did show that EGF/AG1478 was having a similar influence to that found a day later at e16.5 (Figure 5.16).

5.3.1.2.1. Oil Red O Quantification of the EGF/EGFR Pathway

During development of a method of oil red O quantification to support the visual assessments, EGF+ and EGF- cultures were investigated to see if the differences visible could also be quantified. There was little evidence to support the visibility of more adipogenesis with the EGF inhibitor, AG1478 and the values varied between samples.

Although with the inhibitor in 2D cultures there were very few cells, the oil red O values read high, which was not accurate. A bar chart illustrated the averages of each condition (Figure 5.18) and although there was one sample for EGF+ that showed a high value, the other sample was lower than both the control and EGF- values, which was not accurate in relation to what was seen in the culture images.

Table 5.2: Oil Red O quantification of the EGF/EGFR pathway in 2D and 3D to 2D culture

	EGF (+)		AG1478 (-)		DMSO Control	
3D	0.056	0.062	0.058	0.062	0.064	0.057
	0.057	0.069	0.059	0.063	0.066	0.058
	0.054	0.065	0.060	0.062	0.062	0.061
Mean	0.056	0.065	0.059	0.062	0.064	0.059
2D	0.038		0.058		0.042	
	0.037		0.059		0.045	
	0.038		0.055		0.046	
Mean	0.038		0.057		0.044	

Averages means were calculated for both 2D and 3D.

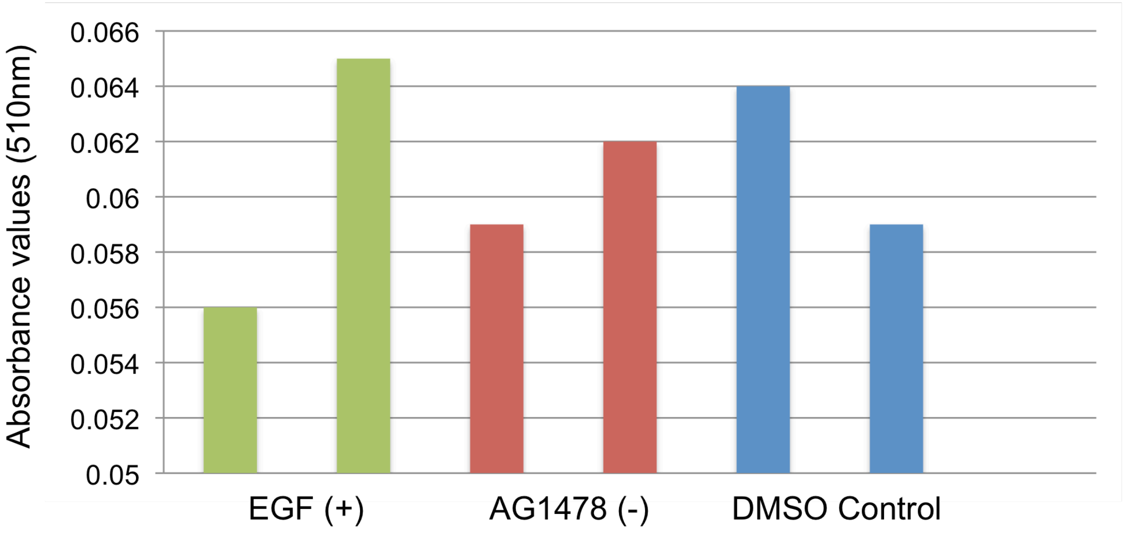

Figure 5.18: Oil red O quantification analysis of 3-dimensional cell spheres put into 2-dimensional culture of 16.5-day embryonic mouse dermis. EGF+/EGF- Readings were taken on a nanodrop using UV-Vis software and read at 510nm absorbance. EGF+, EGF- and Control values are illustrated.

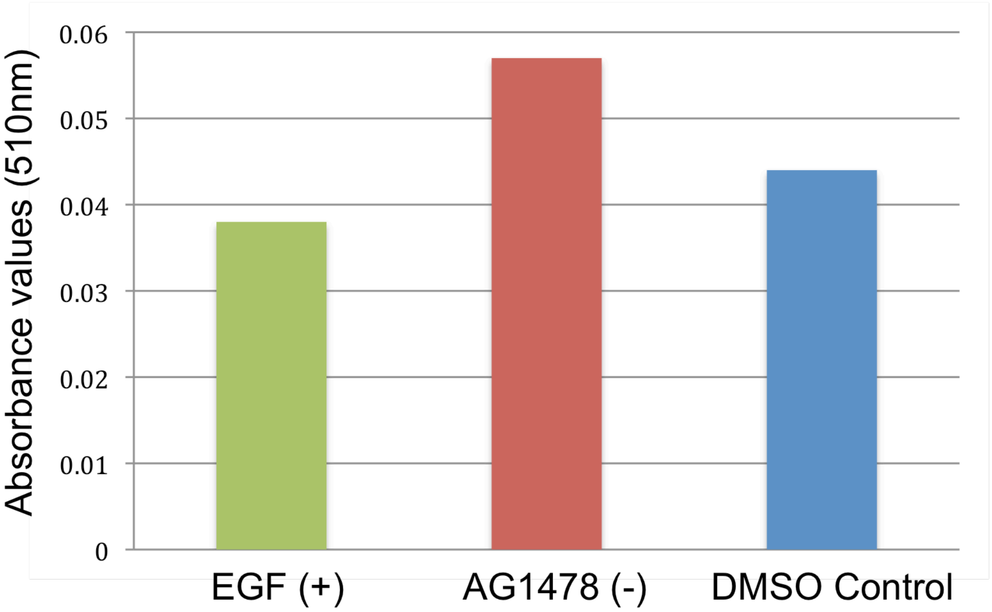

Figure 5.19: Oil red O quantification analysis of 2-dimensional cell culture of 16.5 –day embryonic mouse dermis. EGF+/EGF- Readings were taken on a nanodrop using UV-Vis software and read at 510nm absorbance. EGF+, EGF- and Control values are illustrated.

5.3.2. TGFβ/BMP Pathway

The BMP pathway was investigated using the cell culture model as described in Chapter 4. As both the inhibitor and activator had not been used before with respect to this model, three different concentrations were tried of both BMP4 and DMH1 and applied to 2D, 3D and 3D to 2D culture techniques. Firstly the dermal cells were cultured in 2D with the BMP activator (Figure 5.21) and the BMP inhibitor (Figure 5.22). The cell densities were similar to the controls across both the activator and inhibitor two-dimensional cultures, with the cells more densely packed in the centre of the wells. Representative images in figure demonstrate that the cells that grew near the edge of the cells were of reduced quantity and confluence, e.g. figures 5.21C and 5.22E and F). Unlike that found with the EGF/EGFR pathway, there was little contrast between the effects both the inhibitor and activator of the BMP pathway were having on adipogenesis in 2D culture. This was the same after oil red O analysis of the 2D cultures of both the activator and the inhibitor (Figures 5.24 and 5.25). While inseparable in terms of adipocyte number, they were still present to some degree and it was noticed that the distribution was uneven. Often clusters of red stained adipocytes were seen, while other groups of cells had no adipocytes (Figures 5.23C and 5.24C).

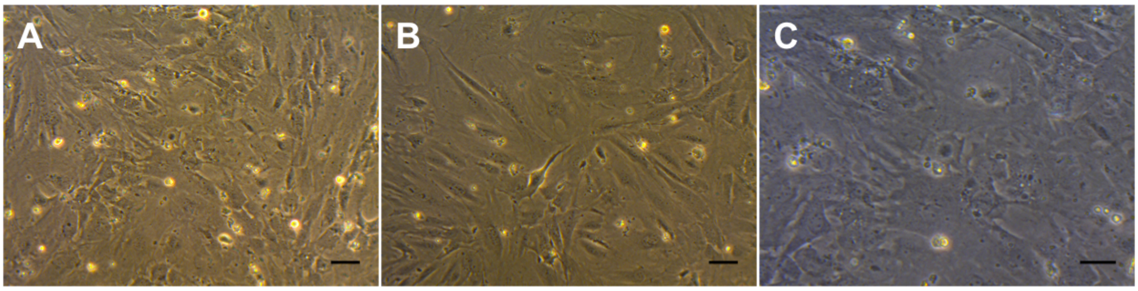

Figure 5.20: 2-dimensional cell culture of 16.5-day embryonic mouse dermis. Control images with DMSO taken of culture after 6 days. Images taken on a Zeiss Axiovert 10. (**A,B**) Images of two different frames from the centre (**A**) and edge (**B**) of the well, scale bar = 65μm. (**C**) Image taken at a higher magnification, scale bar = 40μm.

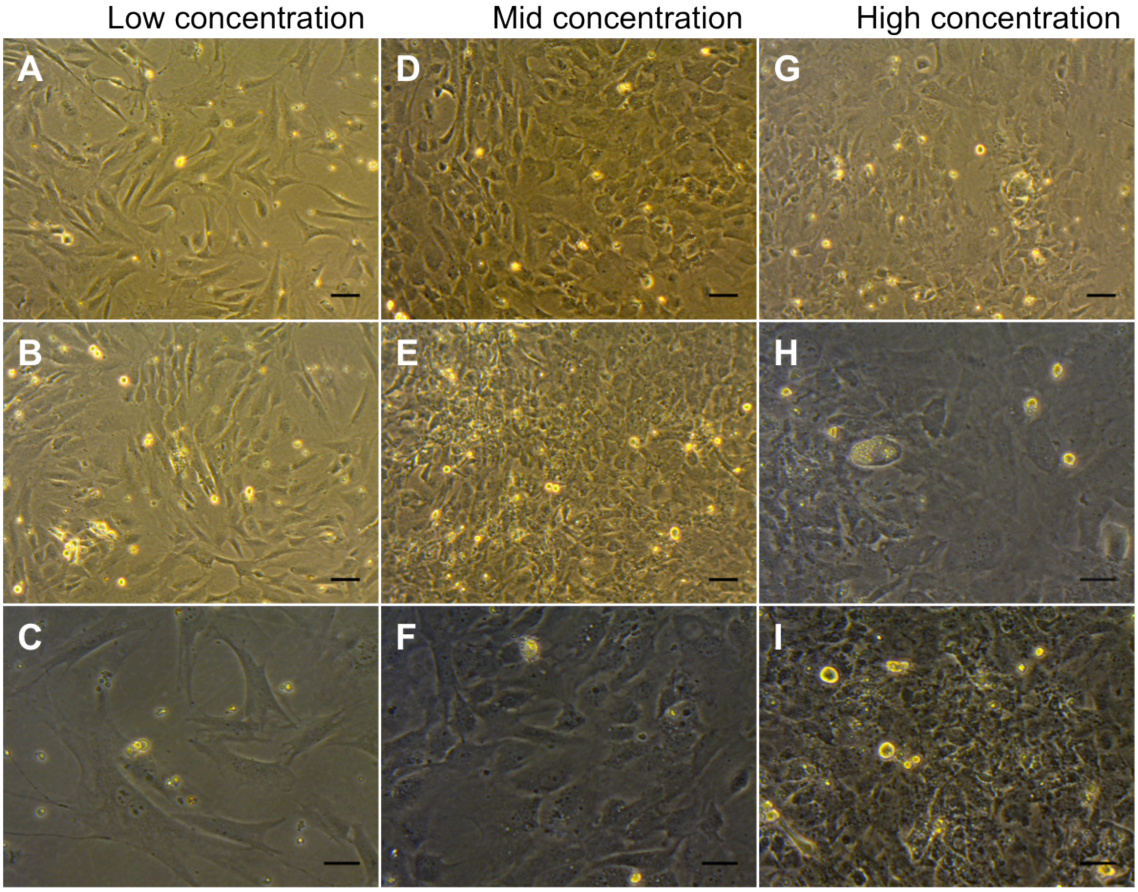

Figure 5.21: 2-dimensional cell culture of 16.5-day embryonic mouse dermis supplemented with BMP4. Images taken of culture after 6 days. From left to right, Low (1ng/ml), mid (10ng/ml) and high (100ng/ml) concentrations. Images taken on a Zeiss Axiovert 10. (**A,B,D,E,G**) scale bar = 65μm. (**C,F,H,I**) scale bar = 40μm.

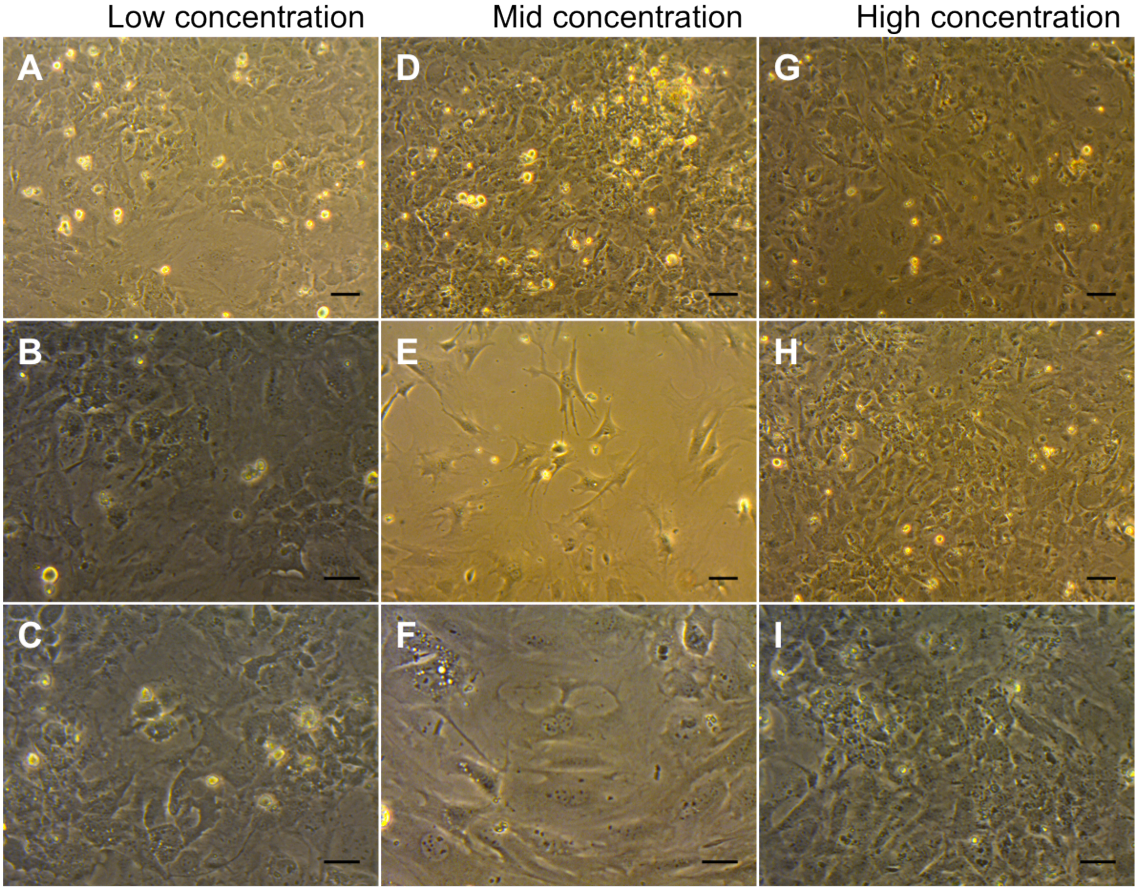

Figure 5.22: 2-dimensional cell culture of 16.5-day embryonic mouse dermis supplemented with the BMP inhibitor, DMH1. Images taken of culture after 6 days. From left to right, Low (19ng/ml), mid (190ng/ml) and high (1.9µg/ml) concentrations. Images taken on a Zeiss Axiovert 10. (**A,D,E,G,H**) scale bar = 65µm. (B,**C,F,I**) scale bar = 40µm.

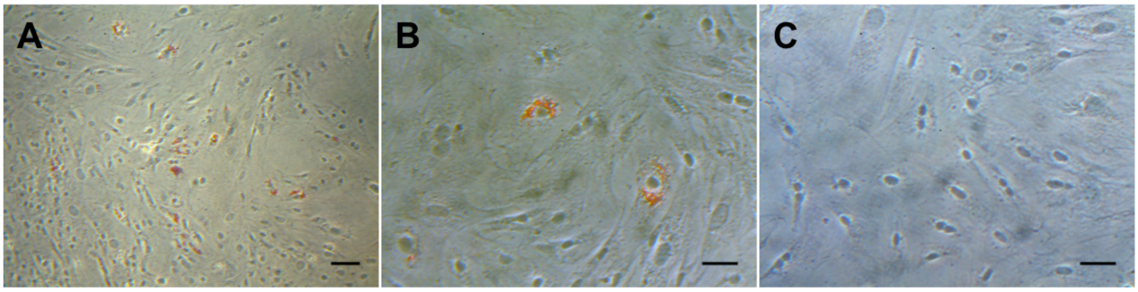

Figure 5.23: Oil red O analysis of 2-dimensional cell culture of 16.5-day embryonic mouse dermis. Control images with DMSO taken of culture after 6 days. Images taken on a Zeiss Axiovert 10. (**A**) scale bar = 65µm. (**B,C**) scale bar = 40µm.

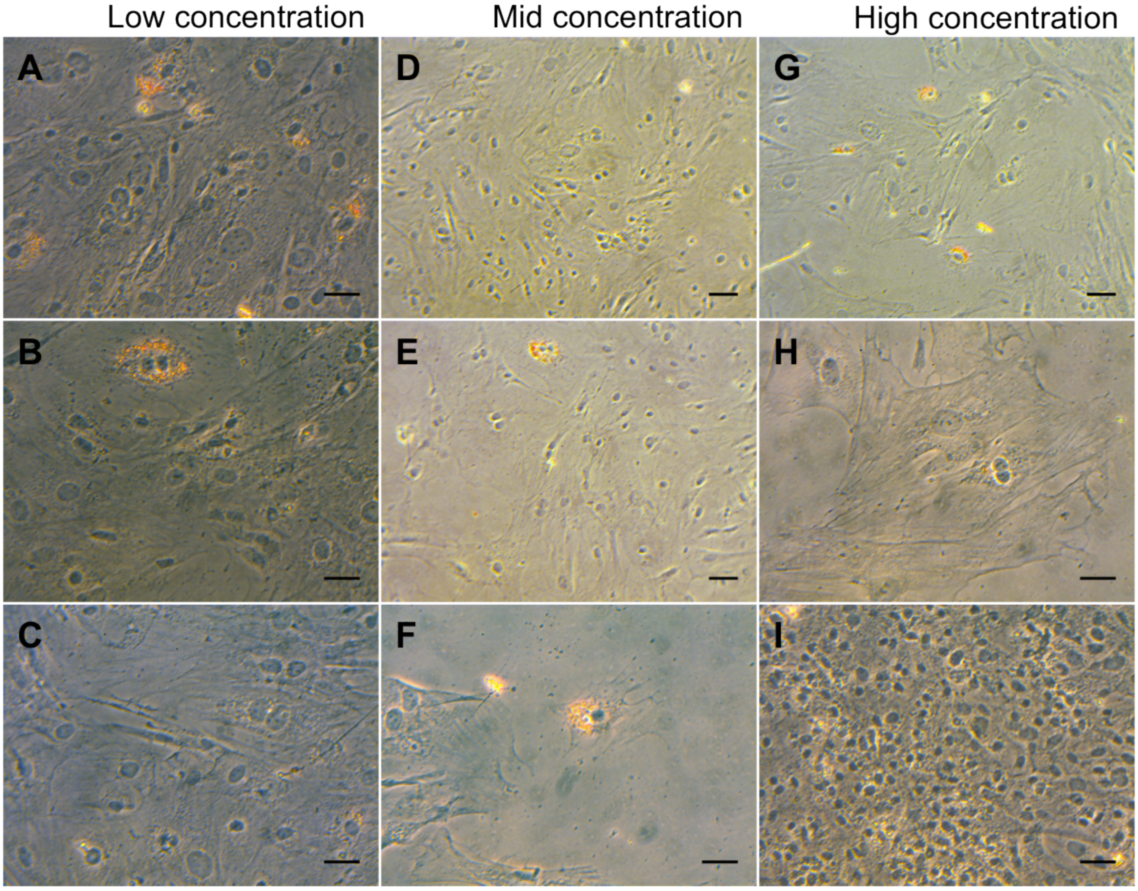

<u>Figure 5.24:</u> **Oil red O analysis of 2-dimensional cell culture of 16.5-day embryonic mouse dermis supplemented with BMP4.** Images taken of culture after 6 days. From left to right, Low(1ng/ml), mid (10ng/ml) and high (100ng/ml) concentrations. Images taken on a Zeiss Axiovert 10. (**D,E,G**) scale bar = 65μm. (**A-C,F,H,I**) scale bar = 40μm.

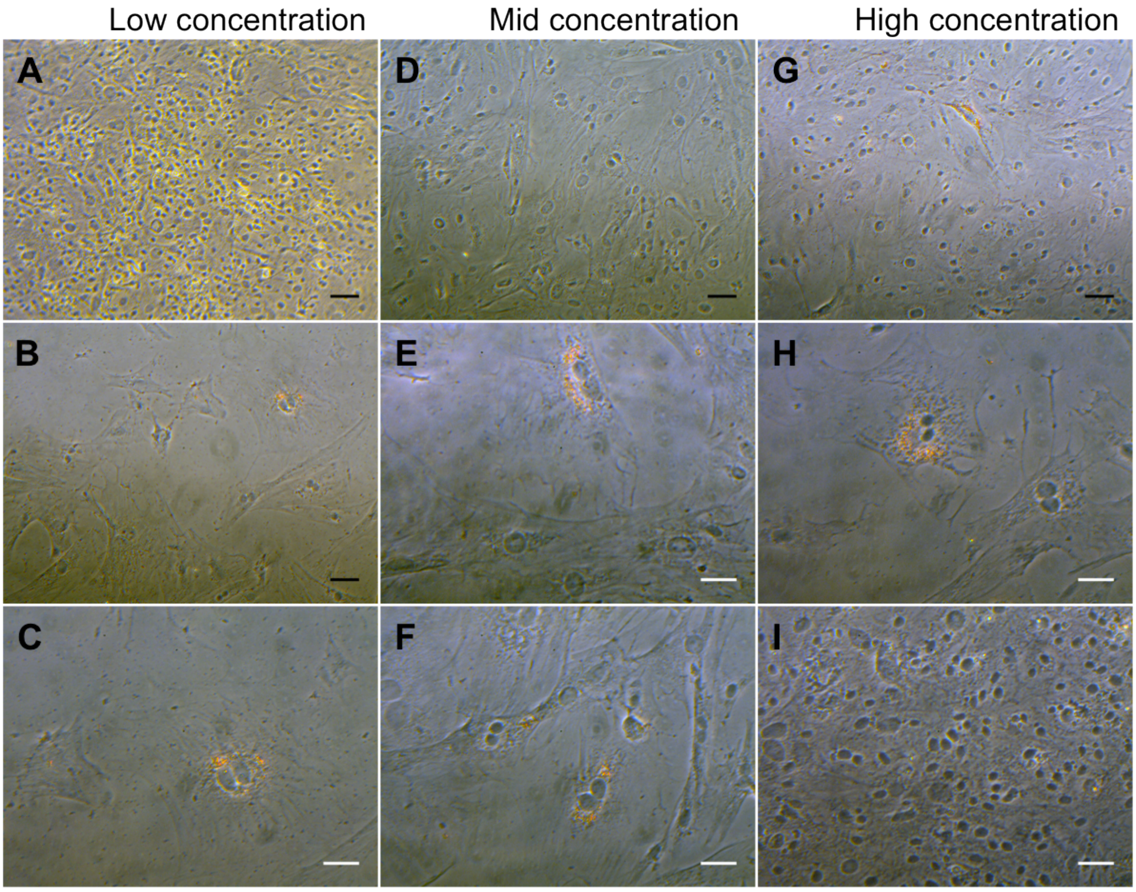

Figure 5.25: Oil red O analysis of 2-dimensional cell culture of 16.5-day embryonic mouse dermis supplemented with the BMP inhibitor, DMH1. Images taken of culture after 6 days. From left to right, Low (19ng/ml), mid (190ng/ml) and high (1.9µg/ml) concentrations. Images taken on a Zeiss Axiovert 10. (**A,D,G**) scale bar = 65µm. (**B,C,E,F,H,I**) scale bar = 40µm.

Like the 2-dimensional cultures, the conclusions drawn were the same from the 3-dimensional into 2-dimensional culture set up (Figures 5.27 and 5.28). As well as recognising the adipocyte-type cells in culture through the appearance of circular lipid droplets within some of the cells, little difference was inferred after these cells were stained with oil red O. This experiment was repeated twice more with similar results as shown by the representative oil red O stained images from both the 2-dimensional culture and the 3D to 2D culture. However with the activator, BMP4 (Figures 5.27 and 5.30) there were a few more adipocytes compared with the inhibitor, DMH1 (Figures 5.28 and 5.31) though considering that in general less adipocytes can be seen after oil red O staining compared with prior to staining, it was difficult to confirm this as a reliable observation.

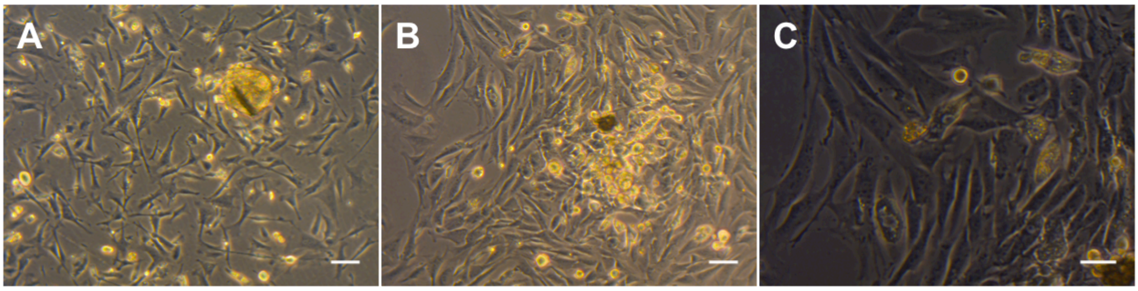

Figure 5.26: 3 dimensional into 2-dimensional cell culture of 16.5-day embryonic mouse dermis. Control images with DMSO taken of culture after 4 days. In 3D and 2 days in 2D. Images taken on a Zeiss Axiovert 10. (**A,B**) scale bar = 65μm. (**C**) scale bar = 40μm.

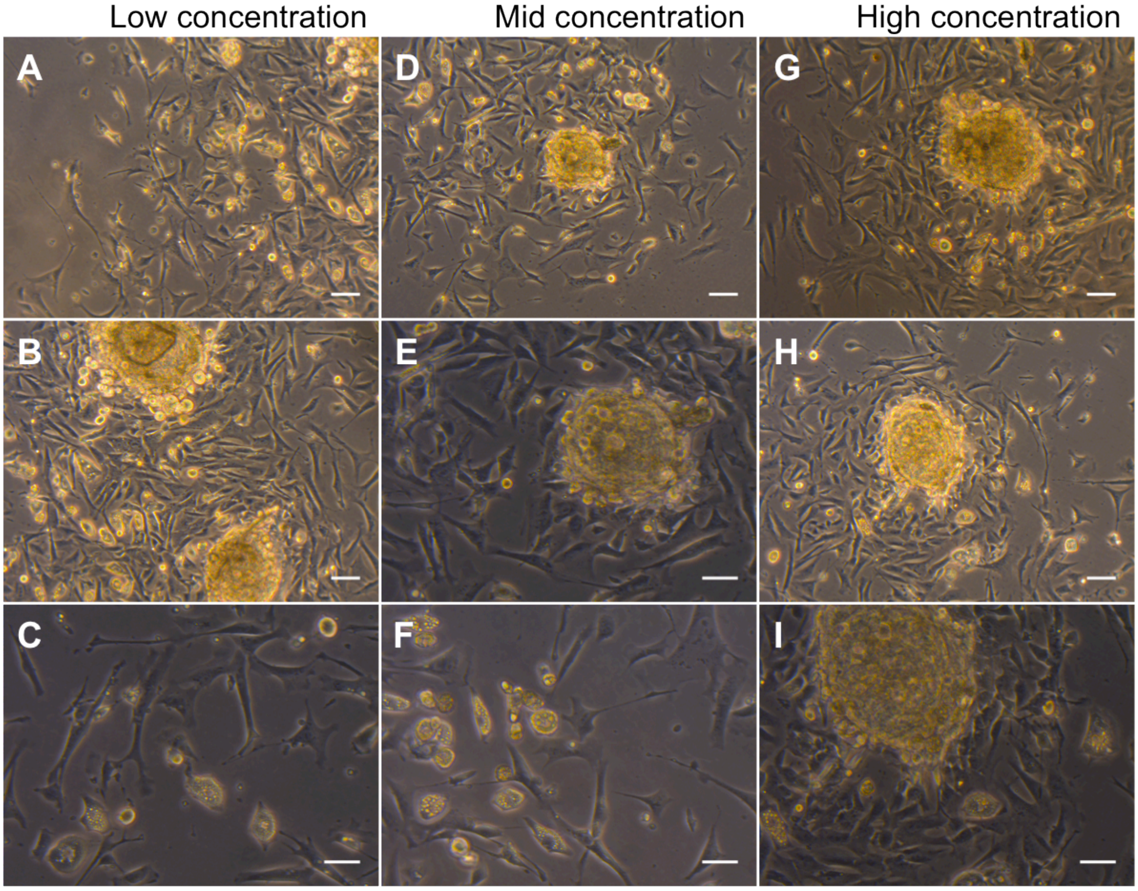

Figure 5.27: 3 dimensional into 2-dimensional cell culture of 16.5-day embryonic mouse dermis supplemented with BMP4. Images taken of culture after 6 days. From left to right, Low (1ng/ml), mid (10ng/ml) and high (100ng/ml) concentrations. Images taken on a Zeiss Axiovert 10. (**A,B,D,G,H**) scale bar = 65μm. (**C,E,F,I**) scale bar = 40μm.

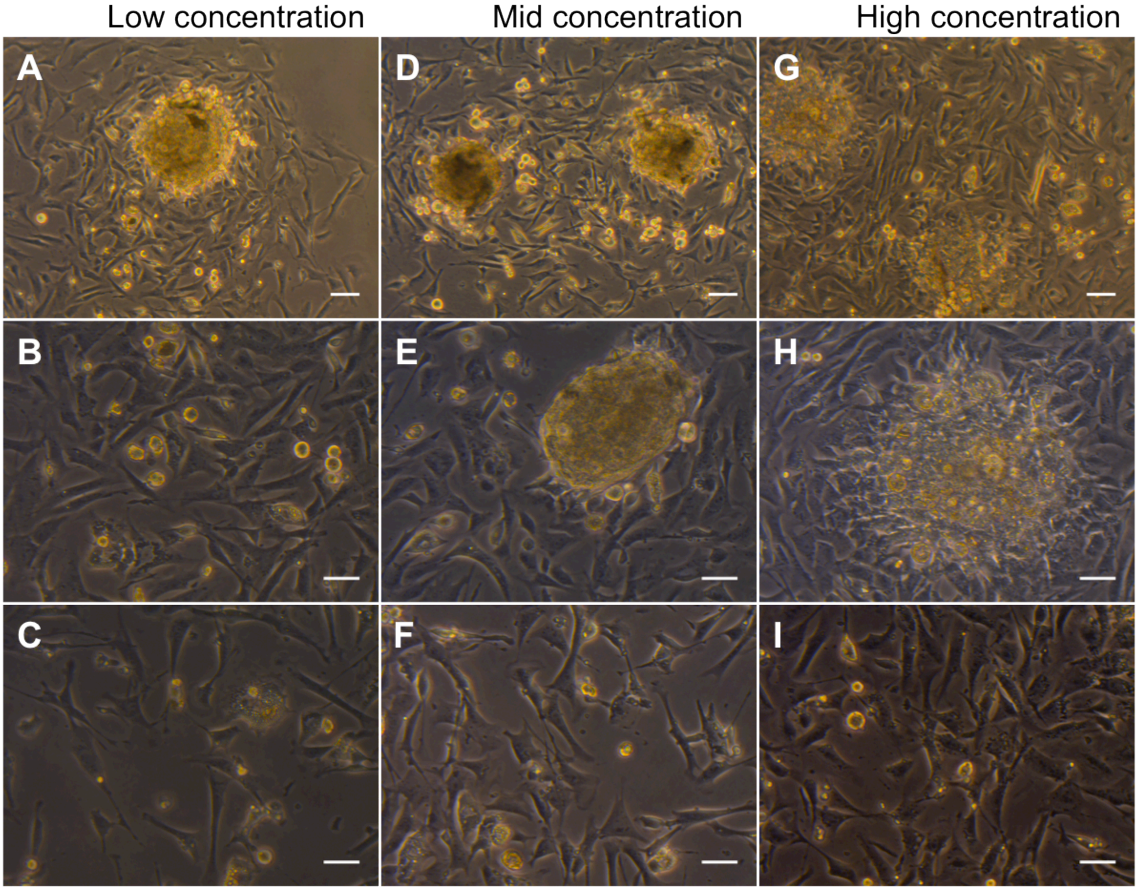

<u>Figure 5.28:</u> 3 dimensional into 2-dimensional cell culture of 16.5-day embryonic mouse dermis supplemented with the BMP inhibitor, DMH1. Images taken of culture after 6 days. From left to right, Low (19ng/ml), mid (190ng/ml) and high (1.9μg/ml) concentrations. Images taken on a Zeiss Axiovert 10. (**A,D,G**) scale bar = 65μm. (**B,C,E,F,H,I**) scale bar = 40μm.

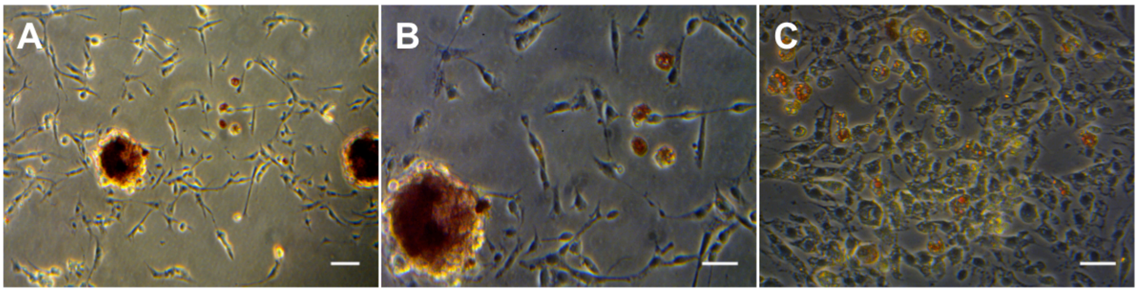

<u>Figure 5.29:</u> Oil red O analysis of 3 dimensional into 2-dimensional cell culture of 16.5 – day embryonic mouse dermis. Images taken after 6 days in culture. Images taken on a Zeiss Axiovert 10. (**A**) scale bar = 65μm. (**B,C**) scale bar = 40μm.

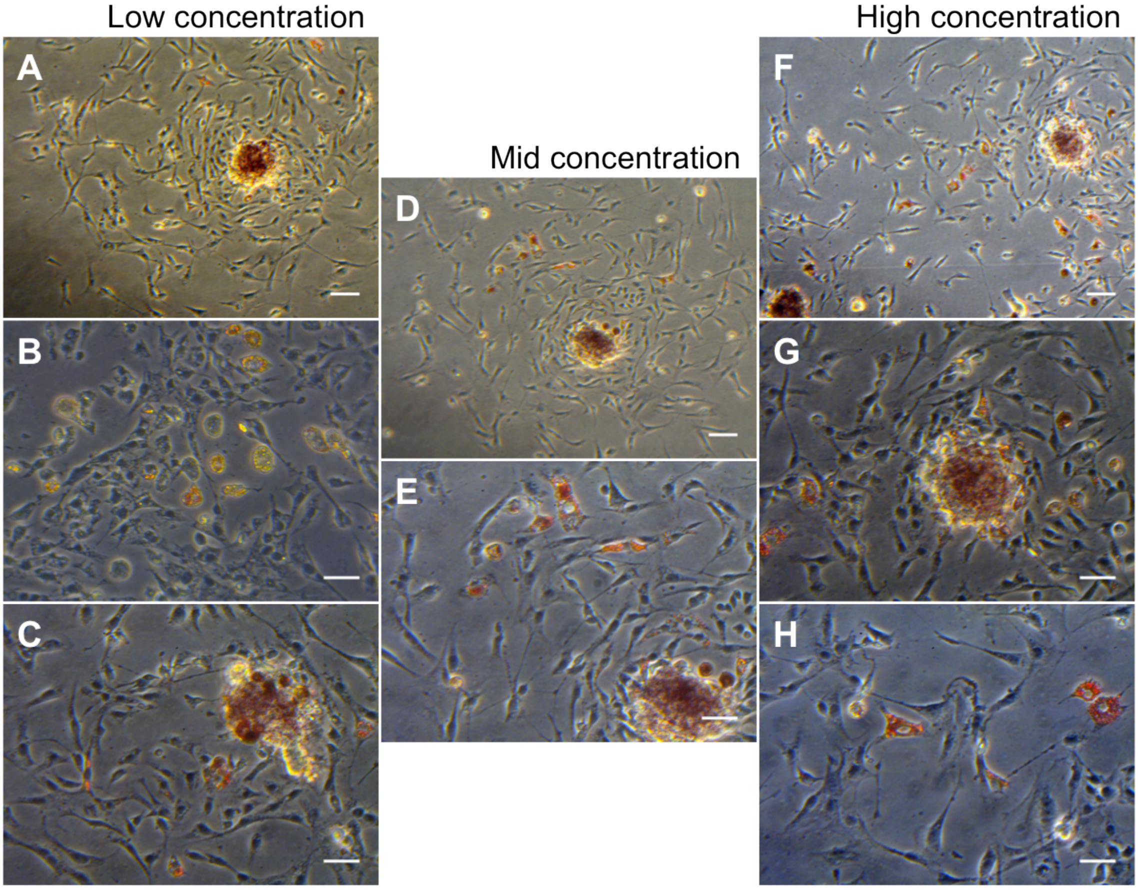

Figure 5.30: Oil red O analysis of 3 dimensional into 2-dimensional cell culture of 16.5-day embryonic mouse dermis supplemented with BMP4. Images taken of culture after 6 days. From left to right, Low(1ng/ml), mid (10ng/ml) and high (100ng/ml) concentrations. Images taken on a Zeiss Axiovert 10. (**A,D,F**) scale bar = 65μm. (**B,C,E,G,H**) scale bar = 40μm.

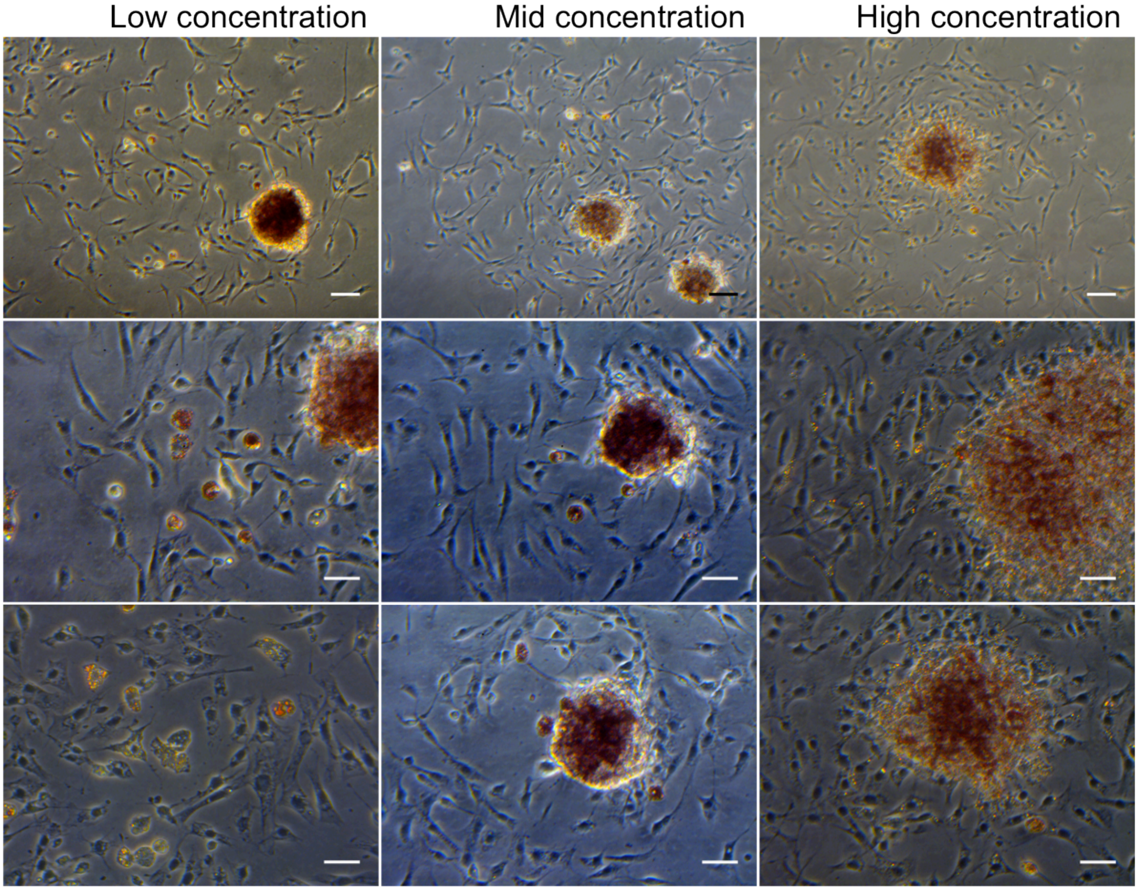

Figure 5.31: Oil red O analysis of 3 dimensional into 2-dimensional cell culture of 16.5-day embryonic mouse dermis supplemented with DMH1. Images taken of culture after 6 days. From left to right, Low (19ng/ml), mid (190ng/ml) and high (1.9µg/ml) concentrations. Images taken on a Zeiss Axiovert 10. (**A,D,G**) scale bar = 65µm. (**B,C,E,F,H,I**) scale bar = 40µm.

Some of the spheres remained in culture for the full 6-day incubation period. However there was not a significant difference between the sizes of the spheres between the activator and inhibitor unlike that found with EGF compared with AG1478.

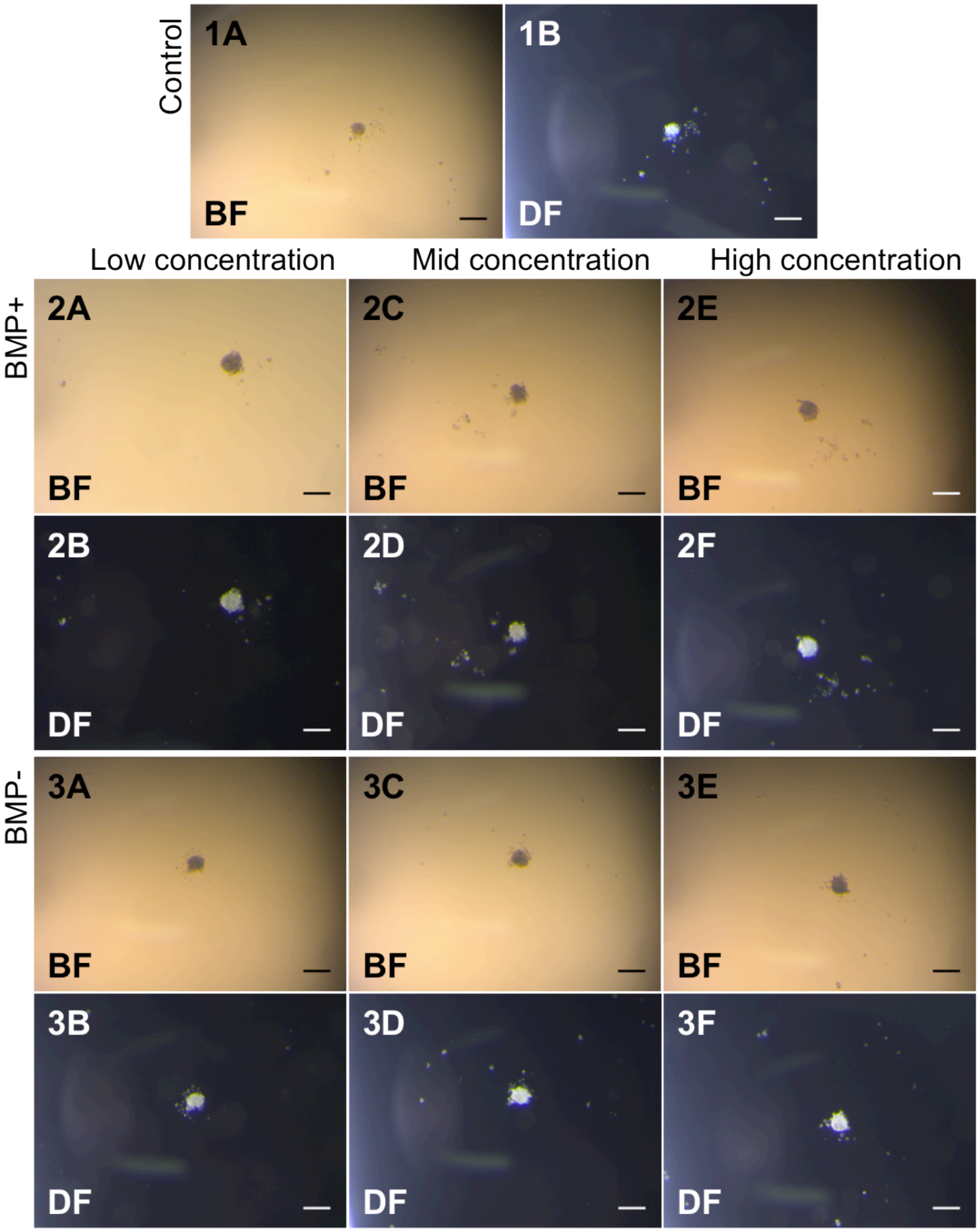

<u>Figure 5.32:</u> **3 dimensional cell culture of 16.5-day embryonic mouse dermis subjected to BMP+/- treatment.** (**1**) Control spheres. (**2**) Cultured with BMP4 of 3 different concentrations (BMP+) Low (1ng/ml), mid (10ng/ml) and high (100ng/ml). (**3**) Cultured with DMH1 of three different concentrations (BMP-) Low (19ng/ml), mid (190ng/ml) and high (1.9µg/ml). Images taken of culture after 6 days. Images taken on a Zeiss Stemi SVII. Scale bar = 0.2mm. BF = bright field. DF = dark field.

The spheres were frozen and sectioned before being stained with oil red O (Figures 5.33-5.35). Comparatively with what might have been observed in 3-dimensional to 2-dimensional culture, it could be suggested that there was a higher degree of red staining of the spheres treated with the BMP inhibitor, DMH1 (Figure 5.35). The fat droplets were a variety of sizes, some of which were clearly larger than others, more easily distinguished in figure 5.35.

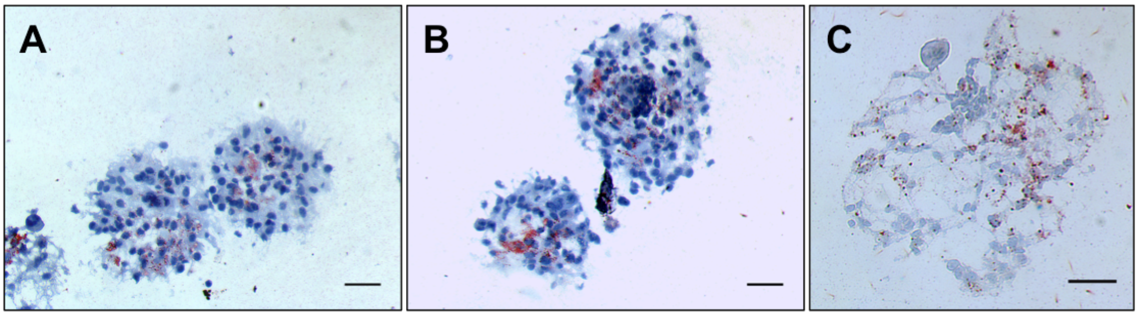

Figure 5.33: Oil red O analysis of 3-dimensional control cell spheres of 16.5-day embryonic mouse dermis supplied with DMSO. Sections cut at 10μm and stained with Oil red O and counterstained with haematoxylin after 6 days in culture. Images taken on a Zeiss Axio Imager M1. Scale bar = 40μm.

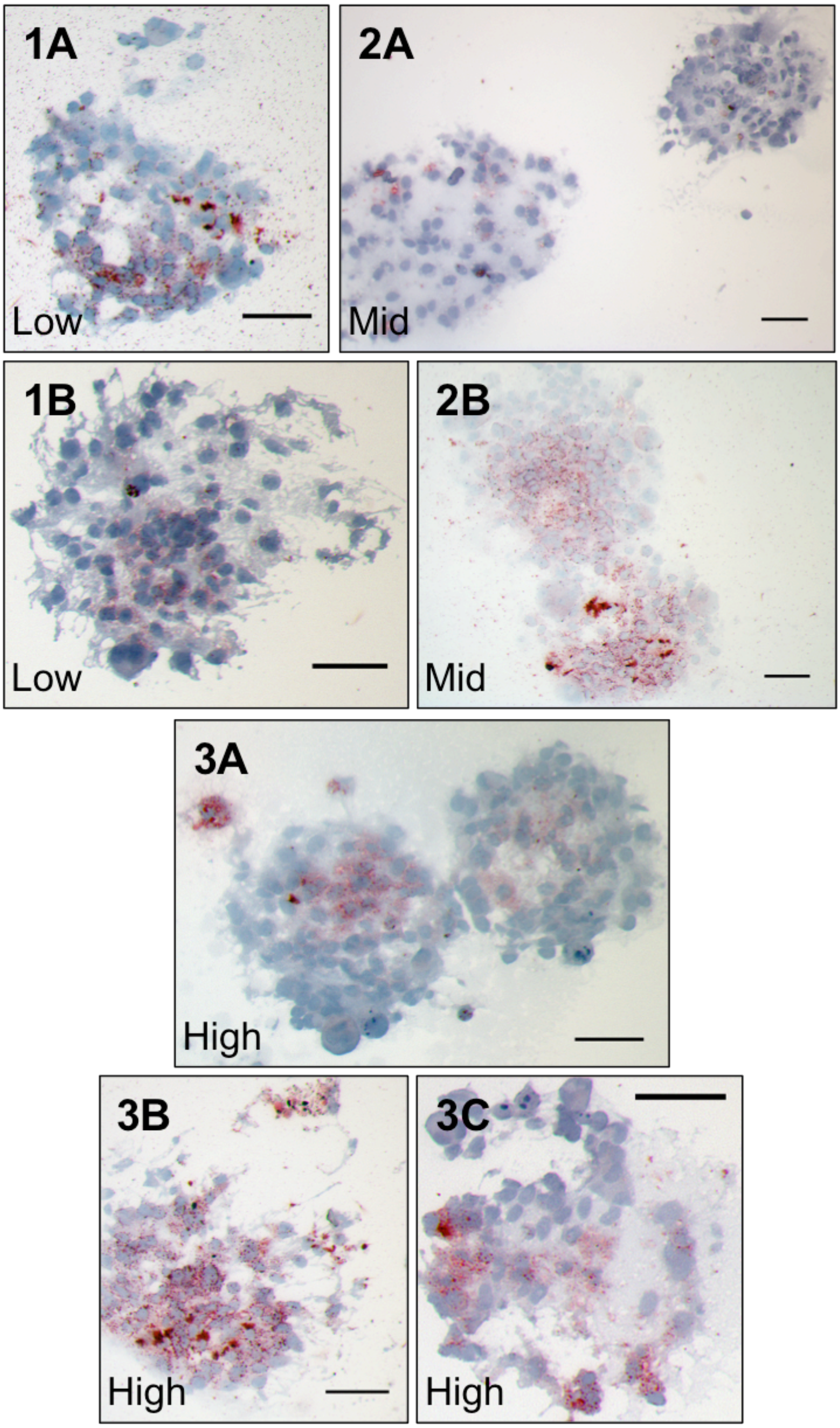

Figure 5.34: Oil red O analysis of 3-dimensional cell spheres of 16.5-day embryonic mouse dermis supplied with BMP4. Sections cut at 10µm and stained with Oil red O and counterstained with haematoxylin after 6 days in culture. (**1**) Low concentration of BMP4, 1ng/ml. (**2**) Mid concentration of BMP4 10ng/ml. (**3**) High concentration of BMP4 100ng/ml. Images taken on a Zeiss Axio Imager M1. Scale bar = 40µm.

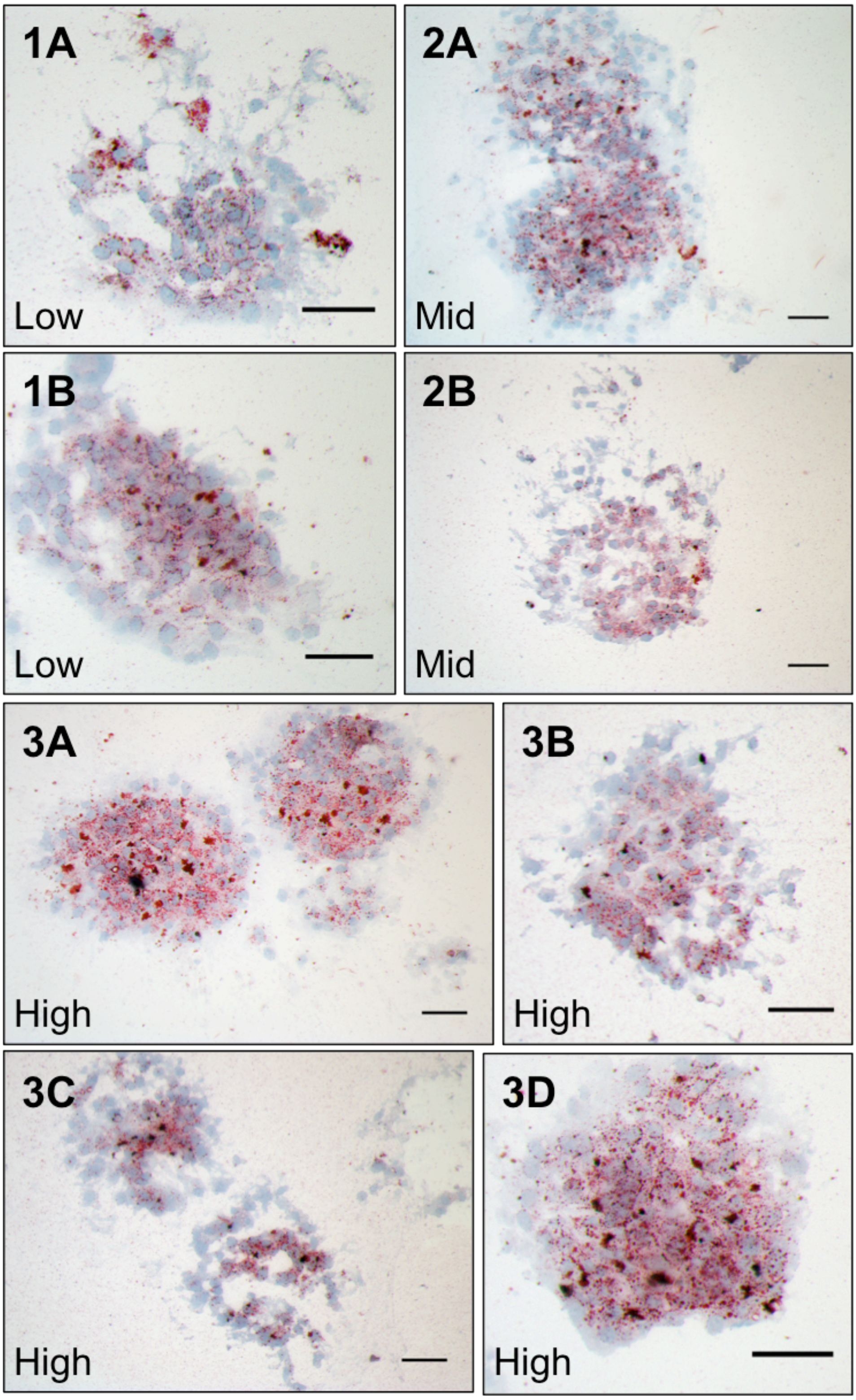

<u>Figure 5.35:</u> **Oil red O analysis of 3-dimensional cell spheres of 16.5-day embryonic mouse dermis supplied with the BMP inhibitor, DMH1.** Sections cut at 10μm and stained with Oil red O and counterstained with haematoxylin after 6 days in culture. (**1**) Low concentration of DMH1 19ng/ml. (**2**) Mid concentration of DMH1 190ng/ml. (**3**) High concentration of DMH1 1.9μg/ml. Images taken on a Zeiss Axio Imager M1. Scale bar = 40μm.

5.3.2.1. Oil Red O Quantification of the TGFβ/BMP Pathway

As well as the EGF/EGFR pathway, the BMP pathway was quantified during establishment of the cell culture method. There was no significant difference between the different conditions in both 3D and 2D (Figures 5.36 and 5.37), which was the same found in culture images.

Table 5.3: Oil red O quantification analysis of 3D and 2D cultures of e16.5 dermal cells under the TGFβ/BMP pathway

	BMP4 low		BMP4 mid		BMP4 high	
3D	0.055	0.062	0.064	0.062	0.057	0.064
	0.052	0.062	0.064	0.066	0.057	0.063
	0.055	0.062	0.066	0.066	0.060	0.060
Mean	0.054	0.062	0.065	0.065	0.058	0.062
	DMH1 low		DMH1 mid		DMH1 high	
3D	0.058	0.058	0.064	0.056	0.056	0.055
	0.059	0.059	0.065	0.055	0.054	0.055
	0.059	0.059	0.064	0.054	0.056	0.053
Mean	0.059	0.059	0.064	0.055	0.055	0.054
	BMP4 low		BMP4 mid		BMP4 high	
2D	0.044		0.053		0.051	
	0.045		0.058		0.051	
	0.043		0.057		0.050	
Mean	0.044		0.056		0.051	
	DMH1 low		DMH1 mid		DMH1 high	
2D	0.051		0.046		0.057	
	0.054		0.044		0.058	
	0.054		0.045		0.057	
Mean	0.053		0.045		0.057	

Average means were calculated for both 3D and 2D.

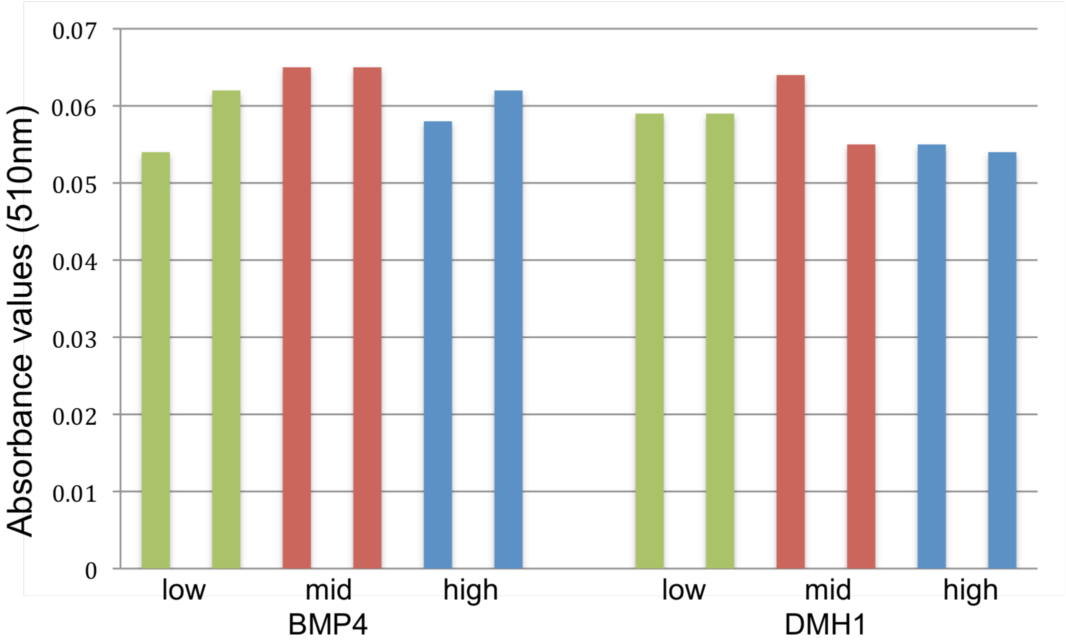

<u>Figure 5.36:</u> Oil red O quantification analysis of 3-dimensional cell spheres put into 2-dimensional culture of 16.5 embryonic-day mouse dermis. BMP4/DMH1 Readings were taken on a nanodrop using UV-Vis software and read at 510nm absorbance. BMP4 and DMH1 values are illustrated.

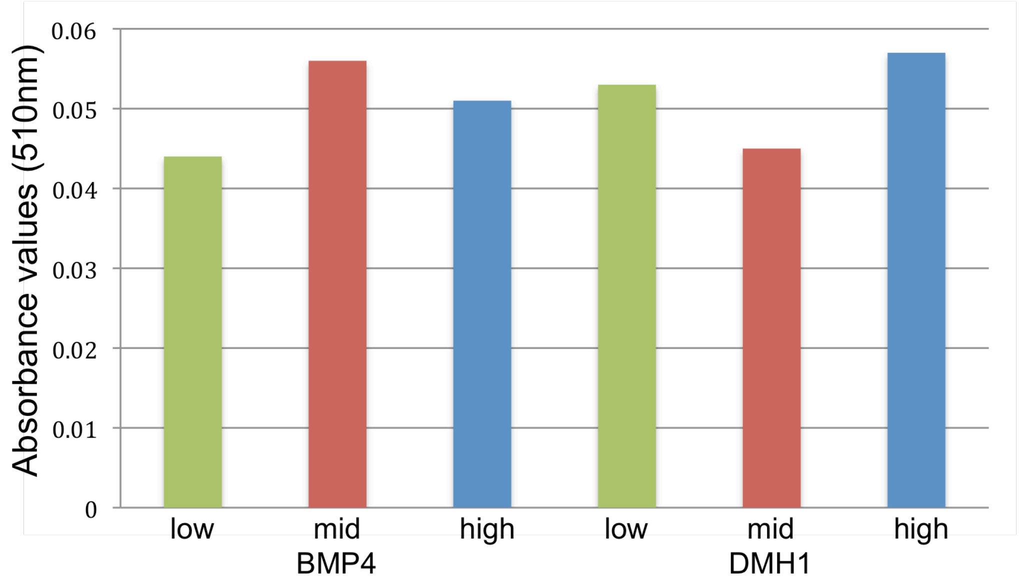

<u>Figure 5.37:</u> Oil red O quantification analysis of 2-dimensional cell culture of 16.5 –day embryonic mouse dermis. BMP4/DMH1 Readings were taken on a nanodrop using UV-Vis software and read at 510nm absorbance. BMP4 and DMH1 values are illustrated.

5.3.3. KGF/KGFR Pathway

Thirdly, the KGF/KGFR pathway was investigated using the cell culture model previously described. KGF was supplied to the cultures at three varying concentrations; 1ng/ml, 10ng/ml and 100ng/ml. Primarily spheres were cultured and later put into 2-dimensionl culture. The spheres supplied with a high concentration of KGF seemed to have an overall larger size than those with the smaller concentrations or no KGF at all (Figure 5.38).

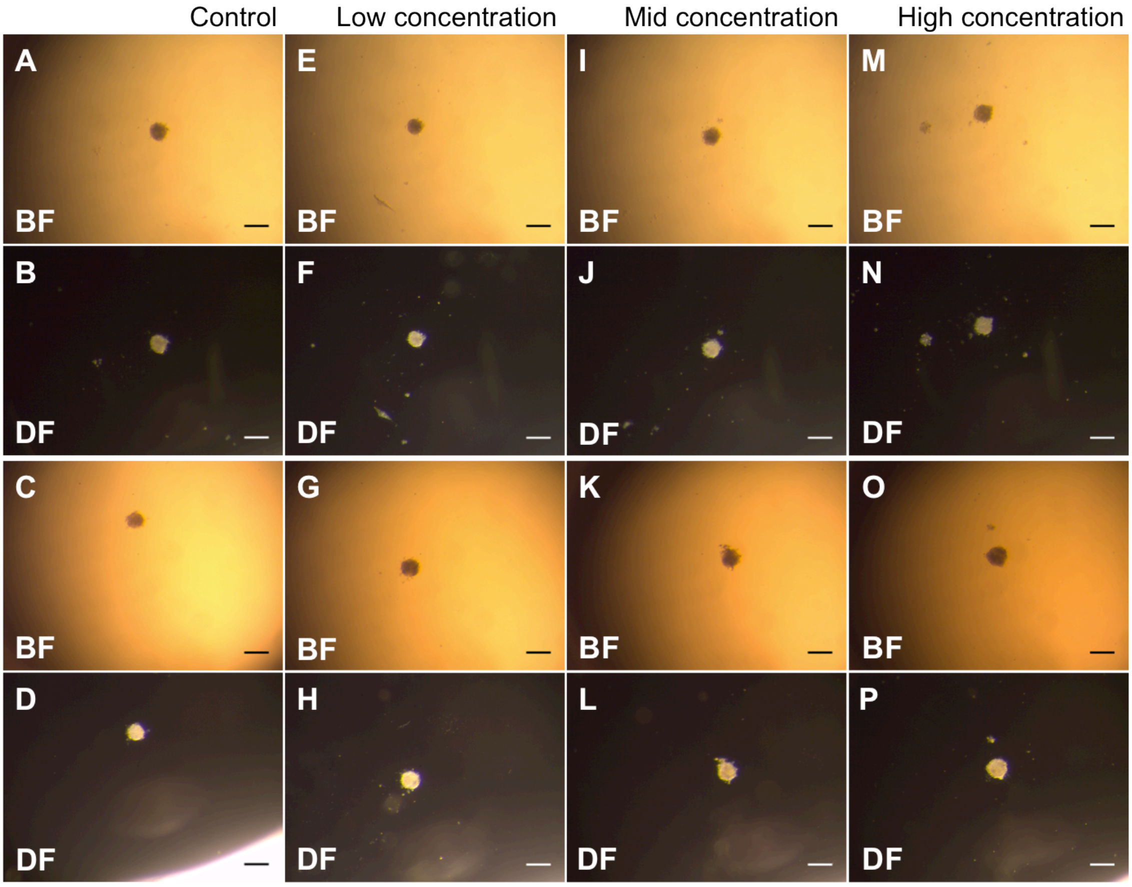

Figure 5.38: 3 dimensional cell culture of 16.5-day embryonic mouse dermis subjected to KGF treatment. (**A-D**) Control spheres. Cultured with DMH1 of 3 different concentrations. Images taken of culture after 6 days. Images taken on a Zeiss Stemi SVII. Scale bar = 0.2mm. BF = bright field. DF = dark field.

From the spheres that were put into 2-dimensional culture, an increase in adipocytes was observed from those spheres treated with KGF (Figure 5.40) compared with those untreated (Figure 5.39). The experiment was repeated twice to produce 3 sets of data and the figures showed representative images across these replicas.

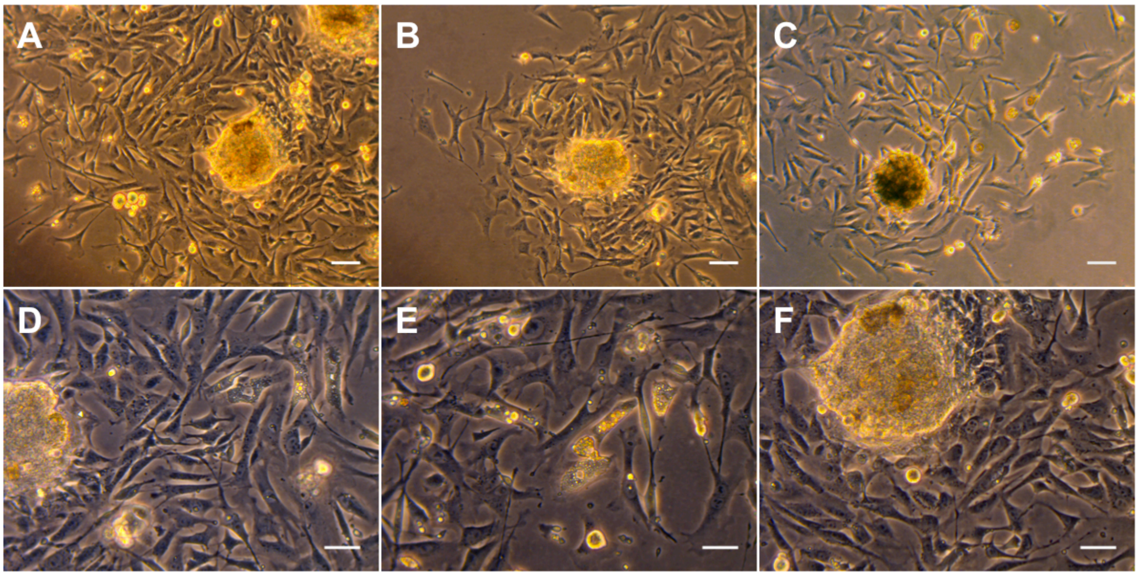

<u>Figure 5.39:</u> 3 dimensional into 2-dimensional cell culture of 16.5-day embryonic mouse dermis. Images taken of culture after 4 days in 3D and 2 days in 2D. Images taken on a Zeiss Axiovert 10. (**A-C**) scale bar = 65μm. (**D-F**) scale bar = 40μm.

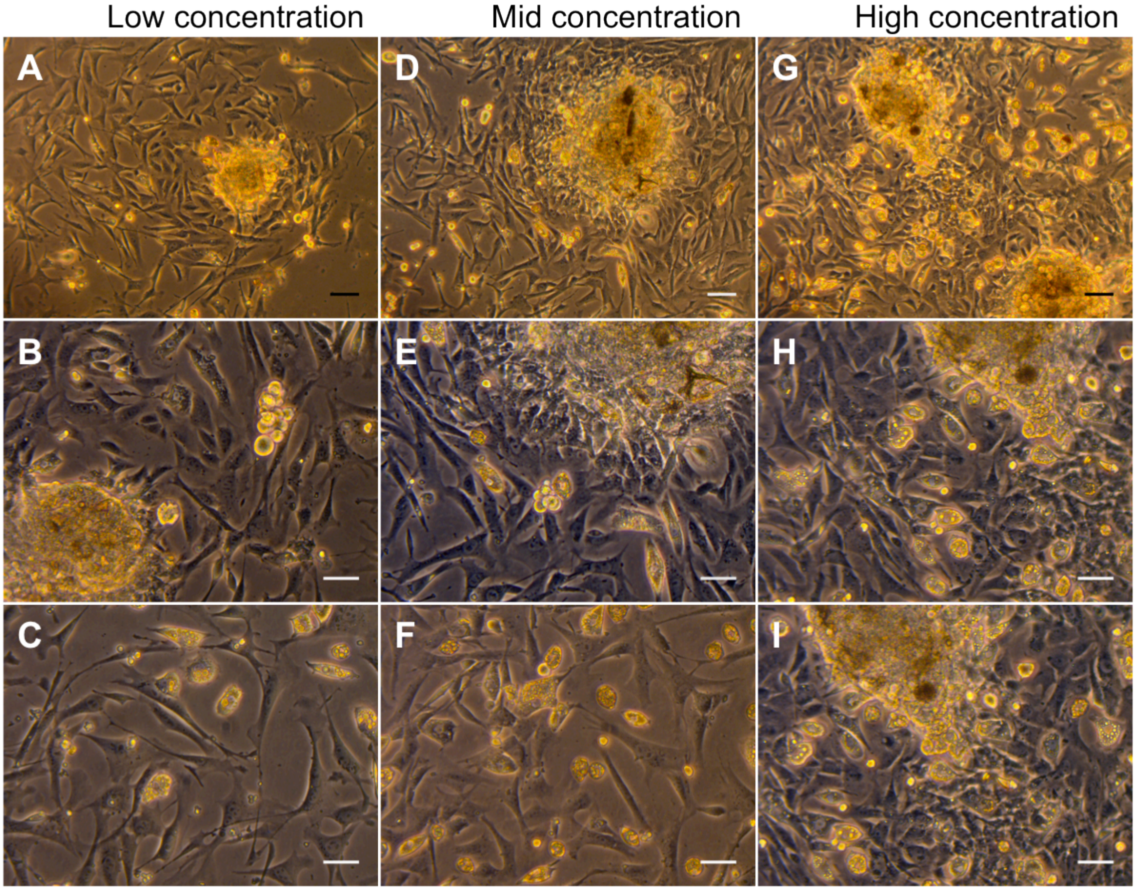

<u>Figure 5.40:</u> 3 dimensional into 2-dimensional cell culture of 16.5-day embryonic mouse dermis supplied with KGF. (**A-C**) Low concentration of KGF. (**D-F**) Mid concentration of KGF. (**G-I**) High concentration of KGF. Pictures taken of culture after 4 days in 3D and 2 days in 2D. Images taken on a Zeiss Axiovert 10. (**A,D,G**) scale bar = 65μm. (**B,C,E,F,H,I**) scale bar = 40μm.

The oil red O staining of these cultures showed that in general across all the spheres there seemed to be an increase in adipocytes present as the concentration of KGF was increased, in particular with the higher two concentrations (Figures 5.42D-I) compared with the controls (Figure 5.41). There were also cells not directly near the spheres, because the cells grew out with more adipocytes in the higher concentrations (Figures 5.42F and I). As well as this, some of the adipocytes within the spheres were more easily, which suggests that not all the adipocytes spread out of the spheres.

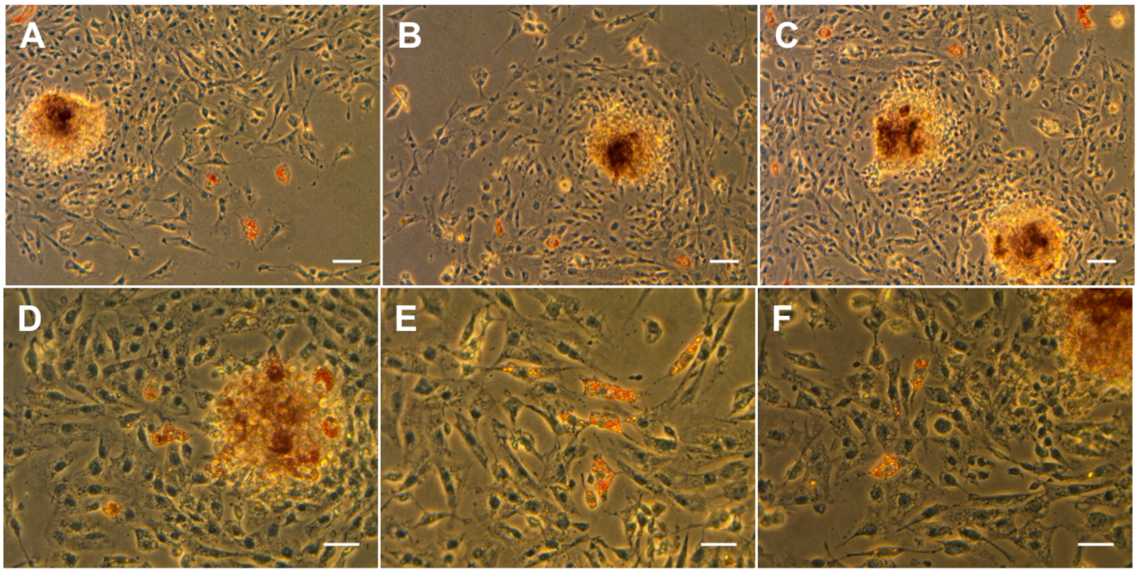

Figure 5.41: **Oil red O analysis of 3 dimensional into 2-dimensional cell culture of 16.5 – day embryonic mouse dermis.** Images taken of culture after 4 days in 3D and 2 days in 2D. Images taken on a Zeiss Axiovert 10. (**A-C**) scale bar = 65µm. (**D-F**) scale bar = 40µm.

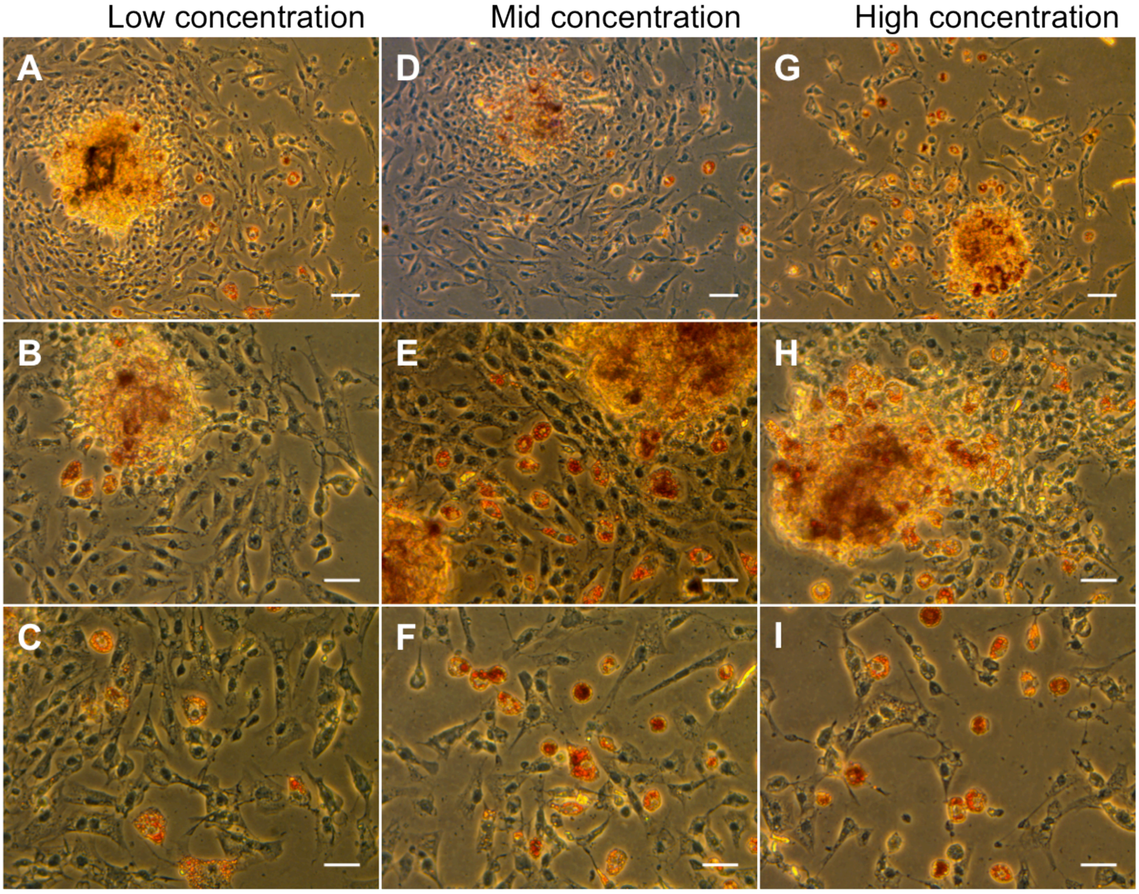

<u>Figure 5.42:</u> Oil red O analysis of 3 dimensional into 2-dimensional cell culture of 16.5-day embryonic mouse dermis supplied with KGF. (**A-C**) Low concentration of KGF. (**D-F**) Mid concentration of KGF. (**G-I**) High concentration of KGF. Pictures taken of culture after 4 days in 3D and 2 days in 2D. Images taken on a Zeiss Axiovert 10. (**A,D,G**) scale bar = 65µm. (**B,C,E,F,H,I**) scale bar = 40µm.

Since the high adipocyte content of the spheres treated with the EGF inhibitor also was associated with low cell survival and overall cell count in the two dimensional culture, the KGF treatments were conducted in 2D culture to see if there was an association between high adipocyte content in 3D and low cell viability in 2D (Figure 5.44). This however was not the case as the cells thrived when treated with all concentrations of KGF. In fact, compared with all other 2D experiments, KGF seems to encourage more fat development in 2D relative to the usual numbers found in 2D in relation to that found in the same treatments in 3D

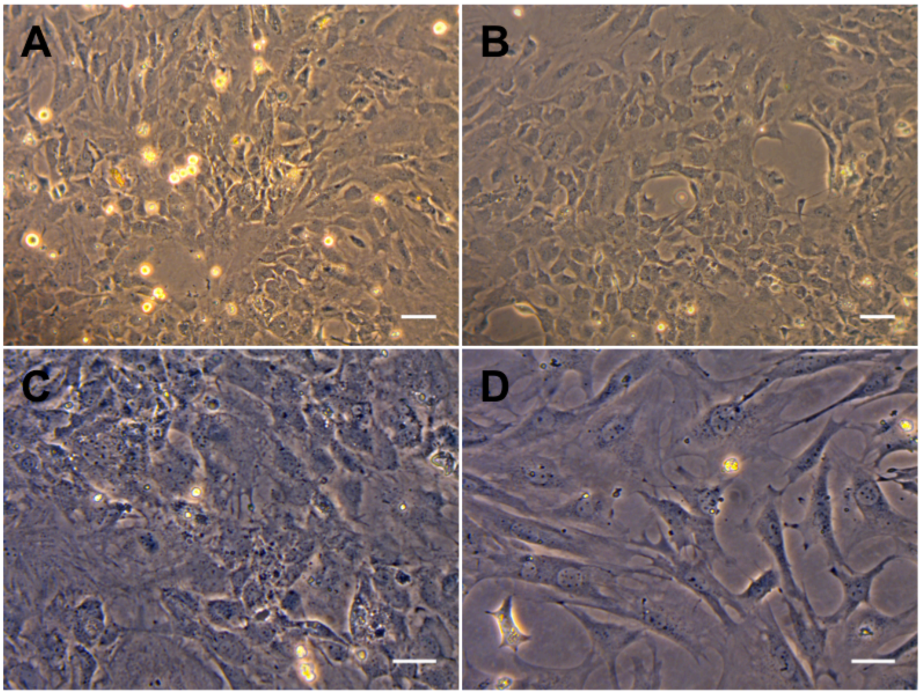

Figure 5.43: **2-dimensional cell culture of 16.5-day embryonic mouse dermis.** Images taken after 6 days in culture. Images taken on a Zeiss Axiovert 10. (**A,B**) scale bar = 65µm. (**C,D**) scale bar = 40µm.

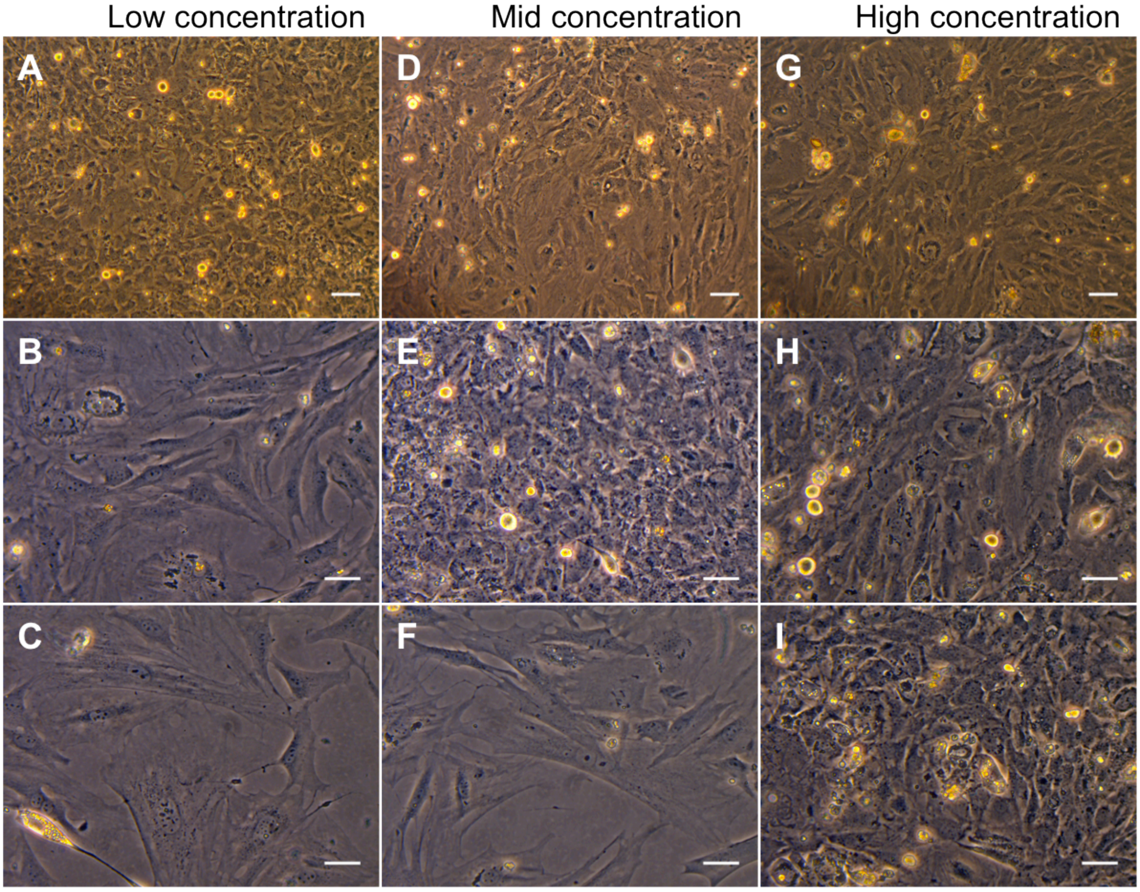

Figure 5.44: **2-dimensional cell culture of 16.5-day embryonic mouse dermis treated with KGF.** (**A-C**) Low concentration of KGF. (**D-F**) Mid concentration of KGF. (**G-I**) High concentration of KGF. Pictures taken after 6 days in culture. Images taken on a Zeiss Axiovert 10. (**A,D,G**) scale bar = 65µm. (**B,C,E,F,H,I**) scale bar = 40µm.

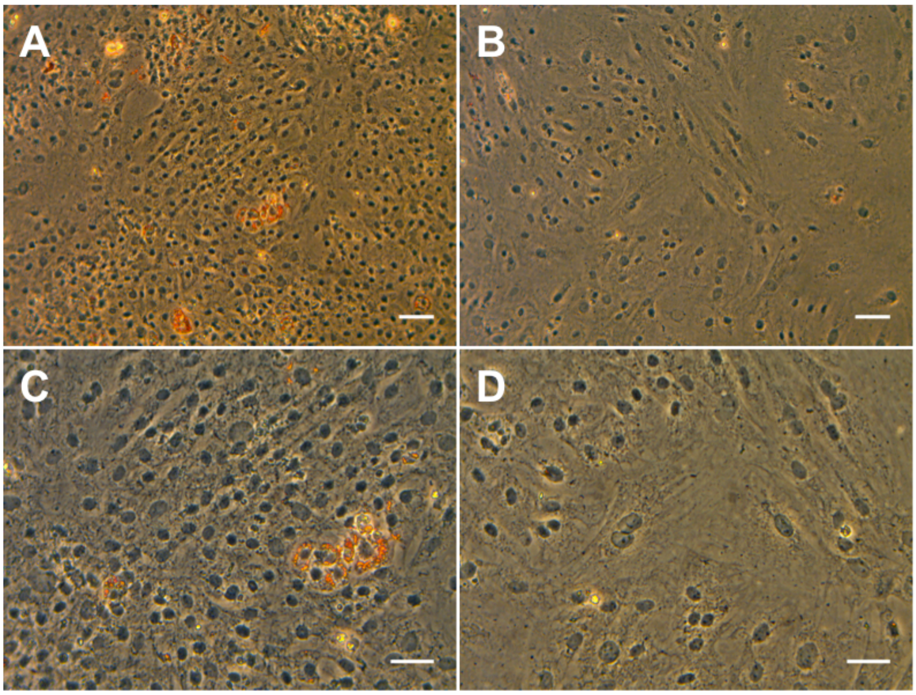

Figure 5.45: **Oil red O analysis of 2-dimensional cell culture of 16.5-day embryonic mouse dermis.** Pictures taken after 6 days in culture. Images taken on a Zeiss Axiovert 10. (**A,B**) scale bar = 65μm. (**C,D**) scale bar = 40μm.

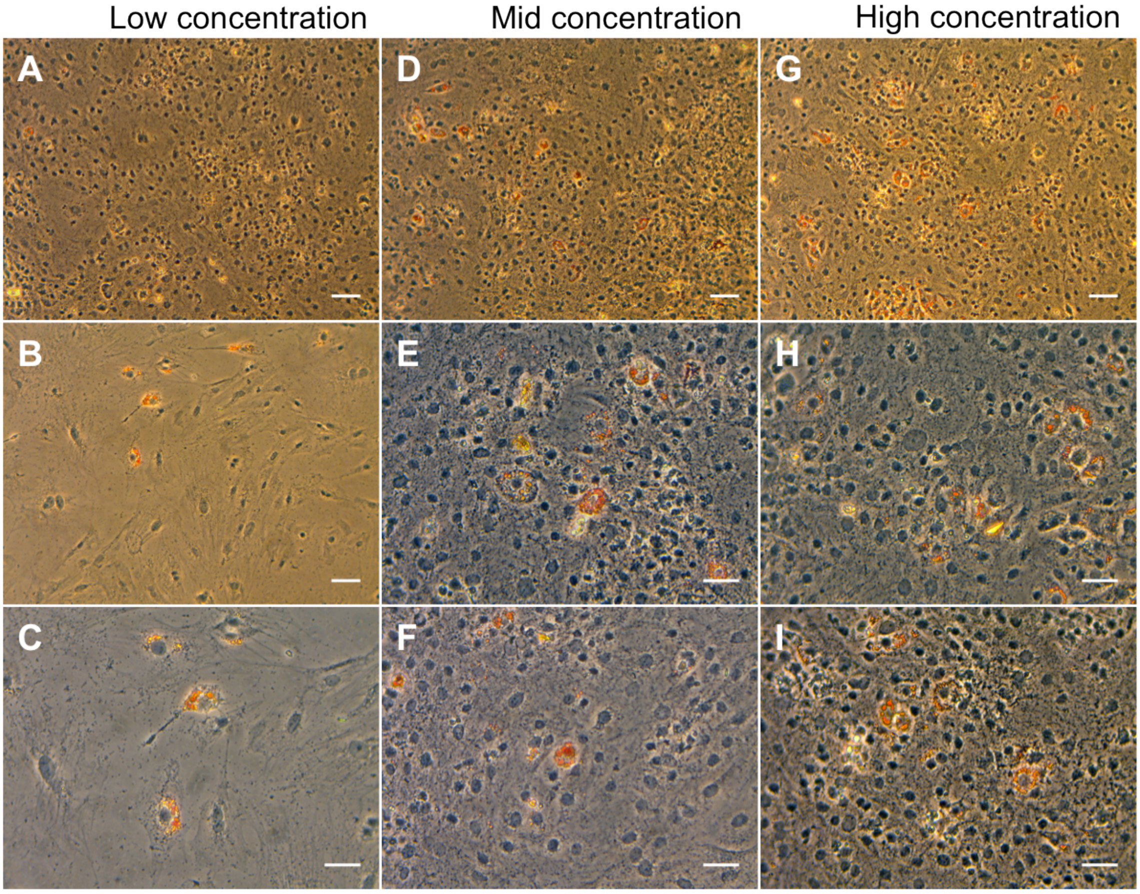

Figure 5.46: **Oil red O analysis of 2-dimensional cell culture of 16.5-day embryonic mouse dermis treated with KGF.** (**A-C**) Low concentration of KGF. (**D-F**) Mid concentration of KGF. (**G-I**) High concentration of KGF. Pictures taken after 6 days in culture. Images taken on a Zeiss Axiovert 10. (**A,B,D,G**) scale bar = 65μm. (**C,E,F,H,I**) scale bar = 40μm.

The 3-dimensional spheres stained with oil red O showed irregular distribution of adipocytes though they tended to group in clusters within the spheres (Figure 5.49). There was substantially more adipocyte staining found in the spheres treated with the mid concentration 10ng/ml of KGF and this tended to be concentrated in the centre of the sphere (Figure 5.49B).

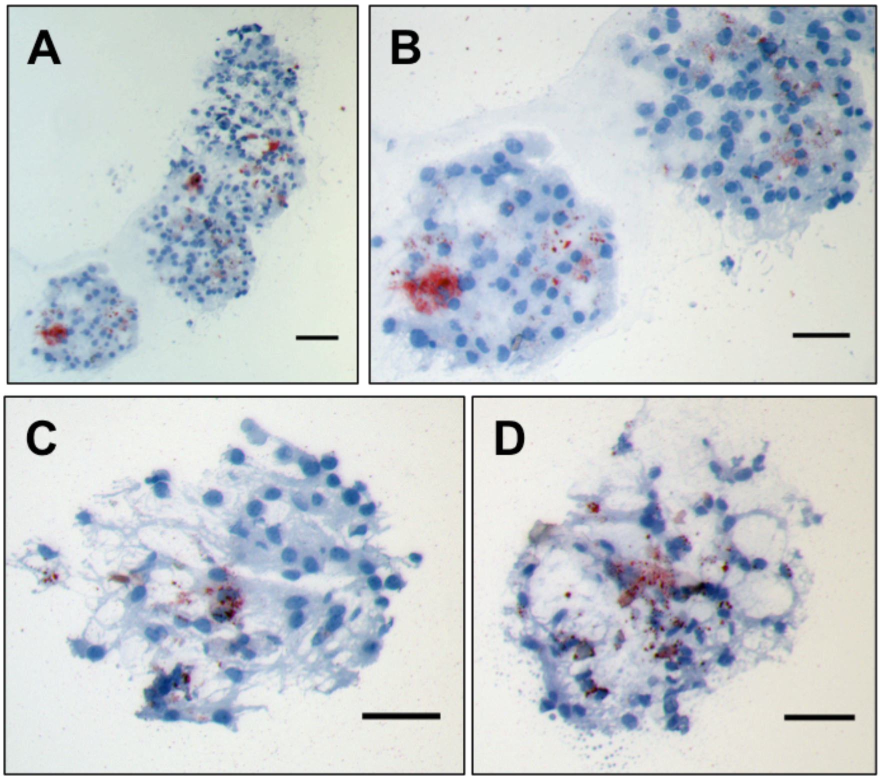

<u>Figure 5.47:</u> Oil red O analysis of 3-dimensional cell spheres of 16.5-day embryonic mouse dermis Sections cut at 10µm and stained with Oil red O and counterstained with haematoxylin after 6 days in culture. Images taken on a Zeiss Axio Imager M1. Scale bar = 40µm.

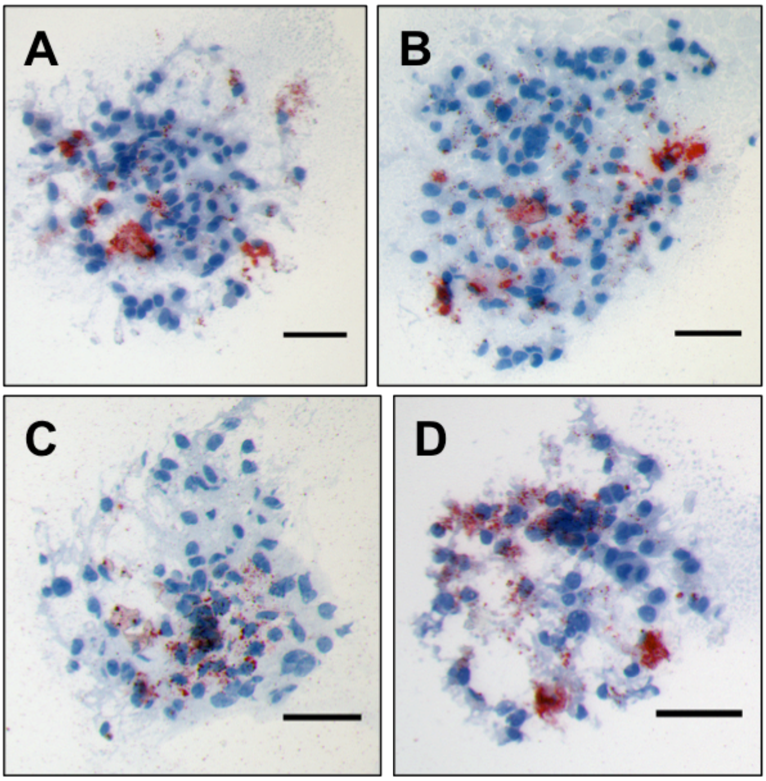

Figure 5.48: Oil red O analysis of 3-dimensional cell spheres of 16.5-day embryonic mouse dermis treated with the low concentration of KGF. Sections cut at 10μm and stained with Oil red O and counterstained with haematoxylin after 6 days in culture. Images taken on a Zeiss Axio Imager M1. Scale bar = 40μm.

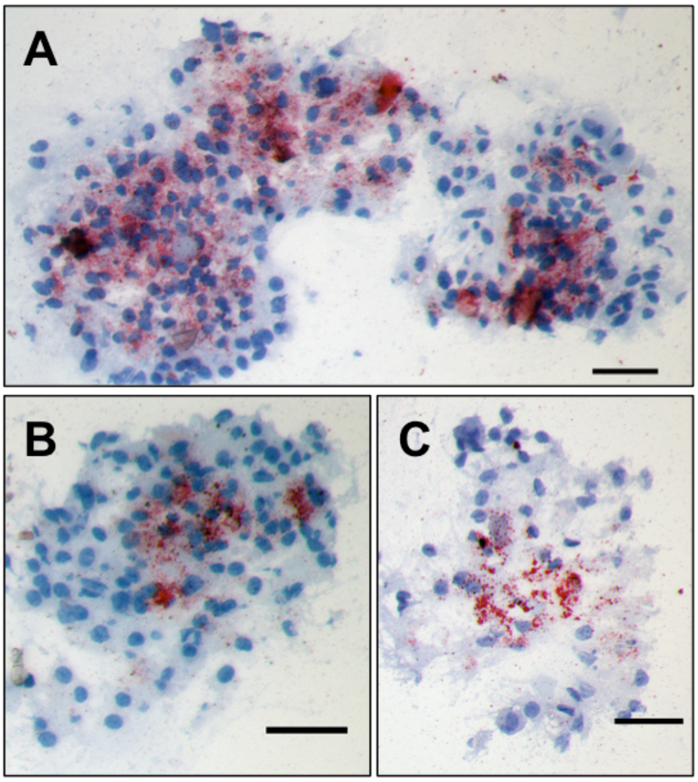

Figure 5.49: Oil red O analysis of 3-dimensional cell spheres of 16.5-day embryonic mouse dermis treated with the mid concentration of KGF. Sections cut at 10μm and stained with Oil red O and counterstained with haematoxylin after 6 days in culture. Images taken on a Zeiss Axio Imager M1. Scale bar = 40μm.

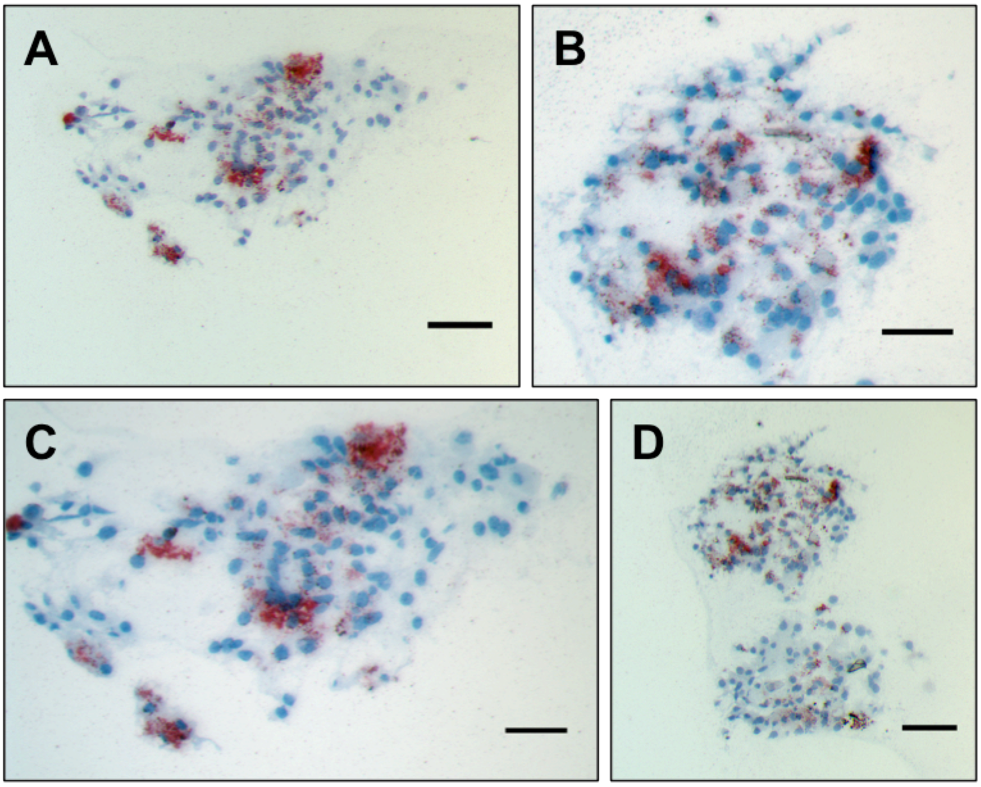

<u>Figure 5.50:</u> Oil red O analysis of 3-dimensional cell spheres of 16.5-day embryonic mouse dermis supplied with the high concentration of KGF. Sections cut at 10μm and stained with Oil red O and counterstained with haematoxylin after 6 days in culture. Images taken on a Zeiss Axio Imager M1. Scale bar = 40μm.

5.3.3.1. EDU Labelling of Spheres

All three KGF concentrations allowed more adipocyte formation than without KGF (Figure 5.47). However, KGF has been implicated in cell proliferation, so it may be that the cell numbers were higher and therefore proportionally there were not more adipocytes. EDU was used to detect proliferation. As described in the methods, a 4 hour pulse of EDU was conducted on spheres treated with KGF (Figure 5.51) and contrasted with spheres not treated with anything to determine if KGF induced more proliferation to occur (Figure 5.52).

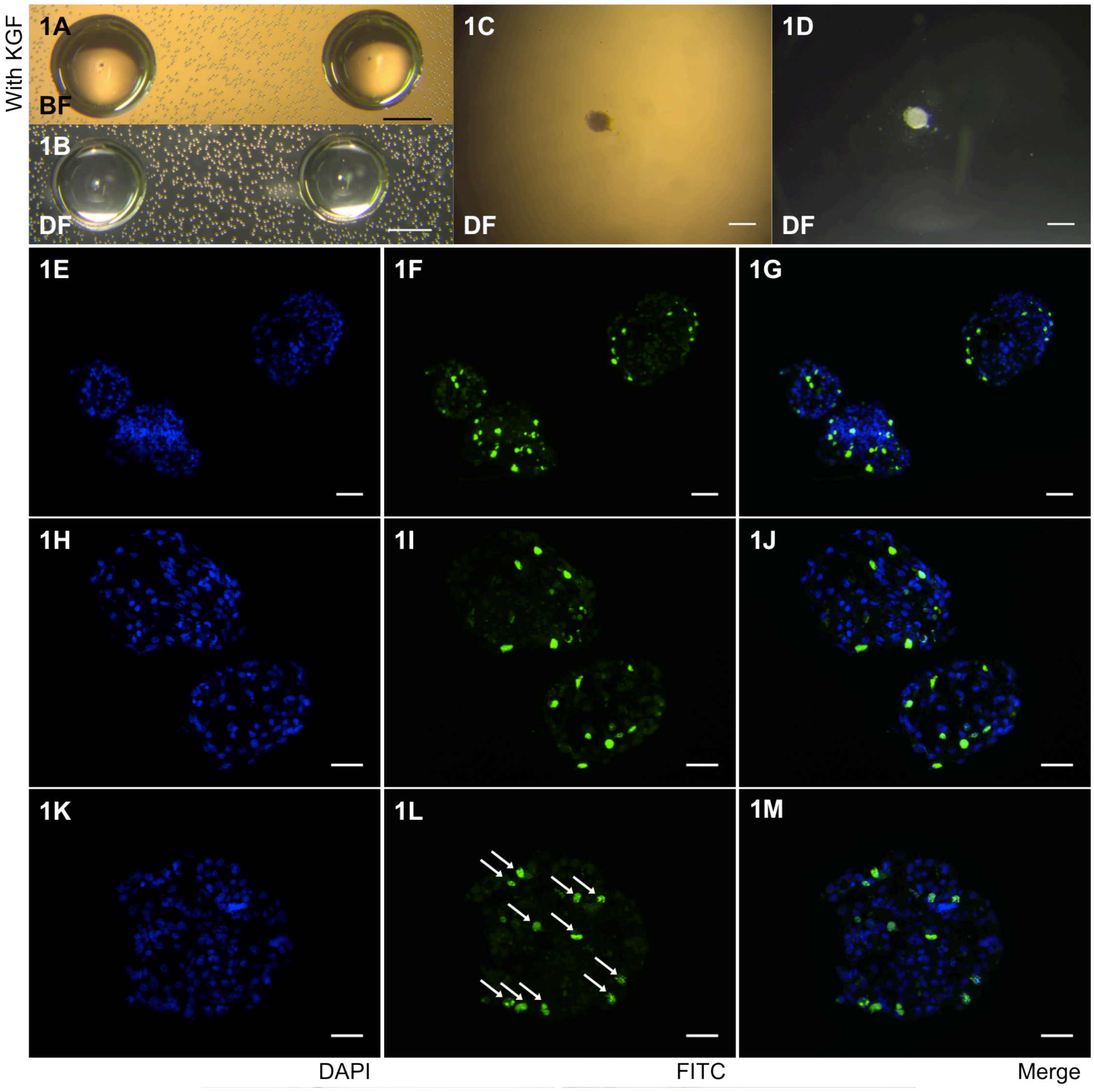

<u>Figure 5.51:</u> Analysis of Cell Proliferation using EDU on e14.5 + 3 day spheres with 10ng/ml KGF. (**1A-D**) Images were taken after 3 days in 3-dimensional culture using Zeiss Stemi SVII with a 4 hour incubation with EDU. (**1E-M**) Sections were cut at 7mm, stained with for EDU labelling and counterstained with DAPI. From left to right; DAPI, FITC, and merge (DAPI/FITC). FITC represents the fluorescent labelling of EDU. Fluorescent images were taken using a Zeiss Axio Imager M1. (**1A,B**) scale bar = 2mm. (**1C,D**) scale bar = 0.2mm (**1E-G**) scale bar= 65µm. (**1H-M**) scale bar = 40µm. Arrows label example positive EDU labelling where cell proliferation has occurred.

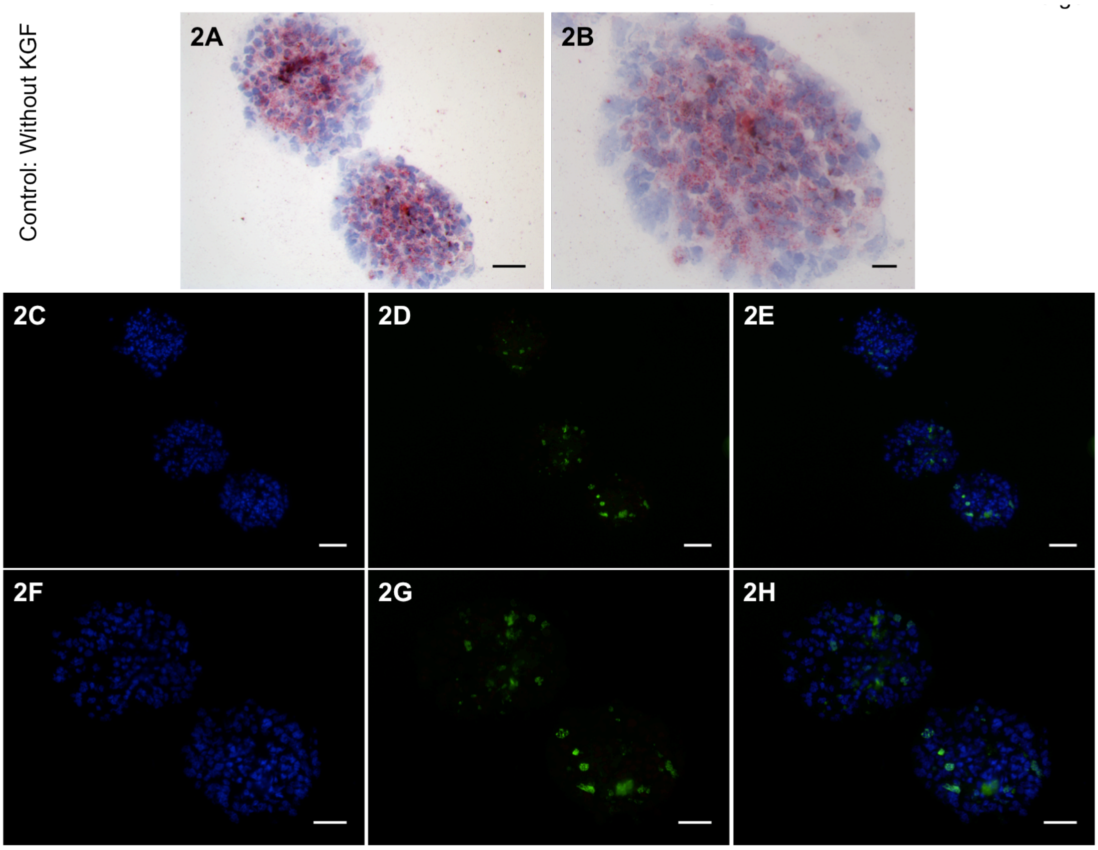

Figure 5.52: Analysis of Cell Proliferation using EDU on control e14.5 + 3 day spheres without KGF. (**1A-D**) Oil red O staining on spheres shows adipocytes (**2A,B**). (**2C-H**) Sections were cut at 7mm, stained with for EDU labelling and counterstained with DAPI. From left to right; DAPI, FITC, and merge (DAPI/FITC). FITC represents the fluorescent labelling of EDU. Fluorescent images were taken using a Zeiss Axio Imager M1. (**2C-E**) scale bar= 65µm. (**2A, F-H**)) scale bar = 40µm. (**2B**) scale bar = 15µm.

In order to quantify if more proliferation occurred in the spheres treated with KGF, three sphere images were taken and the top left quarter of each corner was selected. All the cells and the proportion that was labelled with EDU (green) were counted (Table 5.4).

Table 5.4: Comparison of cell proliferation between spheres treated with KGF and spheres not treated with KGF.

	Total number of cells			EDU labelled cells			Percentage of cells labelled with EDU (%)			Average Percentage (%)
	1	**2**	**3**	**1**	**2**	**3**	**1**	**2**	**3**	
With KGF	29	22	12	3	3	2	10.3	13.6	16.7	13.5
Without KGF	43	29	31	2	1	1	4.65	3.45	3.23	3.78

When the level of proliferation was observed, there was 3.57 fold more EDU present in the spheres treated with KGF, which suggested that KGF was influencing proliferation.

5.4. Discussion

5.4.1. EGF/EGFR Pathway

It was found using the cell culture model that the inhibitor of EGF, AG1478 induced adipocyte formation, while EGF could be thought to inhibit adipocyte formation. There could be many different ways by which this occurs. It is unclear as to whether this pathway is here influencing the commitment or differentiation steps of adipogenesis. That is, the inhibitor may be inducing more cells to become committed or EGF could be inhibiting the preadipocytes from differentiating though they may already be committed. Considering it is becoming increasingly more likely that adipogenesis starts earlier than previously expected prior to embryonic day 16.5 when this pathway was looked at, the more likely scenario is that the cells have already become committed to the adipocyte lineage at this stage and the EGF+ and EGF+ treatments are affecting the differentiation of these cells into terminal adipocytes. EGF disrupts normal hair follicle formation in vitro and in vivo (Philpott *et al.* 1994; Kashiwagi e*t al.* 1997)) and so may change the results of adipogenesis in the culture model due to their linked development (Hausman *et al.* 1981). On the other hand, by e16.5 follicles are already developing so the EGF influence may be too late and therefore acting in a different way

While this result was consistently found with the inhibitor, it seems to be opposite to that previously found using the organ culture model (Wojciechowicz 2012). This is by no means an indication that the results found can be deemed false, but more that it gives an interesting insight into the many roles this pathway may be playing in relation to adipogenesis. For example, it could be that the cell culture model not only has unorganised the dermal cells but also that there are no developing hair follicles or epidermal cells present during culture. Might the EGF/EGFR pathway regulate adipogenesis through the hair follicles or epidermis, thus a different effect is produced when these elements are eliminated? This result therefore could suggest that there is a definite link between adipogenesis and hair follicle formation and/or potential signalling between the epithelial and mesenchymal cell layer. In support of this when the organ culture model was repeated, it was found that when treated with the EGF inhibitor, increasingly defined placodes were observed, which inferred that this is having an effect on the hair follicles. Previous experiments, including the use of knockout mouse models have produced a number of effects on hair follicles which could be observed by the abnormal phenotypes of the hair structures, e.g. Waved-2 (Threadgill *et al.* 1995) or CF-

1 (Yamanishi 1998). It is therefore known that the EGF/EGFR pathway is involved in hair follicle formation, but interestingly this project supports the idea that many of the pathways and their growth factors are having an indirect effect on development, i.e. there is a developmental link between these hair follicles and developing adipose tissue.

As well as this, as Wojciechowicz had previously tried two concentrations and found the skin was unhealthy with one of them, only one concentration of both the activator and inhibitor was used. Considering many growth factors act in a concentration-dependent manner this may influence the results. EGF was found to influence adipocyte formation in a time and dose dependent manner (Hauner *et al.* 1995; Harrington *et al.* 2007). To further the analysis of this pathway, it would therefore be important to experiment with a number of different concentrations to determine if it is indeed concentration-dependent. EGF may already have been expressed and be being produced in culture, thus the addition of more EGF or the inhibitor may be adding to this effect.

The EGF/EGFR signalling pathway is required for normal adipocyte development only during a particular time period of postnatal murine skin development, though microarrays suggest it may be having an earlier influence as well. The inhibitor of EGF, producing a large increase in adipocytes may actually be an abnormal result, in that the normal number of adipocytes that should be produced from these 24,000 cultured cells per well should be a lot less. It is difficult to tell which variable produces more realistic results, e.g. the controls may be equally less realistic, in that they are not in a normal dermis organization. However it was found that addition of EGF to human adipose tissue stromal cells did decrease adipose formation and lipid content (Hauner *et al.* 1995), so perhaps the results here are reliable.

Another characteristic observed from this experiment was that of the 3-dimensional spheres after they had been stained with oil red O and counterstained with haematoxylin. In the dermal cell spheres that had been treated with EGF, the cells appeared to be more tightly packed and the spheres were also larger. This could suggest that EGF had induced cell proliferation to occur (Yaish *et al.* 1988; Anchan *et al.* 1991). As well as this, the cells might spread out or expand prior to differentiation into adipocytes. There might therefore be a link between proliferation or cell number with a decrease in adipocyte formation. Are the developing adipocytes more spread out or outcompeted by the proliferating fibroblasts? Cell-to-cell signalling may also be playing a role here in producing an adipose depot (Section 4.4).

5.4.2. TGFβ/BMP Pathway

Out of all three pathways looked at, this pathway showed the least distinctive results, i.e. there was not a significant difference between the controls and either activator or the inhibitor. Unlike the EGF/EGFR pathway, three different concentrations of both BMP4 and the BMP receptor inhibitor, DMH1 were experimented with to prevent concentration-dependence being a determining factor of the results given. There was little difference as the concentration was changed, also shown when the oil red O was quantified. Rather than this suggesting that members of the BMP pathway do not act in a concentration-dependent manner it may be that the pathway is not playing a role at this point in development: it could be acting earlier or later. To further the investigation of this pathway, which has been implicated in adipogenesis, it would be valuable to look at its effects earlier in development, by using this model and conducting microarray analysis earlier than e17 (Wojciechowicz 2012).

There was clearly a greater degree of red staining of the spheres than controls of those that were not put into 2-dimensional culture, but stained in 3-dimensional intact spheres. Perhaps the 2-dimensional culture technique is having more of a difference on the BMP pathway than the other pathways? It is known that the BMP pathway is involved in pattern formation (Pearson *et al*. 2005), so the lack of effects may be due to the fact that it only works when localised in the correct position and in cell culture the cells are not in a realistic organisation and so the BMP pathway is not effective.

Little or no effect does not necessarily deem these experimental results incorrect; it could infer that the BMP pathway regulated by the release of BMP4 is not necessary to adipogenesis at this stage of the process, e16.5. It would be interesting not only to look at this pathway at different time points, but also using a different model, like that of the organ culture model. BMP may only have an impact if the BMP receptors are present in great numbers or if other ligands are not binding to it. A different BMP inhibitor, e.g. AMPK could also be investigated in the future. A possibility is that endogeneous BMP may be enough to satisfy the BMP receptors and therefore any addition is not influencing the development (Macotela *et al.* 2012).

5.4.3. KGF/KGFR Pathway

Like that found in the transgenic mice where the level of expression determined the degree of hair follicle loss and epidermal thickness, KGF seems to work in a concentration-dependent manner, which has been previously been suggested as the theory behind its effect on hair follicle morphogenesis (Botchkarev *et al.* 1999; Richardson *et al.* 2009). As well as this, the effects of KGF were concentration-dependent when using 3T3-L1 cells and rat primary preadipocytes (Zhang *et al.* 2010). Some of the spheres were larger with the higher concentration, which links in with KGF previously being found to be involved in proliferation (Zhang *et al.* 2010). *In vitro*, KGF is significantly more able to generate proliferation of keratinocytes than EGF or TGFα (Guo *et al.* 1993). KGF may not be acting alone but also with TGFα. EDU was used to understand the proliferative activity in the KGF spheres to see if when keratinocytes are eliminated, proliferation still occurs in the fibroblasts. While usually there is limited cell proliferation in 3D sphere culture, the cells induced with KGF were found to proliferate (Section 5.3.3.1). However, there was also some proliferation detected in the control spheres without KGF. The spheres were not treated with a pulse of EDU till after a couple of days because the spheres had not formed, however there may have been an initial burst of proliferation when KGF was first supplied. If this is the case, the EDU did not measure this, but instead its proliferation at a later stage. In order to establish if this is the case, a method of measuring the proliferation rate at the beginning of KGF treatment should be used. This may be difficult in the spheres considering they don't aggregate till after 48 hours or often longer. This could potentially be tested in the organ culture method, or by separating the dermis from the epidermis and culturing solely the dermis in one piece, rather than the whole skin or needing to dissociate the dermal cells. Cell proliferation may be that KGF triggers preadipocyte cells to multiply so more adipocytes are produced. It could be useful to track the cells that proliferate and determine if they all become adipocytes, because not all the cells in the dermis become adipocytes.

In contrast to the EGF/EGFR pathway, those treatments that produced more adipocytes also thrived in 2-dimensional culture. While KGF and EGF roles are more so understood in relation to their roles in epidermal development, it has been suggested that mesenchymal development is influenced by this, e.g. through the hair follicles, so as described in terms of the EGF/EGFR pathway they may be having indirect effects on adipogenesis in the lower dermis of the skin. KGF knockout mice clearly show that it is important in hair follicle formation (Guo *et al.* 1996). As KGF inhibits follicle development, using it to block early follicle development in organ culture, could be useful to prevent the follicles influence the study of adipogenesis. A preliminary experiment showed it is possible to inhibit follicle growth around e13.5. This might now be a useful method to look at how much adipose tissue develops in culture after the follicles have been eliminated. It may also be useful to clarify the distribution of the FGFR2 receptors; are they present on adipocytes or mesenchymal cells as well as keratinocytes or is this how the regulation is mediated through epithelial cells? It has previously been found that the FGFR2b isoform (KGFR) is found on epithelial cells while FGFR2c is found on mesenchymal cells (Orr-Urtreger *et al.* 1993; Eswarakumar and Schlessinger 2005). This has been thought to allow an interaction between the epithelial and mesenchymal tissue layers during development (Eswarakumar and Schlessinger 2005). This would further support the idea that responses to KGF may be mediated through the epithelium rather than directly affecting the dermis.

KGF (FGF7) is not the only FGF that could be involved in adipogenesis. If you impact KGF activity this may be influencing the expression and effects of other growth factors and interacting signalling pathways. Western blotting could be used to look at the levels of different growth factors after KGF treatment and it would also be useful to observe endogenous levels of KGF already present.

5.4.4. In Conclusion

There are many general observations, which apply to all the pathways. For example, it has been noticed that often the adipocytes are found in clusters and are not evenly distributed throughout the cultured cells. As the adipocytes in vivo form a layer, this could be put down to cell-to-cell signalling either to trigger each other's development or for them to group together. Having been dissociated before being put into culture the cells might be reorganizing into a general upper and lower dermis distribution.

While this chapter has shown some interesting results, they are by no means conclusive. Not only have they provided more insight into potential avenues that need to be explored, they have also posed questions over what is already known. For example, the clear increase in adipocyte development when treated with an EGF inhibitor compared with little or no development when treated with EGF. This is a surprising result, but one that should not be ignored. Like that found in chapter 4 whereby the cells seem to develop into adipocytes a lot earlier than previously expected, it is appropriate to not only investigate gene expression much earlier, around e13/13.5 but also at the influence these signalling pathways may be having earlier as well. Are their effects limited to a certain time point? Do they act differently earlier in development? Not only this, but whether these signalling pathways act in the same way in a different model e.g. the organ culture model. E14.5 spheres were capable of producing fat. It has already been shown by Wojciechowicz (2012) in relation to the EGF/EGFR pathway, though are the effects similar with different pathways with this organ culture model?. It may be that the fact that the epidermis and developing hair follicles are present and capable of influencing the results is what is determining how the signalling pathways act. The activator and inhibitor treatments are unspecific as both the epidermis and dermis receive the signals. On the other hand, the organization of the cells in the cell culture model, which are less realistic than that of the dermal cells in the organ culture model may be the reason for the way these cells respond to the signalling pathways. The organ culture model showed that the effects of EGF were limited to certain time-points, i.e. beyond e18/19 the treatments had no effect on adipose tissue development (Wojciechowicz 2012). Perhaps there is a degree of inhibition of adipogenesis in the skin, which is unable to occur when the cells are dissociated and disorganized in the cell culture model. The development of a successful model, however, is fundamental to the study of adipogenesis and useful for the functional study of genes so to better understand the pathways involved in dermal adipose tissue development. It could be concluded from the development and use of this cell culture model that a number of different types of model should be used in conjunction with each other to build up a better picture of the control adipogenesis.

The results of the inhibition and activation using receptor ligands may not actually depend on the level of endogenous ligands supplemented, but in actual fact the number of receptors present and capable of receiving these growth factors. How much of the growth factor supplied is used by the cells?

While only three different pathways were used in this project, it is important to be aware that there are many other signalling pathways implicated in adipogenesis e.g. the Wnt pathway (Christodoulides e*t al.* 2008). As well as looking at their individual roles, how they interact is an interesting factor (Kanazawa *et al.* 2005; Christodoulides *et al.* 2008). It seems the pathways can influence each other to generate an overall effect, thus combining different growth factor inhibitor and activator treatments may be an insightful experiment to develop our understanding of this process of adipocyte formation and how the pathways impact each other.

Background research into these pathways shows that their roles in hair follicle formation are better characterized and it is less clearly defined whether and what roles these pathways might have in adipogenesis. Guo *et al.* (1993) did however show that there was suppression of both hair follicles and adipogenesis alongside each other when targeted expression of human KGF cDNA in mice was used. This suggests that there is a degree of interaction between these two processes, which is increasingly becoming the consensus (Jahoda *et al.* 2003; Schmidt and Horsley 2013).

CHAPTER 6:

Closing Discussion and Further Experiments

Many signalling pathways and factors regulate the process of adipogenesis. Extracellular signals trigger transcriptional cascades to occur. Not only this, but the cells interact with each other to organise the tissues. Development is therefore a very complex process. While there is a great deal still to understand about adipogenesis, in particular, the dermal adipose layer, this project focused on particular aspects of the process and developing a suitable model to study adipogenesis earlier than e17. It is easier to study the later stages of differentiation when morphological changes have started to occur, but what induces and regulates the commitment to the adipocyte lineage step is more difficult to investigate. Microarrays previously conducted started at embryonic day 17 and examined the lower dermis. However, this project showed that adipocytes can form from cells taken as early as embryonic day 14.5 and previously adipocytes formed in the kidney capsule from cells taken from e14 (Wojciechowicz *et al.* 2013). The cells are already committed, or perhaps all dermal cells are capable of becoming adipocytes and those in the upper dermis require a negative signal. With the production of upper dermis microarrays and the genes flagged up strongly in these, future work can aim to investigate this hypothesis of a negative signal on adipogenesis.

What triggers the difference between the upper and lower dermis? Is it a signal from the dermis or epidermis or even the epithelial part of the follicle. Simply, to investigate adipocyte development, it is necessary to find out what signals are directly influential. It is important to consider that other cell types may be involved in the development, e.g. hair follicles and blood vessels as well as their process of development may be implicated in adipogenesis (Hausman *et al.* 1981).

This project removed the epidermis to observe what occurs in the dermis independently. Adipocytes successful formed from the dermal cells and were influenced by growth factors, e.g. EGF and KGF. Next, it would be interesting to investigate how the epithelial and mesenchymal components influence each other. Dermis, taken from a non-fat producing mouse could be recombined with a wild-type epidermis and wild-type dermis recombined with a non-fat producing mouse epidermis and observed to see which one produces adipocyte development. This should be tried at different ages to show when the dermis becomes committed. Literature research was conducted to find a mouse model that does not produce fat tissue in the skin to provide the tissue for this experiment. Elbe-Bürger and colleagues (2002) found that overexpression of Interleukin-4 (IL-4) causes loss of the dermal adipose tissue. This IL-4 transgenic mouse could be used in a recombinant experiment. When Interleukin-7 (IL-7) is overexpressed, adipose tissue is also reduced (Lucas *et al.* 2012).

Cells are thought to be committed to the adipocyte lineage earlier than e16.5, according to this project (Chapters 4 and 5) The upper and lower dermis may be being establishing at the time of hair follicle formation. However what markers can be used to follow this? Perhaps microarrays can now be conducted earlier than e17.

Adipocytes only form in the lower dermis. Originally this project aimed not only to separate the dermis from the epidermis and look at solely dermal effects, but also what signals a difference between the upper and lower dermis. However, creating the cell-culture model was a time-consuming process. FABP4 labelling of the lower dermis has suggested that it has already separated from the upper dermis by e16/e17 (Wojciechowicz et al. 2013), though it may be that differences develop even earlier in association with hair follicle initiation. A potential way to investigate this is by a recombination type experiment. The dermis is flipped so that the lower dermis interacts with the epidermis and the upper dermis becomes the lower dermis, to see what effect this has on which cells turn into fat in the dermis. This may also enable a better understanding of the timings at which the lower dermal cells become committed. There is however, a muscle layer (panniculus carnosus) which could prevent this experiment from being successful, thus this may need to be taken out of the equation first. Using a transgenic mouse without this muscle layer so only the dermis is in contact with the epidermis and not muscle tissue.

There is an obstacle in terms of hair follicle formation and the influence it has on adipogenesis. Are the signals indirect to the preadipocytes? The hair follicle specific signals could be separated out. Blocking pathways may be blocking follicles at an early stage, and this could be influencing adipogenesis and not the signals directly. With follicles, later stages are better because the signals for formation have already been received, which is why e16.5 was investigated. Another potential experiment could be conducted with a mouse model that does not develop follicles to prove if there is follicular involvement. Or an early blocking agent of hair follicle formation, e.g. KGF could be used in organ culture. For example, KGF could be supplied at e13.5 to block follicle formation before looking at dermal adipose tissue development. However, it may be difficult for the skin to continue to grow and survive after this treatment: the presence of the hair follicles may be necessary to accurately observe the functions of different growth factors and signalling pathways in adipogenesis. Either way, it could provide a useful insight.

While increasing progress is being made, there is still extensive research that needs to be done to understand the adipose organ, both its origins and processes of development. Knowledge of the timing and localization of many events would be greatly improved with the availability of markers specific to MSCs and preadipocytes (Gesta *et al*. 2007). Microarray data and antibody labelling of those found to be upregulated might help to find suitable markers. Use FACs and CD36 to separate the upper and lower dermis and evaluate if signalling occurs between the upper and lower dermis to prevent all the cells differentiating. It was often found in this project that in the spheres, clusters of cells differentiated into adipocytes, so potentially there is a degree of cell-to-cell signalling. To investigate if all the cells are capable of differentiating or if cells are early committed, adipogenic medium can be applied to all the cells to see if they all differentiate.

Bibliography

Aaronson, S.A., Bottaro, D.P., Miki, T., Ron, D., Finch, P.W., Fleming, T.P., Ahn, J., Taylor, W.G. & Rubin, J.S. (1991) Keratinocyte growth factor: a fibroblast growth factor family member with unusual target cell specificity. *Annals of the New York Academy of Sciences;* **638,** 62-77.

Adachi, H., Kurachi, H., Homma, H., Adachi, K., Imai, T., Morishige, K., Matsuzawa, Y. & Miyake, A. (1994) Epidermal growth factor promotes adipogenesis of 3T3-L1 cell in vitro. *Endocrinology;* **135,** 1824–1830.

Ahn, J., Oh, S-A., Suh, Y., Moeller, S.J. & Lee, K. (2013) Porcine G0/G1 Switch Gene 2 (G0S2) Expression is Regulated During Adipogenesis and Short-Tern In-Vivo Nutritional Interventions. *Lipids;* **48,** 209-218.

Ali, A.A., Weinstein, R.S., Stewart, S.A., Parfitt, M., Manolagas, S.C. & Jilka, R.L. (2005) Rosiglitazone Causes Bone Loss in Mice by Suppressing Osteoblast Differentiation and Bone Formation. *Endocrinology;* **146(3),** 1226-1235.

Allison, R. Spheroid Cultures for Cancer Research and Treatment. *Safer Medicines Campaign;* Available from www.safermedicines.org/reports/Perspectives/vol_2_1990/Spheroid.html [Accessed August 2014].

Anchan, R.M., Reh, T.A., Angello, J., Balliet, A. & Walker, M. (1991) EGF and TGF-α stimulate retinal neuroepithelial cell proliferation in vivo. *Neuron;* **6(6),** 923-936.

Atit, R., Sgaier, S.K., Mohamed, O.A., Taketo, M.M., Dufort, D., Joyner, A.L., Niswander, L. & Conlon, R.A. (2006) β-catenin activation is necessary and sufficient to specify the dorsal dermal fate in the mouse. *Developmental Biology;* **296(1),** 164-176.

Avram, A.S., Avram, M.M. & James, W.D. (2005) Subcutaneous fat in normal and diseased states: 2. Anatomy and physiology of white and brown adipose tissue. *Journal of the American Academy of Dermatology;* **53(4),** 671-683.

Bachner, D., Ahrens, M., Schroder, D., Hoffmann, A., Lauber, J., Betat, N., Steinert, P., Flohe, L. & Gross, G. (1998) Bmp-2 downstream targets in mesenchymal development identified by subtractive cloning from recombinant mesenchymal progenitors (C3H10T1/2). *Developmental Dynamics;* **213,** 398-411.

Banerjee, S.S., Feinberg, M.W., Watanabe, M., Gray, S., Haspel, R.L., Denkinger, D.J., Kawahara, R., Hauner, H. & Jain, M.K. (2003) The Krüppel-like factor KLF2 inhibits peroxisome proliferator-activated receptor- gamma expression and adipogenesis. *Journal of Biological Chemistry;* **278,** 2581–2584.

Barak, Y., Nelson, M.C., Ong, E.S., Jones, Y.Z., Ruiz-Lozano, P., Chien, K.R., Koder, A. & Evans, R.M. (1999) PPAR gamma is required for placental, cardiac, and adipose tissue development. *Molecular Cell*; **4**, 585–595.

Billon, N., Iannarelli, P., Monteiro, M.C., Glavieux-Pardanaud, C., Richardson, W.D., Kessaris, N., Dani, C. & Dupin E. (2007) The generation of adipocytes by the neural crest. *Development;* **134,** 2283–2292.

Billon, N., Monteiro, M.C. & Dani, C. (2008) Developmental origin of adipocytes: new insights into a pending question. *Biology of the Cell;* **100(10),** 563-575.

Birsoy, K., Chen, Z. & Friedman, J. (2008) Transcriptional Regulation of Adipogenesis by KLF4. *Cell Metabolism;* **7,** 339-347.

Birsoy, K., Berry, R., Wang, T., Ceyhan, O., Tavazoie, S., Friedman, J.M. & Rodeheffer, M.S. (2011) Analysis of gene networks in white adipose tissue development reveals a role for ETS2 in adipogenesis, *Development;* **138(21),** 4709-4719.

Bishop-Bailey, D. & Wray, J. (2003) Peroxisome proliferator-activated receptors: a critical review on endogenous pathways for ligand generation. *Prostaglandings and Other Lipid Mediator;* **71(1),** 1-22.

Bjare, U. (1992) Serum-free cell culture. *Pharmacology and Therapeutics;* **53,** 355-374.

Botchkarev V.A. (2003) Bone Morphogenetic Proteins and Their Antagonists in Skin and Hair Follicle Biology. *Progress in Dermatology;* **120,** 36-48.

Botchkarev, V.A., Botchkareva, N.V., Roth, W., Nakamura, M., Chen, L-H., Herzong, W., Lindner, G., McMahon, J.A., Peters, C., Lauster, R., McMahon, A.P. & Paus R. (1999) Noggin is a mesenchymally-derived stimulator of hair follicle induction. *Nature Cell Biol* **1.** 158-164.

Botchkarev, V.A. & Sharov, A.A. (2004) BMP signalling in the control of skin development and hair follicle growth. *Differentiation;* **72,** 512-526.

Bouwstra, J.A., Honeywell-Nguyen, P.L., Gooris, G.S. & Ponec, M. (2003) Structure of the skin barrier and its modulation by vesicular formulations. *Progress in Lipid Research;* **42,** 1-36.*et al*. 2003

Brun, R. P., Tontonoz, P., Forman, B. M., Ellis, R., Chen, J., Evans, R. M. & Spiegelman, B. M. (1996) Differential activation of adipogenesis by multiple PPAR isoforms. *Genes and Development;* **10,** 974–984.

Burkhart, C.G. & Ruppert, E.S. (1981) Dystrophic Epidermolysis Bullosa. *Clinical Pediatrics*; **20**(8), 493-496.

Camp, H.S., Ren, D. & Leff, T. (200) Adipogenesis and fat-cell function in obesity and diabetes. *Trends in Molecular Medicine;* **8,** 442-447.

Cao, Y. (2007) Angiogenesis modulates adipogenesis and obesity. *Journal of Clinical Investigation;* **117(9),** 2362-2368.

Cao, Z., Umek, R.M., and McKnight, S.L. (1991) Regulated expression of three C/EBP isoforms during adipose conversion of 3T3–L1 cells. *Genes and Development*; **5,** 1538–1552.

Chen, Z., Torrens, J.I., Anand, A., Spiegelman, B.M., and Friedman, J. (2005)Krox20 stimulates adipogenesis via C/EBPbeta-dependent and –independent mechanisms. *Cell Metabolism;* **1**, 93–106.

Cheon, H.G., LaRochelle, W.J., Bottaro, D.P., Burgess, W.H. & Aaronson, S.A. (1994) High-affinity binding sites for related fibroblast growth factor ligands reside within different receptor immunoglobulin-like domains. *Proceedings of the National Academy of Sciences;* **91(3),** 989-993.

Choi, H., Lee, H., Kim, T-H., Kim, H.J., Lee, Y.J., Lee, S.J., Yu, J.H., Kim, D., Kim, K-S., Park, S.W. & Kim, J-W. (2014) *Cell Death and Differentiation;* **21,** 1071-1080.

Choy, L. & Derynck, R. (2003) Transforming growth factor-β inhibits adipocyte differentiation by Smad3 interacting with CCAAT/enhancer-binding protein (C/EBP) and repressing C/EBP transactivation function. *Journal of Biological Chemistry;* **278,** 9609–9619.

Christodoulides, C., Lagathu, C., Sethi, J.K. & Vidal-Puig, A. (2008) Adipogenesis and Wnt Signalling. *Trends in Endocrinology and Metabolism;* **20(1),** 16-25.

Cinti, S. (2007) In: Fantuzzi G and Mazzone T (Eds.) *Nutrition and Health: Adipose Tissue and Adipokines in Health and Disease*, pp. 3-19. Humana Press Inc., Totowa, NJ.

Cooper, G.M. (2000) Chapter 12: The Cell Surface, *taken from, The Cell; A Molecular Approach.* 2nd edition. Sinauer Associates, Sunderland (MA). Available from: http://www.ncbi.nlm.nih.gov/books/NBK9839/

Couillard, C., Mauriege, P., Imbeault, P., Prud'homme, D., Nadeau, A., Tremblay, A., Bouchard, C. & Despres, J.P. (2000) Hyperleptinemia is more closely associated with adipose cell hypertrophy than with adipose tissue hyperplasia. *International Journal of Obesity Related Metabolic Disorders;* **24,** 782–788.

Cristillo, A.D., Heximer, S.P., Russell, L. & Forsdyke, D.R. (1997) Cyclosporin A inhibits early mRNA expression of G0/G1 switch gene 2 (G0S2) in cultured human blood mononuclear cells. *DNA Cell Biology;* **16,** 1449-1458.

Darlington, G.J., Ross, S.E. & MacDougald, O.A. (1998) The Role of C/EBP genes in Adipocyte Differentiation. *Journal of Biological Chemistry;* **273,** 30057-30060.

Doi, H., Masaki, N., Takahashi, H., Komatsu, H., Fujimori, K. & Satomi, S. (2005) A New Preadipocyte Cell Line, AP-18, Established from Adult Mouse Adipose Tissue. *The Tohoko Journal of Experimental Medicine;* **207,** 209-216.

Downing, D.T. (1992) Lipid and protein structures in the permeability barrier of mammalian epidermis. *Journal of Lipid Research;* **33(3),** 301-313.

Driskell, R:R., Lichtenberger, B.M., Hoste, E., Kretzschmar, K., Simons, B.D., Charalambous, M., Ferron, S.R., Herault, Y., Pavlovic, G., Ferguson-Smith, A.C. & Watt, F.M. (2013) Distinct fibroblast lineages determine architecture in skin development and repair. *Nature;* **504,** 277-281.

Du, X., Tabeta, K., Hoebe, K., Liu, H., Mann, N., Mudd, S., Crozat, K., Sovath, S., Gong, X. & Beutler, B. (2004) Velvet, a dominant Egfr mutation that causes wavy hair and defective eyelid development in mice. *Genetics;* **166**, 331–340.

Eguchi, J., Yan, Q-W., Schones, D.E., Kamal, M., Hsu, C-H., Zhang, M.Q., Crawford, G.E. & Rosen, E.D. (2008) Interferon regulatory factors are transcriptional regulators of adipogenesis. *Cell Metabolism;* **7**, 86–94.

Elbe-Bürger, A., Egyed, A., Olt, S., Klubal ;R., Mann, U., Rappersberger, K., Rot, A. & Stingl, G (2002) Overexpression of IL-4 Alters the Homeostasis in the Skin. *Investigative Dermatology;* **118(5),** 767-778.

EMBL-EBI. GO:0035425 autocrine signalling. *Databases-QuickGo.* Available from www.ebi.ac.uk/QuickGO/GTerm?id=GO:0035425 [Accessed August 2013].

Eswarakumar, V.P., Lax, I. & Schlessinger J. (2005) Cellular signalling by fibroblast growth factor receptors. *Cytokine and Growth Factor Reviews;* **16,** 139-149.

Evans, R.M., Barish, G.D. & Wang, Y-X (2004) PPARs and the complex journey to obesity. *Nature Medicine;* **10,** 355-361.

Farmer, S.R. (2006) Transcriptional control of adipocyte formation. *Cell Metabolism*; **4,** 263-273.

Farmer, S.R. (2008) Molecular determinants of brown adipocyte formation and function. *Genes and Development;* **22,** 1269-1275.

Festa, E., Fretz, J., Berry, R., Schmidt, B., Rodeheffer, M., Horowitz, M. & Horsley, V. (2011) Adipocyte lineage cells contribute to the skin stem cell niche to drive hair cycling. *Cell;* **146(5),** 761-771.

Fève, B. (2005). Adipogenesis : cellular and molecular aspects. *Endocrinology and Metabolism ;* **19,** 483-499.

Fitch, K.R., McGowan, K.A., van Raamsdonk, C.D., Fuchs, H., Lee, D., Puech, A., Herault, Y., Threadgill, D.W., Hrabe de Angelis, M. & Barsh, G.S. (2003) Genetics of dark skin in mice. *Genes and Development ;* **17,** 214–228.

Finch, P.W., Rubin, J.S., Miki, T., Ron, D. & Aaronson,S.A. (1989) Human KGF is FGF-related with properties of a paracrine effector of epithelial cell growth. *Science;* **245,** 752-755.

Fischer-Posovszky, P., Newell, F.S., Wabitsch, M. & Tornqvist, H.E. (2008) Human SGBS cells – a unique tool for studies of human fat cell biology. *Obesity Facts;* **1(4),** 184-189.

Franssen, M.E.J., Boezeman, J.B.M., van der Kerkhof, P.C.M. & van Erp, P.E.J. (2004) Monitoring hyperproliferative disorders in human skin: Flow cytometry of changing cytokeratin expression. *Clinical Cytometry;* **57B(1),** 32-39.

Fukumura, D., Ushiyama, A., Duda, D.G., Xu, L., Tam, J., Krishna, V., Chatterjee, K., Garkavstev, I. & Jain, R.K. (2003) Paracrine Regulation of Angiogenesis and Adipocyte Differentiation During In Vivo Adipogenesis. *Circulation Research*; **93**, e88-e97.

Fukazawa, T., Miyake, S., Band, V. & Band, H. (1996) Tyrosine phosphorylation of Cbl upon epidermal growth factor (EGF) stimulation and its association with EGF receptor and downstream signalling proteins. *Journal of Biological Chemistry;* **271,** 14554-14559.

Gerhold, D.L., Liu, F., Jiang, G., Li, Z., Xu, J., Lu, M., Sachs, J.R., Bagchi, A., Fridman, A., Holder, D.J., Doebber, T.W., Berger, J., Elbrecht, A., Moller, D.E. & Zhang, B.B. (2002) Gene Expression Profile of Adipocyte Differentiation and Its Regulation by Peroxisome Proliferator-Activated Receptor-γ Agonists. *Endocrinology*; **143(6),** 2106-2118 .

Gesta, S., Bluher, M., Yamamoto, Y., Norris, A.W., Berndt, J., Kralisch, S., Boucher, J., Lewis, C. & Kahn, C.R. (2006) Evidence for a role of developmental genes in the origin of obesity and body fat distribution. *Proceedings of the National Academy of Sciences USA;* **103,** 6676-6681.

Gesta, S., Tseng, Y.H. & Kahn, C.R. (2007) Developmental origin of fat: tracking obesity to its source. *Cell*; **131(2),** 242-256.

Graves, C.B., Goewert, R.R. & McDonald, J.M. (1985) The insulin receptor contains a calmodulin binding domain. *Science;* **230,** 827-829.

Gray, S.L., Nora, E.D., Backlund, E.C., Manieri, M., Virtue, S., Noland, R.C., O'Rahilly, S., Cortright, R.N., Cinti, S., Cannon, B. & Vidal-Puig, A. (2006) Decreased Brown Adipocyte Recruitment and Thermogenic Capacity in Mice with Impaired Proliferator-Activated Receptor (P465L PPAR_) Function. *Endocrinology;* **147,** 5708-5714.

Green, E.L. (1966) Biology of the Laboratory Mouse (2nd ed). Dover Publications Inc. New York. Available from http://www.informatics.jax.org/greenbook/index.shtml [Accessed July 2013]

Greenberg, A.S., Egan, J.J., Wek, S.A., Garty, N.B., Blanchette-Mackie, E.J., & Londos, C. (1991) Perilipin, a major hormonally regulated adipocyte-specific phosphoprotein associated with the periphery of lipid storage droplets. *Journal of Biological Chemistry;* **266,** 11341–11346.

Green, H. & Kehinde, O. (1976) Spontaneous heritable changes leading to increased adipose conversion in 3T3 cells. *Cell*; **7,** 105–113.

Gregoire, F.M., Smas, C.M. & Sul, H.S. (1998) Understanding Adipocyte Differentiation. *Physiological Reviews;* **78(3),** 783-809.

Gstraunthaler, G. (2003) Alternatives to the Use of Fetal Bovine Serum: Serum-free Cell Culture. *Altex;* **20,** 275-281.

Guo, L., Yu, Q-C. & Fuchs, E. (1993) Targeting expression of keratinocyte growth factor to keratinocytes elicits striking changes in epithelial differentiation in transgenic mice. *EMBO Journal;* **12(3),** 973-986.

Guo, L., Degenstein, L. & Fuchs, E. (1996) Keratinocyte growth factor is required for hair development but not for wound healing. *Genes and Development;* **10,** 165–75.

Gurnell, M., Wentworth, J.M., Agostini, M., Adams, M., Collingwood, T.N., Provenzano, C., Browne, P.O., Rajanayagam, O., Burris, T.P., Schwabe, J.W., Lazar, M.A. & Chatterjee, V.K. (2000) A dominant-negative peroxisome proliferator-activated receptor gamma (PPARγ) mutant is a constitutive repressor and inhibits PPARγ-mediated adipogenesis. *Journal of Biological Chemistry*; **275,** 5754–5759.

Hadari, Y.R., Gotoh, N., Kouhara, H., Lax, I. & Schlessinger, J. (2001) Critical role for the docking-protein FRS2α in FGF receptor-mediated signal transduction pathways. *Proceedings of the National Academy of Sciences;* **98(15),** 8578-8583.

Hardy, M.H. (1992) The secret life of the hair follicle. *Trends in Genetics;* **8,** 55-60.

Harrington, M., Pond-Tor, S. & Boney, C.M. (2007) Role of Epidermal Growth Factor and ErbB2 Receptors in 3T3-L1 Adipogenesis. *Obesity;* **15(3),** 563-571.

Hauner, H., Rohrig, K. & Petruschke, T. (1995) Effects of epidermal growth factor (EGF), platelet-derived growth factor (PDGF) and fibroblast growth factor (FGF) on human adipocyte development and function. *European Journal of Clinical Investigation;* **25(2),** 90-96.

Hausman, G.J., Campion, D.R., Richardson, R.L. & Martin, R.J. (1981) Adipocyte development in the rat hypodermis. *American Journal of Anatomy;* **161(1),** 85-100.

Hausman, G.J. & Hausman, D.B. (2006). Search for the preadipocyte progenitor cell. *The Journal of Clinical Investigation*; **116**, 3103-3106.

Hausman, G.J. & Martin, R.J. (1982) The development of adipocytes located around hair follicles in the foetal pig. *Journal of Animal Science;* **54(6),** 1286-1296.

Hausman, G.J. & Richardson, R.L. (2004) Adipose tissue angiogenesis. *Journal of Animal Science*; **82**, 925-934.

Heckmann, B.L., Zhang, X., Xie, X. & Liu, J. (2013) The G0/G1 switch gene 2 (G0S2): Regulating metabolism and beyond. *BBA-Molecular and Cell Biology of Lipids;* **1831,** 276-281.

He, W., Barak, Y., Hevener, A., Olson, P., Liao, D., Le, J., Nelson, M., Ong, E., Olefsky, J.M. & Evans, R.M. (2003) Adipose-specific peroxisome proliferator-activated receptor gamma knockout causes insulin resistance in fat and liver but not in muscle. *Proceedings of the National Academy of Sciences;* **100,** 15712–15717.

Higgins, C.A., Richardson, G.D., Ferdinando, D., Westgate, G.E. & Jahoda, C.A. (2010) Modelling the hair follicle dermal papilla using spheroid cell cultures. *Experimental Dermatology;* **19(6),** 546-8.

Hogan, B.L.M. (1996) Bone morphogenetic proteins: multifunctional regulators of vertebrate development. *Genes and Development;* **10,** 1580-1594.

Hotamisligil, G.S., Arner, P., Caro, J.F., Atkinson, R.L. & Spiegelman, B.M. (1995) Increased adipose tissue expression of tumor necrosis factor-alpha in human obesity and insulin resistance. *Journal of Clinical Investigation;* **95(5),** 2409-2415.

Huang, S.M. & Harari, P.M. (1999) Epidermal growth factor receptor inhibition in cancer therapy: biology, rationale and preliminary clinical results. *Invest New Drug* **17,** 259-269.

Hu, E., Tontonoz, P. & Spiegelman, B.M. (1995) Transdifferentiation of myoblasts by the adipogenic transcription factors PPARgamma and C/EBPalpha. *Proceedings of the National Academy of Sciences;* **92(21),** 9856-9860.

Igarashi, T., Nishino, K. & Nayar, S.K. (2005) *Technical Report: The Appearance of Human Skin.* Department of Computer Science, Columbia University. NY. CUCS-024-05

Imai, T., Takakuwa, R., Marchand, S., Dentz, E., Nornert, J-M., Messaddeq, N., Wendling, O., Mark, M., Desvergne, B., Wahli, W., Chambon, P. & Metzger, D. (2004) Peroxisome proliferator-activated receptor gamma is required in mature white and brown adipocytes for their survival in the mouse. *Proceedings of the National Academy of Sciences;* **101**, 4543–4547.

Insenser, M., Montes-Nieto, R., Vilarrasa, N., Lecube, A., Simo, R., Vendrell, J. & Escobar-Morreale, H.F. (2012) A nontargeted proteomic approach to the study of visceral and subcutaneous adipose tissue in human obesity. *Molecular and Cellular Endocrinology;* **363,** 10-19.

Jahoda, C.A.B., Whitehouse, C.J., Reynolds, A.J. & Hole, N. (2003) Hair follicle dermal cells differentiate into adipogenic and osteogenic lineages. *Experimental Dermatology;* **12(6),** 849-859.

Jin, W., Takagi, T., Kanesashi, S-N., Kurahashi, T., Nomura, T., Harada, J. & Ishi S. (2006) Schnurri-2 controls BMP-dependent adipogenesis via interaction with Smad proteins. *Developmental Cell;* **10,** 461–471.

Johnson, D.E. & Williams, L.T. (1993) Structural and functional diversity in the FGF receptor multigene family. *Advances in Cancer Research;* **60,** 1-41.

Kanitakis, J. (2002) Anatomy, Histology and Immunohistochemistry of Normal Human Skin. *European Journal of Dermatology*, **12(4),** 390-399.

Kao, J., Hall, J. & Holland, J.M. (1983) Quantitation of cutaneous toxicity: An in vitro approach using skin organ culture. *Toxicology and Applied Pharmacology;* **68(2),** 206-217.

Kanazawa, A., Tsukada, S., Kamiyama, M., Yanagimoto, T., Nakajima, M., Maeda, S. (2005) Wnt5b partially inhibits canonical Wnt/β-catenin signalling pathway and promotes adipogenesis in 3T3-L1 preadipocytes. *Biochemical and Biophysical Research Connections;* **330,** 505–510.

Kashiwagi, M., Kuroki, T. & Huh, N. (1997) Specific inhibition of hair follicle formation by epidermal growth factor in an organ culture of developing mouse skin. *Developmental Biology;* **189,** 22–32.

Kaur, G & Dufour, J.M. (2012) Cell lines: Valuable tools or useless artifacts. *Spermatogenesis;* **2(1),** 1-5.

Keeler, C.E. (1935) A second rexoid coat character in the house mouse. *Journal of Hereditary;* **26,** 189–91.

Kim, J.B. & Spiegelman, B.M. (1996) ADD1/SREBP1 promotes adipocyte differentiation and gene expression linked to fatty acid metabolism. *Genes and Development;* **10,** 1096–1107.

Kliewer, S. A., Lenhard, J. M., Willson, T. M., Patel, I., Morris, D. C. & Lehmann, J. M. (1995) A prostaglandin J2 metabolite binds peroxisome proliferator-activated receptor γ and promotes adipocyte differentiation. *Cell*; **83**, 813–819.

Koutnikova, H., Cock, T-A., Watanabe, M., Houten, S.M., Champ, M-F., Dierich, A. & Auwerx, J (2003) Compensation by the muscle limits the metabolic consequences of lipodystrophy in PPARγ hypomorphic mice. *Proceedings of the National Academy of Sciences;* **100,** 1457-1462.

Lau, D. C., Dhillon, B., Yan, H., Szmitko, P. E. & Verma, S (2005) Adipokines: molecular links between obesity and atherosclerosis. *American Journal of Physiology. Heart Circulation Physiology;* **288,** 2031–2041.

Lee, D., Cross, S.H., Strunk, K.E., Morgan, J.E., Bailey, C.L., Jackson, I.J. & Threadgill, D.W. (2004) Wa5 is a novel ENU-induced antimorphic allele of the epidermal growth factor receptor. *Mammalian Genome;* **15,** 525-536.

Lefterova, M.I. & Lazar, M.A. (2009) New developments in Adipogenesis. *Trends in Endocrinology and Metabolism;* **20(3),** 107-114.

Lefterova, M.I., Zhang, Y., Steger, D.J., Schupp, M., Schug, J., Cristancho, A., Feng, D., Zhuo, D., Stoeckert Jr3, C.J., Liu, S. & Lazar, M. (2008) PPARγ and C/EBP factors orchestrate adipocyte biology via adjacent binding on a genome-wide scale. *Genes and Development;* **22,** 2941-2952.

Lehmann, J. M., Moore, L. B., Smith-Oliver, T. A., Wilkison, W. O., Willson, T. M., & Kliewer, S. A. (1995) An antidiabetic thiazolidinedione is a high affinity ligand for peroxisome proliferator-activated receptor γ (PPARγ). *Journal of Biological Chemistry;* **270,** 12953–12956.

Lehrke, M. & Lazar, M.A. (2005) The many faces of PPARγ. *Cell;* **123,** 993–999.

Li, D., Yea, S., Li, S., Chen, Z., Narla, G., Banck, M., Laborda, J., Tan, S., Friedman, J.M., Friedman, S.L. & Walsh, M.J. (2005). Krüppel-like factor-6 promotes preadipocyte differentiation through histone deacetylase 3-dependent repression of DLK1. *Journal of Biological Chemistry;* **280,** 26941–26952.

Linhart, H.G., Ishimura-Oka, K., DeMayo, F., Kibe, T., Repka, D., Poindexter, B., Bick, R.J. & Darlington, G.J. (2001) C/EBPα is required for differentiation of white, but not brown, adipose tissue. *Proceedings of the National Academy of Sciences;* **98,** 12532–12537.

Lin, J., Handschin, C. & Spiegelman, B.M. (2005) Metabolic control through the PGC-1 family of transcription coactivators. *Cell Metabolism*; **1**, 361–370.

Lin, F.-T. & Lane, M. D. (1994) CCAAT/enhancer binding protein alpha is sufficient to initiate the 3T3-L1 adipocyte differentiation program. *Proceedings of the National Academy of Sciences*; **91,** 8757–8761.

Liu, M., Guo, L., Liu, Y., Pei, Y., Li, N., Jin, M., Ma, L., Li, Z., Sun, B. & Li, C. (2014) Adipose stromal-vascular fraction-derived paracrine factors regulate adipogenesis. *Molecular and Cellular Biochemistry;* **385,** 115-123.

Liu, Y., Mukhopadhyay, P., Pisano, M.M., Lu, X., Huang, L., Lu, Q. & Dean, D.C. (2013) *Stem Cells;* **31(7),** 1550-1362.

Lu, Z., Hasse, S., Bodo, E., Rose, C., Funk, W. & Paus, R. (2007) Towards the development of a simplified long-term organ culture method for human scalp skin and its appendages under serum-free conditions. *Investigative Dermatology;* **16(1),** 37-44.

Lucas, S., Taront, S., Magnan, C., Fauconnier, L., Delacre, M., Macia, L., Delanoye, A., Verwaerde, C., Spriet, C., Salue, P., Goormachtigh, G., He' liot, L., Ktorza, A., Movassat, J., Polakowska, R., Auriault, C., Poulain-Godefroy, O., Santo, J., Froguet, P. & Wolowczuk (2012) Interleukin-7 Regulates Adipose Tissue Mass and Insulin Sensitivity in High-Fat Diet-Fed Mice through Lymphocyte-Dependent and Independent Mechanisms. *Public Library of Science;* **7,** 1-10.

MacNeal, R.J. (2014) Structure and Function of the Skin. *Merck Manuals.* Available from www.merckmanuals.com/home/skin_disorders/biology_of_the_skin/structure_and_function_of_the_skin.html [Accessed June/2014].

Macotela, Y., Emanuelli, B., Mori, M.A., Gesta, S., Schulz, T.J., Tseng, Y-H. & Kahn, C.R. (2012) Intrinsic Differences in Adipocyte Precursor Cells From Different White Fat Depots. *Diabetes;* **61,** 1691-1699.

Mandrup, S. & Lane, M.D. (1997) Regulating Adipogenesis. *The Journal of Biological Chemistry;* **272,** 5367-5370.

Martin, R.J., Hausman, G.J. & Hausman, D.B. (1998) Regulation of Adipose Cell Development *In Utero*. *Proceedings of the Society for Experimental Biology*; **219**, 200-210.

Massagué, J. & Chen, Y.-C. (2000) Controlling TGF-β signalling. *Genes and Development;* **14,** 627-644.

Massagué, J. & Pandiella, A. (1993) Membrane-Anchored Growth Factors. *Annual Review of Biochemistry;* **62,** 515-541.

Massague, J. & Weis-Garcia, F. (1996) Serine/threonine kinase receptors: Mediators of Tgf-β family signals. *Cancer Surveys;* 2**6,** 41-64.

Massuti, B. (2003) EGFR-Signalling Pathway. *In Fifth Congress on Lung Cancer, Barcelona;* 141-145.

Matsusue, K., Haluzik, M., Lambert, G., Yim, S-H., Gavrilova, O., Ward, J.M., Brewer, B., Reitman, M.L. & Gonzalez, F.J. (2003) Liver-specific disruption of PPARγ in leptin-deficient mice improves fatty liver but aggravates diabetic phenotypes. *Journal of Clinical Investigation;* **111,** 737-747.

McGrath, J.A., Eady, R.A.J. & Pope, F.M. (2004) Anatomy and Organisation of Human Skin. In *Rook's Textbook of Dermatology* (7th ed.). Chapter 3. Blackwell Publishing. Available from: www.blackwellpublishing.com. [Accessed 01/2012].

Michalik, L., Desvergne, B., Dreyer, C., Gavillet, M., Laurini, R.N. & Wahli. W (2002) PPAR expression and function during vertebrate development. *International Journal of Developmental Biology;* **46,** 105-114.

Miki, T., Bottaro, D.P., Fleming, T.P., Smith, C.L., Burgess, W.H., Chan, A.M. & Aaronson, S.A. (1992) Determination of ligand-binding specificity by alternative splicing: two distinct growth factor receptors encoded by a single gene. *Proceedings of the National Academy of Sciences;* **89,** 246–50.

Miles, P.D., Barak, Y. & Evans, R.M. (1999) Metabolic characterization of mice heterozygous for PPARγ deficiency. *Diabetes;* **48,** supplement 1, A68.

Millar, S.E. (2002) Molecular Mechanisms Regulating Hair Follicle Development. *Journal of Investigative Dermatology;* **118,** 216-225.

Millar, S.E. (2005) An Ideal Society? Neighbors of Diverse Origins Interact to Create and Maintain Complex Mini-Organs in the Skin. *Public Library of Science-*

Biology; **3(11),** 1873-1877.

Millar, S.E., Willert, K., Salinas, P.C., Roelink, H., Nusse, R., Sussman, D.J. & Barsh, G.S. (1999). WNT signalling in the control of hair growth and structure. *Developmental Biology;* **207,** 133-149.

Montagna, W. & Parakkal, P.F. (1974) The Structure and Function of Skin. Chapter 1. Academic Press. Available from: www.googlebooks.com. [Accessed 08/2013].

Moore, K.A. & Lemischka, I.R. (2006) Stem Cells and their niches. *Science;* **311,** 1880-1885.

Moreno-Naverrete, J.M. & Fernández-Real, J.M. (2012) Chapter 2: Adipocyte Differentiation. *In Adipose Tissue Biology (Symonds, M.E. ed).* Springer Science + Business Media. DOI 10.1007/978-1-4614-0965-6_2,

Mori, T., Sakaue, H., Iguchi, H., Gomi, H., Okada, Y., Takashima, Y., Nakamura, K., Nakamura, T., Yamauchi, T., Kubota, N., Kadowaki, T., Matsuki, Y., Ogawa, W., Hiramatsu, R. & Kasuga, M.(2005) Role of Krüppel-like factor 15 (KLF15) in transcriptional regulation of adipogenesis. *Journal of Biological Chemistry;* **280,** 12867–12875.

Morrison, R.F. and Farmer, S.R. (1999) Role of PPARγ in regulating a cascade expression of cyclin-dependent kinase inhibitors, p18(INK4c) and p21(Waf1/Cip1), during adipogenesis. *Journal of Biological Chemistry;* **274,** 17088–17097.

Murillas, R., Larcher, F., Conti, C.J., Santos, M., Ulrich, A. & Jorcano, J.L. (1995) Expression of a dominant negative mutant of epidermal growth factor receptor in the epidermis of transgenic mice elicits striking alterations in hair follicle development and skin structure. *EMBO Journal*; **14** , 5216–5223.

Nanba, D., Hieda, Y. & Nakanishi, Y. (2000) Remodeling of desmosomal and hemidesmosomal adhesion systems during early morphogenesis of mouse pelage hair follicles. *Journal of Investigative Dermatology;* **114,** 171-177.

Nanney, L:B., Stoscheck, C.M., Magid, M. & King Jr, L.E. (1986) Altered [^{125}I] epidermal growth factor binding and receptor distribution in psoriasis. *Journal of Investigative Dermatology;* **86,** 260-265.

Neels, J.G., Thinnes, T. & Lokustuff, D.J. (2004) Angiogenesis in an in vivo model of adipose tissue development. *FASEB Journal;* **18(9),** 983-985.

Nie, J. & Sage, E.H. (2009) SPARC inhibits adipogenesis by its enhancement of β-catenin signalling. *Journal of Biological Chemistry;* **284,** 1279-1290.

Nohe, A., Hassel, S., Ehrlich, M., Neubauer, F., Sebald, W., Henis, Y.I. & Knaus, P. (2002) The mode of bone morphogenetic protein (BMP) receptor oligomerization determines different BMP-2 signalling pathways. *Journal of Biological Chemistry;* **277,** 5330-5338.

O'Flaherty, J.T., Rogers, L.C., Paumi, C.M., Hantgan, R.R., Thomas, L.R., Clay, C.E., High, K., Chen, Y.Q., Willingham, M.C., Smitherman, P.K., Kute, T.E., Rao, A., Cramer, S.D. & Morrow, C.S. (2005) %-Oxo-ETE analogs and the proliferation of cancer cells. *Biochimica et Biophysica Acta, Molecular and Cell Biology of Lipids;* **1736/3),** 228-236.

Oishi, Y., Manabe, I., Tobe, K., Tsushima, K., Shindo, T., Fujiu, K., Nishimura, G., Maemura, K., Yamauchi, T., Kubota, N., Suzuki, R., Kitamura, T., Akira, S., Kadowaki, T. & Nagai, R. (2005). Krüppel-like transcription factor KLF5 is key regulator of adipocyte differentiation. *Cell Metabolism;* **1**, 27–39.

Oliver, R.F. & Jahoda, C.A. (1988) Dermal-epithelial interactions. *Clinical Dermatology;* **6,** 74-82.

Orr-Urtreger, A., Givol, D., Yayon, A., Yarden, Y. & Lonai, P. (1991) Developmental expression of two murine fibroblast growth factor receptors, flg and bek. *Development;* **113***,* 1419-1434.

Oshima, H., Rochat, A., Kedzia, C., Kobayashi, K. & Barrandon, Y. (2001) Morphogenesis and renewal of hair follicles from adult multipotent stem cells. *Cell;* **104,** 233-245.

Otto, T.C. & Lane, M.D. (2005) Adipose development: from stem cell to adipocyte. *Crit. Rev. Biochem. Molecular Biology;* **40,** 229–242.

Pairault, J. & Green, H. (1979) A study of the adipose conversion of suspended 3T3 cells by using glycerophosphate dehydrogenase as differentiation marker. *Proceedings of the National Academy of Sciences;* **76,** 5138-5142.

Paus, R., Muller-Rover, S., Van Der Veen, C., Maurer, M., Eichmuller, S., Ling, G., Hofmann, U., Foitzik, K., Mecklenburg, L. & Handjiski, B. (1999) A comprehensive guide for the recognition and classification of distinct stages of hair follicle morphogenesis. *Journal of Investigative Dermatology;* **113,** 523-532.

Pearson, J.C., Lemons, D. & McGinnis, W. (2005) Modulating Hox gene functions during animal body patterning. *Nature Reviews;* **6,** 893-904.

Perera, R.J., Marcusson, E.G., Koo, S., Kang, X., Kim, Y., White, N. & Dean, N.M. (2006) Identification of novel PPARγ target genes in primary human adipocytes. *Gene*; **369,** 90–99.

Peters, K.G., Werner, S., Chen, G. & Williams, L.T. (1992) Two FGF receptor genes are differentially expressed in epithelial and mesenchymal tissues during limb formation and organogenesis in the mouse. *Development;* **114,** 233-243.

Petiot, A., Conti, F. J., Grose, R., Revest, J. M., Hodivala-Dilke, K. M. & Dickson, C. (2003). A crucial role for Fgfr2-IIIb signalling in epidermal development and hair follicle patterning. *Development;* **130,** 5493-5501.

Petrovic, N., Walden, T.B., Shabalina, I.G., Timmons, J.A., Cannon, B., Nedergaard, J. (2010) Chronic peroxisome proliferator-activated receptor gamma (PPARgamma) activation of epididymally derived white adipocyte cultures reveals a population of thermogenically competent, UCP1-containing adipocytes molecularly distinct from classic brown adipocytes. *Journal of Biological Chemistry;* **285,** 7153–7164.

Philpott, M.P., Sanders, D., Westgate, G.E. & Kealey, T. (1994) Human hair growth in vitro: a model for the study of hair follicle biology. *Journal of Dermatological Science;* **7(S1),** S55-S72.

Picard, F., Kurtev, M., Chung, N., Topark-Ngarm, A., Senawong, T., Machado De Oliveira, R., Leid, M., McBurney, M.W., and Guarente, L. (2004) Sirt1 promotes fat mobilization in white adipocytes by repressing PPARgamma. *Nature*; **429,** 771–776.

Poulos, S.P., Hausman, D.B. & Hausman, G.J. (2009) The development and endocrine functions of adipose tissue. *Molecular and Cellular Endocrinology;* **323,** 20-34.

Rahimi, N., Tremblay, E., McAdam, L., Roberts, A. & Elliott, B (1998) Autocrine secretion of TGF-β and TGF-β2 by pre-adipocytes and adipocytes: a potent negative regulator of adipocyte differentiation and proliferation of mammary carcinoma cells. *In Vitro Cell Developmental Biology – Animal;* **34**, 412–420.

Razani, B., Combs, T.P., Wang, X.B., Frank, P.G., Park, D.S., Russell, R.G., Li, M., Tang, B., Jelicks, L.A., Scherer, P.E. & Lisanti, M.P. (2002) Caveolin-1-deficient Mice Are Lean, Resistant to Diet-induced Obesity, and Show Hypertriglyceridemia with Adipocyte Abnormalities. *Journal of Biological Chemistry ;* **277,** 8635-8647.

Reiners, J.J. & Slaga, T.J. (1983) Effects of tumor promoters on the rate and commitment to terminal differentiation of subpopulations of murine keratinocytes. *Cell ;* **32(1),** 247-255.

Richardson, G.D., Bazzi, H., Fantauzzo, K.A., Waters, J.M., Crawford, H., Hynd, P., Christiano, A.M. & Jahoda, C.A.B. (2009) KGF and EGF signalling block hair follicle induction and promote interfollicular epidermal fate in developing mouse skin. *Development;* **136,** 2153-2164.

Rodeheffer, M.S., Birsoy, K., Friedman, J.M (2008) Identification of White Adipocyte Progenitor Cells In Vivo. *Cell ;* **135,** 240-249.

Rodriguez-Viciana, P., Warne, P.H., Dhand, R., Vanhaesebroeck, B., Gout, I., Fry, M.J., Waterfield, M.D. & Downward, J. (1994) Phosphatidylinositol-3-OH kinase as a direct target of Ras. *Nature;* **370**, 527-532.

Rosen, E.D., Hsu, C-H., Wang, X., Sakai, S., Freeman, M.W., Gonzalez, F.J. & Spiegelman, B.M. (2002) C/EBPα induces adipogenesis through PPARγ: a unified pathway. *Genes and Development*; **16**, 22-26.

Rosen, E.D. & MacDougald, O.A. (2006) Adipocyte differentiation from the inside out. *Nature Reviews Molecular Cell Biology;* **7,** 885–896.

Rosen, E.D., Sarraf, P., Troy, A.E., Bradwin, G., Moore, K., Milstone, D.S., Spiegelman, B.M. & Mortensen, R.M. (1999) PPARγ Is Required for the Differentiation of Adipose Tissue In Vivo and In Vitro. *Molecular Cell*; **4**, 611-617.

Rotman, N., Michalik, L., Desvergne, B. & Wahli, W (2006) PPARs in fetal and early postnatal development. *Advances in Developmental Biology;* **16,** 1574-3349.

Rubin, J.S., Bottaro, D.P., Chedid, M., Miki, T., Ron, D., Cheon, G., Taylor, W.G., Fortney, E., Sakata, H., Finch, P.W. & LaRochelle, W.J. (1995) Keratinocyte growth factor. *Cell Biology International;* **19,** 399–411.

Schmidt, B.A. & Horsley, V. (2012) Unravelling hair follicle-adipocyte communication. *Experimental Dermatology;* **21,** 827-830.

Schmidt, B.A. & Horsley, V. (2013) Intradermal adipocytes mediate fibroblast recruitment during skin wound healing. *Development;* **140,** 1517-1527.

Schmidt, S.F., Jorgensen, M., Chen, Y., Nielsen, R., Sandelin, A. & Mandrup, S. (2011) Cross species comparison of C/EBPα and PPARγ profiles in mouse and human adipocytes reveals interdependent retention of binding sites. *BMC Genomics;* **12(152),** 1-16.

Schoonjans, K., Peinado-Onsurbe, J., Lefebvre, A.M., Heyman, R.A., Briggs, M., Deeb, S., Staels, B. & Auwerx J. (1996) PPARalpha and PPARgamma activators direct a distinct tissue-specific transcriptional response via a PPRE in the lipoprotein lipase gene. *EMBO Journal;* **15(19),** 5336-5348.

Seale, P., Bjork, B., Yang, W., Kajimura, S., Chin, S., Kuang, S., Scime, A., Devarakonda, S., Conroe, H.M., Erdjument-Bromage, H., Tempst, P., Rudnick, M.A., Beier, D.R. & Spiegelman, B.M. (2008) PRDM16 controls a brown fat/skeletal muscle switch. *Nature;* **454**, 961–967.

Sears, I.B., MacGinnitie, M.A., Kovacs, L.G. & Graves, R.A. (1996) Differentiation dependent expression of the brown adipocyte uncoupling protein gene: regulation by peroxisome proliferator-activated receptor γ. *Molecular Cell Biology;* **16,** 3410–3419.

Serrero, G. & Mills, D. (1991) Physiological role of epidermal growth factor on adipose tissue development in vivo. *Proceedings of the National Academy of Sciences;* **88,** 3912–3916.

Sibilia, M., Wagner, B., Hoebertz, A., Elliott, C., Marino, S., Jochum, W. & Wagner, E.F. (2003) Mice humanised for the EGF receptor display hypomorphic phenotypes in skin, bone and heart. *Development*; **130,** 4515–25.

Siersbæk, R., Nielsen, R., John, S., Sung, M-H., Baek, S., Loft, A., Hager, G.L. & Mandrup, S. (2011) Extensive chromatin remodelling and establishment of transcription factor 'hotspots' during early adipogenesis. *EMBO Journal;* **30,** 1459-1472.

Siersbæk, R., Nielsen, R. & Mandrup, S. (2012) Transcriptional networks and chromatin remodeling controlling adipogenesis. *Trends in Endocrinology and Metabolism;* **23,** 56-64.

Soltoff, S.P., Carraway, K.L. III., Prigent, S.A., Gullick, W.G. & Cantley, L.C. (1994) ErbB3 is involved in activation of phosphatidylinositol 3-kinase by epidermal growth factor. *Molecular and Cellular Biology;* **14**, 3550-3558.

Soukas, A., Socci, N.D., Saatkamp, B.D., Novelli, S. & Friedman, J.M. (2001) Distinct Transcriptional Profiles of Adipogenesis *in Vivo* and *in Vitro. The Journal of Biological Chemistry;* **276,** 34167-34174.

Sperling, L.C. (1991) Hair anatomy for the clinician. *Journal of American Academic Dermatology;* **25,** 1-17.

Spiegelman, B.M. (2013) Regulation of Adipogenesis: Toward New Therapeutics for Metabolic Disease. *Diabetes;* **62,** 1774-1783.

Suga, J., Yoshimasa, Y., Yamada, K., Yamamoto, Y., Inoue, G., Okamoto, M., Hayashi, T, Shigemoto, M., Kosaki, A., Kuzuya, H. & Nakao, K. (1997) Differential Activation of Mitogen-Activated Protein Kinase by Insulin and Epidermal Growth Factor in 3T3-L1 Adipocytes: A Possible Involvement of PI3 Kinase in the Activation of the MAP Kinase by Insulin. *Diabetes;* **46,** 735-741.

Sugawara, K., Schneider, M.R., Dahlhoff, M., Kloepper, J.E. & Paus, R. (2010) Cutaneous consequences of inhibiting EGF receptor signalling *in vivo*: Normal hair follicle development, but retarded hair cycle induction and inhibition of adipocyte growth in Egfr^{Wa5} mice. *Journal of Dermatological Science;* **57,** 155-161.

Sundberg, J.P & Hogan, M.E. (1994) Hair types and subtypes in the laboratory mouse. *Handbook of mouse mutations with skin and hair abnormalities*. Pp 57-68.

Takashima, Y., Era, T., Nakao, K., Kondo, S., Kasuga, M., Smith, A.G. & Nishikawa, S. (2007) Neuroepithelial cells supply an initial transient wave of MSC differentiation. *Cell;* **129,** 1377–1388.

Tanaka, T., Yoshida, N., Kishimoto, T. & Akira, S. (1997) Defective adipocyte differentiation in mice lacking the C/EBPβ and/or C/EBPδ gene. *European Molecular Biology Organisation Journal;* **16**, 7432–7443.

Tang, Q.Q., Otto, T.C. & Lane, M.D. (2003) Mitotic clonal expansion: a synchronous process required for adipogenesis. *Proceedings of the National Academy of Sciences;* **100,** 44–49.

Tang, Q. Q., Otto, T. C. & Lane, M.D. (2004) Commitment of C3H10T1/2 pluripotent stem cells to the adipocyte lineage. *Proceedings of the National Academy of Sciences;* **101,** 9607–9611.

Taylor, G., Lehrer, M.S., Jensen, P.J., Sun, T.T. & Lavker, R.M. (2000) Involvement of follicular stem cells in forming not only the follicle but also the epidermis. *Cell;* 102, 451-461.

Threadgill, D.W., Dlugosz, A.A., Hansen, L.A., Tennenbaum, T., Lichti, U., Yee, D., LaMantia, C., Mourton, T., Herrup, K., Harris, R.C. (1995) Targeted disruption of mouse EGF receptor: effect of genetic background on mutant phenotype. *Science*; **269,** 230–234.

Tontonoz, P., Hu, E. & Spiegelman, B.M. (1994). Stimulation of adipogenesis in fibroblasts by PPARγ2, a lipid-activated transcription factor. *Cell;* **79**, 1147–1156.

Tontonoz, P. & Spiegelman, B.M. (2008) Fat and beyond: the diverse biology of PPARγ. *Annual Review of Biochemistry*; **77,** 289–312.

Trayhurn, P. (2005) Endocrine and signalling role of adipose tissue: new perspectives on fat. *Acta Physiologica Scandinavica;* **184**, 285–293.

Tsai, F-J., Yang, C-F., Chen, C-C., Chuang, L-M., Lu, C-H., Chang, C-T., Wang, T-Y., Chen, R-H., Shiu, C-F., Liu, Y-M., Chang, C-C., Chen, P., Chen, C-H., Fann, C.S.J., Chen, Y-T. & Wu, J-Y. (2010) A Genome-Wide Association Study

Identifies Susceptibility Variants for Type 2 Diabetes in Han Chinese. *Public Library of Science, Genetics;* **6(2),** 1-9.

Tumbar, T., Guasch, G., Greco, V., Blanpain, C., Lowry, W.E., Rendl, M. & Fuchs, E. (2003) Defining the epithelial stem cell niche in skin. *Science;* 303, 359-363.

Unger, R.H. (2002) Lipotoxic diseases. *Annual Review of Medicine;* **53,** 319–336.

Vernochet, C., Milstone, D.S., Lehlé, C., Belmonte, N., Phillips, B., Wdziekonski, B., Villageois, P., Amri, E.Z., O'Donnell, P.E., Mortensen, R.M., Ailhaud, G. & Dani, C (2002). PPARγ-dependent and PPARγ-independent effects on the development of adipose cells from embryonic stem cells. *FEBS Letters;* **510,** 94-98.

Wang, N.D., Finegold, M.J., Bradley, A., Ou, C.N., Abdelsayed, S.V., Wilde, M.D., Taylor, L.R., Wilson, D.R. & Darlington, G.J. (1995) Impaired energy homeostasis in C/EBP alpha knockout mice. *Science;* **269,** 1108–1112.

Wang, E. A., Israel, D. I., Kelly, S. & Luxenberg, D. P. (1993) Bone morphogenetic protein-2 causes commitment and differentiation in C3H10T1/2 and 3T3 cells.. *Growth Factors;* 9**,** 57–71.

Wang, H.C., Ko, Y.H., Mersmann, H.J., Chen, C.L. & Ding, S.T. (2006) The expression of genes related to adipocyte differentiation in pigs. *Journal of Animal Science*; **84**, 1059-1066.

Watanabe, S., Takeuchi, Y., Fukumoto, S., Fujita, H., Nakano, T. & Fujita, T. (2003) Decrease in serum leptin by troglitazone is associated with preventing bone loss in type 2 diabetic patients. *Journal of Bone and Mineral Metabolism;* **21,** 166-171.

Werner, S., Smola, H., Liao, X., Longaker, M.T., Krieg, T., Hofschneider, P.H. & Williams, L.T. (1994) The function of KGF in morphogenesis of epithelium and reepithelialization of wounds. *Science;* **266**(5186), 819-822.

Winnier, G., Blessing, M., Labosky, PA. & Hogan, B.L. (1995) Bone morphogenetic protein-4 is required for mesoderm formation and patterning in the mouse. *Genes and Development;* **9,** 2105-2116.

Wojciechowicz, K. (2012) PhD Thesis. Durham University. In vivo and in vitro studies of adipogenesis with particular reference to adipocyte development in rodent skin.

Wojciechowicz, K., Gledhill, K., Ambler, C.A., Manning, C.B. & Jahoda, C.A.B. (2013) Development of the Mouse Dermal Fat Layer Occurs Independently of Subcutaneous Fat and is Marked by Restricted Early Expression of FABP4. *Public Library of Science;* **8(3),** 1-15.

Wojciechowicz, K., Markiewicz, E. & Jahoda, C.A. (2008) C/EBPα identifies differentiating preadipocytes around hair follicles in foetal and neonatal rat and mouse skin. *Experimental Dermatology*; **17(8),** 675-680.

Wu, J., Srinivasan, S.V., Neumann, J.C. & Lingrel, J.B. (2005) The KLF2 transcription factor does not affect the formation of preadipocytes but inhibits their differentiation into adipocytes. *Biochemistry;* 4**4,** 11098–11105.

Wu, Z., Bucher, N.L. & Farmer, S.R. (1996) Induction of peroxisome proliferator-activated receptor gamma during the conversion of 3T3 fibroblasts into adipocytes is mediated by C/EBPalpha, C/EBPdelta, and glucocorticoids. *Molecular and Cellular Biology;* **16,** 4128-4136.

Wu, Z., Rosen, E.D., Brun, R., Hauser, S., Adelmont, G., Troy, A.E., McKeon, C., Darlington, G.J. & Spiegelman, B.M. (1999) Cross-regulation of C/EBP alpha and PPAR gamma controls the transcriptional pathway of adipogenesis and insulin sensitivity. *Molecular Cell;* **3,** 151–158.

Yaish, P., Gazit, A., Gilon, C. & Levitzki, A. (1988) Blocking of EGF-dependent cell proliferation by EGF receptor kinase inhibitors. *Science;* **242,** 933-935.

Yamaguchi, K., Nagai, S-I., Ninomiya-Tsui, J., Nishita, M., Tamai, K., Irie, K., Ueno, N., Nishida, E., Shibuya, H. & Matsumoto, K. (1999) XIAP, a cellular member of the inhibitor of apoptosis protein family, links the receptors to TAB1-TAK1 in the BMP signalling pathway. *EMBO Journal;* **18,** 179-187.

Yamanishi, K. (1998) Gene-knockout mice with abnormal epidermal and hair follicle development. *Journal of Dermatological Science;* **18(2),** 75-89.

Yang, J., Croniger, C.M., Lekstrom-Himes, J., Zhang, P., Fenyus, M., Tenen, D.G., Darlington, G.J. & Hanson, R.W. (2005) Metabolic response of mice to a postnatal ablation of CCAAT/enhancer-binding protein alpha. *Journal of Biological Chemistry;* **280,** 38689–38699.

Yang, X., Lu, X., Lombe, M., Rha, G.B., Chi, Y-I., Guerin, T.M., Smart, E.J. & Liu, J. (2010) The G0/G1 Switch Gene 2 Regulates Adipose Lipolysis through Association with Adipose Triglyceride Lipase. *Cell Metabolism;* **11,** 194-205.

Yarden, Y. & Shilo, B.Z. (2007) SnapShot:. EGFR signalling pathway. *Cell;* **131,** 1018.

Yasuoka, H., Larregina, A.T., Yamaguchi, Y. & Feghali-Bostwick, C.A. (2008) Human Skin Culture as an *Ex Vivo* Model for Assessing the Fibrotic Effects of Insulin-Like Growth Factor Binding Proteins. *Open Rheumatology Journal;* **2,** 17-22.

Yu, C., Markan, K., Temple, K.A., Deplewski, D., Brady, M.J. & Choen, R.N. (2005)

The nuclear receptor corepressors NCoR and SMRT decrease peroxisome proliferator-activated receptor gamma transcriptional activity and repress 3T3-L1 adipogenesis. *Journal of Biological Chemistry;* **280,** 13600–13605.

Zamani, N. & Brown, C.W. (2011) Emerging roles for the transforming growth factor-beta superfamily in regulating adiposity and energy expenditure. *Endocrinology Reviews;* **32,** 387–403.

Zandbergen, F., Mandard, S., Escher, P., Tan, N.S., Patsouris, D., Jatkoe, T., Rojas-Caro, S., Madore, S., Wahli, W., Tafuri, S., Müller, M. & Kersten. (2005). The G0/G1 switch gene 2 is a novel PPAR target gene. *Biochemical Journal;* **392,** 313–324.

Zehentner, B. K., Leser, U. & Burtscher, H. (2000) BMP-2 and sonic hedgehog have contrary effects on adipocyte-like differentiation of C3H10T1/2 cells. *DNA and Cell Biology;* **19,** 275–281.

Zhang, J., Fu, M., Cui, T., Xiong, C., Xu, K., Zhong, W., Xiao, Y., Floyd, D., Liang, J., Li, E.,Song, Q. & Chen, Y.E. (2004) Selective disruption of PPARγ2 impairs the development of adipose tissue and insulin sensitivity. *Proceedings of the National Academy of Sciences;* **101,** 10703–10708.

Zhang, T., Guan, H. & Yang, K. (2010) Keratinocyte Growth Factor Promotes Preadipocyte Proliferation via an Autocrine Mechanism. *Journal of Cellular Biochemistry;* **109,** 737-746.

Zhu, H., Kavsak, P., Abdollah, S.,Wrana, J.L. & Thomsen, G.H. (1999) A SMAD ubiquitin ligase targets the BMP pathway and affects embryonic pattern formation. *Nature;* **400,** 687-693.

Zhu, Y., Chao, Q., Korenberg, J.R., Chen, X-N., Noya, D., Rao, M.S. & Reddy, J.K. (1995) Structural organization of mouse peroxisome proliferator-activated receptor gamma (mPPARγ) gene: alternative promoter use and different splicing yield two mPPARγ isoforms. *Proceedings of the National Academy of Sciences;* **92,** 7921–7925.

zur Nieden, N. I., Kempka, G., Rancourt, D. E. & Ahr, H. J. (2005) Induction of chondro-, osteo- and adipogenesis in embryonic stem cells by bone morphogenetic protein-2: effect of cofactors on differentiating lineages. *BMC Developmental Biology;* **5,** 1.

Appendix I

Working Solutions and Reagents for Tissue Staining

<u>For Immunofluorescence, Oil Red O and H&E staining</u>

Phosphate buffered saline (PBS)

- 40g NaCl
- 9.03g Na2HPO4.2H2O
- 1.45g KH2PO4
- 1g KCL

Adjust pH to 7.4 and stir to dissolve in 1 litre distilled H20

Calcium formal solution

- 20g paraformaldehyde or 50ml of 37% formaldehyde solution
- 5g calcium chloride (Sigma)
- 450ml distilled water.

Mowiol (when not using Vectashield)

- 6g glycerol,
- 2.4g mowiol (mowiol 4-88)
- 6ml H20
- 12ml 0.2M Tris (ph 6.8)

Stir overnight , centrifuge and add supernatant to DABCO (1.4-diazobicylo-(2.2.2.)-octane) to a concentration of 2.5%.

4% Paraformaldehyde

- Add 4g paraformaldehyde (Sigma) to 100ml PBS and heat to 50°C.
- Stir until transparent.

0.5% Triton X

- 0.5ml TritonX (Sigma) and make up to 100ml with PBS
- Further dilute for 0.1%

Oil Red O stock solution

- Add 300mg oil red O powder (Sigma) to 100ml 99% isopropanol (Sigma).
- Dissolve before use.

Oil Red O working solution

- Add 3 parts oil red O stock solution to 2 parts distilled water.
- Leave to settle for a few minutes and then filter 2-3 times until the red solution is transparent.

Appendix II

Working Solutions and Reagents for Chapter 3

Mouse on Mouse Kit (FMK-2207; Vector Labs Inc)

Mouse Ig Blocking Reagent

- 2 drops of stock solution
- 2.5ml PBS

Diluent

- 600µl Protein Concentrate
- 7.5ml PBS

Biotinylated Anti-mouse IgG Reagent

- 10µ stock solution
- 2.5ml of prepared Diluent

Fluorescein Avidin DCS

- 40µl stock solution
- 2.5ml PBS
-

For Inducing Adipogenesis in 3T3 F442A cells

3T3 cell medium

- DMEM (4.5g/1 D-glucose) (Gibco)
- 10% foetal bovine serum (Sigma)
- 2mM L-glutamine
- Antibiotics: Fungizone, 2µg/ml (Sigma), Penicillin, 100units/ml and Streptomycin, 100µg/ml (Gibco)

Differentiation medium

- 1µg/ml insulin (Sigma)
- 0.5mM IBMX
- 0.25mM dexamethasone
- Add Insulin, IBMX and dexamethasone to the 3T3 cell medium

Insulin medium

- 3T3 cell medium
- 1µg/ml insulin

Appendix III (A)

Working Solutions and Reagents for Chapters 4 and 5

For Organ and Cell Culture Model set ups

5% Agar Plates

- For approx. 4 petri dishes, add 10grams of agar (Sigma) to 200ml distilled water.
- Heat in a microwave with the lid loosed for 2 minutes, stirring frequently.
- Leave to cool then pour into the petri dishes.
- When set, store upside-down in the fridge.

Collagen coated filters

- Coat Nucleopore filters (Whatman) with rat-tail collagen type 1 (Sigma) for 40 seconds on each side.
- Adhere them to a petri dish lid and place under UV light overnight for sterility

DNase I stock solution

- 1 mg/ml DNase I (Stock): 0.01 g DNase I (Roche)
- 10 ml DPBS (Gibco)
- Mix slowly.

Collagenase II/DNase I working solution

- 3900 units of collagenase II (Worthington)
- 100µg of 1mg/ml DNase I in 15ml of MEM-minimal essential medium (Sigma) with antibiotics: 2µg/ml fungizone and 100U/ml penicillin and 100µg/ml streptomycin (Gibco)

Earle's Solution

Two solutions (A and B) were mixed in equal quantities and sterile filtered.

Solution A	Solution B
NaCl 6.8g	NaHCO3 1g
KCl 0.4g	dH20 150ml
Nah2PO4 0.14g	
Glucose 1g	
dH20 950ml	

*These quantities make 1x, though for solutions A and B, using 95ml and 15ml of distilled water respectively can make a 10x solution which can be diluted prior to use.

6% Pancreatin

- Add 6g pancreatin (Sigma) to 100ml sterile Earles (1x) and leave stirring overnight at 4°C
- Aliquots (500 **ml**) kept in -20°C. Filter before use.

5% Trypsin

- Add 5 g trypsin (BD) to 100ml sterile Earle's (1x) solution.
- Aliquots (1ml) kept in -20°C. Filter before use.

Before use to create single cell suspension, 6% Pancreatin, 5% Trypsin and 1x Earle's solution were mixed in a 1:1:2 ratio respectively.

Appendix III (B)

Working Solutions and Reagents for Chapters 4 and 5

Activation and Inhibition Factors

- EGF (Sigma) 100ng/ml, dissolved in DMSO
- AG1478 (Calbiochem) was bought in solution dissolved in DMSO at 10mM
- BMP4 (Calbiochem)
- DMH1 (Calbiochem) was dissolved in DMSO at 16.6mg/ml in a water bath overnight and then further diluted in sterile PBS at 190μg/ml.
- KGF (Peprotech) was dissolved in 0.1% BSA (Sigma) in sterile PBS

EDU Reaction Cocktail (Click.-IT® EDU Imaging Kit, Invitrogen, Alexa Fluor kit)

- 86μl Reaction (RX) buffer (1x RX buffer in deionised water)
- 4μl $CuSO_4$
- 0.24μl Alexa Fluor 488 Azide
- 10μl RX buffer additive (1X RX buffer additive in deionised water)

Appendix IV

Calculations for Cell Culture

Calculating cell numbers

A cell pellet was resuspended in 1ml of media.
10µl was pipetted under the coverslip adhered to a haemocytometer.
Under a microscope, the number of cells in 10 squares was counted (or 5 squares and multiplied by 2).
This was multiplied by 10,000 to get the number of cells in the 1ml.